Thermal Modelling of Feedwater Heaters

Prepared by:

Mohammed Nazier Allie

ALLMOH013

Department of Mechanical Engineering

University of Cape Town

Supervisor: Dr Wim Fuls

Industrial Mentor: Dr Francois Du Preez

February 2016

Submitted to the Department of Mechanical Engineering at the University of Cape Town in partial fulfilment of the academic requirements for a Masters of Science degree in Mechanical Engineering

Key Words: Feedwater heaters; tube plate type; header type; Eskom; thermal modelling; Mathcad

Abstract

Manufacturers of feedwater heaters (FWHs) are obliged to disclose a specification sheet to the client that describes their FWH design. However, the client is unable to verify the performance of this FWH design without comparing it to the results that are predicted by a thermal model. An additional limitation is that the manufacturer will only disclose the minimum number of design parameters. The purpose of this study was to develop a thermal model that can predict the performance of a FWH. The model requires the minimum design input data to predict the performance parameters that may be compared to values predicted by the vendor.

A FWH in a regenerative water-steam Rankine cycle achieves heat transfer to the feedwater by condensing steam on the shell side. This is called a single zone FWH. The tube plate type FWH is the most common type of FWH referenced in literature but the following variations may exist:

- The Eskom fleet consist of both tube plate and header type FWHs.
- FWHs may be orientated vertically or horizontally.
- Internal shrouded regions, that define it as a 2 or 3 zone FWH, may be present in the FWH.
- The length of the drains cooler (DC) zone may either be identified as long or short.

A general model was required to capture all these design variations. Plant visits were arranged with engineers at several power stations to obtain the minimum input data and to confirm that these FWH design variations existed within the Eskom fleet. The model was based on existing tube plate models found in literature. It was then extended to accommodate the FWH variations mentioned above. A further improvement was made by including an additional heat transfer sub-zone that removes excess superheat in the condensing (COND) zone.

The vendor does not disclose the correlations used to predict the film heat transfer coefficients (h) in their design. Therefore, the user is granted the option of selecting a correlation from a list of popular correlations, specific to a heat transfer mode. Note that the uncertainty associated with this thermal model is affected by the uncertainty of each correlation selected in the model.

The FWHs of 6 power stations, within the Eskom fleet, were analysed in order to capture all possible FWH design variations and thus test the thermal model. The thermal model results were generated using multiple combinations of correlations including their associated uncertainty. Therefore, a performance parameter is not just represented by a nominal value but by a statistical range of possible values. The testing revealed that most of the performance values reported by vendors fell within the range of values predicted by the model for the particular FWH. Some concerns and exceptions were noted but could be explained and future thermal model improvements have been recommended such as including wet de-superheating in the COND zone.

Declaration

I, Mohammed Nazier Allie, hereby declare I know the meaning of plagiarism and declare that all the work in the document, save for that which is properly acknowledged, is my own. I have not allowed, and will not allow, anyone to copy my work with the intention of passing it off as their own work or part thereof.

Mohammed Nazier Allie

Acknowledgements

I wish to firstly acknowledge Eskom and the management of EPPEI for sponsoring my research and hope that this study will add value to the organisation. I am grateful to the management at Koeberg Nuclear Power Station for releasing me from my responsibilities during this 2 year MSc programme. I wish to highlight specific individuals such as Wahid Taliep for approving my initial application, to Brandon Taylor for obtaining final the approval from the Power Station Manager (Riedewaan Bakardien), to Xolisiwe Booi and Christine Simpson for allowing me to remotely complete the necessary organisational administration.

I wish to thank the system engineers at the power stations (PS) for arranging plant access and obtaining the necessary data that was used in this study. These individuals are Alain Michaels (Kriel PS), Adriaan van Niekerk and Sujen Balakisson (Duvha PS), Musawenkosi Ngwenyama (Arnot PS), Abel Rudman (Kendal PS), John Clark (Tutuka PS), Wiets Roos (Hendrina PS) and Sulaiman Bapeekee (Majuba Power Station).

I also visited three local factories that manufacture FWHs for Eskom and witnessed aspects of construction. I wish to thank the following individuals for arranging the factory visits and allowing me to witness the manufacturing process of the following FWHs: Alan van Rooyen (SPX DB Thermal – Grootvlei PS FWH), Alex Dreyer (GEA – Matla PS FWH) and Mohamed Khan (Steinmuller Africa – Arnot PS FWH).

I wish to thank the following individuals from the Eskom engineering departments that either developed my MSc topic or provided me with technical feedback and support during my study. To Dr Francois Du Preez and Gary De Klerk (Chief Engineers with Turbine Engineering CoE), Ockert Augustyn (Engineer with Turbine Engineering CoE), Nicolaas Hallatt (Engineer with Production Engineering Integration (Coal)).

However, the largest contributor to my MSc was from my research supervisor Dr. Wim Fuls. He was able to monitor my progress and provided me with guidance during our weekly meetings. I also wish to thank him for painstakingly reviewing my thesis and for assisting me with programming relating obstacles.

Finally, I wish to acknowledge the support of my wife, Shameema Noordien, especially during the time that there was a new addition to our family. She made many sacrifices during the preparation of this text and for assisting with the proof reading the document. To my daughter Zahrah and son Muhammad Zaeem for being patient with me during the final months of my study.

I am grateful to the Almighty for granting me the strength to complete this study.

Table of Contents

List of Figures

List of Tables

List of Nomenclature

General symbols

A	Heat transfer surface area or cross section area [m^2]
B_{cut}	Baffle cut [%]
C	heat capacity rate ($\dot{m}Cp$) [kW/K]
C^*	Heat capacity rate ratio C_{min}/C_{max} [ ]
Cp	Specific heat capacity [kJ/kgK]
C_{RB}	Turbulent heat transfer geometry factor used in the Gentry method [ ]
c_T	Clearance between tubes along the transverse pitch (P_T) axis [m]
D	Diameter of bundle or shell or equivalent diameter [m]
DCA	Performance parameter measuring the drains cooler approach [K]
F	Friction factor [ ]
f	Proportion of steam flowrate utilised in each condensation sub-zone [ ]
G_s	Shell-side mass velocity [kg/m^2s]
g	Gravitational acceleration [9.81 m/s^2]
$\hbar$	Specific Enthalpy [kJ/kg]
H	Height of DC or DS [m]
h	average film heat transfer coefficient [$W/m^2 K$]
h_N	film heat transfer coefficient on tube N of the vertical column of the tube array [$W/m^2 K$]
h_x	local film heat transfer coefficient [$W/m^2 K$]
k	Thermal conductivity [W/mK]
L	Length [m]
$\dot{m}$	mass flow rate [kg/s]
n	Number of tube n_t [ ]
NTU	Number of transfer units C_{min}, UA/C_{min}
Nu	Nusselt number [ ]
P	Pressure [Pa or bar]
P_L	Longitudinal tube pitch [m]
Pr	Prandtl number [ ]
P_T	Transverse tube pitch [m]
Q	Heat transfer rate [MW]
R	Radius of shell or bundle [m]
r	Radius of tube [m]
Re	Reynolds number [ ]

R	Thermal resistance [K/W]
S	Entropy [kJ/kgK]
T	Temperature [K or ^{o}C]
t	Thickness of plane/plate [m]
TTD	Performance parameter measuring the terminal temperature difference [K]
U	overall heat transfer coefficient [W/m^2 K]
v	Fluid velocity [m/s]
W	Work done by turbine [MW]
X_{tt}	Lockhart-Martinelli parameter [ ]
x	steam quality [ ]

Greek symbols

Δ	Difference or deviation
δ	Condensate film thickness [m]
ε	effectiveness
μ	Dynamic viscosity [Pa.s]
θ	Angle [^{o}]
ρ	Density [kg/m^3]
ξ	Turbulent heat transfer correction using in the Gentry method or enhancement (Shiina)

Subscripts

Bi	Bundle ring inside diameter
Bo	Bundle ring outside diameter
b	baffle
bs	Baffle-to-shell or baffle-to-shroud
bt	Baffle-to-tube
bundle	Tube bundle
C	Cold streams or feedwater streams
ccf	Counter current flow
cf	Cross flow
DCpf	This the area through which water flows through a baffled DC
DCpf_freeflow	This the area through which water flows through an unbaffled DC
e	Equivalent e.g. tube diameter D_e
fi	Fouling layer on the inside of the tube
fo	Fouling layer on the outside of the tube
g	Vapour or gas
gr	Gravity controlled condensation

H	Streams: Hot stream, extraction steam or condensate streams
H	Area: Surface area calculated using the outer tube diameter
Hsat	Saturation conditions on the outside of the tube or on the shell side
in	Inside
id	Ideal
l	Liquid *or* Leakage, e.g. leak flow area A_l
lg	Liquid-vapour
M	Cascading stream
m	Mean or average
max	Maximum
min	Minimum
OTL	Outer tube limit
o	Outside
p	Projected
pf	Parallel flow
r	Rod
sh	Vapour shear controlled condensation
shell	Shell side
t	tubes
tDC	Tubes in DC
unit	This is the free flow area though a unbaffled unit cell
unitgrid	This is the free flow area though a baffled (grid baffle) unit cell
w	Tube wall

Acronyms and Abbreviations

COND	Condensing zone
*COND**C***	Condensing sub-zone responsible for latent heat transfer to tubes not passing through DC
*COND**C1***	The *COND**C*** minus the surface area in the last pass
*COND**C2o***	The *COND**C*** surface area in the last pass (*COND**C2*** **+** *COND**S***)
*COND**C2***	The *COND**C*** surface area in the last pass that only participates in condensation
*COND**R***	Condensing sub-zone responsible for latent heat transfer to tubes passing through DC
*COND**S***	COND sub-zone responsible for removing excess superheat from the steam exiting the DS
DC	Drains cooler or sub-cooling zone
DS	De-superheating zone
DWA	Dry wall approach
EdF	Électricité de France
EPPEI	Eskom Power Plant Engineering Institute

ESP	Egg-crate support plates or baffles
FWH	Feedwater heater
HEI	Heat Exchanger Institute, Inc.
HP	High pressure
IAPWS	International association for the properties of water and steam
LMTD	Log mean temperature difference
LP	Low pressure
MCR	Maximum continuous rating
seg	Segmented baffles
STHE	Shell and tube heat exchanger
TEMA	Tubular Exchanger Manufacturers Association, Inc.
PS	Power Station

1. Introduction

1.1 Background to the study

All Eskom thermal power stations are fitted with a series of shell and tube heat exchangers (STHE) on the feedwater pipe line routed between the condenser and the boiler. The STHE gradually increases the temperature of the feedwater flowing inside the tubes of these STHEs by condensing extraction steam on the outside of the tubes. This special type of condenser is called a single zone feedwater heater (FWH) and collectively improves the cycle efficiency of the thermal plant because less heat is discarded to the heat sink [1].

Tube failures may occur during the life of a FWH which will require tube plugging. This will result in a drop in heat transfer area and a consequential reduction in FWH performance. A drop in FWH performance will result in a drop in cycle efficiency if the plugging limit of the particular FWH is exceeded. There are several FWHs in the existing fleet that have experienced a drop in thermal performance. Several FWHs have been replaced already while some have been scheduled for replacement. Eskom is also increasing the capacity of the grid with the construction of two new thermal power stations, which also involves the installation of new FWHs.

Eskom deems it prudent to assess the performance of a new FWH during a technical tender evaluation. However, they do not have a software package that can perform the thermal analysis of a proposed FWH. Hence, a modelling tool was required that would enable Eskom to reasonably predict the performance of any FWH using the minimum design information supplied by the vendor.

1.2 Purpose of the study

The purpose and primary objective of this study was to develop a thermal model for FWHs that utilises the minimum number of inputs in order to generate thermal performance results. It is endeavoured that Eskom engineers will utilise this thermal model as one of their tools to evaluate a technical tender for new/replacement FWHs. A more detailed analysis of the design, with the aid of this tool, may reveal a thermal design oversight or deviation that would otherwise have been encountered later in the project. This oversight or deviation may translate to additional project cost and delays with project completion.

1.2.1 Problem to be investigated

The following questions or secondary objectives will be investigated and answered in this study:

- Identify applicable film heat transfer coefficient (*h*) correlations for thermal modelling of FWHs and review those applied to existing FWH thermal models in open literature.
- What internal zone definitions are needed to allow the model to properly capture the heater performance? This is specifically important for the condensing zone where most models assume saturated exit conditions from the de-superheater, though in practice this does not happen. The model needs to predict the performance based on the design input, and not assume any internal conditions.
- Do the results from case studies demonstrate the robustness of the model and is there acceptable agreement of the model results with vendor specifications on existing power stations?

1.3 Scope of study

The model should be more versatile in comparison with those observed in literature, as it should be able to analyse the full spectrum of heater types utilized within Eskom. The model should therefore incorporate the following FWH variations:

- **Type**: tube plate or header type
- **Orientation**: vertically or horizontally mounted
- **Zones**: condensing only; de-superheater added; short or long drains cooler added
- **Support type**: segmented or grid baffle type

The thermal model is an analytical heat exchanger computation that systematically tracks the heat transfer from the inlet to the exit of the FWH. The heater is divided into several systems or zones depending on the physical arrangement inside the heater and the associated system boundaries may be arbitrary or coincide with a physical boundary like the DC or DS shroud. The boundaries are subject to a geometric calculation that assumes that regions are symmetrically arranged within the FWH. The heat transfer is computed analytically across the particular zone. The overall heat transfer coefficient is assumed to be uniform in a particular zone.

Pressure drop is not incorporated in this model and hence it is referred to as a thermal model and not thermal hydraulic model. The pressure drop across the de-superheating zone determines the saturation temperature of this particular FWH [2]. Therefore, this assumption is a shortcoming of the thermal model proposed in this study but only when applied to a FWH fitted with a de-superheating zone. The performance parameters are only predicted under steady state 100% load

conditions. The liquid level in the FWH, where applicable, is assumed to be maintained at the desired level i.e. the DC completely flooded. The model assumes no fouling layer on either side of the tubes because the vendors do not disclose if this allowance was incorporated into the original design.

The name of the Eskom power station corresponding to the presented input data or results will not be released due to the sensitivity of the information. Instead, a coding system was developed within the research centre in order to identify a particular Eskom power station.

1.4 Plan of development

The theory that is applicable to FWHs is presented in Chapter 2. It commences with a motivation of the benefits of a FWH in the context of a regenerative Rankine cycle. The fundamental thermodynamic principles and basic design of FWHs is then described in more detail. The largest uncertainty in predicting the heat transfer in a FWH is associated with the selection of correlations that describe the boundary layer heat transfer coefficients. Hence, an in depth review of applicable correlations is described and discussed in terms of its application to the development of a FWH thermal model. The application of FWH models in literature is reviewed in Chapter 3 which was the basis for the development of the methodology which is described in Chapter 4. The application of the model and discussion of results is presented in Chapter 5. Chapter 6 discusses the usability of the model, shortfalls and recommendations for further work on the topic.

2. Theory

A FWH is a STHE that is installed on solar thermal, fossil and nuclear power stations for the primary purpose of improving the Rankine cycle efficiency. A consequence of this improvement is that less primary fuel (coal or nuclear fission) is required for sensible heat addition in the boiler [3] in order to increase the feedwater temperature to the saturation temperature in the boiler. The improvement in cycle efficiency must offset the costs associated with the manufacture, installation and maintenance of FWHs.

The hot stream enters the shell side of the STHE as steam, which is extracted from a particular stage of the turbine, and is allowed to condense over a series of tubes. The cold stream that flows inside the tubes of the STHE is called feedwater. Hence, these particular STHE are called feedwater heaters (FWH). The feedwater is conveyed from the condenser back to the boiler via several LP and HP FWHs. The pressure class of the FWHs are identified based on whether they are located before or after the boiler feed pump. The low pressure (LP) FWHs are located between the condenser and the boiler feed pump while the high pressure (HP) FWHs are located between the boiler feed pump and the steam generator or boiler.

The following topics will be discussed in this chapter:

- The regenerative Rankine cycle will be presented and the location of FWHs in this cycle will be identified.
- The fundamentals needed to analyse a basic STHE using thermodynamics and heat transfer theory is described. This includes a description of the various thermal resistances such as the convective heat transfer coefficient of the boundary layers (h) and tube conductivity (k).
- The heat transfer design analysis, whether using the LMDT or effectiveness-NTU method, is subject to the flow arrangement inside the zones that is determined by the physical design. The variation of design will determine which NTU relation and convective film heat transfer correlations (h) are applicable. Hence, a thorough review of FWH design variations will be introduced in this section. The type of FWH design is largely determined by cost and tube longevity considerations. The latter is primarily affected by frequent plant transients and operating conditions.
- Quantifying the resistances to heat transfer, notably h, is associated with the largest uncertainty in the heat transfer computation. Thus, the uncertainty associated with each correlation will also be presented.

2.1 Regenerative Rankine cycle

A power station is essentially a heat engine that converts thermal energy into mechanical energy. The most efficient heat engine operates within the bounds of a Carnot cycle. The purpose of a power station is to convert the thermal energy released by combustion or fission into mechanical energy. The mechanical energy, in the form of a rotating turbine rotor that in turn rotates the rotor of a generator, is finally converted into electrical energy. A diagram that depicts this simple closed loop process is illustrated in Figure 2-1. The working fluid is water and will be present in either the liquid phase, gas phase or both phases at a particular point in the cycle. Hence, this cycle is referred to as a water/steam cycle. The cycle is a closed loop because a condenser is utilised to condense the steam exiting the turbine in order that it may be pumped back to the evaporator/boiler or steam generator where saturated steam will be produced. This particular closed loop cycle is referred to as a Rankine cycle.

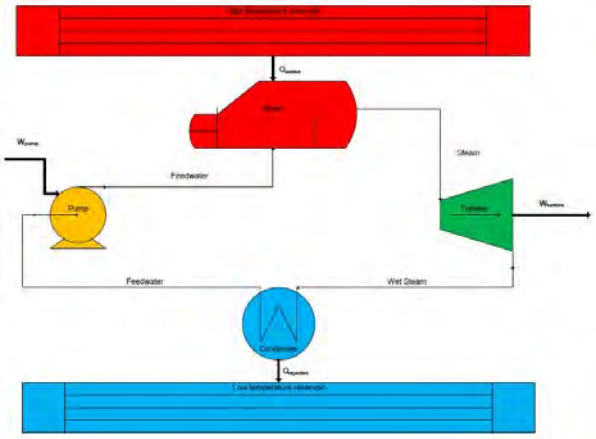

Figure 2-1. Illustration of a basic power generation cycle

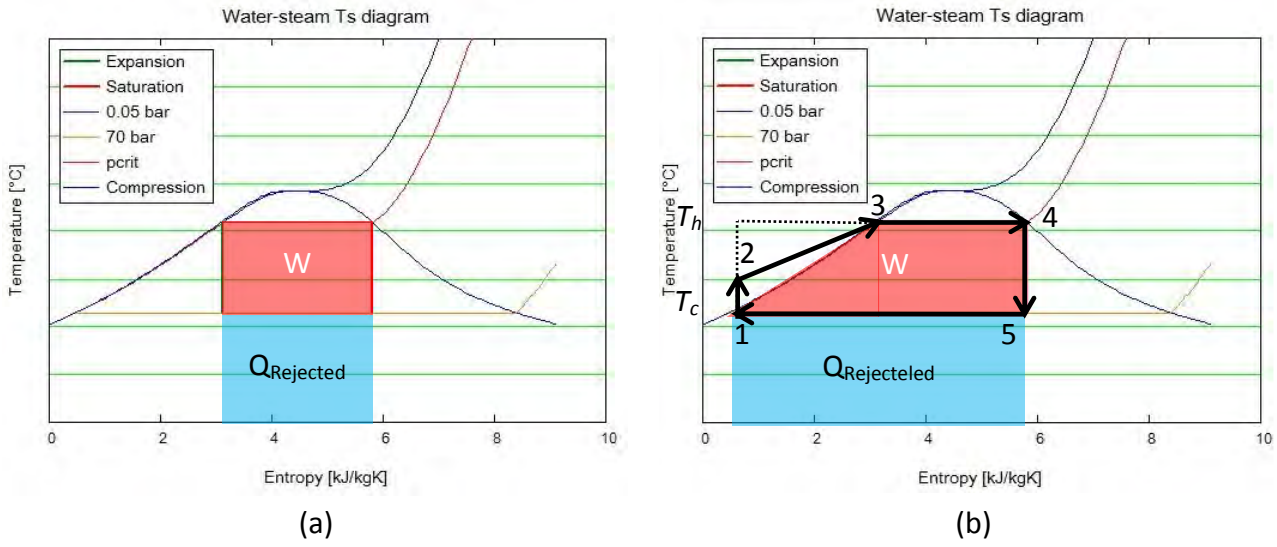

Figure 2-2. T-S diagram of a Carnot (a) and Rankine cycle (b) for a hypothetical power station

The T-S diagrams of a hypothetical power station, operating within the bounds of a Carnot and Rankine cycle, producing saturated steam at 70 bar and condensing the exhaust steam at 0.05 bar is illustrated in Figure 2-2(a) and Figure 2-2(b), respectively. The penalty associated with the Rankine cycle is illustrated in Figure 2-2(b). The Carnot cycle is only concerned with the maximum and minimum fluid temperature in the cycle and does not concern itself with fluid phase limitations imposed by the vapour dome in T-S diagrams or irreversibilities in the process.

The sum of the two rectangular areas on a T-S diagram represents the total heat transferred (Q). The area enclosed by the bottom rectangle represents the heat rejected ($Q_{Rejected}$). The difference represents the work done (W) by the turbine, assuming the work required by the pump is negligible. The ratio of W to Q, visualised in Figure 2-2(a), represents the Carnot cycle efficiency. The efficiency of the Rankine cycle, which is more representative of a plant process, is less than that of the Carnot cycle because of the limitation imposed by the liquid saturation line.

The Carnot efficiency for a typical fossil station operating between 230 bar and 0.05 bar is about 54% and for a typical nuclear station operating within the bounds of Figure 2-2(b) is about 44% [4]. The larger efficiency is attributed to the fact that fossil stations generate superheated steam while nuclear stations are designed to only produce saturated steam. However, the typical Rankine cycle efficiency may be less than 40%. The efficiency may be improved by reducing the $Q_{Rejected}$, which is achieved by installing FWHs in the cycle.

A series of FWHs, located between the condenser and evaporator, systematically increases the temperature of the feedwater before it enters the evaporator. This thermodynamic cycle is referred to as a regenerative Rankine cycle. A basic loop for a fossil station is illustrated in Figure 2-3. On a nuclear power station thermal energy released from fission is transferred from the reactor coolant system (primary loop) to the steam system (secondary loop) via the steam generator, the basic loop for a nuclear station is illustrated in Figure 2-4.

The feedwater temperature is systematically increased as it is conveyed from the condenser back to the boiler via several LP and HP FWHs. In a regenerative Rankine cycle, feedwater enters the furnace slightly below the saturation temperature. Heating steam that would have passed through the turbine is utilised as the feedwater heating source. This would imply that the work done by the turbine would have been reduced. However, also note that less heat is now required in the boiler. There is a limit to the improvement in cycle efficiency with the addition of FWHs due to their consumption of steam that would otherwise have passed through the turbine. The fuels consumed for primary heat addition in the boiler will also reduce as less heat is required for sensible heat transfer in the boiler.

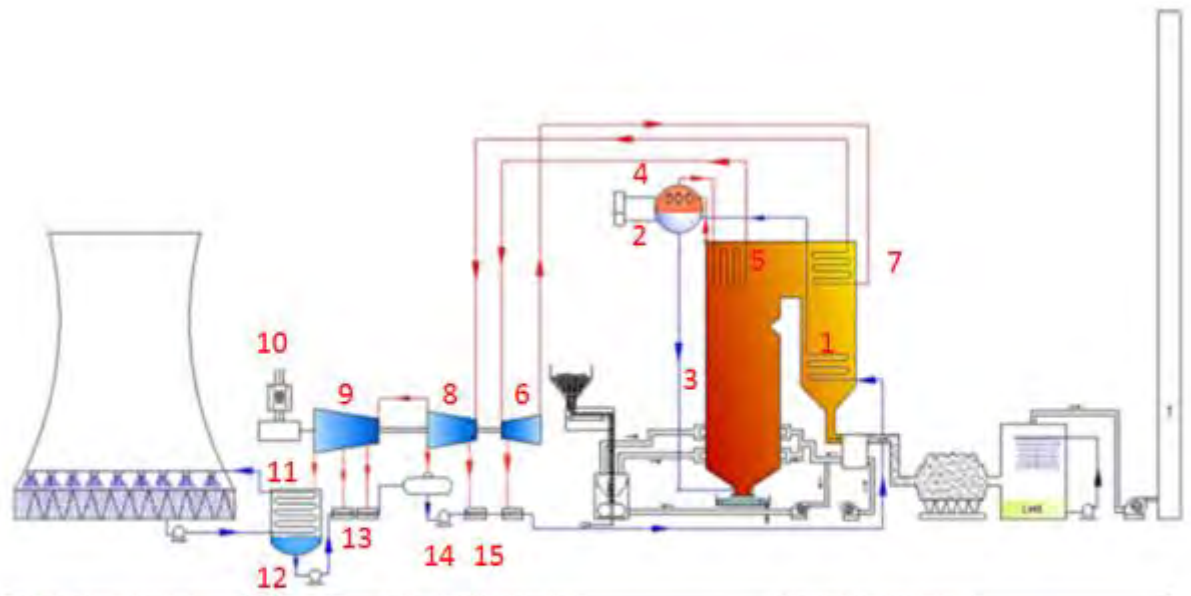

1 – Economiser	6 – HP Turbine	11 – Condenser
2 – Drum Boiler Condensate	7 – Re-heater	12 – Condensate Pump
3 – Evaporator (Furnace Walls)	8 – IP Turbine	**13 – LP Feedwater Heaters**
4 – Drum Boiler	9 – LP Turbine	14 – Boiler Feed Pump
5 – Super-heater	10 – Generator	**15 – HP Feedwater Heaters**

Figure 2-3. Schematic of a typical fossil power station [5]

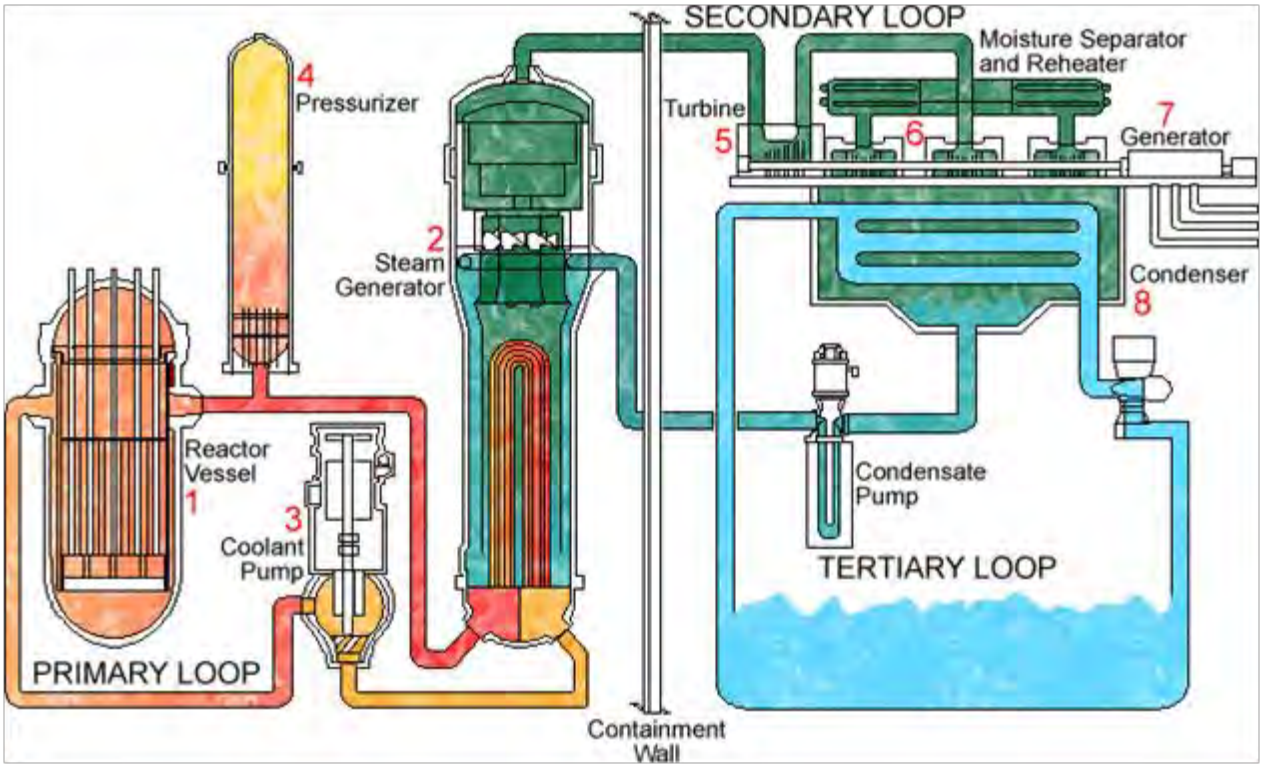

Figure 2-4. Schematic of a PWR nuclear power station [6]

2.2 Fundamentals of heat transfer

A FWH transfers heat (Q) from a hot stream initially at a temperature (T_{H1}) to a cold stream initially at a temperature (T_{C1}), which is illustrated in Figure 2-5. This may be achieved by mixing the streams in a vessel. This vessel is identified as a contact or open heat exchanger [3] and is called a de-arator. FWHs achieve heat transfer between the hot and cold streams across a tube wall and this type of heat exchanger is referred to as a closed heat exchanger, or shell and tube heat exchanger. The construction of a basic thermodynamic model for a closed heat exchanger is the topic of this section, which is illustrated in Figure 2-5.

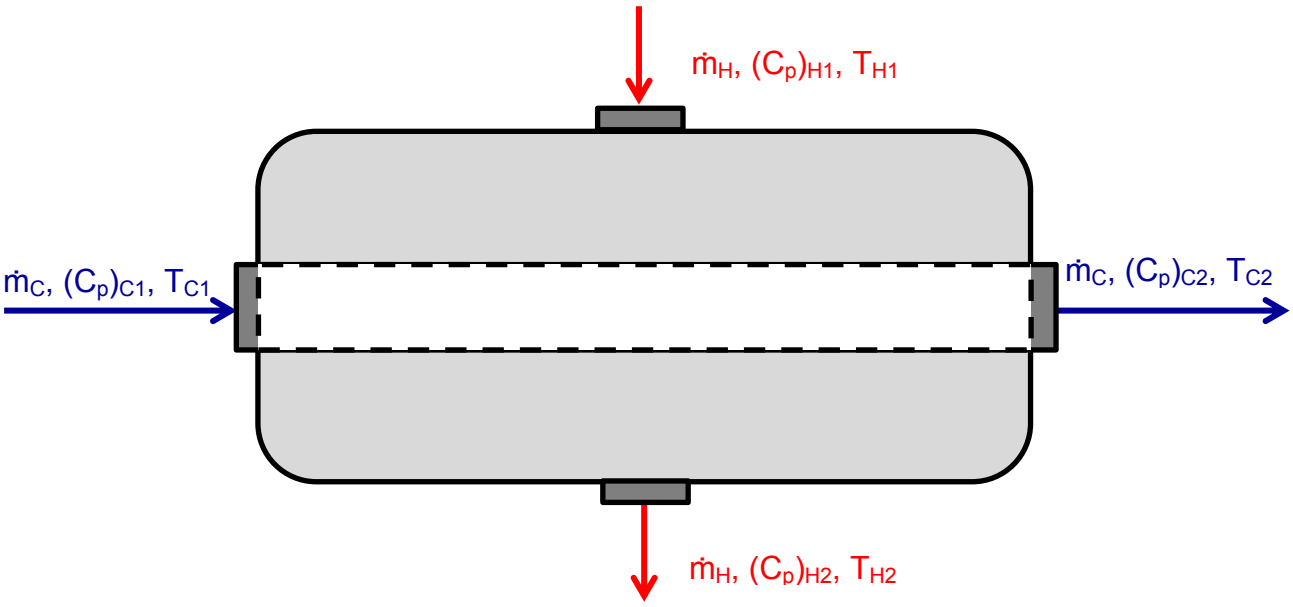

Figure 2-5. Schematic of a basic heat exchanger

2.2.1 Thermodynamics

In this particular example of a heat exchanger illustrated in Figure 2-5, the continuity equations are defined in Equations (2.1) and (2.2), where $\dot{m}$ is the mass flow rate:

$$\dot{m}_{C1} = \dot{m}_{C2} \tag{2.1}$$

$$\dot{m}_{H1} = \dot{m}_{H2} \tag{2.2}$$

The first law of thermodynamics, for an open system under steady state, steady flow conditions, with negligible kinetic and potential energy can be written as:

$$Q = \dot{m}\left(\hbar_2 - \hbar_1\right) \tag{2.3}$$

where $\hbar$ is the specific enthalpy of the stream entering (1) and exiting (2) the system. The symbol $\hbar$ should not be confused with the convective film heat transfer coefficient defined as h and Q is the heat transfer rate to the particular fluid stream.

If the STHE was assumed to be very well insulated then the heat transferred from the hot fluid to the cold fluid would equate, see Equation (2.4):

$$Q = \dot{m}_C\left(\hbar_{C2} - \hbar_{C1}\right) = -\dot{m}_H\left(\hbar_{H2} - \hbar_{H1}\right) = \dot{m}_H\left(\hbar_{H1} - \hbar_{H2}\right) \tag{2.4}$$

where the subscripts H and C refer to the hot and cold fluids, respectively.

If the fluids do not undergo a phase change and have constant specific heat capacities over the particular temperature range then Equation (2.4) may be written as:

$$Q = \left(\dot{m}C_p\right)_C\left(T_{C2} - T_{C1}\right) = \left(\dot{m}C_p\right)_H\left(T_{H1} - T_{H2}\right) \tag{2.5}$$

where the grouping of ($\dot{m}C_p$) is referred to as the heat capacity rate or abbreviated as C.

$$Q = C_C\left(T_{C2} - T_{C1}\right) = C_H\left(T_{H1} - T_{H2}\right) \tag{2.6}$$

2.2.2 Heat transfer

The heat that is transferred may be achieved using different internal configurations and tube material specifications. However, some equipment configuration may not be optimum and may require a larger surface area to achieve the desired heat transfer. This size or tube surface area (A) of the STHE is calculated from heat transfer theory which accounts for the various thermal resistances including geometry, flow configuration and material specification.

Heat transfer theory relates the required heat transfer duty to the thermal resistances, heat transfer surface area and the temperature driving force. The temperature driving force, with reference to an incremental heat transfer area (dA), is described as the temperature difference between the hot and cold fluids ($\Delta T = T_H - T_C$) and is illustrated in Figure 2-6. However, this difference may vary along the length of the heat exchanger, which makes it convenient to formulate a mean or equivalent temperature difference between the fluids (ΔT_m).

The heat transfer rate between two counter current fluid stream across a tube wall may be determined from the following equation:

$$Q = UA\Delta T_{LMTD} \tag{2.7}$$

where *U* is the average overall heat transfer coefficient based on the external heat transfer area (A). The ΔT_{LMTD} is defined in Equation (2.8).

$$\Delta T_m = \left(\Delta T_m\right)_{ccf} = \Delta T_{LMTD} = \frac{\left(T_{H1} - T_{C2}\right) - \left(T_{H2} - T_{C1}\right)}{\ln\left(\frac{T_{H1} - T_{C2}}{T_{H2} - T_{C1}}\right)} \tag{2.8}$$

The classical flow arrangement analysed in open literature is counter current flow and is illustrated in Figure 2-6.

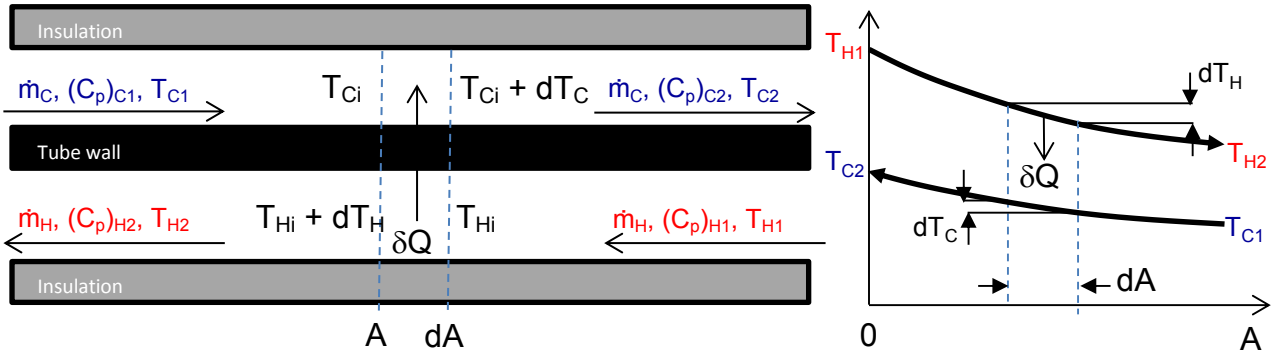

Figure 2-6. Assignment of thermal parameters and the associated temperature profiles for hot and cold streams for a two-fluid heat exchanger

where the subscript *ccf* implies counter current flow.

In a FWH, heat transfer occurs across a partition or tube that separates the two fluid streams. The average overall heat transfer coefficient, *U*, comprises of the thermal resistance of the tube, the thermal resistance of the boundary layer on the outside of the tube and the thermal resistance of the boundary layer on the inside of the tube. Thermal resistances such as fouling will not be analysed in this study. Fins are often machined on the tube surface to improve heat transfer but this practice is not adopted with FWHs and will therefore not be reviewed.

Tube thermal conductivity (*k*)

The HP FWHs are typically fitted with carbon steel tubes while the LP FWHs are typically fitted with stainless tubes. The conductivity of tube material used in the Eskom fleet is listed in Table 2-1. The thermal resistance due to the tube conductivity (*1/k*) is low in comparison to the boundary layer thermal resistance in single phase heat transfer applications. However, this is not necessarily the case in the condensing region. This makes a FWH design sensitive to tube material selection as alternating the tube material between these two options can reduce the heat transfer by almost 10%, using the HP6 FWH from station PS00 as a case study.

Table 2-1 Conductivity values of tubes used in the construction of FWHs [7]

Metal	Thermal conductivity *k*(100°C) [W/mK]	FWH pressure class
St35.8/1.0305	57	HP
A42/1.0425	50	
15Mo3	50	
15Mo6	50	
304L/1.4306	17	LP
S347/1.4550	17	

Outer and inner boundary layer convective heat transfer coefficients (*h*)

The two remaining resistances to heat transfer across a tube is the thermal resistance imposed by the thermal boundary layer of the fluids on either side of the tube, see Figure 2-7. These two resistances are typically more dominant than the conductive resistance of the tube except in a scenario where a two phase boundary layer (condensation) is present. The bulk temperature of the two fluids is T_H and T_C. The fluid on the shell side may be in the gas phase and therefore exhibits a larger thermal resistance to heat transfer compared to the resistance that would be exhibited by the fluid if it was in the saturated gas or liquid phase. The measure of the film boundary layer resistance is denoted as *R*, where the subscript will denote the outer or inner thermal boundary layer. *R* for the thermal boundary layer is defined as the reciprocal of the product of the film heat transfer coefficient *h* and the associated heat transfer area *A* in Equation (2.9).

$$R = \frac{1}{hA} \tag{2.9}$$

It can be concluded from Equation (2.9) that a larger *h* will result in a lower thermal resistance. A FWH may have water present in 1 or 2 fluid phases on the shell side, which implies that the external boundary layer may vary considerably along the length of the tube. However, the water on the inside of the tube remains in the liquid phase.

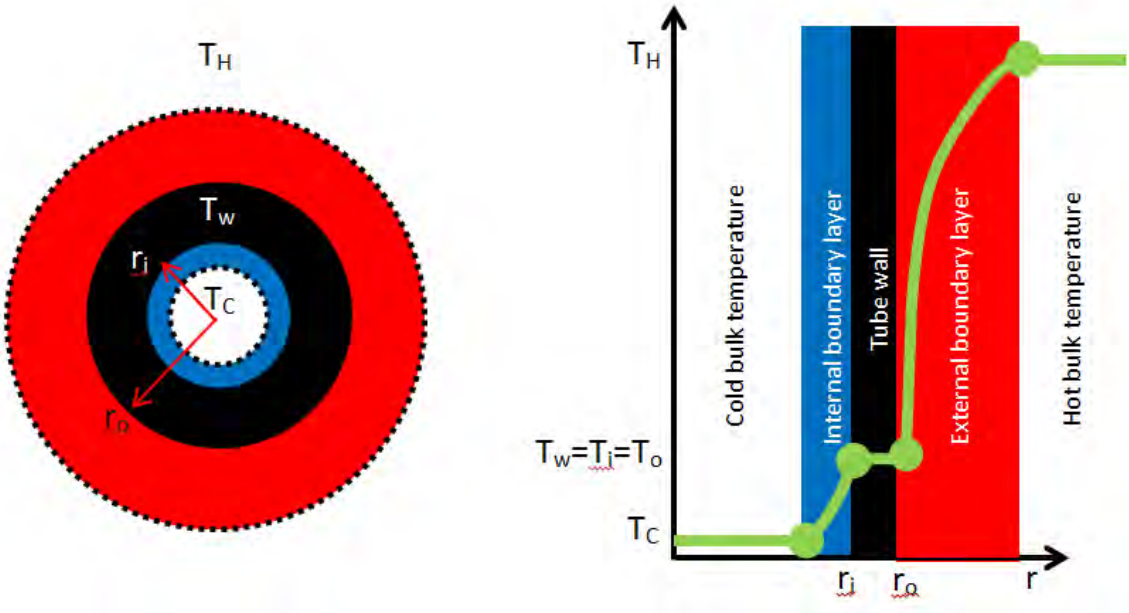

Figure 2-7. Radial temperature profile across a single tube of a heat exchanger

Table 2-2 Order of magnitude film heat transfer coefficients [8]

Fluid	***h* [W/m^{2}K]**
Gases (natural convection)	3 – 25
Gases	50 - 1000
Flowing liquids inside tubes	100 – 10 000
Condensation – Vertical tubes	4000 – 11 000
Condensation – Horizontal tubes	9000 – 25 000

Order of magnitude values for *h* are presented in Table 2-2 and it is notable that the largest value *h* occurs during condensation. The overall heat transfer coefficient (*U*) for a single smooth and clean plane wall is formulated as follows:

$$\mathrm{UA} = \frac{1}{R} = \frac{1}{\frac{1}{h_{in}A} + \frac{t}{kA} + \frac{1}{h_o A}} \tag{2.10}$$

where R is the total thermal resistance to heat transfer across the contact area between the flowing fluids on either side of the tube. The thickness of the plane is denoted as t, the film heat transfer coefficient of the boundary layer for the inside and outside tube flows is denoted as h_{in} and h_o, respectively.

The equation is then applied to a clean (no fouling on tubes) un-finned tube and is presented as Equation (2.11). In this study the no fouling U_o is used and is calculated relative to the outside surface area (A_o). The equation is expanded further and presented as Equation (2.12):

$$\mathrm{U}_o\mathrm{A}_o = \mathrm{U}_{in}\mathrm{A}_{in} = \frac{1}{R} = \frac{1}{\frac{1}{h_{in}A_{in}} + R_w + \frac{1}{h_o A_o}} \tag{2.11}$$

$$\mathrm{U}_o = \frac{1}{\frac{r_o}{h_{in}r_{in}} + \frac{r_o \ln\left(\frac{r_o}{r_{in}}\right)}{2\pi k} + \frac{1}{h_o}} \tag{2.12}$$

A designer may also include up to two additional thermal resistance layers. The accumulation of fouling layers on either side of the tube is a consideration on a Heat Exchanger Institute (HEI) standard specification sheet [9]. The inclusion of these two thermal resistances requires additional heat transfer area to meet the Q originally calculated with no fouling. The U_o relation for fouled tubes is formulated as follows:

$$\mathrm{U}_o = \frac{1}{\frac{r_o}{h_{in}r_{in}} + \frac{r_o}{r_{in}}R_{fin} + \frac{r_o \ln\left(\frac{r_o}{r_{in}}\right)}{2\pi kL} + R_{fo} + \frac{1}{h_o}} \tag{2.13}$$

where R_{fin} and R_{fo} are the inside and outside fouling factors, respectively (m^2K/W). The HEI standard recommends a R_{fin} and R_{fo} of $3.5\text{x}10^{-5}$ m^2K/W and $5.3\text{x}10^{-5}$ m^2K/W but this may vary depending on the client's specifications. However, the effect of following is not considered and no Eskom FWH specification sheet, reviewed in this study, reported a fouling factor consideration.

2.3 Heat transfer design analysis

There are essentially two basic methods for analysing a heat exchanger. The first method uses the mean or equivalent temperature difference (Equation (2.7)), which requires all the terminal temperatures to be known. The ΔT_m is replaced with ΔT_{LMTD} for the counter current flow arrangement. This method is referred to as the LMTD method and is preferred when sizing a heat exchanger i.e. when computing the surface area of the heat exchanger (*A*).

The second method is called the effectiveness - number of transfer units (ε-NTU) method. This method was developed by Nusselt [10] in order to eliminate the iterative steps associated with the LMTD method when only the inlet stream temperatures and *A* are known. Hence, the ε-NTU method only requires the inlet stream temperatures to calculate the *Q*. This method is preferred when comparing the calculated exit temperatures to the actual exit temperatures. This approach is called a performance or rating evaluation of an existing STHE. The NTU method defines the exit temperatures in terms of known variables only. This derivation can be reviewed in several heat transfer books but suffice to say that the derivation requires the formulation of a unitless measure of heat transfer area called the number of transfer units or NTU. NTU comprises of three parameters namely U_o, A_o and C_{min}, which is presented in Equation (2.14).

$$NTU = \frac{U_o A_o}{C_{\min}} \tag{2.14}$$

Capacity rate is defined as the product of *Cp* and $\dot{m}$. There are two capacity rates for a two-stream heat exchanger i.e. $C_H = Cp_H \cdot \dot{m}_H$ and $C_C = Cp_H \cdot \dot{m}_H$, where C_{min} is the minimum of the two capacity rates.

2.3.1 LMTD Method

The heat transfer for an ideal two stream counter current heat exchanger can be calculated using Equation (2.15). However, the heat transfer regions in a FWH are not ideal counter current two-stream heat exchangers. The STHE and may have a combination of counter current flow and cross flow regions, with multiple passes. Equation (2.15) must be adapted with a correction factor in order to accurately predict the heat transfer for the particular STHE.

$$\mathrm{Q} = \mathrm{U}_o \mathrm{A}_o \Delta T_{LMTD} = \mathrm{U}_o \mathrm{A}_o \frac{\left(T_{H1} - T_{C2}\right) - \left(T_{H2} - T_{C1}\right)}{\ln\left(\frac{T_{H1} - T_{C2}}{T_{H2} - T_{C1}}\right)} \tag{2.15}$$

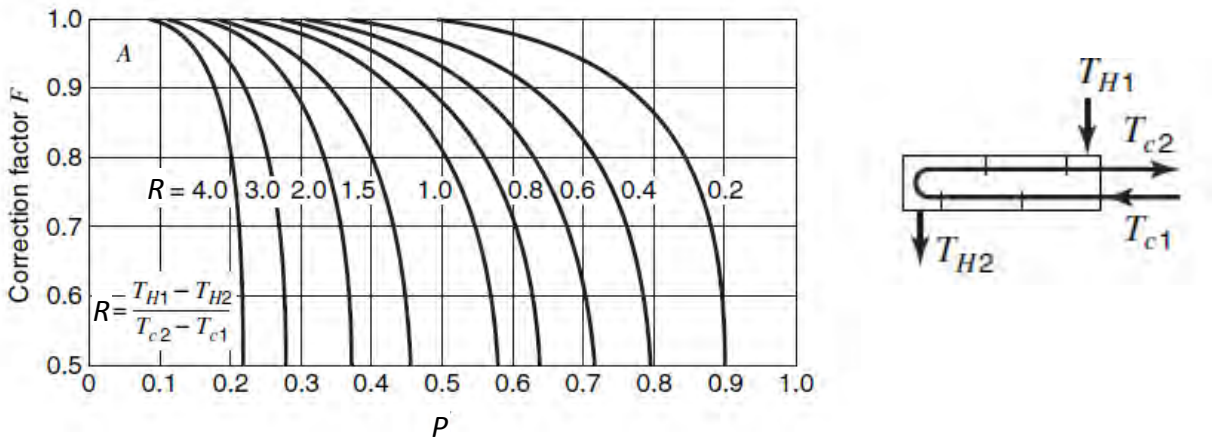

Figure 2-8. Correction chart for a heat exchanger with one shell pass and multiple tube passes[10]

The correction factor *F* is used to adjust the ideal counter current result to suit the actual flow arrangement. The correction factor is less than 1 for cross flow and multipass arrangements and is a function of three parameters as defined in Equation (2.17).

$$F = f(\text{P,R,arrangement}) \tag{2.16}$$

$$\text{Q} = F\text{U}_o\text{A}_o\Delta T_{LMTD} = F\text{U}_o\text{A}_o \frac{\left(T_{H1} - T_{C2}\right) - \left(T_{H2} - T_{C1}\right)}{\ln\left(\frac{T_{H1} - T_{C2}}{T_{H2} - T_{C1}}\right)} \tag{2.17}$$

The type of flow arrangement must be known in order to select the applicable chart from the TEMA standard [11] or any other reference material. The remaining two parameters are then used to intercept the *F* value off the chart.

A correction chart is illustrated in Figure 2-8 for a baffled STHE with one shell pass and 2 tube pass arrangement. There will be no further discussion of the LMTD method since the ε-NTU method was used in this study because it is the favoured method for rating of STHE.

2.3.2 ε-NTU Method

The effectiveness-NTU or ε-NTU method compares the actual heat transfer to the maximum possible heat transfer. The ratio of these two values is termed the effectiveness (ε) of the STHE and is defined in Equation (2.18). The maximum temperature difference would correspond to the difference of the two inlet stream temperatures. The *C* associated with this maximum temperature difference will be the stream with the smallest *C* value or called C_{min}.

$$\varepsilon = \frac{\left|C_H\left(T_{H1}-T_{H2}\right)\right|}{C_{\min}\left(T_{H1}-T_{C1}\right)} = \frac{\left|C_C\left(T_{C1}-T_{C2}\right)\right|}{C_{\min}\left(T_{H1}-T_{C1}\right)} = \frac{Q}{C_{\min}\left(T_{H1}-T_{C1}\right)} \tag{2.18}$$

where C is the capacity rate, the subscript identifies the hot or cold stream and C_{min} is smallest value of the two capacity rates.

Nusselt defined the capacity rate ratio C^* and NTU parameters, that were substituted into the equations derived from the LMTD method in order to compute ε. The ε is therefore a function of C^*, NTU and the flow arrangement as defined below:

$$\varepsilon = f\left(\left\lfloor C^* = \frac{C_{\min}}{C_{\max}}\right\rfloor, NTU, \text{arrangement}\right) \tag{2.19}$$

The exit temperatures in the numerator of Equation (2.18) may be solved if ε is computed and substituted into the equation. Only the ε relations applicable for the flow arrangements found in the Eskom FWH are presented. The architecture of the various regions or zones inside a FWH will be presented in detail in Section 3.1 suffice to say that there may be a maximum number of 3 flow arrangements in a FWH.

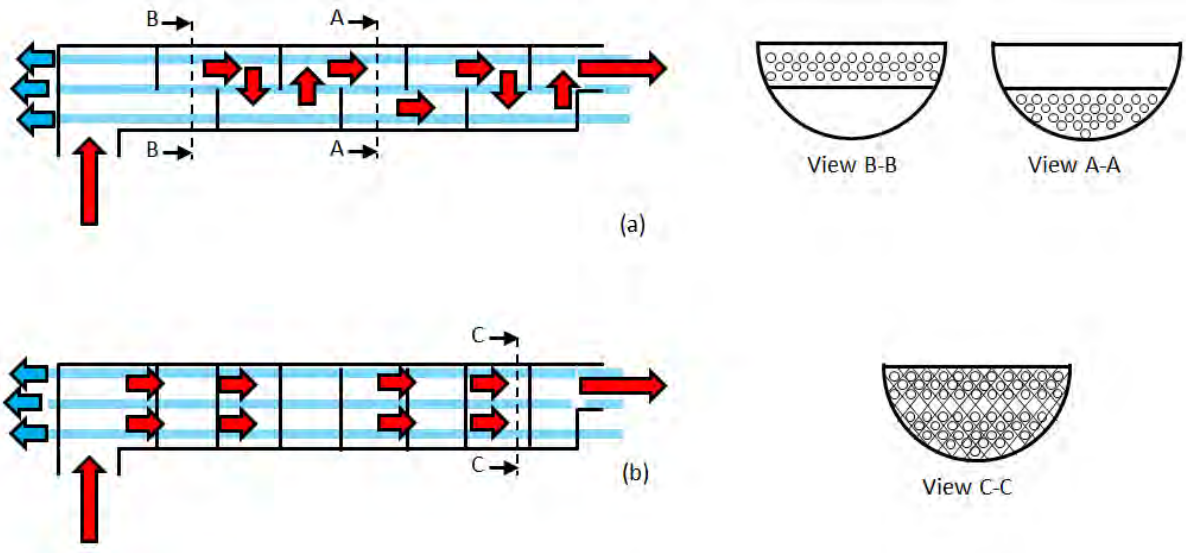

Figure 2-9. Shell side flow arrangement through a STHE installed with (a) segmented baffles resulting in cross and counter current flow or (b) grid tube supports resulting in counter current flow only

The fluid on the shell side may flow across the tubes, in a counter current direction or a combination of both. The latter two flow arrangements are depicted in Figure 2-9. The fluid also remains in one phase, on either side of the tube, for these flow arrangements. The cross and counter current flow arrangement is illustrated in Figure 2-9(a), which is experienced if segmented

baffles are installed to support the tubes. In this particular type of STHE, the addition of baffles forces the fluid to flow through narrow windows, thereby increasing the fluid velocity. Only counter current flow will be experienced if a grid type baffle support is used, see Figure 2-9(b). The ε relation applicable for these flow arrangements is presented in Table 2-3.

Table 2-3 Effectiveness relation for STHE fitted with segmented or grid baffles [8]

Tube support	Flow arrangement	ε relation	Equation
Segmented	Cross and counter current	$\varepsilon = \frac{1-e^{(C^*-1)NTU}}{1-C^*e^{(C^*-1)NTU}}$	(2.20)
Grid	Counter current		

In Figure 2-9 the fluid on both the shell and tube side flows once through the STHE, this is referred to as a single tube and shell pass. However, the literature applies these relations to a two pass STHE. Thulukkanam [12] states that ε can be assumed to be 1 for a single tube pass STHE where there are more than 5 segmented baffles otherwise Equation (2.20) may be used to calculate ε. The flow arrangement for the grid supports will also be modelled as a counter current STHE. Therefore, the ε relation for both a segmented baffle and grid baffle STHE will be identical.

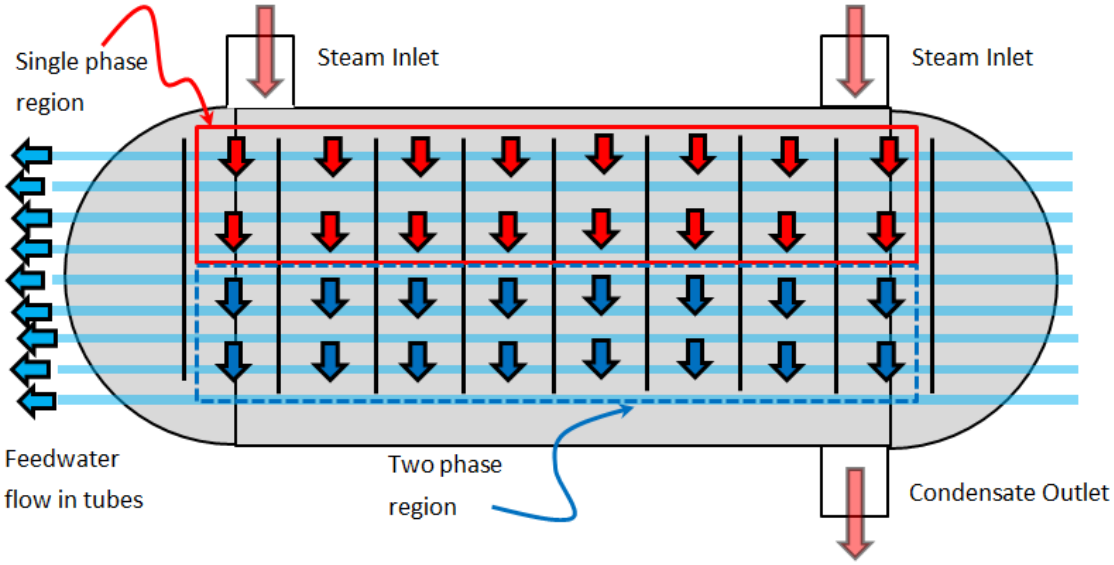

Figure 2-10. Shell side flow arrangement through a STHE where there (a) single phase cross flow and (b) two phase cross flow

The third type of flow arrangement is where a fluid flows in a cross flow manner only and does not undergo a phase change. The effectiveness ε relation for a cross flow heat exchanger, with no phase change, depends on whether C_{max} occurs on the tube side (unmixed) or on the shell side (mixed). In general the *Cp* is larger for the liquid compared to the steam. The mass flowrate of the feedwater ($\dot{m}_C$) is always larger than that of the extraction steam ($\dot{m}_H$), which would allow a

general prediction of C_{min} (Equation (2.21)) to be defined as being C_C. However, $\dot{m}_C$ may be distributed between a single phase region and a two phase region which make a general prediction of C_{max} and C_{min} difficult, see Figure 2-10. Hence, the capacity rate must be calculated before the ε relation (Equation (2.22) or Equation (2.23)) can be assigned for a single phase cross flow arrangement.

$$Cp_C\dot{m}_C > Cp_H\dot{m}_H \tag{2.21}$$

The table below shows the various ε relations for pure cross flow. The zone defined as COND**S** is where the entering steam is still superheated, even after passing through a de-superheating zone, and as is treated as an additional de-superheating zone. This de-superheating zone is treated as a single phase heat transfer zone with cross flow only. It is possible for condensation to occur while the steam is superheated, however, this is not modelled in this study. The region where the steam starts condensing, hence becomes two phase, is called the condensing zone (COND) that may be subdivided further into sub-zones (COND**R** and COND**C**), which will be explained later. The inlet and exit shell temperatures of this region does not change because it remains at saturated conditions.

Table 2-4 Tube support arrangement in condensing zone with the applicable ε relation [8]

Sub-zone	**Fluid**	**ε relation**	**Equation**
COND**S**	$Cp_C\dot{m}_C > Cp_H\dot{m}_H$	$1-e^{\left(\frac{1-e^{\left[-C^*NTU\right]}}{-C^*}\right)}$	(2.22)
	$Cp_C\dot{m}_C < Cp_H\dot{m}_H$	$\frac{1}{C*}\left(1-e^{-C^*\left(1-e^{-NTU}\right)}\right)$	(2.23)
COND**C**	Removing latent heat	$1-e^{-NTU}$	(2.24)
COND**R**			

An energy balance of the shell side in the COND zone will reveal that no sensible heat is transferred during the phase change i.e. C_H cannot be used to quantify the energy transfer. However, the NTU method still requires a comparison of the capacity rates and hence Equation (2.25) is formulated to derive a fictitious value for C_H, which is computed to be $C_H = \infty$. The capacity rate ratio will therefore be $C^* = 0$ and the result of the derivation using this special case is presented as Equation (2.24) in Table 2-4.

$$C_H = \frac{Q}{\left(T_{Hsat} - T_{Hsat}\right)} = \infty \tag{2.25}$$

2.4 Thermal boundary layer theory

A review of the film heat transfer correlations applicable to the resistance to heat transfer across the boundary layer is presented in this section. In a FWH, heat transfer may occur across a single phase or two phase boundary layer. There are several single phase regions in the FWH such as:

- **Entire tube-side:** Feedwater remains in the liquid phase inside the tubes
- **De-superheater (DS) shell side:** Bled steam remains in the steam phase
- **Drains cooler (DC) shell side:** Condensed steam remains in the liquid phase
- **Excess superheat removal:** Excess superheat is removed in this single phase cross flow STHE

Two phase heat transfer occurs in the condensing zone, where steam condenses in a thin liquid film on the outer surface of the tubes.

2.4.1 Critical dimensionless parameter for forced convection

The most important dimensionless number associated with heat transfer in FWHs is the Prandtl (*Pr*) number, Reynolds (*Re*) number and Nusselt (*Nu*) number. The *Pr* number compares the rate at which the velocity profile changes to the rate at which the temperature profile changes. The *Pr* number is computed using Equation (2.26) where μ is the fluid dynamic viscosity, ρ is the density of the fluid, *k* is the fluid thermal conductivity and *Cp* is the specific heat capacity of the fluid at a particular temperature and pressure. It can be considered a dimensionless fluid property, as it is independent of the flow characteristics.

$$\mathrm{Pr} = \frac{\mu / \rho}{\mathrm{k}/ \rho \mathrm{Cp}} = \frac{\mu}{\mathrm{k}/ \mathrm{Cp}} \tag{2.26}$$

The Reynolds (*Re*) number is computed using Equation (2.27) where *v* is the fluid velocity and d_o is a characteristic length particular to the geometry, e.g. the pipe diameter. It should be noted that the shell side *v* is the most challenging parameter to calculate because the free flow area on the shell side may vary and an equivalent pipe diameter (D_e) is used. The *Re* number is an indication of the flow regime, of which turbulent flow is the most common in industrial FWHs.

$$\mathrm{Re} = \frac{\rho v d_o}{\mu} = \frac{\rho v D_e}{\mu} \tag{2.27}$$

The selection of the applicable correlations for computing the film heat transfer coefficient *h* is dependent on the flow regime. Only correlations applicable to turbulent flow regimes will be

considered in this study. The exact definition of the fluid velocity and characteristic length applicable to the *Re* number formulation depends on the correlation selected.

The third dimensionless number used in this study is established when performing an energy balance on the boundary layer. Note that the fluid velocity at the tube wall is zero, which conveniently permits the heat transfer to be modelled as conduction. In the energy balance the heat transfer by conduction is equated to the heat transfer by convection, see Equation (2.28). The Nusselt (*Nu*) number is established with some rearranging, see Equation (2.29). Here, the subscript *x* is identifying a specific length along the pipe while *y* is identified as the distance normal to the wall. The local film heat transfer coefficient is identified as h, d_o is identified as the pipe diameter, the fluid temperature at the wall is taken as the tube wall temperature T_w and the bulk fluid temperature is T_b.

$$\frac{\delta Q}{dA} = h\left(T_w - T_b\right)_x = -k\left(\frac{dT}{dy}\right)_x \tag{2.28}$$

$$Nu = \frac{hd_o}{k} = d_o\left(\frac{dT}{dy}\right)_x \Big/ \left(T_b - T_w\right)_x \tag{2.29}$$

The right hand side of Equation (2.29) indicates that only the temperature profile must be known to solve for the local *h*. The right hand side of this equation is solved using dimensional analysis and corrected with results from empirical studies.

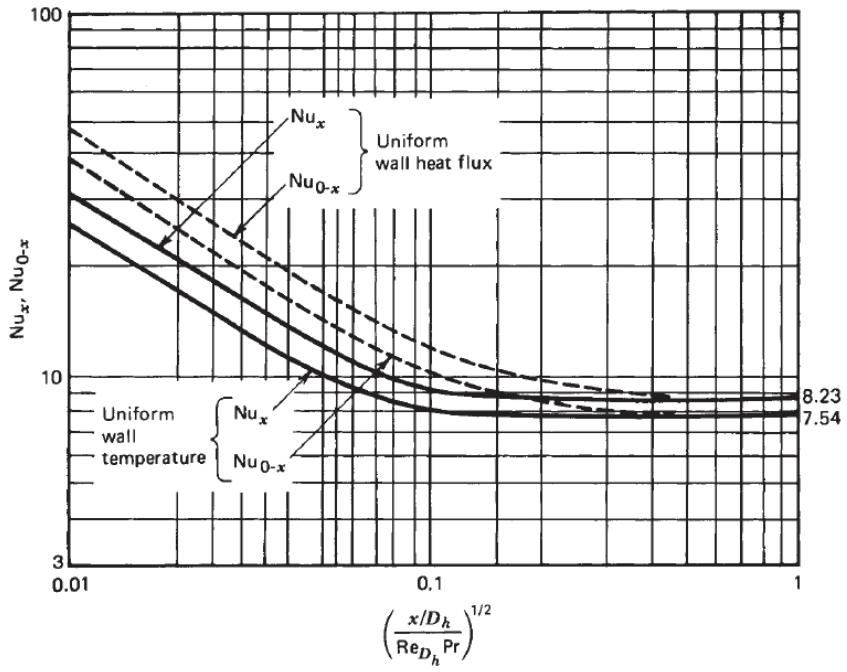

Figure 2-11. Plot of Nu number vs length from entrance region until fully developed flow is achieved [13]

The *Nu* number is assumed to be uniform along a pipe length after fully developed flow is achieved. The magnitude of the *Nu* number is considerably larger by almost a factor of two at the entrance region and along the developing thermal boundary region in comparison to the fully developed thermal boundary region (Figure 2-11). Hence, heat transfer can be improved if the fluid flows through a sequence of obstructions which breaks up the developed boundary layer. This is achieved in a FWH by using a set sequence of grids or rod baffles. The obstructions cause vortex shedding, which increases the turbulence in the boundary layer and thus further enhances the heat transfer [14].

A single fluid stream will typically have an inlet and outlet with the fluid temperature and pressure varying between these two points. Analytical heat transfer computation and numerical computation will require a single temperature and pressure input in order to calculate the fluid properties needed to compute the dimensionless parameters. Developers of heat transfer correlations have either used average bulk fluid temperature (Equation (2.30)) or an average film temperature (Equation (2.31)). The average bulk temperature is preferred in this study as the wall temperature is seldom a known value.

$$T_{bulk} = \frac{T_{in} + T_{outlet}}{2} \tag{2.30}$$

$$T_{film} = \frac{T_{wall} + T_{bulk}}{2} \tag{2.31}$$

2.4.2 Dimensional analysis and film heat transfer coefficient (*h*)

In 1909 Nusselt applied dimensional analysis and obtained a general equation for turbulent flow in pipes that describes the right hand side of Equation (2.29)[15]:

$$Nu = \frac{h_x D}{k} = f\left(\frac{Dv\rho}{\mu}, \frac{\mu}{k/Cp}, \frac{L}{D}\right) \tag{2.32}$$

The right hand side of Equation (2.32) states that the *Nu* number is a function of three grouped parameters and can be rewritten as a power function, where *a*, *n*, *m* and *e* are constants (Equation (2.33)):

$$Nu = \frac{h_x D}{k} = a\left(\frac{Dv\rho}{\mu}\right)^n \left(\frac{\mu}{k/Cp}\right)^m \left(\frac{L}{D}\right)^e \tag{2.33}$$

McAdams [15] reported that data collected during the early development of heat transfer theory, from experiments conducted with air and liquid water, validated that these 8 factors had some

effect in estimating the *Nu* number. Re-writing the parameters with their assigned grouped name reveals Equation (2.34). The (L/D) term tries to address the effect of flow development.

$$Nu = \frac{h_x D}{k} = a\mathrm{Re}^n \mathrm{Pr}^m \left(\frac{L}{D}\right)^e \tag{2.34}$$

The viscosity of petroleum fractions is higher in comparison to water and very sensitive to temperature. This results in a difference in viscosity between the bulk region and the film region which greatly influences heat transfer. Pioneering work by Allen and Eckert including work by Deissler resulted in the development of a forth grouped parameter that accounts for the variation of viscosity between the wall and the bulk region [16]. To incorporate this temperature difference Equation (2.34) is adapted with this forth grouped parameter in Equation (2.35). Equation (2.35) is applicable for liquids while Equation (2.36) is applicable for gases.

$$Nu = \frac{h_x D}{k} = a\mathrm{Re}^n \mathrm{Pr}^m \left(\frac{L}{D}\right)^e \left(\frac{\mu}{\mu_w}\right)^j \tag{2.35}$$

$$Nu = \frac{h_x D}{k} = a\mathrm{Re}^n \mathrm{Pr}^m \left(\frac{L}{D}\right)^e \left(\frac{T}{T_w}\right)^j \tag{2.36}$$

The subscript *w* denotes viscosity and temperature computed or selected at the tube wall, respectively. The exponent *j* is selected based on whether for fluid stream is heating or cooling. Particular focus will be placed on liquid phase correlations since the fluid remains in the liquid phase inside the tubes. The general correlation for liquid inside a tube can be further reduced by noting that the medium used in FWHs is water which has low viscosities in comparison to petroleum fractions. The varying of viscosity in the boundary layer, caused by a difference in the tube wall and adjacent fluid bulk temperature, will also be ignored. Since we are concerned with fully developed flow the exponent value for *e* is zero which reduces Equation (2.35) to Equation (2.37). Developing flow is only of interest to grid or rod baffles and is discussed in Section 2.6.5.

$$Nu = \frac{h_x D}{k} = a\mathrm{Re}^n \mathrm{Pr}^m \tag{2.37}$$

Other researchers have attempted to derive a theoretical equation for a three layer boundary condition and then correct it with data obtained from extensive experimental work. Petukhov and Popov attempted this in 1963 including several other subsequent researchers such as Sleicher and Gnielinski. Their correlation assumes that fully developed flow is achieved, constant fluid

properties over the length of the tube and a constant heat flux at the boundary. These conditions are not always satisfied in a FWH and hence the analytical results from these correlations are approximations. However, these conditions are satisfied if the tube length is discretised such that the properties do not change appreciably along the length of tube. An improved approximation should be achieved with 3D computational fluid dynamics, which is not within this scope of this study.

2.5 Review of the single phase forced convection correlations applied to the internal tube boundary layer

Several correlations have been proposed by a number of researchers based on their experimental data where the fluid remains in a single phase inside a tube. The values of the constants, published by several researchers that used water as the tested medium in their experiments, are listed in Table 2-5 and these correlations may have uncertainties of the order of +/- 25%[17].

Table 2-5 Values of constants assigned to general dimensional equation for calculating the Nu number in horizontal tubes (Re > 10000) [15][17]

Researcher/s	**Year**	***Constants***					**Properties computed at**
		a	***n***	***m***	***e***	j	
Nusselt	1913	0.0302	0.786	0.786	0.054	0	Film Temp.
Rice	1924	0.0157	0.83	0.50	0	0	Film Temp.
McAdams I	1925	0.0178	0.83	0.38	0	0	Film Temp.
Eagle & Ferguson	1930	This is a chart referenced by Kern [18]					Bulk Temp.
Dittus & Boelter (T_w>T_C)	1930	0.0243	0.80	0.4	0	0	Bulk Temp.
Dittus & Boelter (T_w<T_H)	1930	0.0265	0.80	0.3	0	0	Bulk Temp.
Lawrence &Sherwood	1931	0.0561	0.70	0.50	0	0	Bulk Temp.
Nusselt[17]	1931	0.036	0.8	1/3	0.055	0	Bulk Temp.
Sherwood & Petrie	1932	0.024	0.8	0.40	0	0	Bulk Temp.
Colburn*	1933	$St = 0.023Re^{-0.2}Pr^{-2/3}$					Film Temp.
McAdams II	1933	0.0225	0.8	0.4	0	0	Fluid Temp.
Sieder & Tate†	1936	0.027	0.8	1/3	0	0.014	Fluid Temp.

* The *St* number is defined as $St = \frac{Nu}{RePr}$ and the dimensionless parameters in the *St* are evaluated at the fluid temperature [10].

† This correlation was developed using petroleum fractions and includes the fourth grouped parameter included in Equation (2.35) [18].

The Dittus and Boelter correlation for a heated fluid ($T_w > T_H$) will be one of the relations used in this study. In 1970, Petukhov and Kirillov simplified the correlation they proposed in 1963 and it is presented as Equation (2.38)[16]. The accuracy of this correlation is estimated to be 6% [8].

$$Nu = \frac{h_j D}{k} = \frac{(F/2)\mathrm{RePr}}{1.07 + 12.7(F/2)^{1/2}\left(\mathrm{Pr}^{2/3} - 1\right)} \tag{2.38}$$

Where *F* is identified as the friction factor which can be computed for the cooling liquid (feedwater) using Equation (2.39). All properties are evaluated at the film temperature [17], however, it is also reported that they are evaluated at bulk temperature conditions [7]. The latter method has been adopted for the tube side in this study. The effect of temperature variation across the boundary layer has been ignored in this study.

$$F = \left(1.58\ln(\mathrm{Re}) - 3.28\right)^{-2} \tag{2.39}$$

The above mentioned equations are not applicable in the transition region and the upper bounds of the correlations are presented in Table 2-6. In 1976, Gnielinski developed a correlation that was also applicable in the transitional flow regime and is presented as Equation (2.40). The typical accuracy of the Gnielinski correlation is 10% and can be applied to both constant heat flux and constant temperature applications [13].

$$Nu = \frac{h_x D}{k} = \frac{(F/2)(\mathrm{Re} - 1000)\mathrm{Pr}}{1 + 12.7(F/2)^{1/2}\left(\mathrm{Pr}^{2/3} - 1\right)} \tag{2.40}$$

The Dittus and Boelter and Petukhov and Kirillov correlations will be used interchangeably in this study. The former correlation appears in other FWH studies while the latter reports the lowest uncertainty. The original experimental conditions and the uncertainty associated with some important correlations, notably the two correlations used in this study, are presented in Table 2-6.

Table 2-6 Limitations of *Nu* correlations applicable for fluids flowing in pipes

Researcher/s	**Phase**	***Parameters***			
		Pr	***Re***	***L/D***	***Uncertainty***
Dittus & Boelter	Steam/Liquid	0.7 - 100	$< 10^4$	> 60	25%†*
Colburn	-	0.7 - 160	$< 10^4$	> 60	
McAdams II (1933)	Steam	1.2	$< 10^5$	-	-
	Liquid	2.9 - 10.6	$< 10^5$	59 - 224	-
Sieder & Tate	Oils	> 0.7	$< 10^4$	> 60	15%*
Petukhov & Kirillov	Air/Water	0.5 - 200	10^4- 10^6	-	6%‡
Sleicher & Rouse	-	0.1 - 10^4	$< 10^6$	-	10%*
Gnielinski	Air/Liquid	0.5 - 10^6	$< 10^6$	-	10%‡

† Holman [17] reports that these correlations can result in an error of up to 25%

‡ EPRI [19]

* McAdams [15]

The *Pr* number for saturated steam and liquid water was plotted as a function of pressure using the IAPWS-IF97. The *Pr* number for saturated liquid water almost remains constant at 1 for a pressure greater than 100 kPa and less than 4000 kPa and then dramatically increases below this pressure of 100 kPa, see Figure 2-12. The *Pr* number for saturated steam remains almost constant at 1. It was therefore important to investigate the impact of the *Nu* number, calculated using the different correlation, at a *Pr* number of 1 and 4. A graphical comparison of the correlations presented in Table 2-6, with a Pr = 1 and Pr = 4 is presented in Figure 2-13(a) and Figure 2-13(b), respectively. Note that the Pethokhov correlation exceeds the Dittus and Boelter correlation at high *Pr* numbers.

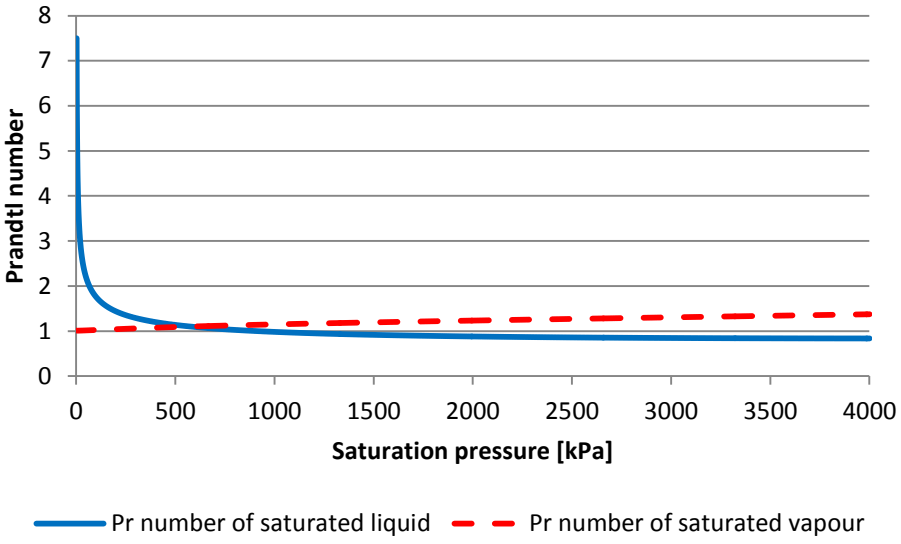

Figure 2-12. Plot of *Pr* number for water at saturated liquid and vapour conditions using IAPWS-IF97

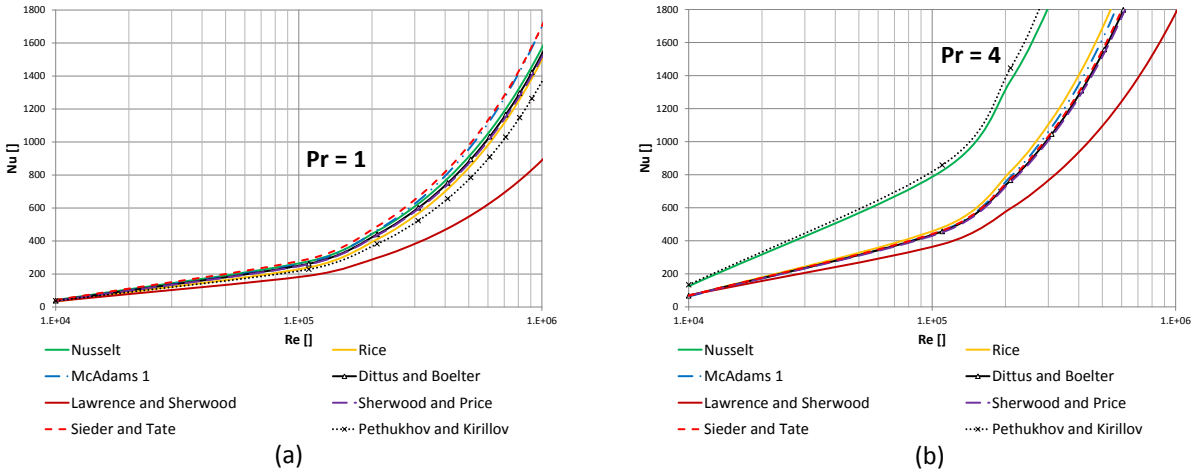

Figure 2-13. Graphical representation of correlations presented in Table 2-6 with *Pr = 1*(a) and *Pr = 4*(b)

2.6 Review of the single phase forced convection correlations applied to the external tube boundary layer

In addition to the flow internal to the tube, referred to as tube side, there is also a more complex flow arrangement external to the tube, referred to as the shell side. Researchers have developed heat transfer correlations using flow arrangements around spheres, cylinders, tubes and banks of tubes. The applicability of the correlations is dependent on how closely the internal FWH geometry matches with the original experimental set-up that was used during its development. A critical input into the correlations is the free flow area, which is dependent on the flow arrangement inside the FWH. Hence, a brief overview of the various zones in a FWH is required to appreciate the shell side flow path through of a FWH. Refer to section 3.1.1 for a more detailed description of the design and configuration of FWHs.

The fluid exists in either the gas phase, liquid phase or in both phases on the shell side. There are discrete zones on the shell side to achieve the optimum heat transfer. The typical range of the film heat transfer coefficient, *h*, in each of the 3 zones of a FWH is presented in Table 2-7.

Table 2-7 Typical film heat transfer coefficients for the three zones of the shell side [8]

Zone	Phase	Film heat transfer coefficient h_o [W/m^{2}K]
De-superheating	steam	80 - 800
Condensing	steam/liquid	8000 – 12000
Drains Cooler	liquid	5000 – 7000

2.6.1 De-superheater (DS) flow arrangement

The design of the DS zone is critical in order to achieve the maximum heat transfer coefficient since it has the lowest *h* of the three zones because the fluid is steam. The general correlation in Equation (2.34) reveals that the film heat transfer coefficient is proportional to the fluid velocity i.e. $h \propto v$. Hence, *h* can be maximised by directing all the superheated steam into the DS compared to distributing the steam across the full length of the FWH. This type of inlet is common across the Eskom fleet but only the fluid path through the DS differs, which is illustrated in Figure 2-14.

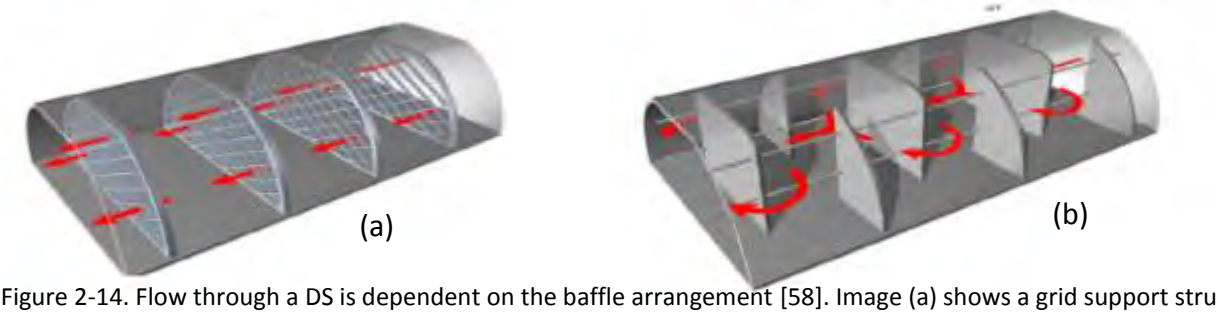

Figure 2-14. Flow through a DS is dependent on the baffle arrangement [58]. Image (a) shows a grid support structure, while (b) shows a segmented baffle arrangement.

Figure 2-15. Tube arrangement in grid supports [20]

Baffles are responsible for supporting the tubes and directing the flow over the tubes to achieve efficient heat transfer. The grid type baffle, illustrated in Figure 2-14(a), ensures that the fluid on the shell side flows counter current to the fluid flowing inside the tube. The flow is longitudinal along the entire length which minimises shell side flow induced vibration and pressure. There is always a trade-off between h and ΔP, and it is reported that grid supports have the highest $h/\Delta P$ ratio [14]. A grid baffle comprises of a series of strips or rods configured in two directions such that the tubes may be supported, which is illustrated in Figure 2-15. The heat transfer analysis for heat exchangers with grid or rod type supports is not well documented in open literature. Donohue [21] discusses the selection of the *Nu* correlation for un-baffled shells i.e. fluid flows parallel to the tube length. Gentry, Gentry and Scanlon [14] provides insight into predicting the shell side h of a STHE fitted with rod baffles. Grid baffles are also identified as egg-crate support plates (ESP) and Hitachi provides insight into the heat transfer analysis associated with these type of baffles [22]. The improved heat transfer characteristics are generated by vortex shedding that is created each time the fluid has to flow across the rod or grid edge.

Segmented baffles are illustrated in Figure 2-14(b). These baffles create cross flow regions in addition to counter flow regions. This is a popular heat exchanger arrangement for conventional heat exchangers in the petrochemical and nuclear industry. A larger film heat transfer coefficient h may be achieved with a combination of cross flow and counter current flow across the tube bank in comparison to only a counter current flow arrangement [8]. Many researchers have proposed correlations for modelling h with segmented baffles and these methods include: McAdams/Kern [18], Jestin [23], Bell Delaware [24] and the Stream Analysis method proposed by Tinker [25].

A conventional single phase STHE will have a shell side large enough to exclude counter current flow by extending the baffle such that all the tubes are supported. This type of design is identified as a no-tube-in-window segmented baffle design as illustrated in Figure 2-16(a). While an arrangement where the baffle supports a portion of the tubes will incorporate counter current flow and cross flow regions as illustrated in Figure 2-16(b). The opening that permits the counter current flow is represented as a percentage of the shell diameter and the ratio is referred to as the baffle cut. The heat transfer improves with the inclusion of baffles because the fluid velocity increases and cross flow regions are introduced.

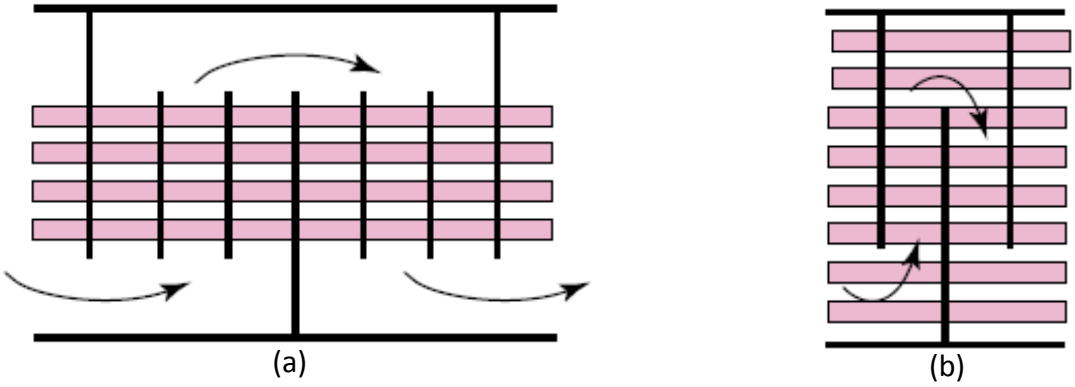

Figure 2-16. No-tubes-in-window vs single segmented baffle design [26]

In summary, a DS is inserted into a FWH to increase the fluid velocity and may be fitted with either segmented or grid baffles. The segmented baffle design incorporates both shell side counter current and cross flow regions while the grid design only allows counter current flow.

2.6.2 Sub-cooling zone or drains cooler (DC) design variation

The variety of internal flow arrangements found in the DC is identical to that found in the DS. The most significant difference is that water is in liquid phase on the shell side. The film heat transfer coefficient is thus much larger in comparison to the DS, see Table 2-7.

2.6.3 Unbaffled STHE

In an unbaffled STHE the tubes are only supported by the tube plates as illustrated in Figure 2-17. It is assumed that the fluid flows parallel to the tubes and counter current relative to the internal fluid. The estimation of the *Nu* number for this design is suggested by Donohue [21]. In this application the constant *a* of the general *Nu* correlation, Equation (2.33), is a function of the equivalent diameter i.e. $a(D_e)$. The correlation is presented in Equation (2.41):

$$Nu = \frac{h_j d_o}{k} = a(\mathrm{D}_e)\mathrm{Re}^{0.6}\,\mathrm{Pr}^{0.33} \tag{2.41}$$

$$a(\mathrm{D}_e) = \frac{1}{1.16^{0.6}}\mathrm{D}_e^{0.6} \tag{2.42}$$

$$\mathrm{D}_e = \frac{4[\text{Free flow area}]}{\text{wetted perimeter}} = \frac{4\left[\frac{P_T^2\sqrt{3}}{4} - \frac{\pi d_o^2}{8}\right]}{\frac{\pi \mathrm{d}_o}{2}} \tag{2.43}$$

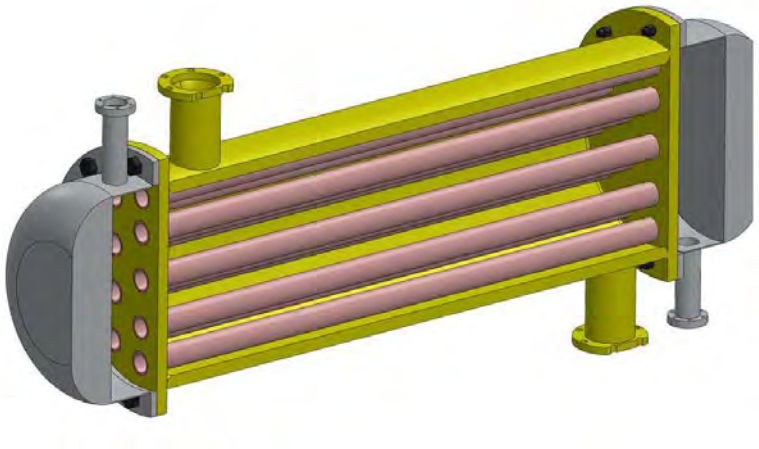

Figure 2-17. Illustration of an unbaffled shell where tubes are only supported at their ends by the tube plates [27]

The velocity used to calculate the *Re* number in Equation (2.41) is calculated by utilising the free flow area on the shell side. This is calculated by subtracting the cross-sectional area of the tubes from the cross-sectional area of the shell. However, in a DC and DS the shell diameter (D_{shell}) corresponds to the bundle diameter (D_{shell}) of the FWH. The uncertainty associated with estimating *h* using this method, assuming STHE is identical to the specific experimental setup, is $\pm$ 25% [21].

2.6.4 Gentry method for rod baffles

From the information available, it appears that none of the FWHs in the Eskom fleet are fitted with rod baffles. However, they have similar physical similarities when compared with grid or plate baffles, which make the inclusion of this method of benefit to this study. Gentry, Gentry and Scanlon [14] reports that rod baffles were originally developed to reduce flow induced tube vibration problems, which is also achieved with grid or plate baffles. The DC and DS are enclosed in a shroud where it is assumed that the shell of the shroud corresponds to D_{bundle} and a bundle ring, to which the baffles are secured, does not exist. The method for determining D_{bundle} is presented in Appendix A.

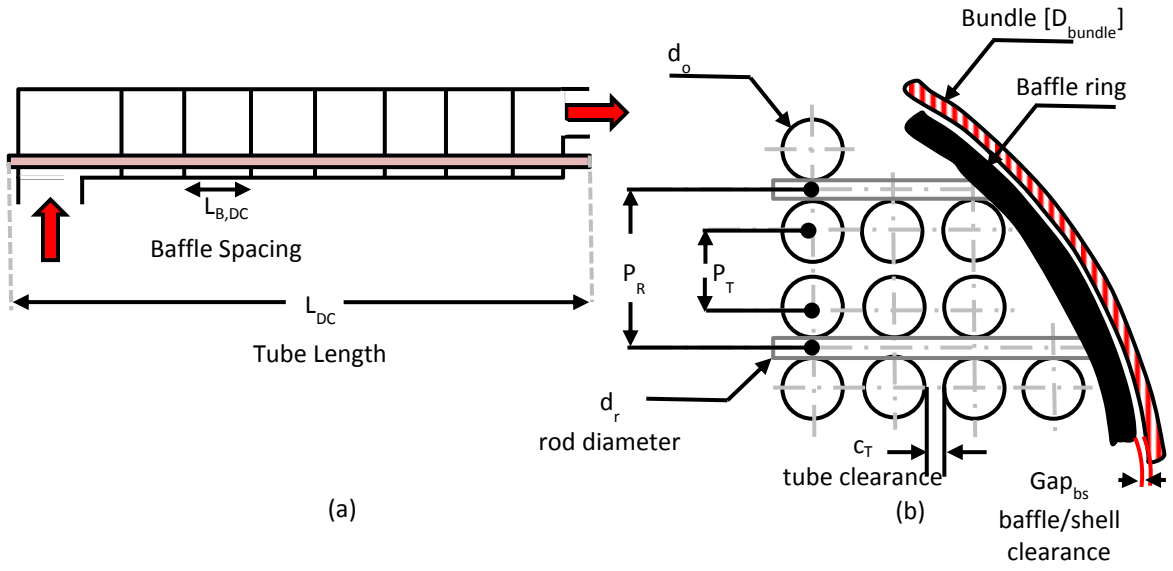

Figure 2-18. Tube and support layout of a rod baffle STHE illustrating overall configuration (a) and details of baffle

Free flow area calculation

The geometric parameters associated with rod baffles are illustrated in Figure 2-18. The geometric variables have to be specified in order to calculate the free flow and leakage areas. The shell side flow area is defined as the cross sectional area of the shell minus the total cross sectional area occupied by the tubes. In the case of FHWs the DS and DC shells are the shrouds and their tube plates are approximated to be semi-circular, see Figure 2-19(a). Hence, the area calculations will differ from the original experimental setup where tubes were arranged on a circular tube plate.

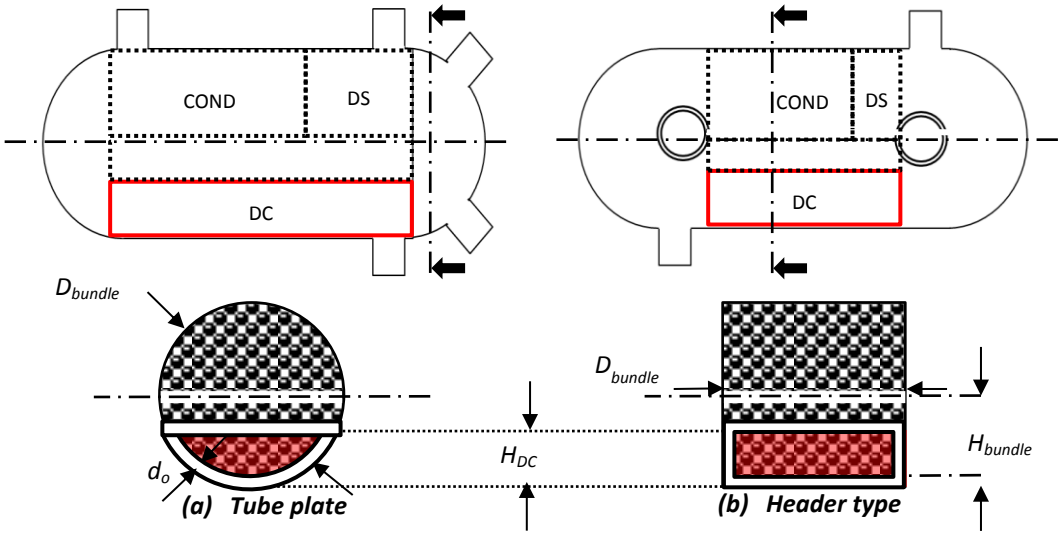

Figure 2-19. Distribution of heat transfer area about a symmetrical axis for a two pass 3 zone tube plate (a) and header (b) type FHW

The tube arrangement differs even further when applying it to a header type FWH, see Figure 2-19(b). The tube arrangement in the DC or DS of a header type FWH is assumed to be rectangular compared to a tube plate type FWH. The cross section area of the window in the DC of a header type FWH is defined by Equation (2.44). The number of tubes in the DC zone is denoted by n_{tDC}.

$$A_{DCpf\_freeflow} = H_{DC} D_{bundle} - n_{tDC} \frac{\pi}{4} d_o^2 \tag{2.44}$$

The leakage flow is a critical parameter in the Gentry method. The leakage flow area for rod baffles is defined as the free flow area between the D_{shell} and the bundle outer diameter (D_{OTL}). However, as was explained earlier the presence of the shroud requires D_{shell} to be substituted with D_{bundle}. The leakage area between D_{bundle} and D_{OTL} is estimated using Equation (2.45) assuming a gap of d_o.

$$A_l = D_{bundle} H_{DC} - \left(D_{bundle} - d_o\right)\left(H_{DC} - d_o\right) \tag{2.45}$$

The leakage flow for a tube plate type FWH is calculated as follows and the estimated leakage gap between the shroud and bundle was assumed to be $3/5 d_o$ after reviewing several FWH drawings:

$$A_l = \pi \frac{D_{bundle}^2 - (D_{bundle} - \frac{3}{5}\mathrm{d}_o)^2}{4} \tag{2.46}$$

The free flow area is defined as the window area minus the total cross sectional area occupied by the total rod length used to manufacture a baffle (Equation (2.47)).

$$A_{DCpf} = A_{DCpf\_freeflow} - d_r L_r \tag{2.47}$$

However, manufacturers only disclose the diameter or thickness of the rod or plate (d_r) but not the length of rod or plate (L_r) used to manufacture a single baffle. Instead a unit cell approach is adopted to calculate the factor by which the free flow area decreases. This is discussed in detail in Appendix A, suffice to say that an area reduction factor is defined ($A_{unitgrid}/A_{unit}$). This factor accounts for the additional obstruction of the rod to free flow and is applied in Equation (2.48).

$$A_{DCpf} = A_{DCpf\_freeflow} \left\lfloor \frac{A_{unitgrid}}{A_{unit}} \right\rfloor = \left(A_{DCpf} - n_{tDC} \left(\frac{\pi \mathrm{d}_o^2}{4} \right) \right) \left\lfloor \frac{A_{unitgrid}}{A_{unit}} \right\rfloor \tag{2.48}$$

Heat Transfer Model

The *Nu* correlation for the shell side of a rod baffle STHE is presented in Equation (2.49) this applies to turbulent flow, which is the predominant regime at nominal operating conditions.

$$Nu = \frac{h_x d_o}{k} = C_{RB}\,\mathrm{Re}_{D_e}^{\,0.8}\,\mathrm{Pr}^{0.4} \tag{2.49}$$

$$C_{RB} = a(\mathrm{L}_b, \mathrm{n}_t, \mathrm{d}_o, \mathrm{d}_r, \mathrm{D}_{\mathrm{shell}}, \mathrm{D}_{OTL}, \mathrm{D}_{Bi}, \mathrm{D}_{Bo}, \mathrm{L}_r, \mathrm{L}_t) \tag{2.50}$$

The exponents of the Re_{De} and *Pr* numbers differ from those suggested by Donohue [21] for unbaffled shells because improved heat transfer is expected with the consideration of baffles.

The flow through the shell side of FWHs, at steady state and rated power level of the station (100% MCR) conditions, is in the turbulent region. Hence, the method applied for turbulent flow is applicable and is presented in Figure 2-20.

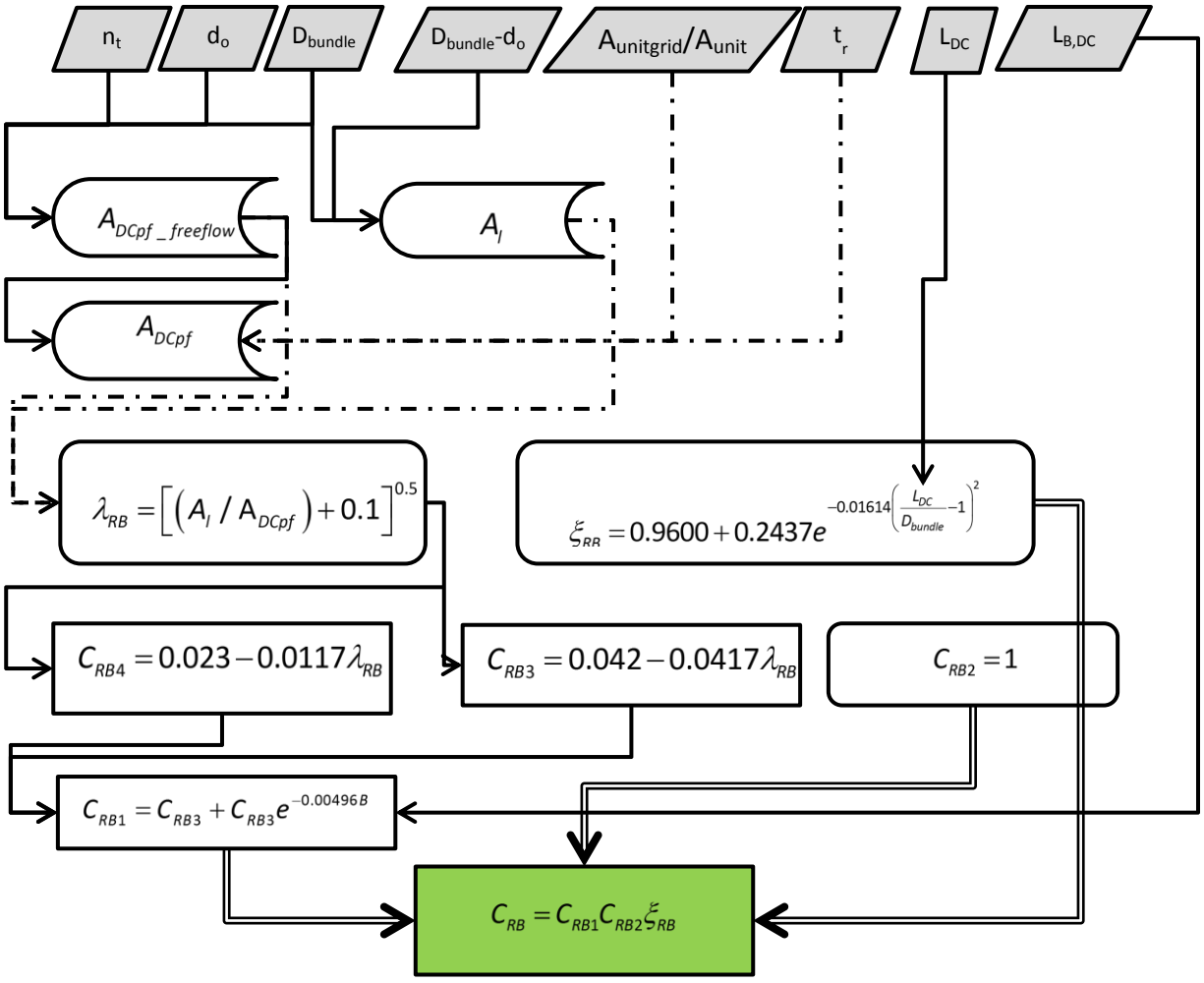

Figure 2-20. Calculation methodology for calculating the turbulent geometric function C_{RB} for a bare tube [14]

The geometric coefficient function (C_{RB}) was found to be sensitivity to baffle spacing (L_b) and the leakage-to-shell ratio ($A_l/A_{DCpf\_freeflow}$). C_{RB} consists of three main parameters:

- $\boldsymbol{C_{RB1}}$ – This parameter is a function of L_B and $A_l/A_{DCpf\_freeflow}$
- $\boldsymbol{C_{RB2}}$ - The external surface profile of the tube i.e. is the tube finned or bare
- $\boldsymbol{\xi_{RB}}$ – This parameter is a function of the length of tube (L_t) to (D_{bundle})

FWH tubes are not finned and by this definition have a C_{RB2} of 1. The error associated with h for this method particular to the specific experimental setup is $\pm$ 25% [21].

2.6.5 Shiina, Nakamura and Matsumura method for grid/plate baffles

The DSs and DCs of the more recent Eskom stations are fitted with grid or plate baffles. Hitachi [22] designates their grid baffles as egg-crate support plates (ESPs) or non-segmented baffles. Thulukkanam [12] distinguishes between grid and plate baffles because they are patented designs but from a flow perspective they are essentially identical. They are both manufactured from stainless steel flat strips and are tack welded to the baffle ring and at the intersection of strips.

Shiina, Nakamura and Matsumura [22] recommends a method for calculating h for egg-crate or grid baffles using previously published correlations and also suggests their own correlation. The maximum uncertainty of this correlation was measured to be approximately 30%, which excludes the measurement uncertainty associated with the experimental results of 20%. Hence, the expected uncertainty associated with their correlation, which is only applicable for transitional flow regime, may be in the order of 50%. Their correlation was not considered but their method for developing the correlation was used to develop a correlation used in this study.

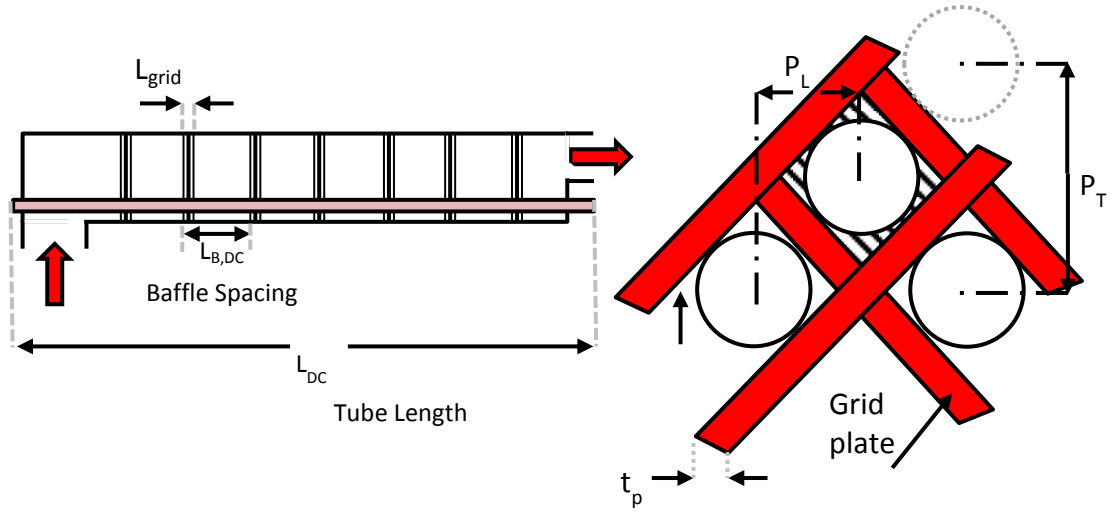

Figure 2-21. Geometry of an egg-grate/ grid baffle

Their method states that there is *h* along the tube between the baffles and along the grid plate (L_{grid}), see Figure 2-21. The latter *h* being larger than the former *h* due to presence of entrance effects along the grid plates. The lower limit of *h* is calculated assuming several correlations including the Dingee correlation that is presented below:

$$Nu_{lower} = \frac{hD_e}{k} = a(\mathrm{P}_T, \mathrm{d}_o)\mathrm{Re}_e^{0.8}\,\mathrm{Pr}^{0.4} \tag{2.51}$$

$$a(\mathrm{P}_T, \mathrm{d}_o) = 0.026\left(\frac{P_T}{d_o}\right) - 0.006 \tag{2.52}$$

The upper limit of *h* is calculated using the same correlation but assumes that the grid obstructs free flow between the tubes thus increasing the fluid velocity. The velocity is then adjusted for the obstructed flow scenario and is used in the *Re* number in Equation (2.54). The increased velocity (v_p) is calculated as follows:

$$v_p = \frac{\dot{m}_H}{A_p \rho_H} \tag{2.53}$$

where A_p is the free flow area that results from subtracting the cross section area of the tubes and the support plates. In Equation (2.54) Re_p is distinguished from *Re* since the velocity v_p is used

$$Nu_{upper} = \frac{hD_e}{k} = a(\mathrm{P}_T, \mathrm{d}_o)\mathrm{Re}_p^{0.8}\,\mathrm{Pr}^{0.4} \tag{2.54}$$

The average *h* is then calculated using a weighted average of the upper and lower predictions, based on the grid spacing.

$$h_j = \xi h_{lower} = \left(1 - \frac{L_{grid}}{L_B}\right)h_{lower} + \left(\frac{L_{grid}}{L_B}\right)h_{upper} \tag{2.55}$$

Where ξ is identified as the heat transfer enhancement factor, which occurs as a result of the vortex shedding effect at the edge of each baffle. Shiina, Nakamura and Matsumura [22] reports that the heat transfer improvement was almost 100% i.e. an enhancement of $\xi \approx 2$. The enhancement is driven by entrance effects, mentioned in Section 2.4.1, rather than the increase in velocity at the grid's edge. Therefore, there appears to be a shortcoming in the development of Equation (2.55). The enhancement cannot be achieved by merely adjusting the free flow area along the grid's length but also has to incorporate the entrance effect enhancement.

As was mentioned earlier, Shiina, Nakamura and Matsumura do not reference a correlation to be used in Equation (2.55) but reviews several correlations in their study. They report that acceptable agreement, with experimental data, was obtained with the Dingee correlation. However, this correlation mainly applies to nuclear fuel assemblies [28], where fuel rods are substantially smaller than tubes. Initial testing of the correlation with FWH geometry revealed an overestimated *h* when compared to the reported h values.

2.6.6 Modified Donohue method for grid/plate baffles

The Donohue correlation [21] was applied to Equation (2.55) as Eskom reports that a derivative of this correlation is popular with grid baffle arrangements [29]. The exact correlation cannot be disclosed due to propriety concerns. Hence, the formulation of this correlation was developed by the author from open source literature and further experimental testing to confirm the uncertainty is recommended.

The h_{upper} is identical to h_{lower} but is assigned with an enhancement of 2 (entrance effects is discussed in Section 2.4.1) and also includes an area reduction factor, $[A_{unitgrid}/A_{unit}]^{0.6}$, that accounts for the reduction in free flow area due to the obstructing grids. Recall that the exponent of the *Re* number in Equation (2.41) is 0.6 and hence the reason for the exponent on the area reduction factor. The Equation (2.55) may therefore be adjusted as follows and is henceforth referred to as the modified Donohue correlation for grid baffles:

$$h_j = \xi h_{lower} = \left(1 - \frac{L_{grid}}{L_B}\right) h_{lower} + \left(\frac{L_{grid}}{L_B}\right) 2h_{lower} \left[A_{unitgrid} / A_{unit}\right]^{0.6} \qquad (2.56)$$

2.6.7 McAdams/Kern method with 25% cut segmented baffles

Kakaç [8] recommends the use of the correlation proposed by McAdams/Kern, Equation (2.57), for segmented baffles. McAdams/Kern developed this correlation by applying a baffle cut of 25% in his experimental set-up. The calculation of the *Re* number for the shell side is specified with a subscript Re_{cf} because the equation utilises D_{bundle} to calculate the cross section area (A_{cf}). It should also be noted that the free flow area increases down the tube rows as more tubes are located in the successive rows. The applicable Re_{cf} for the use of this correlation is presented in Equation (2.58):

$$Nu = \frac{h_o D_e}{k} = 0.36 \mathrm{Re}_{cf}^{0.55} \mathrm{Pr}^{1/3} \left(\frac{\mu_b}{\mu_w} \right)^{0.14} \tag{2.57}$$

$$2x10^3 < \mathrm{Re}_{cf} = \frac{G_s D_e}{\mu} = (\rho v)_{cf} \frac{D_e}{\mu} = \left(\frac{\dot{m}_H}{A_{cf}} \right) \frac{D_e}{\mu} < 1x10^6 \tag{2.58}$$

where the subscript *cf* indicates that the Re number is computed using the cross flow area, h_o is the shell side heat transfer coefficient and G_s is the estimated shell-side mass velocity [kg/m^2.s].

Kern [18] reports the uncertainty to be in the range of ±20% assuming that it is applied to an identical STHE. The properties are evaluated at the average fluid temperature in the shell. D_e is calculated along the axis of the shell and is taken as four times the net flow area divided by the wetted perimeter even though the flow is cross flow. The D_e for a square pitch and triangular/staggered pitch is presented in Equation (2.59) and Equation (2.60), respectively. The arrangement of square and triangular/staggered transverse pitch, P_T, is illustrated in Figure 2-22.

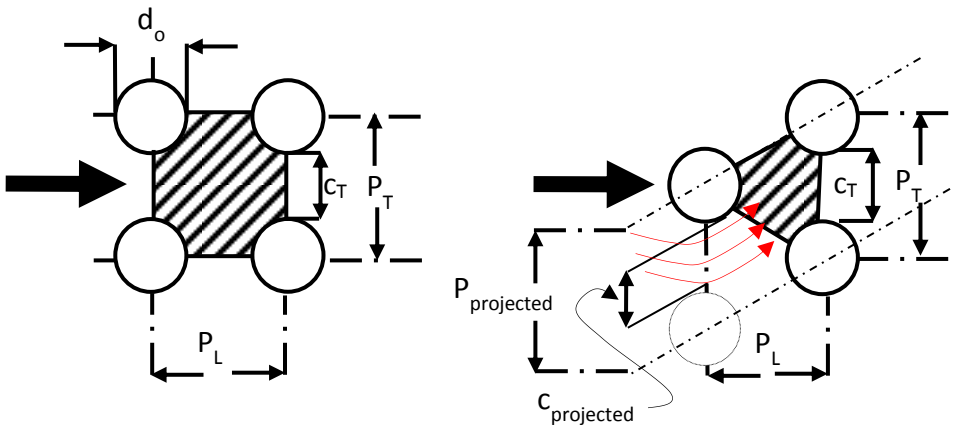

Figure 2-22. Transverse pitch definition for a square and triangular/staggered tube arrangement

$$D_e = \frac{4\left(P_T^2 - \pi d_o^2\right)}{\pi d_o} \tag{2.59}$$

$$D_e = \frac{4\left(\frac{\sqrt{3} P_T^2}{4} - \frac{\pi d_o^2}{8} \right)}{\pi d_o / 2} \tag{2.60}$$

A hypothetical cross flow area is defined in the region that would generate the lowest shell side velocity or in the region with the maximum cross flow area. McAdams [15] applied this method to a conventional STHE where the maximum cross flow area would correspond to the centre of the heater. Thus, the total maximum free flow area would correspond to the tube clearance c_T multiplied by the number of adjacent tube combinations at the tube row with maximum number tubes. The row that contains the maximum number of tubes is located at some offset from the bundle diameter, D_{bundle}. Thus, the row with the maximum number of clearances, c_T, can be approximated as D_{bundle}/P_T. The free flow area (A_{cf}) is computed in Equation (2.61):

$$A_{cf} = length \times breath = L_B \left[c_T \left(\frac{D_{bundle}}{P_T} \right) \right] \tag{2.61}$$

where the length of the free flow area is equated to the baffle spacing, L_B.

2.6.8 Jestin Method

Professor Louis Jestin is the head of the Eskom Power Plant Engineering Institute (EPPEI) and provided some insight from his experience managing the heat exchanger programme at Électricité de France (EdF). The thermal model [23] he described assumes that there is a split between the fluid flowing counter current and cross flow and typically this distribution is 50:50. If this distribution is assumed then the average *h* is calculated using Equation (2.62). The *h* is calculated for each flow regime using correlation similar to that proposed by Dittus and Boelter (Equation (2.63)) and McAdams (Equation (2.64)) for the counter current and cross flow regions, respectively.

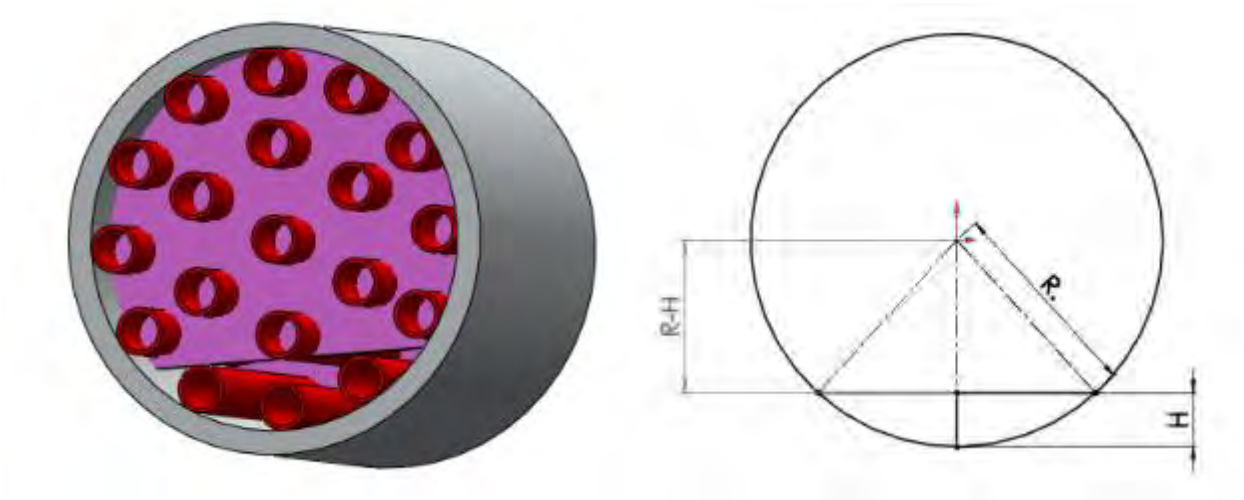

Figure 2-23. Designation of dimensions for calculating the window area

Jestin compared results to actual plant data and applied a factor of 0.65 to correct Equation (2.62), see Equation (2.65). The Jestin model does not require an input for baffle spacing or baffle cut. The baffle spacing L_B in Equation (2.61) was estimated to be 50 pipe diameters as was inferred from the validation exercise.

These two correlations are applied to the DC and DS zones in a FWH that contain tubes that are fitted on a partial tube plate i.e. circular segment, which is illustrated in Figure 2-23. The shell side counter current flow area, which is utilised in calculating the Re_{De} and Re numbers, is calculated based on the assumption that tube bundles are constructed in a circular pattern. Hence, Equation (2.67) is formulated based the area of the sector as illustrated in Figure 2-23.

$$h_{ideal} = 0.5h_{pf} + 0.5h_{cf} \tag{2.62}$$

$$Nu_{pf} = \frac{h_{pf} d_o}{k} = 0.023 \mathrm{Re}_{pf}^{\ 0.8} \mathrm{Pr}^{0.4} \tag{2.63}$$

$$Nu_{cf} = \frac{h_{cf} d_o}{k} = 0.22 \mathrm{Re}_{D_e,cf}^{0.56} \mathrm{Pr}^{1/3} \tag{2.64}$$

$$h_{actual} = 0.65 h_{ideal} \tag{2.65}$$

where the subscripts D_e implies that the cross flow *Re* number is calculated using the equivalent pipe diameter, defined in Equation (2.60), *pf* and *cf* is defined as parallel and cross flow, respectively.

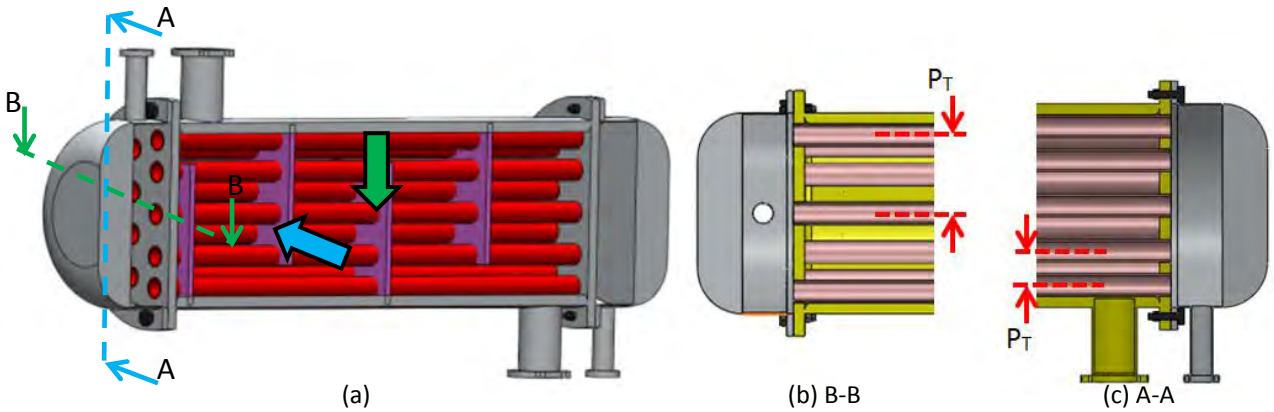

Figure 2-24. Cross section view through a basic STHE with segmented baffles[27]

Note that Jestin assumes that the baffles are located in such a manner that the P_T, the pitch perpendicular to the flow, corresponds to the largest of the two tube pitches. This is illustrated in Figure 2-24(a) and Figure 2-24(b). However, a review of detailed FWH drawings indicates that the

baffle arrangement may be installed in a manner illustrated in Figure 2-14(c). This implies that P_T, for this arrangement, corresponds to the smaller of the two pitches. A larger prediction of *h* would therefore be expected with this tube arrangement. However, the drawback with this configuration is that a larger pressure drop is expected.

The parallel free flow area is calculated by subtracting the cross sectional area of the tubes from the window area. An imported parameter associated with segmented baffles is baffle cut, which is defined as the ratio of the maximum window opening length over the shell diameter; see Equation (2.66) and Figure 2-23.

$$B_{cut} = \frac{H}{D_{bundle}} = \frac{H}{2R} \tag{2.66}$$

The window area is calculated by subtracting the two right angled triangles from the area of the sector, see Equation (2.67) and Figure 2-23. This method of calculating the window and parallel flow area is an approximation of the flow through the shroud of a DC and DS. The approximation deviates even more when applied to a header type heater where the tube arrangement is almost rectangular.

$$\begin{aligned} A_{window} &= \text{sec}tor - 2\left(90^o\ triangle\right) \\ A_{window} &= R^2 \cos^{-1}\left(\frac{R-H}{R}\right) - 2\left(\frac{1}{2}\left[\sqrt{2RH-H^2}\right]\left[R-H\right]\right) \end{aligned} \tag{2.67}$$

$$A_{pf} = A_{window} - n_{t,window}\pi\frac{d_o^2}{4} \tag{2.68}$$

The subscript *pf* is parallel flow, *R* is the radius of the bundle, *H* is the height of the sector and $n_{t,window}$ is the number tubes located in that particular sector of the circle.

2.6.9 Bell-Delaware/Taborek Model

The Bell Delaware model was developed to calculate *h* on the shell side of a single phase heat exchanger with segmented baffles. This was also a circular heat exchanger which differs from the shape of the shroud of the DS and DC zones. Hence, the free flow areas will be calculated using D_{bundle} instead of D_{shell}, where applicable. This method was developed in 1963 and the correction factors were plotted on charts [30]. In 1983, Taborek [31] fitted correlations to the charts which allows for automated calculations. Bell and Meuller [30] also report that even though this model is

the best available model in open literature it has an uncertainty of ± 100%. The uncertainty was determined by the Heat Transfer Research Institute (HTRI) from an extensive experimental study. However, Taborek [31] reports an uncertainty in the range of 25% based on the original experimental set-up.

The basic equation for calculating the average shell-side heat transfer coefficient h is given by:

$$h = h_{id} J_c J_l J_b J_s J_r \tag{2.69}$$

where h_{id} is the ideal heat transfer coefficient for a pure cross flow arrangement (using Colburn j-factor method) and J denotes specific correction factors.

A description of the 5 correction factors is presented in Table 2-8. The method assumes that a tube bundle with single segmented baffles of a specified outer tube limit (D_{OTL}), baffle spacing (L_B) and baffle cut (B_{cut}) is inserted into a shell with internal diameter (D_{shell}). The shroud of the DC and DS now requires the variable D_{shell} to be replaced with D_{bundle} and D_{OTL} is replaced with D_{bundle}-$2d_o$ (see Figure 2-25 and Figure 2-26).

Table 2-8 Definition of correction factors used in the Bell Delaware method

Subscript *J*_	Definition
c	Accounting for deviation from pure cross flow, in window area.
l	Lowers the heat transfer due to tube-to-baffle and shell-to-baffle leakage.
b	Lowers the heat transfer due to fluid flowing on the periphery of bundle.
s	Variable baffle spacing and inlet and outlet nozzle effects. Chosen as 1.
r	Laminar flow correction factor. Equal to unity because shell side *Re > 100*.

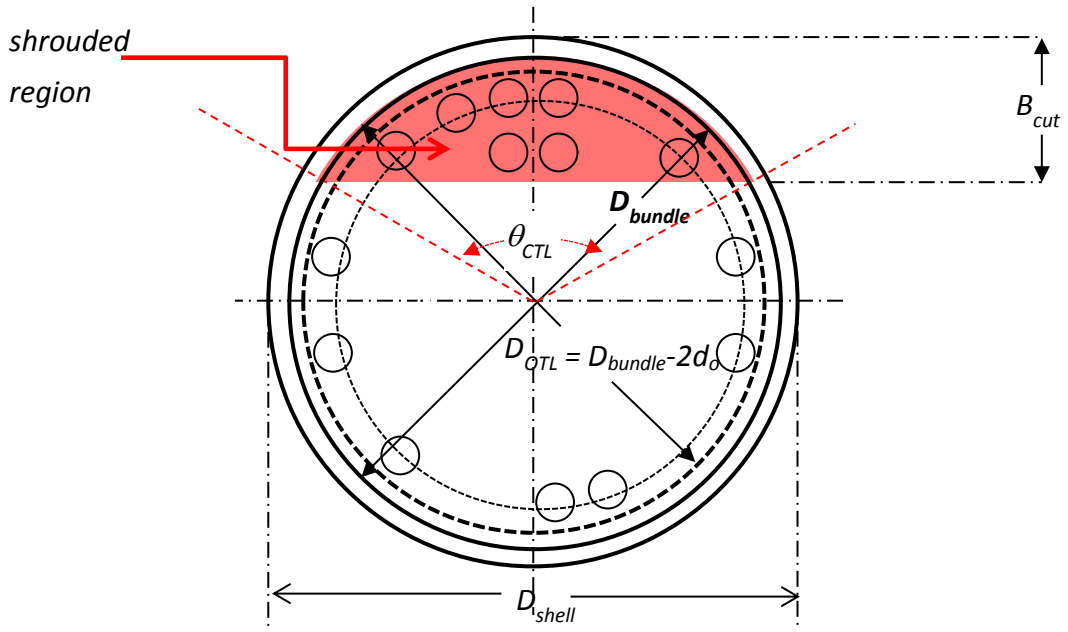

Figure 2-25. Baffle and tube bundle geometry for shrouded region within a STHE applying the Bell-Delaware model

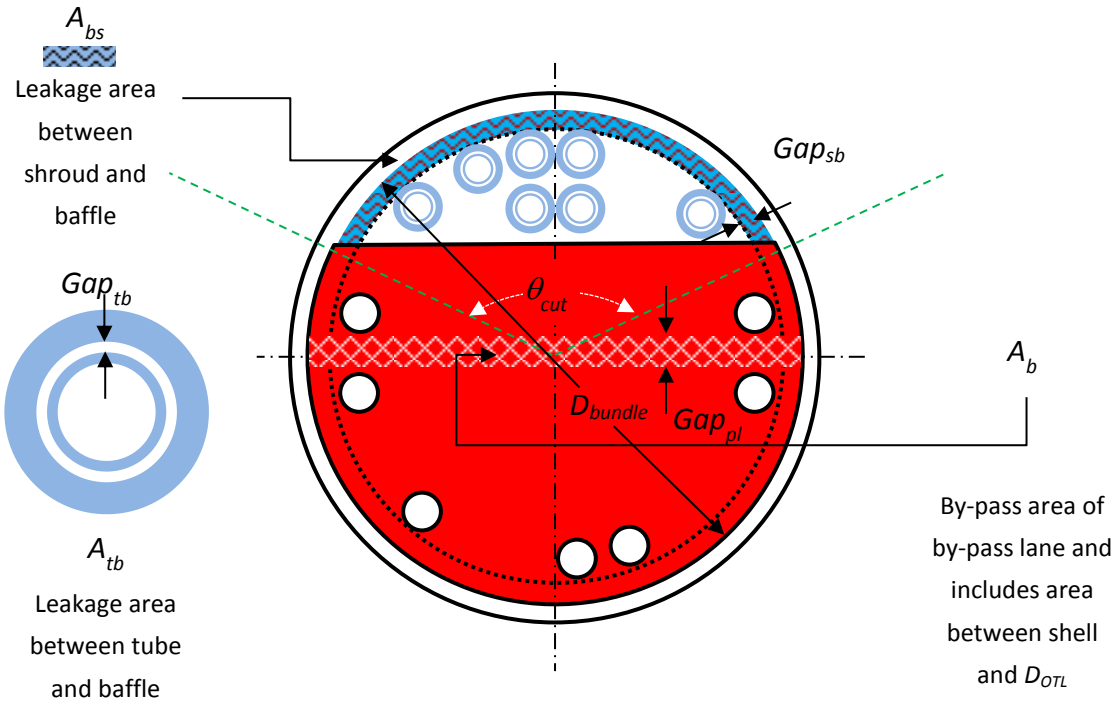

Figure 2-26. Leakage and by-pass areas of a tube bundle

A segmented baffled tube bundle is illustrated in Figure 2-27. The calculation sequence for determining the correction factors is presented in Figure 2-28 and Figure 2-29. It is assumed that the baffles are distributed uniformly in the DS and DC due to the lack of detail on vendor drawings ($J_s = 1$).

Figure 2-27. A classical tube bundle with single segmented baffles inserted into a one pass shell[27]

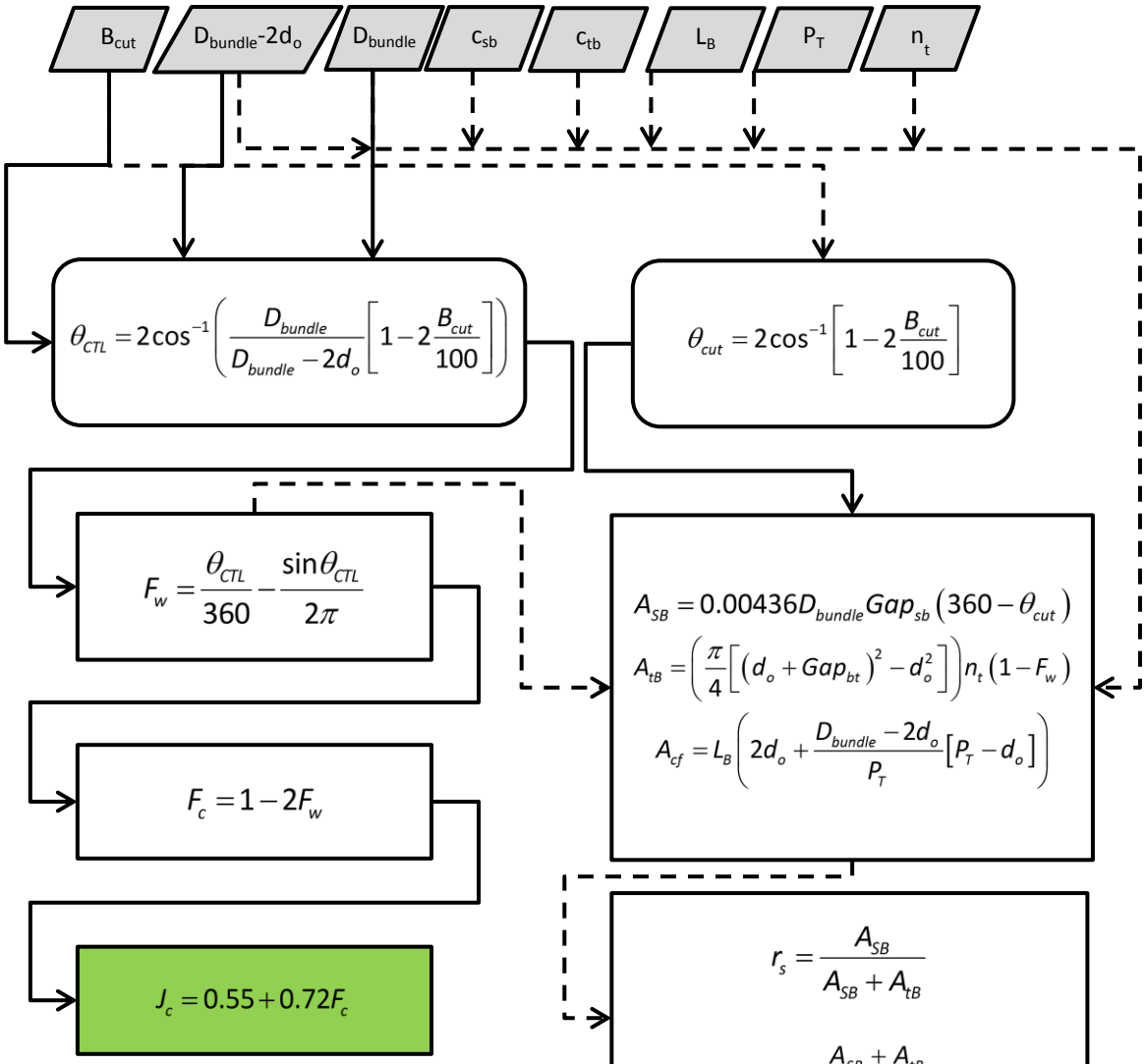

Parameter	Description
B_{cut}	Baffle cut [%]
D_{bundle}	Tube bundle diameter
Gap_{sb}	Clearance btwn shroud and bundle
Gap_{bt}	Clearance btwn tube and baffle
d_o	Tube outer diameter
L_B	Baffle spacing
P_T	Transverse pitch
n_t	Number of tubes
J_c	Correction for cross/parallel flow
J_l	Correction for leakage

Figure 2-28. Calculation sequence for evaluating J_c and J_l utilised in the Taborek model

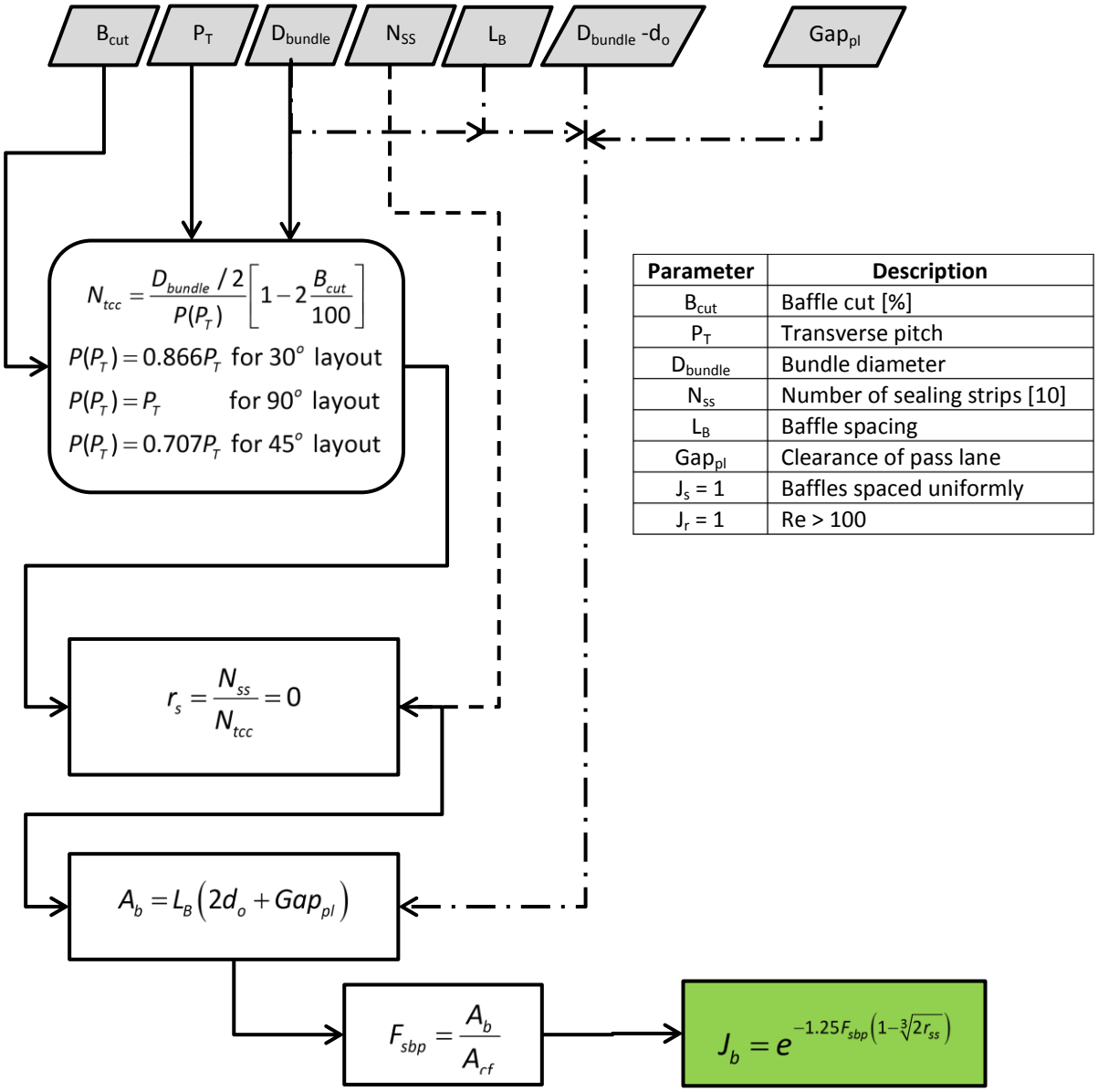

Parameter	Description
B_{cut}	Baffle cut [%]
P_T	Transverse pitch
D_{bundle}	Bundle diameter
N_{ss}	Number of sealing strips [10]
L_B	Baffle spacing
Gap_{pl}	Clearance of pass lane
$J_s = 1$	Baffles spaced uniformly
$J_r = 1$	Re > 100

Figure 2-29. Calculation sequence for evaluating J_b utilised in the Taborek model

The TEMA standard [11] baffle hole clearances is presented and will be utilised for tube baffle leakage in the event that the vendor of an Eskom FWH did not disclose this clearance. The HEI standard [9] reports a baffle-to-tube hole clearance (Gap_{bt}) should be 0.8 mm and the shroud-to-bundle clearance (Gap_{sb}) is assumed to be 0.0 mm as this clearance is not reported in either of these standards. The leakage and by-pass clearances are illustrated on Figure 2-25 and Figure 2-26.

Table 2-9 Baffle hole clearance as applied to segmented baffles [11]

Unsupported span	Tube hole	Over tolerance
d_o > 31.8 mm	d_o + 0.8 mm	0.3 mm
d_o < 31.8 mm	d_o + 0.4 mm	0.3 mm

The ideal heat transfer coefficient for pure cross flow, h_{id}, may be calculated using the Colburn j-factor or Zukauskas approach, although the former method is more common.

2.6.10 Colburn *j*-factor approach to estimating h_{id} for cross flow

The Colburn *j*-factor approach [8] for the ideal heat transfer coefficient (h_{id}) for a pure cross flow arrangement is presented in Equations (2.70) to (2.72).

$$h_{id} = jC_p\left(\frac{\dot{m}_H}{A_{cross}}\right)\left(\frac{k}{C_p\mu}\right)^{2/3}\left(\frac{\mu}{\mu_w}\right)^{0.14} \tag{2.70}$$

$$j = a_1\left(\frac{1.33}{P_T/d_o}\right)^{a}\left(\frac{d_o\dot{m}}{A_{cross}\mu}\right)^{a_2} \tag{2.71}$$

$$a = \frac{a_3}{1+0.14\left(\frac{d_o\dot{m}_H}{A_{cf}\mu}\right)^{a_4}} \tag{2.72}$$

Where *j* is the Colburn-factor for an ideal tube bank, A_{cross} is the cross flow area calculated at the centreline of the shell between baffles. The Colburn-factor is a function of the *Re* number and the area used in the velocity calculation is based on the minimum cross section flow area as calculated at the shell diameter. The effect of temperature variation in the boundary is neglected and the uncertainty associated with this correlation is $\pm$15% [8]. The values of the coefficients in Equations (2.71) to (2.72) is tabulated in Table 2-10.

Table 2-10 Empirical coefficients for calculating the Colburn factor [32]

Layout	Re	a_1	a_2	a_3	a_4	b_1	b_2	b_3	b_4
30°	10^5-10^4	0.321	-0.388	1.450	0.519	0.372	-0.123	7.00	0.500
	10^4-10^3	0.321	-0.388			0.486	-0.152		
	10^3-10^2	0.593	-0.477			4.570	-0.476		
	10^2-10	1.360	-0.657			45.10	-0.973		
	<10	1.400	-0.667			48.00	-1.000		
45°	10^5-10^4	0.370	-0.396	1.930	0.500	0.303	-0.126	6.59	0.520
	10^4-10^3	0.370	-0.396			0.333	-0.136		
	10^3-10^2	0.730	-0.500			3.500	-0.476		
	10^2-10	0.498	-0.656			26.20	-0.913		
	<10	1.550	-0.667			32.00	-1.000		
90°	10^5-10^4	0.370	-0.395	1.187	0.370	0.391	-0.148	6.30	0.378
	10^4-10^3	0.107	-0.266			0.0815	+0.022		
	10^3-10^2	0.408	-0.460			6.0900	-0.602		
	10^2-10	0.900	-0.631			32.100	-0.963		
	<10	0.970	-0.667			35.000	-1.000		

2.6.11 Zukauskas approach to estimating h_{id} for cross flow

The Zukauskas correlations are recommended for estimating h_{id} in a cross flow arrangement for both staggered and in-line tubes. The layout of the tubes in tube plate FWH is typically staggered while they are in-line for header type heaters. Zukauskas uses the following general equation to evaluate the *Nu* number:

$$Nu = \frac{h_o d_o}{k} = a\,\mathrm{Re}^n\,\mathrm{Pr}^m \left(\frac{c_T}{c_{projected}} \right)^p \tag{2.73}$$

where the *Re* number is calculated using d_o as the assigned characteristic length.

The velocity used to calculate the *Re* number is the velocity (v_{max}) calculated in the narrowest clearance of the tube array plane. The clearance, in the array that was illustrated in Figure 2-22, is either at the transverse clearance ($c_T = P_T - d_o$) or at the projected clearance ($c_{projected}$):

$$c_{projected} = P_{projected} - d_o = \sqrt{P_L^2 + \left[\frac{P_T}{2} \right]^2} - d_o \tag{2.74}$$

The upstream velocity between the tubes is first calculated. This result is then used to calculate the maximum velocity by using the following relation of conservation of mass assuming constant density [13]:

$$v_{in}P_T = v_{\max}c_T \text{ or } v_{\max}c_{projected} \tag{2.75}$$

where v_{in} is the fluid velocity flowing through passage c_T.

Zukauskas developed these correlations from experimental work using a square shell i.e. there are an equal number of tubes in each row. However, in a tube plate type FWH the number of tube in a successive tube row increases. Therefore, in addition to the reported uncertainty there is an additional unquantifiable uncertainty associated with a tube arrangement that deviates from the ideal experimental set-up. Nevertheless, the reported uncertainty of $\pm$ 15% [13] will be adopted for this study.

In the case of a tube plate type FWH the circular arrangement of the tubes on the periphery can be converted to a rectangular arrangement in an attempt to adjust the FWH set-up to the experimental set-up of a square shell, this will form part of the methodology which is discussed in Appendix A.

2.7 Review of the external forced convection correlations for two-phase fluids

The surface area allocated to each zone is presented in Figure 2-30(a). The zone responsible for the largest heat transfer is the condensation (COND) zone as illustrated in Figure 2-30(b). This is expected, since FWHs used on power plants mainly function by condensing steam from the turbine extractions. It was observed thus far that the largest uncertainty is associated with estimating *h* on the shell side of a single phase STHE. The two-phase correlations for both a horizontally orientated and vertically orientated surfaces will be presented in this section including their associated uncertainty.

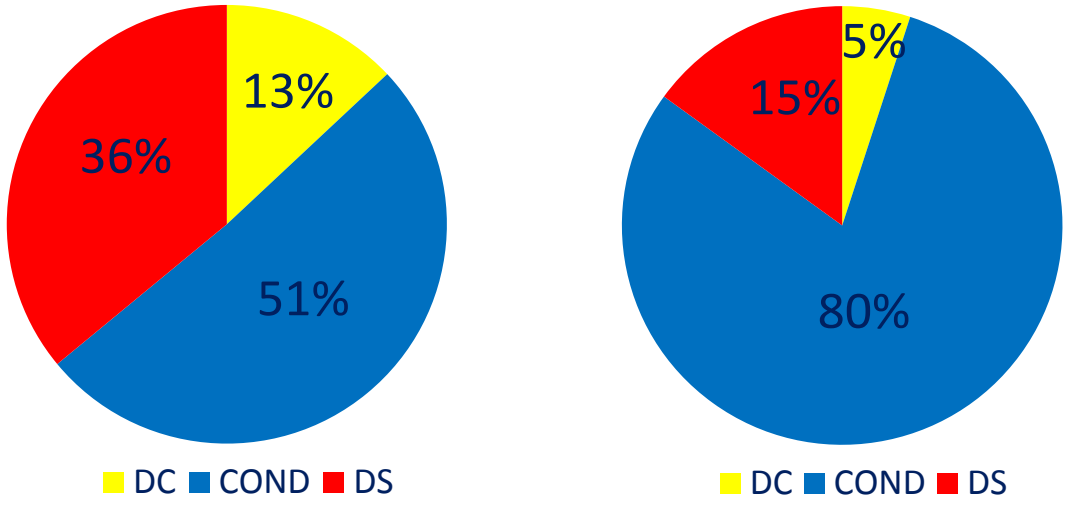

(a) Surface Area (b) Heat Transfer

Figure 2-30. Approximate heat transfer and surface area contribution in each zone of a typical 3 zone FWH [33]

2.7.1 Condensation zone arrangement

The flow arrangement through a horizontal tube plate type heater was illustrated in Figure 2-10 and for a vertical tube plate type heater it is illustrated below in Figure 2-31(a). The flow path of the steam relative to the tubes, whether the tubes are orientated vertical or horizontal, in the COND zone is assumed to be cross flow. Impingement plates are fitted in the region of the steam inlets in order to reduce tube erosion where a DS is not present. The steam then distributes evenly across the length between the support plates. This is also applicable for header type FWHs.

A vertically orientated FWH may result in a reduction of COND zone surface area because a portion of the tubes may be submerged in the condensate. An alternative design philosophy, applicable to vertical header type FWHs, is to allow the DC to occupy the entire bottom region of the vessel as illustrated in Figure 2-31(b).

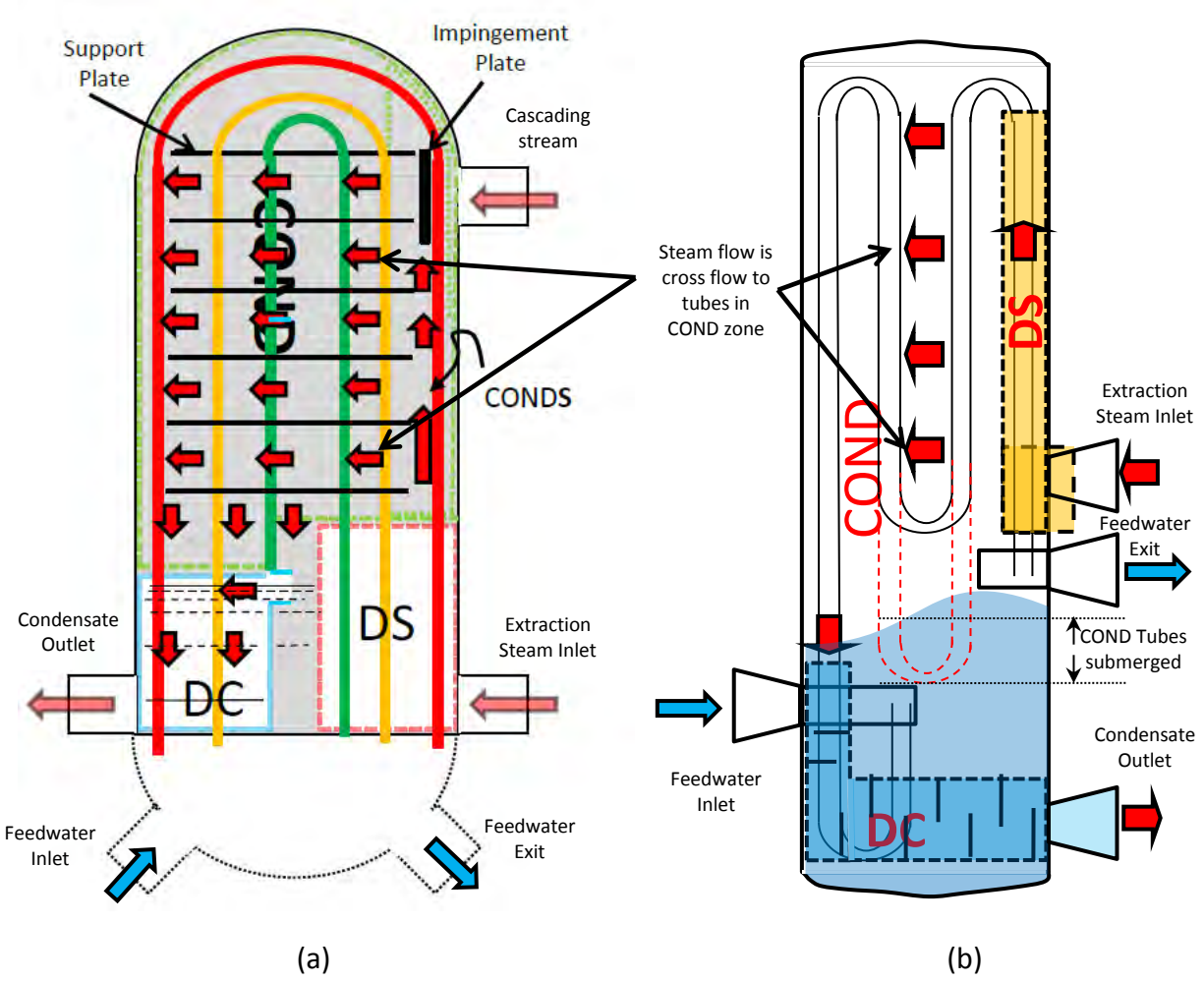

Figure 2-31. Steam and condensate flow path through a vertical tube plate (a) and header type (b) FWH

2.7.2 Condensation

A fluid that is saturated steam (i.e. not superheated) will condense when it comes into contact with a cold surface that is maintained at a temperature below its saturation temperature. Latent heat is transferred to the surface during the condensation process without the fluid temperature changing. The droplets of condensing liquid initially manifest on the surface and coalesce as condensation proceeds. This is called drop-wise condensation. When the boundary layer thickness increases, condensation now occurs at the vapour/liquid surface. At this point the surface will be flooded with layer of water, this is called film-wise condensation. Film-wise condensation is the predominant mechanism in FWHs and is the focus of the study.

2.7.3 Condensation over vertical tubes

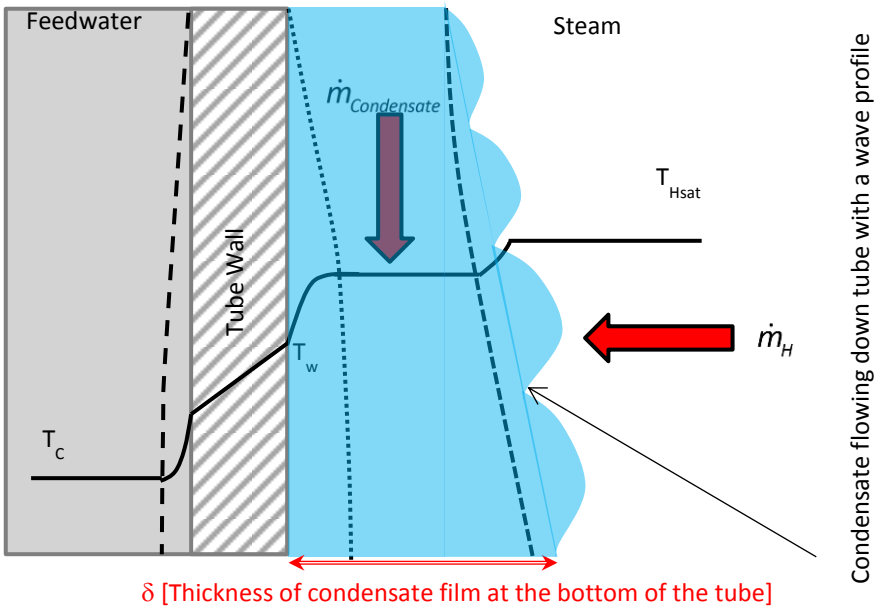

Figure 2-32. Temperature profile through the condensate film with trickling flow in the laminar region in the presence of quiescent steam flow

The steam flow is directed across the tubes by the support plates and the temperature profile in the boundary layers is presented in Figure 2-32. Condensation occurs on the tube length (*L*) between the support plates. The condensate then runs across the support plate to the periphery and overflows to the condensate drain nozzle. Nusselt derived the equation for calculating the average heat transfer coefficient for the condensation of saturated steam over a vertical plate. This expression is presented in Equation (2.76) and is also applicable to condensation over a vertical tube [34] but was formulated under the following assumptions:

- The vapour is saturated and only transfer latent heat i.e. no sub-cooling occurs.
- The flow regime of the condensate film is laminar and the vapour flow is quiescent. This implies that the condensate trickles down the tube under the influence of gravity. This is called gravity condensation and the Nusselt number corresponding to this type of condensation is identified as Nu_{gr}.

  If a large steam flow is present, it will assist the downward flow of condensate and in so doing will decrease the thickness of the condensate boundary layer and improve heat transfer. This assisted type of condensation is called vapour shear condensation (Nu_{sh}) and will only be discussed when covering the topic of condensation over horizontal tubes.
- Heat is transferred through the film via conduction.
- There is no resistance to heat transfer with the vapour at the condensate film surface.

The flow regime in the COND zone of a FWH is assumed to be turbulent since $Re_{vertical}$ (Equation (2.78)) is typically greater than 1800 [35]. This expression for calculating h (Equation (2.76)) can also be written in terms of dimensionless parameters and is presented in Equation (2.77). The expressions for wavy laminar flow conditions and turbulent conditions are also presented. A step change in the h is observed when the $Re_{vertical}$ number is greater than 30. This improvement is attributed to the formation of ripples or waves on the vertical length of the tube. The step change, applicable to the range $30 < Re_{vertical} < 1800$, is reported to be between 20% to 50% higher than that predicted by Nusselt [36]. The following laminar relations are multiplied by the maximum improvement predicted under wavy conditions ($30 < Re_{vertical} < 1800$):

$$h = 150\% \cdot 0.943 \left(\frac{k_l^3 \rho_l^2 \Delta\hbar_{lg} g}{\mu_l L \left[T_{Hsat} - T_w \right]} \right)^{1/4} \tag{2.76}$$

$$h = 150\% \cdot 1.47 \left(\mathrm{Re}_{vertical} \frac{\mu_l^2}{k_l^3 \rho_l^2 g} \right)^{-1/3} \tag{2.77}$$

$$\mathrm{Re}_{vertical} = \frac{\rho_l v_l}{\mu_l} D_e = \frac{\rho_l v_l}{\mu_l} \frac{4(\pi \mathrm{d}_o \delta)}{\pi \mathrm{d}_o} = \frac{4\left(\rho_l v_l \delta \pi \mathrm{d}_o\right)}{\pi \mathrm{d}_o \mu_l} = \frac{4\left(\dot{m}_H / n_t\right)}{\pi d_o \mu_l} \tag{2.78}$$

where $\Delta\hbar_{lg}$ is the latent heat of vapourisation, L is the tube length between support plates, n_t is the number of tubes, δ is the film thickness, T_{Hsat} is the saturation temperature on the shell side and T_w is the average tube wall temperature in the COND zone.

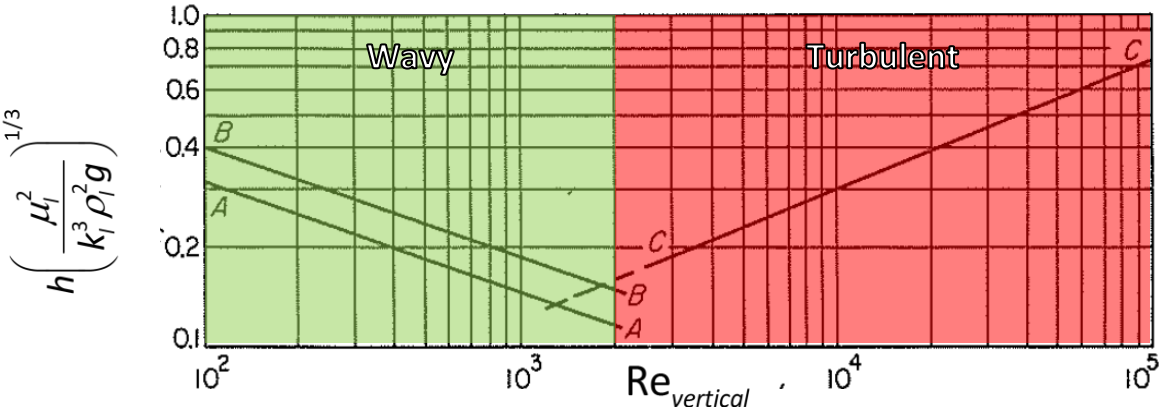

Figure 2-33. The two flow regimes associated with film condensation [36]

The length of tube, *L*, is calculated by dividing the tube's single pass length (L_{pass}) by the standard support spacing recommended by HEI [9], this varies between 0.7 m to 1.2 m. The *h* decreases as the $Re_{vertical}$ increases in the laminar region. This is indicated by line A-A in Figure 2-33 and the Line B-B represents the trend of *h* with regards to condensation over horizontal tubes. A further drop in *h* is experienced in the wavy region as the $Re_{vertical}$ increases, as illustrated in Figure 2-33.

Cengel and Ghajar [35] reports that *h* in the wavy-laminar flow region, $30 < Re_{vertical} < 1800$, can also be estimated using the correlation proposed by Kutateladze in Equation (2.79):

$$h = \frac{\mathrm{Re}_{vertical,wavy}\, k_l}{1.08\mathrm{Re}_{vertical,wavy}^{1.22} - 5.2}\left(\frac{g\mu_l^2}{\rho_l^2}\right)^{1/3} \tag{2.79}$$

where $Re_{vertical,wavy}$ is defined as follows:

$$\mathrm{Re}_{vertical,wavy} = \left\{\left[4.81 + \frac{3.70Lk_l\left(T_{Hsat} - T_w\right)}{\mu_l \Delta\hbar_{\mathrm{lg}}}\right]\left(\frac{g\mu_l^2}{\rho_l^2}\right)^{1/3}\right\}^{0.82} \tag{2.80}$$

McCabe, Smith and Harriott [36] reports that Kirkbride and Badger developed a correlation that envelopes the turbulent region and is presented as Equation (2.81). It is applicable for a $Re_{vertical}$ number greater than 2100 [36]:

$$h = 0.0076\mathrm{Re}_{vertical}^{0.4}\left(\frac{\mu_l^2}{k_l^3\rho_l^2 g}\right)^{-1/3} \tag{2.81}$$

The line C-C in Figure 2-33 was plotted using the Kirkbride and Badger correlation.

Cengel and Ghajar [35] reports that Labuntsov developed the following relation for turbulent flow of condensate over a vertical plate ($Re_{vertical} > 1800$) and is described by Equation (2.82):

$$h = \frac{\mathrm{Re}_{vertical,\mathrm{turb}}\, k_l}{8750 + 58\mathrm{Pr}^{-0.5}\left(\mathrm{Re}_{vertical,turb}^{0.75} - 253\right)}\left(\frac{g\mu_l^2}{\rho_l^2}\right)^{1/3} \tag{2.82}$$

where $Re_{vertical,turb}$ is defined as follows:

$$\mathrm{Re}_{vertical,turb} = \left\{\left[\frac{0.0690Lk_l\mathrm{Pr}^{0.5}\left(T_{Hsat} - T_w\right)}{\mu_l \Delta\hbar_{\mathrm{lg}}}\right]\left(\frac{g\mu_l^2}{\rho_l^2}\right)^{1/3} - 151\mathrm{Pr}^{0.5} + 253\right\}^{4/3} \tag{2.83}$$

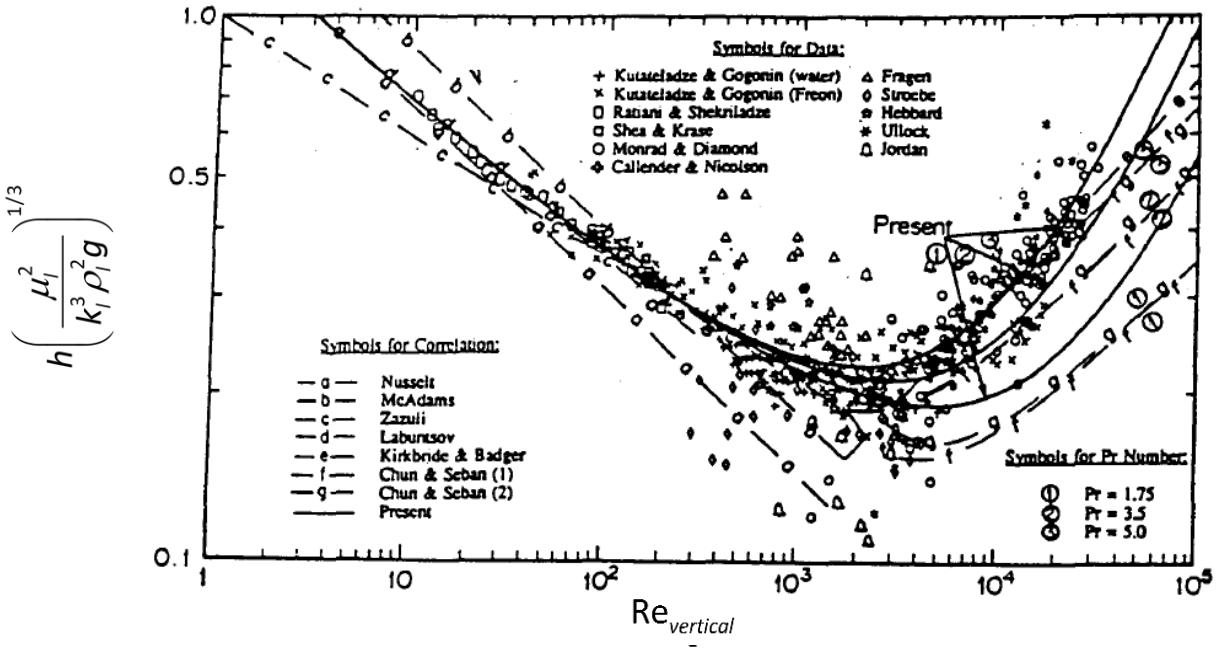

Figure 2-34. Film-wise condensation heat transfer on a vertical surface (Pr = 1.75 for water) [37]

The Nusselt correlation is referenced in other thermal models [38][39] even if the flow regime exceeds the laminar region. One wavy and two turbulent correlations will be applied in this study, see Table 2-11. A comprehensive study was performed by Chun and Kim [37] to determine the uncertainty associated with several correlations including those developed by Nusselt and Labuntsov. Chun and Kim [37] compared the prediction of several correlation to experimental data, that was previously published, which is succinctly illustrated in Figure 2-34. The sharp transition between the wavy-laminar and the turbulent flow regime that was discussed in Figure 2-33 is also observed in Figure 2-34. The uncertainty associated with Nusselt and Labuntsov correlations was determined in the laminar and wavy flow regime and the maximum uncertainty was reported to be 33% and 4%, respectively. The maximum uncertainty associated with the Kirkbride and Badger correlation is reported to be 7% by Kubin, Hirs and Plasek [37].

Table 2-11 Uncertainty associated with correlations used to estimate *h* for condensation over plain vertical plate [37]

Correlation	Uncertainty	Flow regime	Equation
Nusselt (wavy)	33%	wavy -laminar	(2.76)†
Kutateladze	7%‡	wavy-laminar	(2.76)
Kirkbride and Badger	7%	turbulent	(2.81)
Labuntsov	4%*	turbulent	(2.82)

† Use Equation (2.76) and multiply by the 150% wavy-laminar factor

‡ The reference for this uncertainty is [40] and it is for condensation inside a tube

* Although this correlation is applicable to turbulent conditions the uncertainty was determined under wavy-laminar conditions

The consequence of vapour shear, which reduces the film thickness and thereby pre-empts the onset of the turbulent regime, is not considered for vertical condensation. The method proposed by Butterworth, that incorporates vapour shear, is comprehensive and is discussed by Thome [41] but will not be incorporated in this study.

Inundation in vertically orientated FWH

The original formulation of the Nusselt relation (Equation (2.76)) assumes that all the condensate from a given tube drains as a continuous laminar sheet along the vertical length of the tube. However, in a vertically orientated FWH the tube supports are installed horizontally, which breaks the formation of a continuous laminar sheet along the entire length of the tube, as illustrated in Figure 2-35.

The condensate runs radially along the horizontal support to the periphery and then drops vertically. Hence, a continuous laminar sheet is only present between horizontal supports. Therefore, the L to be used in these correlations is the length of tube between horizontal supports ($L_{B,COND}$), which varies between 0.7 m and 1.2 m.

The effect of the entrainment of droplets in the steam, between the successive supports, that may result in a thicker boundary layer (inundation) is not analysed.

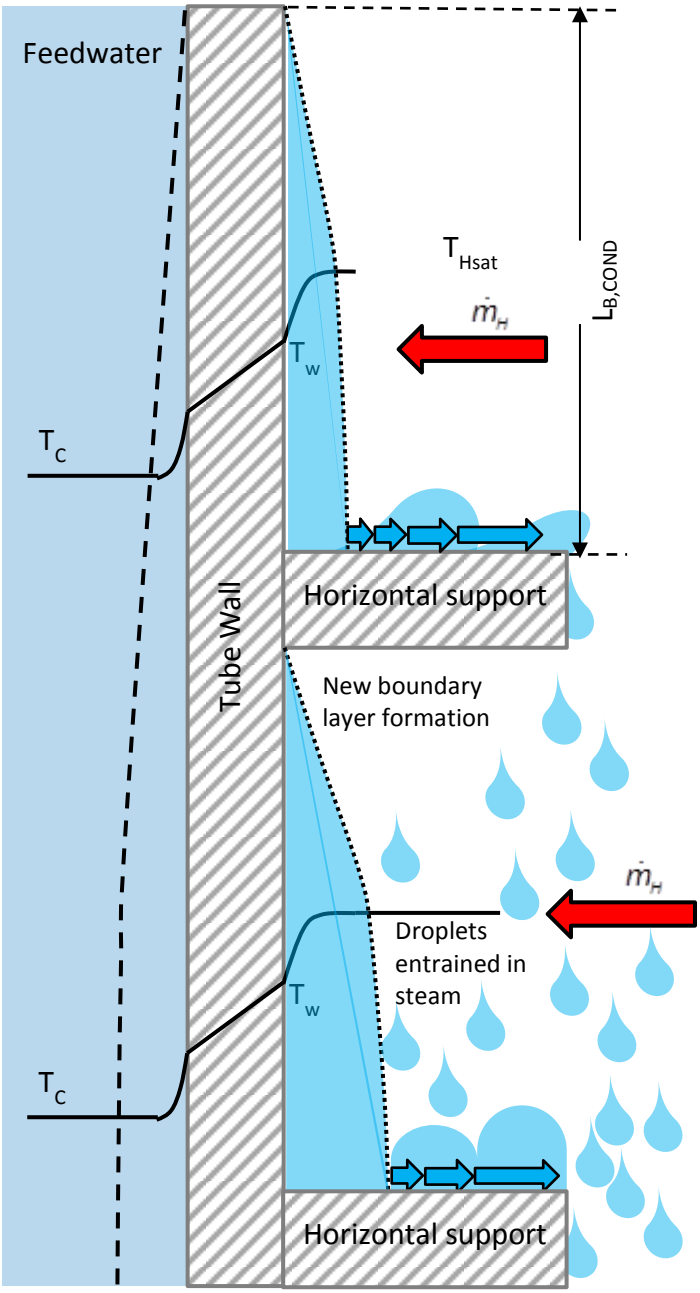

Figure 2-35. Boundary layer formation on vertical tubes between two successive tube bundle supports/baffles

There are extensive correlations that describe the effect of inundation in horizontally orientated tube bundles but no correlation could be obtained for vertical orientated bundles.

2.7.4 Condensation over horizontal tubes

The average heat transfer coefficient for the condensation of saturated steam over a horizontal tube where the film remains in the laminar flow region is described below [8]:

$$h = 0.725\left(\frac{k_l^3 \rho_l^2 \Delta\hbar_{lg} g}{\mu_l d_o \left[T_{Hsat} - T_w \right]} \right)^{1/4} \tag{2.84}$$

The equation also assumes that the tube temperature remains constant but most importantly that the vapour stream is quiescent i.e. the liquid film departs the tube under gravity and is not assisted by vapour velocity, which is also referred to as vapour shear. An alternative equation in terms of dimensionless units is presented below:

$$h = 1.51\left(\mathrm{Re}_{horizontal} \frac{\mu_l^2}{k_l^3 \rho_l^2 g} \right)^{-1/3} \tag{2.85}$$

$$\mathrm{Re}_{horizontal} = \frac{4}{\mu_l} \frac{\dot{m}_H}{L n_t} \tag{2.86}$$

This expression is adjusted for a bank of tubes as the condensate drops under gravity from one tube to another, which is referred to as inundation. The boundary layer thickness will increase on the successive tubes, due to the accumulation of condensate, and will result in a drop in *h* for each successive tube in the stack. Kern suggested the correction to Equation (2.85) that is presented below:

$$h = 0.725\left(\frac{k_l^3 \rho_l^2 \Delta\hbar_{lg} g}{\mu_l d_o \left[T_{Hsat} - T_w \right]} \right)^{1/4} n_{t,\mathrm{column}}^{-1/6} \tag{2.87}$$

where $n_{t,column}$ is the number of tubes in the column of the tube array.

The influence of vapour shear can be incorporated into a single expression Equation (2.88), which was developed by Shekriladze and Gomelauri [13]. The *h* is representative of the heat transfer coefficient on the first tube and the Kern correction will be applied to the column of tubes to account for inundation.

$$h = \frac{k_l}{d_o} 0.64\left(\mathrm{Re}_{TwoPhase} \left(1 + \left(1 + 1.69F \right)^{1/2} \right)^{1/2} \right) \tag{2.88}$$

$$F = \frac{\mu_l \Delta \hbar_{lg} g d_o}{\left(\frac{\dot{m}_H}{\rho_g A}\right)^2 k_l \left[T_{Hsat} - T_w\right]} \tag{2.89}$$

The *Re* number, also called the two phase *Re* number, is calculated using Equation (2.90). This equation uses the steam velocity but liquid properties [13].

$$\mathrm{Re}_{TwoPhase} = \frac{v_g d_o \rho_l}{\mu_l} = \frac{\frac{\dot{m}_H}{A} d_o \frac{\rho_l}{\rho_g}}{\mu_l} \tag{2.90}$$

where the subscripts *l* and *g* designated the phase of the fluid which is liquid and gas, respectively. *A* represents the free flow area through which the steam flows.

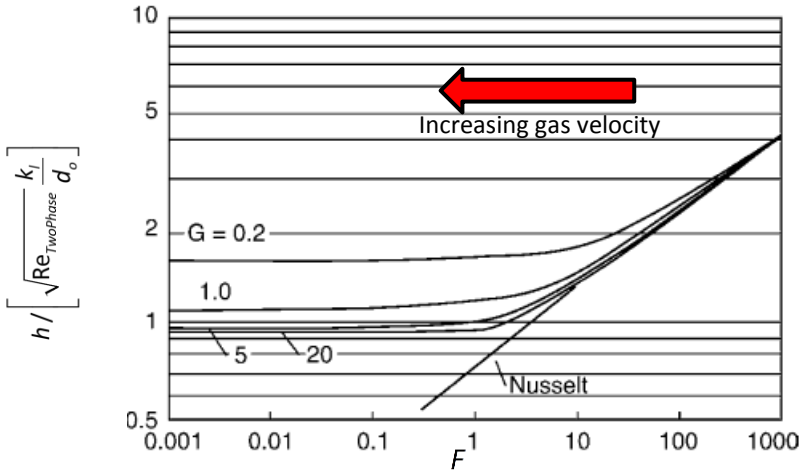

Figure 2-36. Influence of gas velocity on *h* [7]

The *h* is plotted in Figure 2-36 as a function of the dimensionless parameter *F.* The expression on the x-axis is an indirect measure of gas velocity, where the gas velocity squared is inversely proportional to *F*, see Equation (2.89). Hence, *h* coincides with the Nusselt relation (Equation (2.84)) at low gas velocities, which corresponds to large values of *F*.

Several researchers have developed a correlation where both the gravity contribution (Nu_{gr}) and shear contribution (Nu_{sh}) is incorporated. The dominant contributor is then determined by using a Euclidean norm or a variation thereof. The model of Butterworth [8] recommends the following norm to account for the interaction between gravity and shear effects to predict *h* on a particular tube in the column i.e. h_N. The following expression predicts *h* on the first tube (h_1) and the Kern correction will be used to determine an average value over the particular vertical stack of tubes.

$$h_1 = \left(\frac{1}{2} h_{sh}^2 + \left(\frac{1}{4} h_{sh}^4 + h_{gr}^4 \right)^{1/2} \right)^{1/2} \tag{2.91}$$

The Nu_{gr} term in the Butterworth model represents the idealised Nusselt relation in Equation (2.87) while the Nu_{sh} term is computed as follows:

$$Nu_{sh} = 0.59 \frac{k_l}{d_o} \mathrm{Re}_{TwoPhase}^{0.5} \tag{2.92}$$

The model of McNaught [42] recommends the following norm to account for the interaction between gravity and shear effects:

$$h = \frac{k_l}{d_o} \left(Nu_{gr}^2 + Nu_{sh}^2 \right)^{1/2} \tag{2.93}$$

The Nu_{gr} term in the McNaught model represents the idealised Nusselt relation in Equation (2.87) while the Nu_{sh} term is computed as follows:

$$Nu_{sh} = 1.26 Nu_l \left(\frac{1}{X_{tt}} \right)^{0.78} \tag{2.94}$$

where X_{tt} is the Lockhart-Martinelli parameter.

$$X_{tt} = \left(\frac{1-x}{x} \right)^{0.9} \left(\frac{\rho_g}{\rho_l} \right)^{0.5} \left(\frac{\mu_l}{\mu_g} \right)^{0.1} \tag{2.95}$$

The parameter x represents the steam quality and a value of 0.8 is assumed for the analytical calculation since the upper condition of the correlation is 0.8 [8] and it will therefore correspond to the first tube in the column. The Nu_l represents the Nusselt number of a free flowing liquid and is presented in Equation (2.96). The Re_l for FWHs are substantially greater than 300, this was apparent when analysing the data in this study.

$$\begin{gathered} h = \frac{k_l}{d_o} C_1 \mathrm{Re}_{TwoPhase}^{C_2} \mathrm{Pr}_l^{0.34} \\ C_1 = 0.273 \text{ and } C_2 = 0.635 \text{ when } 300 < \mathrm{Re}_l \leq 2x10^5 \\ C_1 = 0.124 \text{ and } C_2 = 0.700 \text{ when } \mathrm{Re}_l > 2x10^5 \end{gathered} \tag{2.96}$$

The model of Honda [42] recommends the following norm to account for the interaction between gravity and shear effects:

$$h = \frac{k_l}{d_o}\left(Nu_{gr}^4 + Nu_{sh}^4\right)^{1/4} \tag{2.97}$$

Gstöhl and Thome [41] modified the Honda model to fit their experimental results and it is presented below:

$$h = \frac{k_l}{d_o}\left(\left(1.2\mathrm{Re}_{TwoPhase}^{-0.3}\right)^4 + \left(0.04\mathrm{Re}_{TwoPhase}^{0.2}\,\mathrm{Pr}_l^{1/3}\right)^4\right)^{1/4} \tag{2.98}$$

Briggs [42] reports the uncertainty of these correlations based on a study he conducted using previously published experimental data. The spread of experimental results, gathered by Briggs [42], is plotted in Figure 2-37 and is visually compared with the prediction of the McNaught correlation that is represented by the diagonal line. The uncertainty of the correlations used in this study is tabulated in Table 2-12.

Table 2-12 Uncertainty associated with correlations used to estimate *h* for condensation on plain horizontal tubes that incorporates both gravity and vapour shear interactions [41]

Correlation	Uncertainty	Flow regime	Equation
Shekriladze and Gomelauri	48%	turbulent	(2.88)
McNaught	27%	turbulent	(2.93)
Gstöhl and Thome / Honda	25%	turbulent	(2.98)

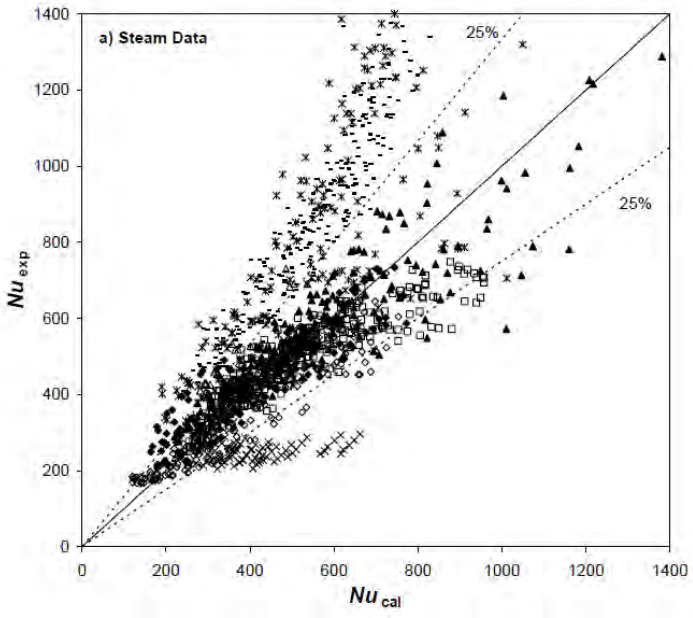

Figure 2-37. Comparison of the McNaught correlation to experimental data [42]

3. Literature review

The flow arrangement through a FWH was discussed briefly in order to explain the selection of the correlations presented in Chapter 2. A review of the literature pertaining directly to FWH layout and subsequent modelling will be reviewed in this chapter, which includes the application of the above correlations.

3.1 Basic geometry of feedwater heaters and flow distribution

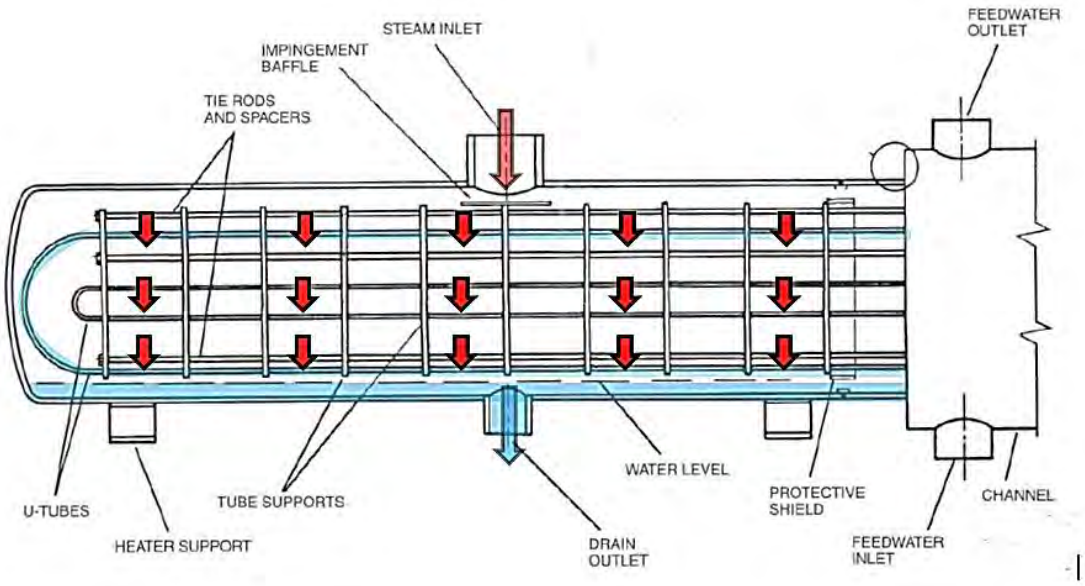

Figure 3-1. Single zone horizontally mounted tube plate type FWH [9]

Figure 3-2. 3D image of a single zone horizontally mounted tube plate type FWH used on a nuclear power station [43]

3.1.1 FWH design

All the FWHs in the Eskom fleet are STHE and are essentially condensers in their most basic form, also called a single zone FWH. Ideally, saturated steam will enter the FWH and condense against horizontally or vertically mounted tubes. The condensate then collects at the bottom of the heater and is conveyed out of the FWH via the drain outlet. On the shell side, the steam flow is distributed across the tube supports and is assumed to flow in a cross flow manner across the FWH bundle. Even though the configuration may be a multi-pass arrangement the ε relation, Equation (2.24), for two phase cross flow is still applicable. The pressure in the shell is determined by the bled steam extraction pressure, which in turn determines the saturation temperature of the outlet condensate. The feedwater flows on the tube side through a multitude of parallel pipes from the inlet to the outlet, each conveying the same mass flow of water.

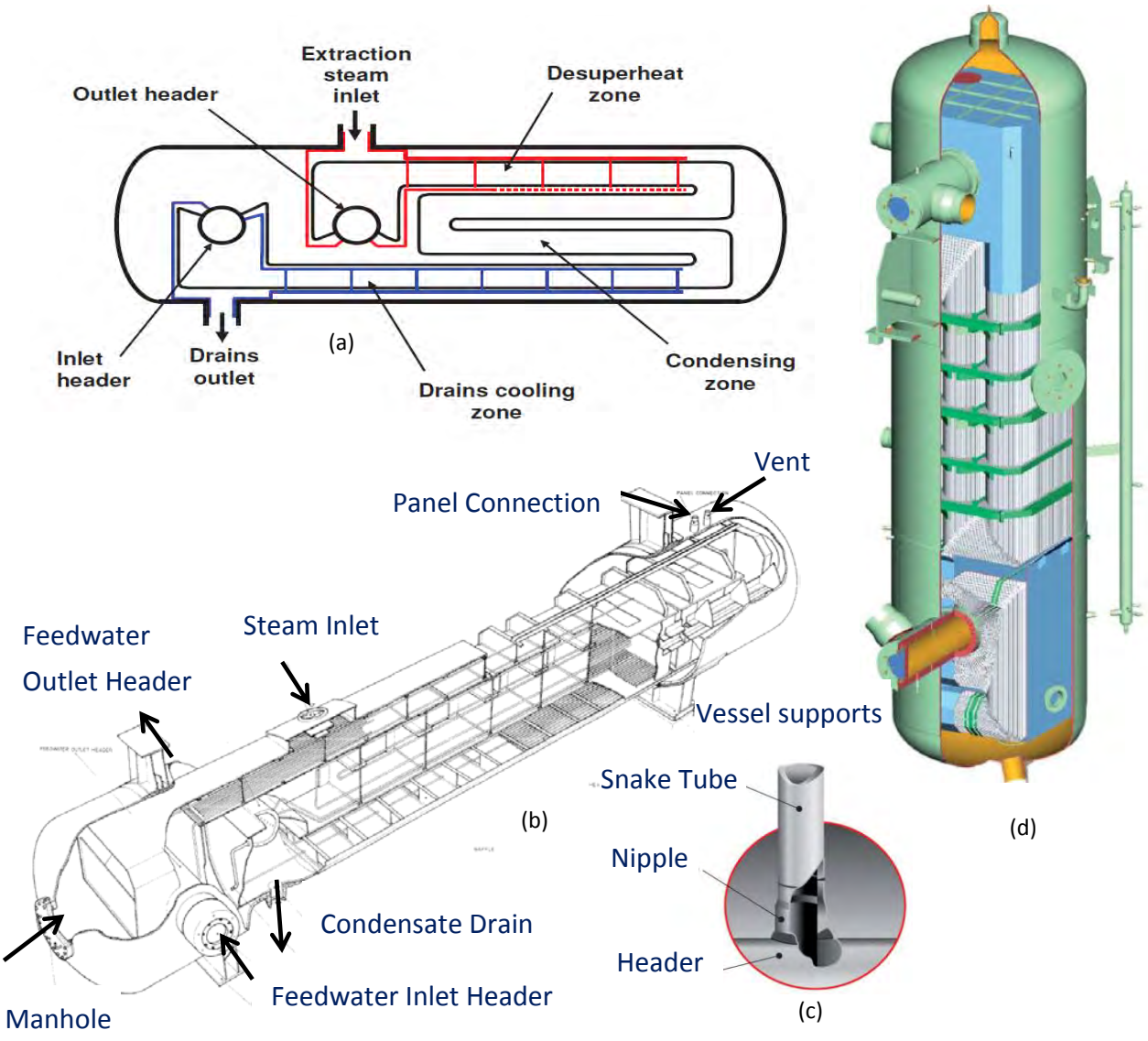

Figure 3-3. Horizontally and vertically mounted header type FWH [44][45][1]

Tube plate vs header type FWHs

The type of FWH is determined by the method used to secure the U tubes to the vessel. There are two types of STHE utilised within the Eskom fleet viz. tube plate type and header type.

In a tube plate type FWH the ends of the U-tubes are attached to a single plate, called the tube plate (see Figure 3-1 and Figure 3-2). The feedwater enters a chamber called the channel and is distributed at the tube plate through each U-tube. The feedwater makes only two passes through a tube plate type FWH shell.

In a header type FWH the inlet and outlet ends of the tubes are attached to separate cylinders or headers (Figure 3-3). The tubes are attached to the headers using nipples as illustrated in Figure 3-3 (c). These headers penetrate the shell where they are connected to the feedwater inlet and outlet nozzle. The number of passes in these heaters varies between 3 to 4 and the zones in header type FWH is illustrated in Figure 3-3 (a).

The decision for selecting the specific type of FWH is dependent on economics and operating conditions. Header type FWHs can better accommodate large thermal expansions which are experienced at higher operating conditions or load flowing plants, but they are expensive to manufacture due to the large magnitude of closely spaced tube-to-nipple welds. A thicker tube plate is required at high operating conditions, which drives up the cost of manufacturing a tube plate type FWH. A header type FWH may become more feasible to manufacture at this stage. The tube plate type is the most common LP FWH because it is more economical to manufacture under these LP conditions. Header type FWHs are therefore utilised as HP heaters if operating conditions are deemed high enough, or if station operation necessitates it. The HP FWHs analysed in this study are all header type except those at stations PS00 and PS05.

Horizontal vs vertical orientation

A FWH may be mounted vertically or horizontally. This choice is driven by layout constraints, as well as the choice to thermal expansion allowance and support design. For tube sheet FHWs, the location of the channel may be up or down as illustrated in Figure 3-4. The FWHs at station PS04 is of the channel up configuration.

For vertical FWHs, it is assumed that the steam flows in a cross flow manner as illustrated in Figure 3-4. The condensate collects at the bottom and the condensation happens on a vertical surface as described in Section 2.7.3. The orientation is of no significance in the single phase DS and DC zones as orientation does not impact single phase heat transfer.

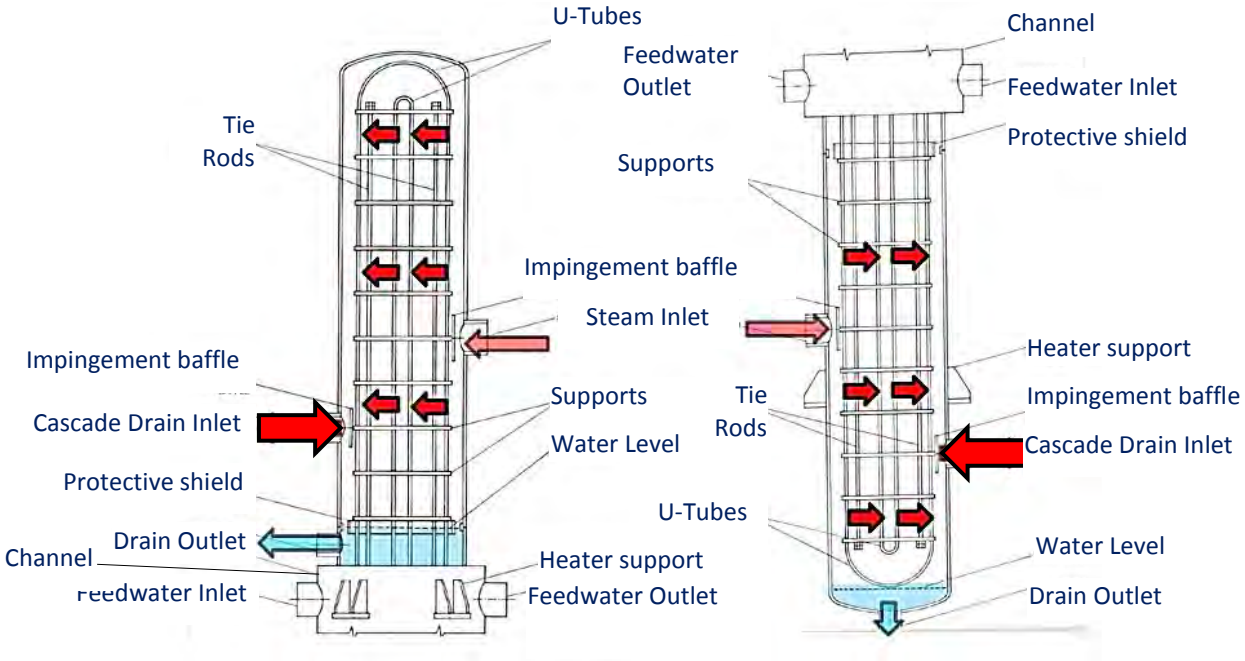

Figure 3-4. Condensing zone vertically mounted channel down and channel up tube plate type FWH [9]

Flash tank

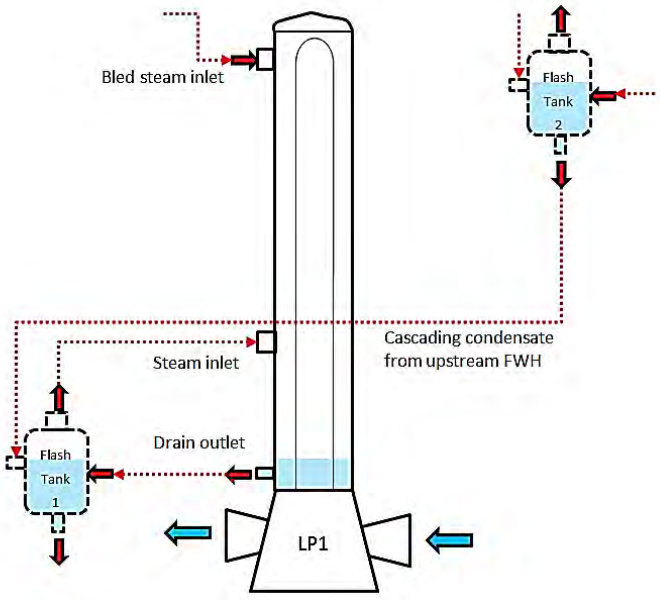

Figure 3-5. Condensing zone horizontally mounted channel down FWH fitted with a flash tank

The hot drains from the shell side are not normally directed to the condenser but may cascade to the lower ordered FWH, as is illustrated for a vertically mounted FWH in Figure 3-5. However, the pressure in the lower ordered FWH will also be lower making flashing of steam a concern on the connecting lines. A flash tank is installed to allow for the separation of saturated steam and water, which is also illustrated in Figure 3-5. The drains of a horizontally mounted FWH may also be fitted with a flash tank as is the case at station PS06.

Drains cooler or sub-cooling (DC) zone

Flashing may also be avoided by sub-cooling the condensate before it exits the drain outlet. This can be achieved by ensuring that the tubes near the outlet drain remains flooded. Not only must the tubes be flooded but a flow path must be created to ensure maximum heat transfer. This flow path is created by constructing a shroud around the flooded tubes. The shroud has an inlet and an outlet that is located at the outlet drain. The region enclosed by the shroud can be viewed as a single pass STHE and is called the drains cooler (DC) zone, see Figure 3-6 and Figure 3-7.

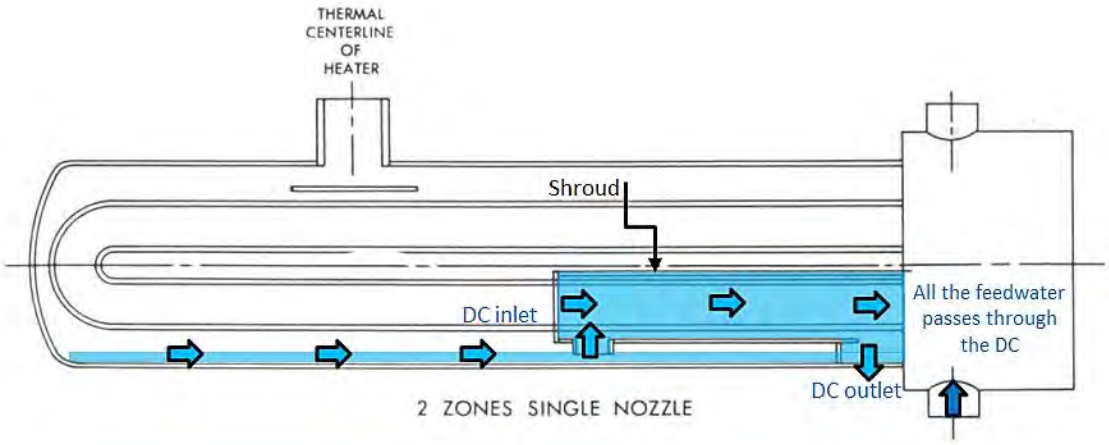

Figure 3-6. Horizontally mounted FWH with COND and short DC zones [9]

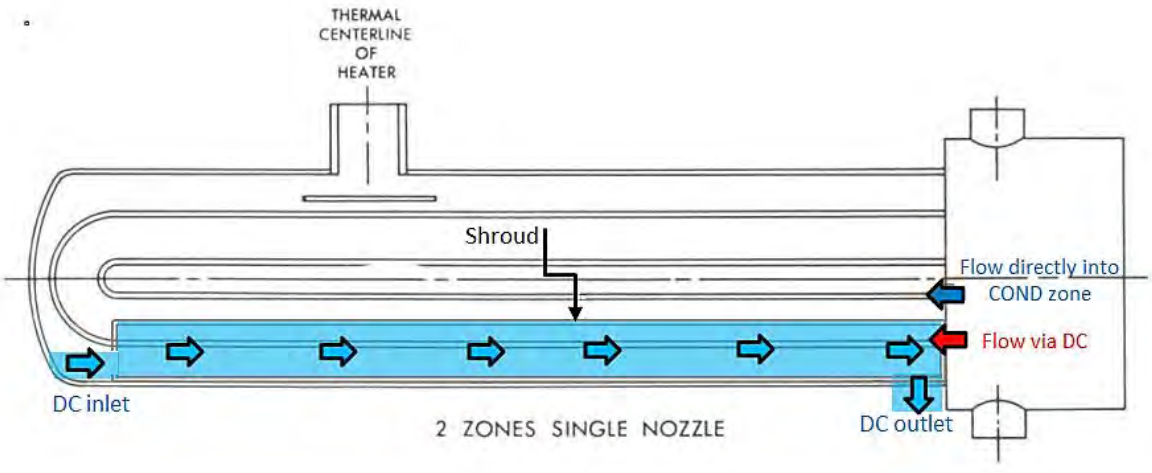

Figure 3-7. Horizontally mounted FWH with COND and long DC zones [9]

The heat transfer through the enclosure can further be improved by installing baffles. These baffles disrupt the flow path by either introducing a series of cross flow regions or vortex shedding regions by installing segmented or grid baffles, respectively. These regions have a larger heat transfer capability than solely having a parallel flow region. In addition to the internal differences, the designer may also alter the length of the DC. A DC that spans a portion of the single pass

length and houses all the tubes in the single pass is called a short DC, see Figure 3-6. A DC that spans the entire length of a single pass and houses a portion of the tubes in the single pass is called a long DC, see Figure 3-7. The advantages and disadvantages of a long DC compared to a short DC are listed in Table 3-1.

Table 3-1 Salient differences between a long DC versus a short DC [46]

Long DC	Short DC
Only a portion of the total feedwater flows through a long DC while the balance of the feedwater flows directly into the COND zone.	All the feedwater flows through a short DC.
The long DC makes use of the normal working level to ensure that the DC remains submerged. There is more effective liquid level control, which allows the performance parameters to be maintained at their optimum values.	The short DC makes use of a barometric effect which is not reliable at low loads.
There are two streams entering the COND zone. The first steam enters the COND zone at the inlet temperature while the second stream enters the COND zone at a slightly elevated temperature after passing through the DC.	In a short DC all the entering feedwater is increased to an elevated temperature before entering the COND zone. A higher exit feedwater temperature is achieved in identical FWHs with a short DC than that of the long DC for the same DC surface area.
A larger shroud is required for a long DC. A long DC is fitted at the bottom of the cylindrical vessel where the number of tube in each successive row decreases towards the bottom.	A smaller shroud is required for a short DC which reduces the total weight of the FWH.

De-superheating (DS) zone

At this stage of the chapter it was assumed that the extraction steam is supplied at saturated conditions to the shell side inlet. However, extraction steam from the HP turbine and some LP turbines are supplied at superheated conditions. This implies that sensible heat must first be removed from the steam before condensation will commence. It has also been established, from Table 2-2, that the magnitude of the heat transfer coefficient (*h*) for steam is substantially lower than that of liquid water or during condensation. This implies that a portion of the surface area that was allocated for condensation in the COND zone would be consumed for sensible heat removal before condensation commences.

This consumed COND zone surface area, used for de-superheating, may be reduced if the *h* is improved for the de-superheating of the steam. This is generally achieved by increasing the velocity of the steam over the dedicated tubes used for de-superheating. The velocity may be increased by constructing a narrow envelope inside the FWH such that the steam does not distribute evenly across the single pass length but rather enters and exits this narrow envelope. The physical boundary of this envelope is called the shroud and this region is referred to as the de-superheating (DS) zone, see Figure 3-8. The heat transfer may be improved further by installing baffles that create cross flow regions, which is also illustrated in Figure 3-8.

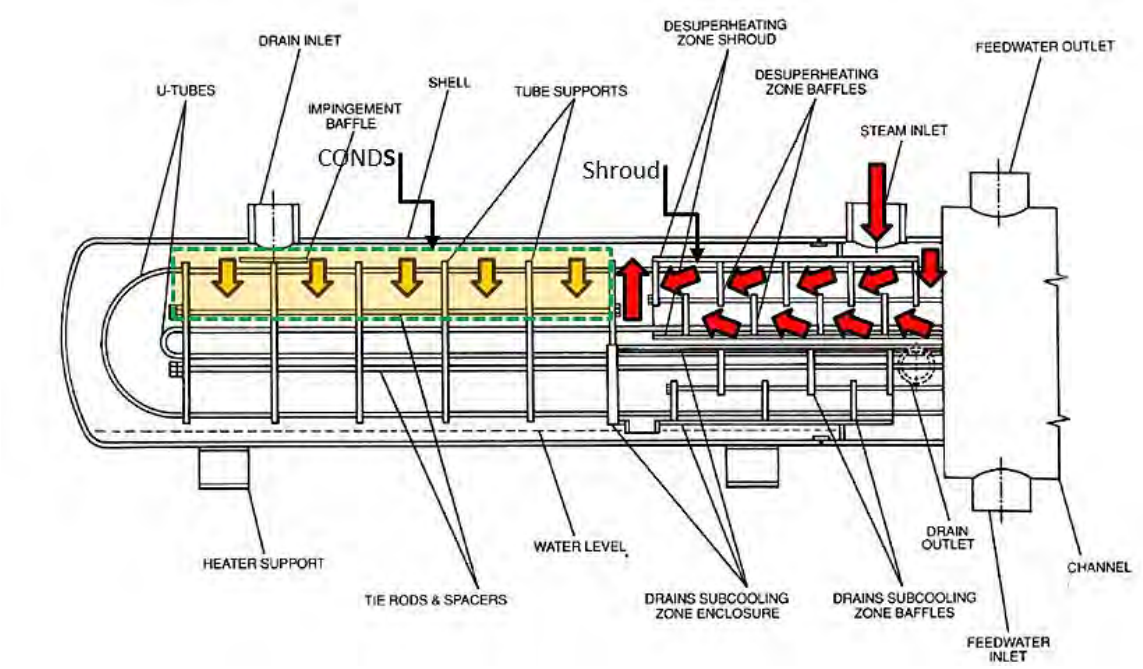

Figure 3-8. Horizontally mounted FWH with COND, short DC and DS zones [3]

Removal of excess superheat (CONDS) sub-zone

A short introduction of this sub-zone is considered here but it will only be discussed in more detail in Section 4.1 as the treatment of this sub-zone is unique to this study. Suffice to say that the steam flow in this region occurs in a cross flow manner. This zone will only exist if the steam enters the COND zone with excess superheat either from the DS exit or directly into the COND zone from the steam nozzle. The presence of both a single phase and two phase region in the same zone was briefly introduced in Section 2.3.2 and was illustrated in Figure 2-10. This single phase sub-zone may either be assigned a single phase or two phase heat transfer correlation depending on the tube wall temperature [47]. However, in this study the single phase heat transfer properties are adopted as a conservative consideration irrespective of the tube temperature. This region will be identified as the COND**S** sub-zone because it is located within the COND zone but does not participate in condensation see Figure 3-8.

Summary

From a modelling point of view, the hierarchy of FWH designs is illustrated in Figure 3-9. At each branch a different set of heat transfer correlations is required. Also, the allocation of heat transfer areas to the various zones is highly dependent on the eventual layout.

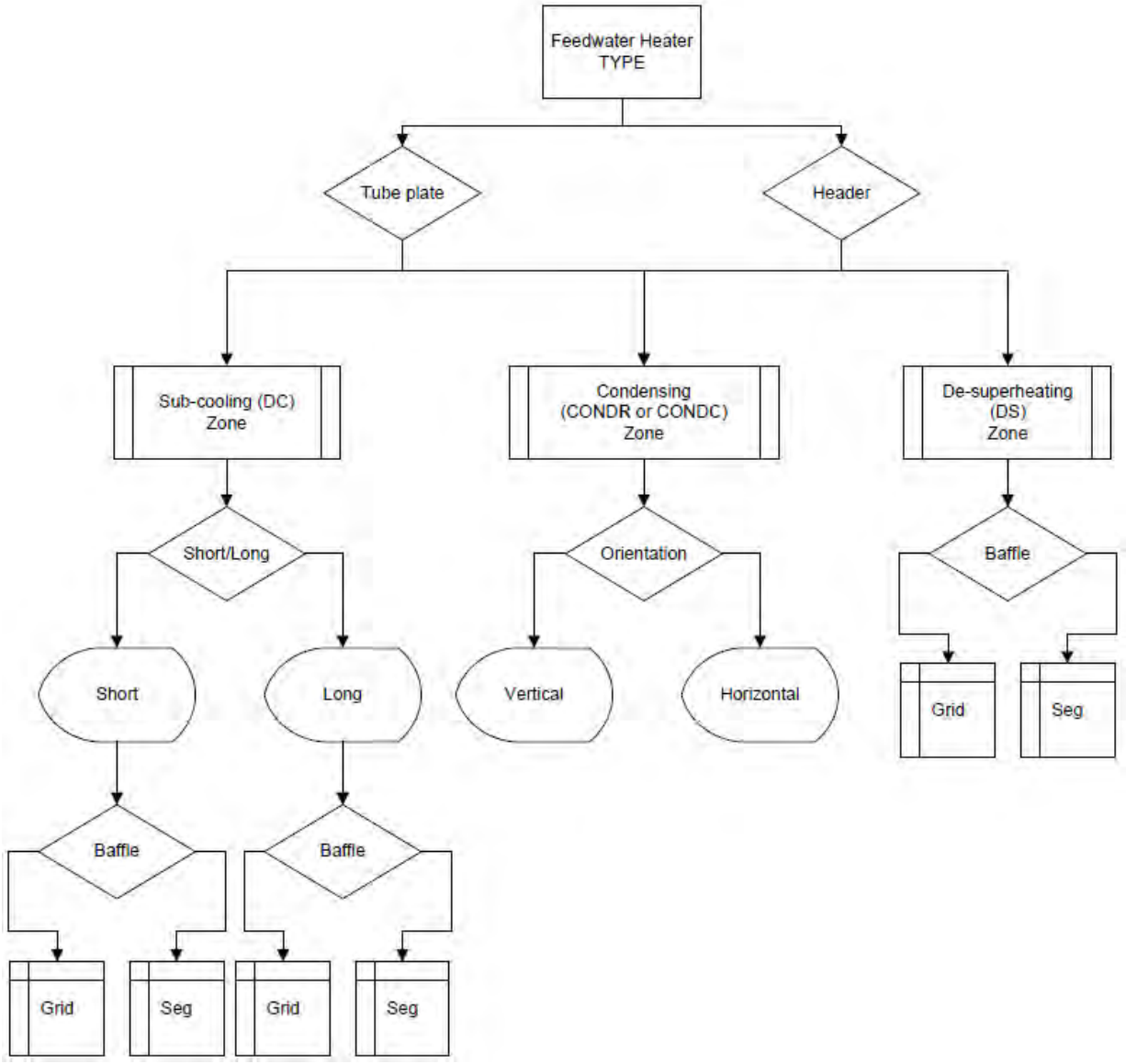

Figure 3-9. The possible zones and configurations of FWHs

3.1.2 Zone, sub-zone and stream assignment

The stream designation for both the feedwater and extraction steam will be described below with the aid of illustrations applicable to a 3 zone tube plate type FWH without a COND**S** sub-zone.

Feedwater streams

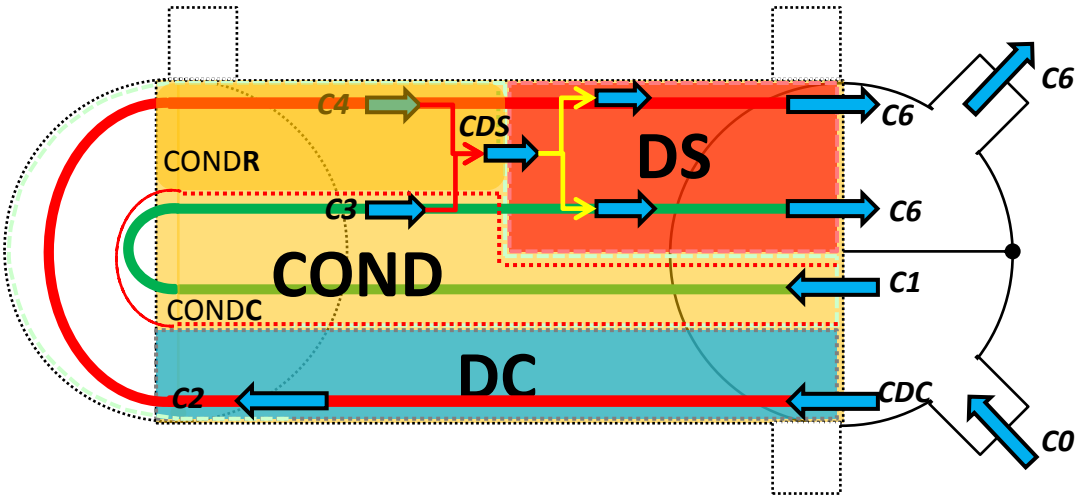

Figure 3-10. Stream designation for the tube side of a tube plate type FWH with 3 zones

The feedwater stream is designated with a subscript *C* as it is the cold stream and the flow path is illustrated in Figure 3-10.

The feedwater inlet stream is designated as stream *C0*. This flow is then distributed at the tube plate either through the DC or directly through the COND zone, which is depicted in Figure 3-10. The region located in the COND zone that convey feedwater through the DC is called the COND**R** sub-zone while the remaining portion of the COND zone is referred to as the COND**C** sub-zone.

The stream *CDC* has the identical thermodynamic properties as stream *C0* but distinguishes the mass flowrate distribution that enters the DC. The feedwater that passes through the DC receives sensible heat from the condensate that is being sub-cooled and exits as stream *C2*.

The stream *C1* that enters the COND zone (or COND**C** sub-zone) directly absorbs the latent heat and exits as stream *C3*. The tubes that exit the DC zone, stream *C2*, will enter the COND**R** sub-zone and also absorb the latent heat from shell side and exit as stream *C4*.

It is assumed that streams *C3* and *C4* are homogenously mixed and exits as stream *CDS* before it enters the DS. Here sensible heat is transferred from the superheated extraction steam to the feedwater, stream *CDS*, and then finally exits as stream *C6*. The reason for assuming the mixed flow *CDS* stream is to ensure an analytical solution is possible for the DS. There is a slight

temperature difference between *C3* and *C4*, less than 1°C was observed for the horizontally mounted 3 zone tube plate FWH from station PS16, which supports the validity of this assumption.

Extraction steam streams

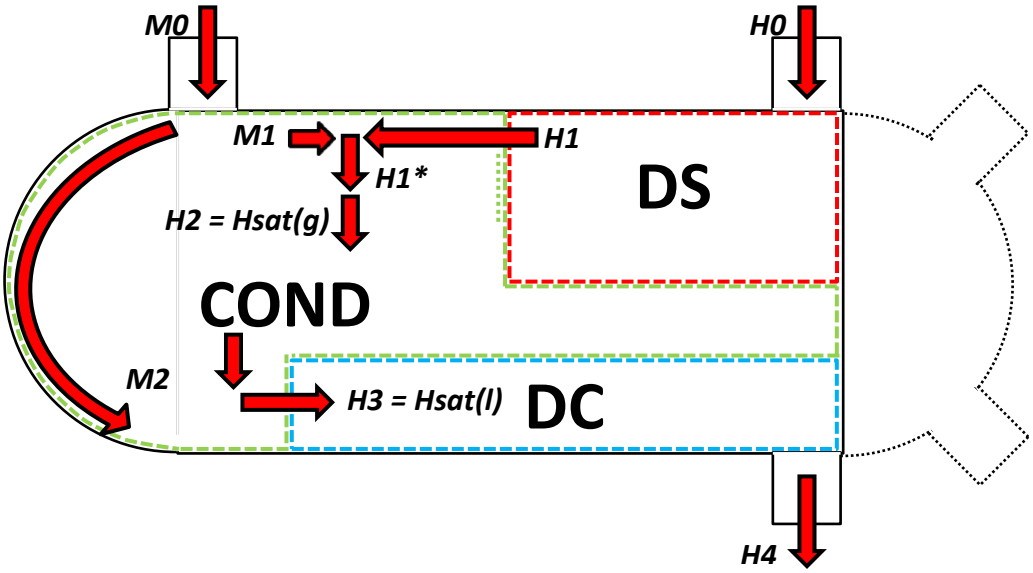

Figure 3-11. Stream designation for the shell side of a tube plate type FWH with 3 zones

The stream assignment for the extraction steam and cascade[1] stream is illustrated in Figure 3-11.

The cascading stream, *M0*, may flash on entry into the FWH during the de-pressurisation. The thermodynamic properties of this depressurised stream are captured by stream *M0**. The most important property will be the steam quality identified as x_{M0*}. The saturated vapour will now be theoretically separated from the saturated liquid as streams *M1* and *M2*, respectively.

Superheated extraction steam enters the shell side of the vessel as stream *H0* and immediately enters the DS. Sensible heat is transferred from the steam and is assumed to exit as saturated steam. The stream is identified as *H1* and is assumed to mix homogenously with the vapour portion of the cascading stream *M0*, if present. The mixed stream is identified as $H1^*$ and it is assumed to be saturated steam and therefore does not require the removal of excess superheat. Therefore, stream *H1** may be equated to stream *H2*.

The saturated steam is then split proportionally between COND**R** and COND**C** sub-zones according to their available surface area. The latent heat is then removed in the COND zone and the streams exits as saturated liquid. These streams then homogenously mix with the saturated liquid portion of the cascade, identified as *M2,* and enter the shell side of the DC as a single stream identified as *H3*. Finally, the saturated liquid is sub-cooled in the DC zone and exits as stream *H4*.

[1] Cascade flow is the condensate coming from higher pressure heaters downstream of the receiving FWH.

The various flow streams are now illustrated on a process flow diagram, see Figure 3-12. This diagram may be adjusted for other combinations e.g. a model with only 1 zone or 2 zones. A basic description of each stream is tabulated in Table 3-2. The condition where *H1** is not saturated steam (i.e. a degree of superheat still remains after DS) is handled by introducing a COND**S** zone. This will be explained in detail in section 4.1.1.

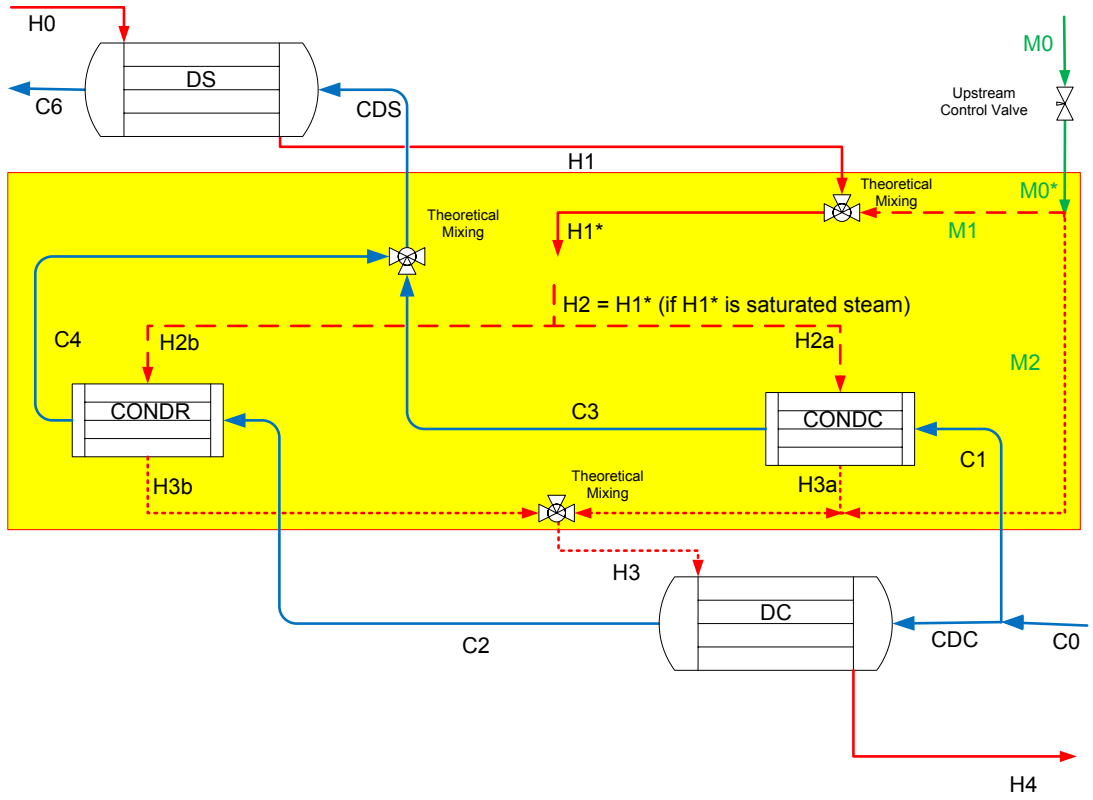

Figure 3-12. General process flow diagram for a 3 zone FWH

Table 3-2 Stream assignment for the process flow diagram describing a 3 zone FWH

Stream	Description	Stream	Description
C0	Inlet feedwater	**H0**	Inlet bled steam extraction
CDC	Fraction of *C0* entering DC	**H1**	Steam at exit of DS
C1	Fraction of *C0* entering COND**C**	**H1***	Steam mixture of H1 and M1
C2	Exit of DC	**H2**	Saturated steam
C3	Feedwater exiting COND**C**	**H2a/b**	Saturated water
C4	Feedwater exiting COND**R**	**H3**	Saturated water
CDS	Feedwater exiting COND	**H3a/b**	Condensate exit from DC
C6	Feedwater exiting DS	**H4**	Condensate exit from DC
		M0	Cascading stream inlet
		M0*	M0 that is depressurised in FWH
		M1	M0 that is saturated steam
		M2	M0 that is saturated liquid

3.1.3 FWH performance parameters

A FWH is required to increase the feedwater temperature such that the contracted terminal temperature difference (*TTD*) and drain sub-cooler approach (DCA) is achieved [9].

TTD is defined as the difference between the saturation temperature on the shell side and the outlet feedwater temperature on the tube side[2]. It is desired that the feedwater outlet temperature approach the saturation temperature on the shell side in order to achieve the maximum performance. The stream temperatures are illustrated in Figure 3-13 and calculated using Equation (3.1), below:

$$TTD = T_{Hsat} - T_{C6} \tag{3.1}$$

where T_{C6} and T_{Hsat} corresponds to the exit feedwater temperature and the shell side saturation temperature, respectively.

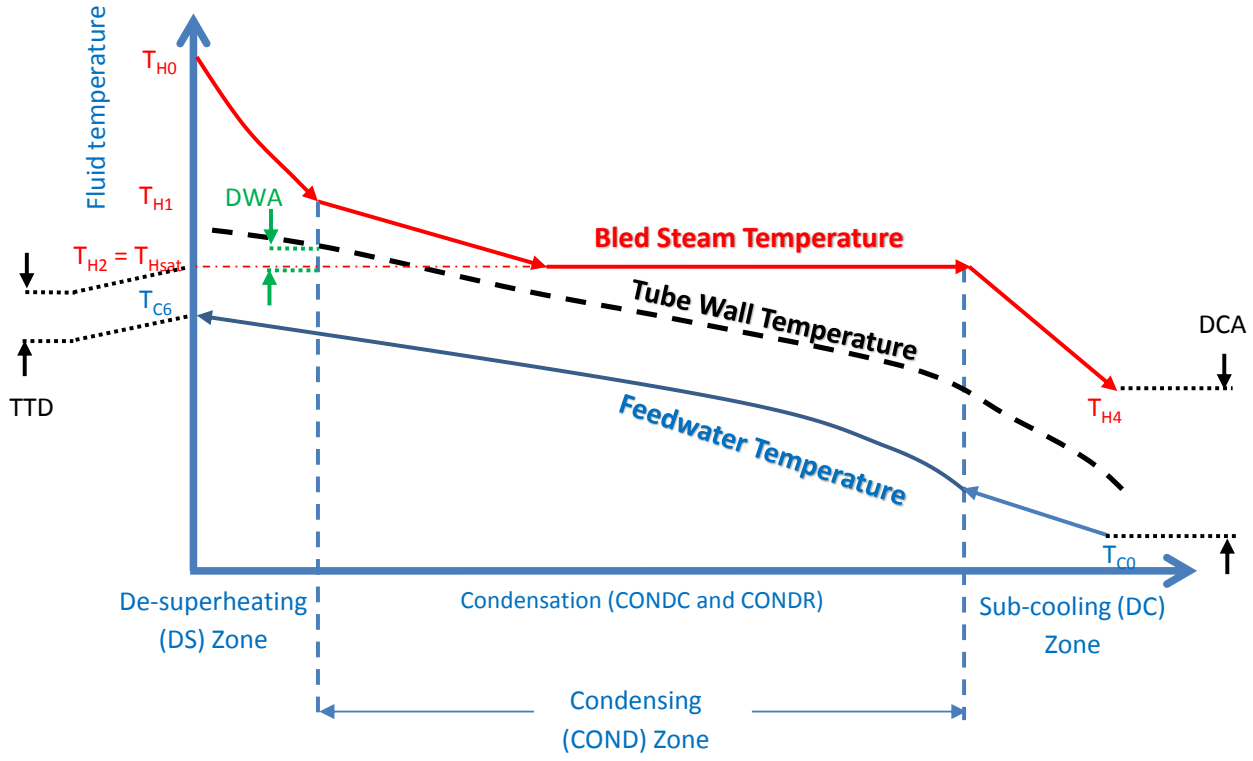

Figure 3-13. Performance parameters (TTD and DCA) depicted on the temperature profile

[2] Note that this definition is specific for FWHs. The more generic definition of TTD for heat exchangers simply considers the difference between the hot inlet and cold outlet temperature.

It is possible for the TTD to be less than zero if the heater is installed with a DS. This means the extraction steam is likely to be superheated and could heat the exiting feedwater above the saturation temperature.

DCA is the temperature difference between condensate leaving the shell side and the feedwater entering the heater on the tube side. Ideally an approach of the condensate temperature (T_{H4}) to the inlet feedwater temperature is desired. DCA is calculated as follows:

$$DCA = T_{H4} - T_{C0} \tag{3.2}$$

where T_{H4} was assigned in Figure 3-11 and corresponds to the exit condensate temperature while T_{C0} corresponds to the inlet feedwater temperature.

The steam temperature exiting the DS (T_{H1}), illustrated in Figure 3-13 and Figure 3-14, must have a degree of superheat such that the tube wall in this region remains above the saturation temperature. If this is not the case, steam will condense on the tube surface and together with the high fluid velocity in the shroud will result in the onset of rapid tube erosion. Hence, another parameter to monitor is the dry wall safety margin or approach (DWA). The DWA is depicted in Figure 3-14 and defined in Equation (3.3). The minimum DWA recommended is reported in literature to be 1^{o}C [9].

$$DWA = T_{wall} - T_{Hsat} \geq 1^{o}C \text{ or approximately } 2^{o}F \tag{3.3}$$

where T_{wall} is the tube wall temperature at the exit if the DS and T_{Hsat} corresponds to the shell side saturation temperature.

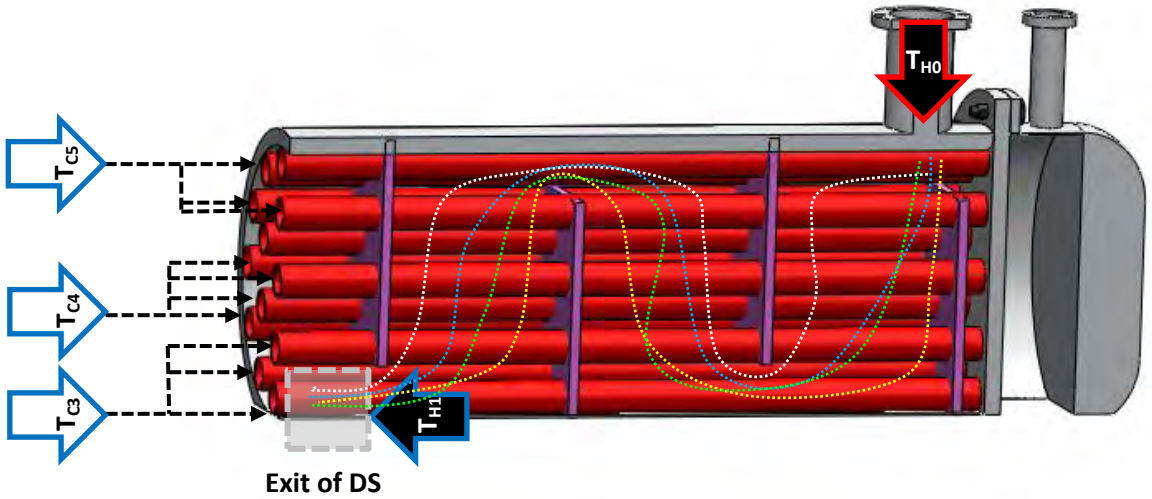

Figure 3-14. Cross section view through DS with the possibility of three different inlet tube temperatures applicable for a three zone heater [27]

The tube plate type FWH will have a maximum of three different tube side temperature streams for the 3 zone model, which will be explained later. Of the three temperatures, T_{C3} is likely to be the lowest temperature. The exit DS tube wall temperature can be estimated by equating the convective heat transfer across the tube at this point and re-arranging the equation to yield Equation (3.4):

$$T_{wall} = \frac{h_{H1} d_o T_{H1} + h_{C3} d_{in} T_{C3}}{h_{H1} d_o + h_{C3} d_{in}} \tag{3.4}$$

where the subscript *C3* and *H1 i*s assigned with reference to Figure 3-14 and corresponds to the tube side stream applicable to the tubes not passing through a DC and the steam stream exiting the DS, respectively.

3.2 Overview of FWH thermal models

In this section we will review previous thermal models that were published in open literature. The purpose of this review is to identify the methodology used in these models in order to establish a baseline model for the current study. The literature review revealed that only tube plate type FWHs, fitted with segmented baffles, where previously modelled. However, the area calculations are consistent for any FWH orientation and variation. The baseline model would later be expanded to make it applicable for any FWH variation in the Eskom fleet.

What is clear from the review is that there are 4 basic steps when developing a thermal model for a FWH:

- **Input step**: The inputs into the model must be fully specified.
- **Area calculation step**: The specification of *h* correlations requires flow area inputs. The flow areas for the cross and counter current flow regions are calculated using basic geometry. Surface area calculations are required for sub-zones in order to calculate their effectiveness.
- **Initialisation step**: Generate results for the entire stream by performing a crude once through calculation. A better approximation of the thermal properties can now be made with the inlet and the computed outlet temperatures in the next step.
- **Iterative step**: The initialisation step is then compiled into a programme loop that keeps iterating until all temperatures converge.

Results from thermal FWH models will differ based on the selection of *h* correlations and the associated area calculations. Hence, aspects from similar studies will be highlighted and discussed.

3.2.1 Antar, Zubair, Hussaini and Zubair model

Hussaini, Zubair and Antar [48] applied the LMTD method as well as a numerical model to a 3 zone FWH. They report that the maximum error between the analytical and numerical model was 0.8% when comparing the heat transfer rate (Q).

Heat transfer correlations

Table 3-3. Inputs

Geometric Data	
Orientation	0 []
A_{HCOND}	193.2 [m^2]
A_{HDC}	57 [m^2]
A_{HDS}	100 [m^2]
D_S	0.94 [m]
n_t	429
d_o	15.8 [mm]
th	1.3 [mm]
Baffle type	1 []
Operational Data	
m_{C0}	86.91 [kg/s]
T_{C0}	196.3 [^oC]
P_{C0}	120.569 [bars]
T_{H0}	372.16 [^oC]
PH0	30.337 [bars]
x_{H0}	1 []
m_{M0}	0.0001 [kg/s]
T_{M0}	234.5 [^oC]
P_{M0}	30.337 [bars]
x_{M0}	0 []
Detail geometric data	
B	482 [mm]
Bc	40.00% [%]
B	241.3 [mm]
Bc	30.00% [%]
Passes	2 []
Layout	30 [^{o}]
P_T	21.4 [mm]
P_L	21.4 m
th_{plate}	2.5 [mm]
th_{grid}	100 [mm]

The geometry and the operating conditions of the FWH analysed in their study is presented in Table 3-3. Their model was reconstructed from the information in the paper. This baseline model was the skeleton of the current model. A detailed description of the surface area calculations was not provided in this paper so the method used in another study (Koehler and Weber [46]) was adopted.

The following heat transfer correlations were used:

- h_{in}: Dittus and Boelter correlation (see Table 2-5)
- h_o: McAdams/ Kern correlation (see Equation (2.57))
- h_{COND}: Nusselt correlation (see Equation (2.84))

These *U* values were recalculated using the correlations and inputs from Table 3-3 and compared with the data reported in the paper [48], which is presented in Table 3-4. They use a short DC in their study and report that 17 baffles are installed and spaced at intervals of 0.07 m. However, when the baffles spacing is calculated using the DC surface area a value of 0.16 m is obtained. A larger U_{DC} is calculated with the reported baffle spacing of 0.07 m.

Table 3-4 Comparison of U reported and re-calculated

U **[W/m^{2}K]**	**Hussaini**	**Reconstructed short DC**
U_{DC}	1135	2734
U_{COND}	4185	4159
U_{DS}	592	621

Geometry and area calculations

The free flow area is an input to the *Nu* correlations. The method used by the McAdams correlation, applied to the shell side of the DC and DS, was described in Section 2.6.7.

The difference between a short and long DC is illustrated in Figure 3-15. Note that the McAdams method (Section 2.6.7) requires the longest chord to be used. The chord for a short DC corresponds to D_{shell} while it is shorter for a long DC.

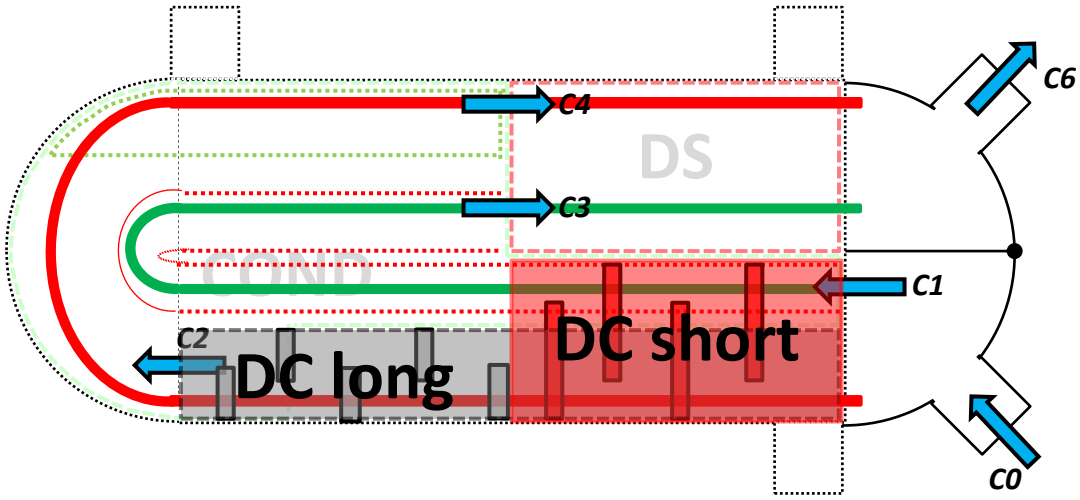

Figure 3-15. FWH fitted with either a long or short DC

The impact of using a long DC with the reconstructed model was also analysed and the results are presented in Table 3-5. Recall that Table 3-1 predicted that a FWH fitted with short DC would transfer more *Q* than the identical FWH fitted with a long DC, this is supported by the statement made in Table 3-1.

Table 3-5 Comparison of performance parameters under clean conditions

Parameter	Hussaini, Zubair and Antar	Reconstructed long DC	Reconstructed short DC
TTD	-1.5°C	-1.0°C	-1.2°C
DCA	0.8°C	0.3°C	0.3°C
Q_{DC}	1.04 MW	1.14 MW	1.15 MW
Q_{COND}	12.32 MW	12.02 MW	12.60 MW
Q_{DS}	2.33 MW	2.24 MW	1.74 MW
Q	15.69 MW	15.40 MW	15.49 MW
$\dot{m}_{H0}$	6.87 kg/s	6.61 kg/s	6.65 kg/s

Hussaini, Zubair and Antar [48] assumes that the steam exits the DS at the saturation temperature. However, they emphasise that the exit temperature will corresponds to a tube wall temperature that is equal to the shell side saturation temperature (T_w - T_{Hsat} = 0^oC).

Antar and Zubair [38] extended their work and evaluated the impact of fouling on the performance of the identical heater. The numerical model is used and the heat transfer in the COND zone, on shell side, is assumed to occur via latent heat transfer only. The sensible heat transfer that will also occur in the COND zone is not discussed in the numerical method i.e. the steam exits the DS zone at T_{Hsat}.

The shortcoming of the Hussaini, Zubair and Antar model is that it does not incorporate the dry wall limiting criteria i.e. that the steam will exit at a temperature (T_{H1}) in equilibrium with a tube temperature maintained at T_{Hsat}. This was incorporated in the reconstructed model and it is observed that the heat transfer increases and decreases in the COND and DS zones, respectively. However, instead of specifying the exit temperature it may be more prudent to calculate it and verify how far the tube wall temperature, T_{wDS} deviates from T_{Hsat}.

3.2.2 Koehler and Weber model

Koehler and Weber [46] developed a general thermal model for FWHs with long DCs for the purpose of evaluating vendor bids when FWHs have to be replaced once the 10% plugging limit is exceeded. They reported that the model was necessary to challenge the vendor before an ASME PT 12.1 performance commissioning test is performed. It should also be noted that the thermal model derivations in ASME PT 12.1 applies to a short DC only.

Heat transfer correlations

The heat transfer correlations is not mentioned in the 1992 report [46] but it is documented by Weber and Minner [49]. The following heat transfer correlation was used while the remaining coefficients are computed arithmetically using the manufacturers reported values:

- h_{in}: Dittus and Boelter correlation (see Table 2-5)
- h_o: Uses manufacturer's value for U_{DS} and U_{DC} then solves for h_o using Equation (2.12)
- h_{COND}: Uses manufacturer's value for U_{COND} then solves for h_{COND} using Equation (2.12)

The use of the vendors values is acceptable for performance testing but an empirical correlation is required if the vendors results are to be challenged before commissioning.

Geometry and area calculations

Koehler and Weber used the standard PEPSE® design mode sub-model whereby each zone is represented by a separate heat exchanger and the surface area calculations was performed as follows:

- The feedwater flowrate distributes proportionally to the number of tubes present in that zone i.e. $\dot{m}_{C0} \propto n_t$. The number of tubes in a long DC zone is calculated as follows:

$$n_{tDC} = \frac{A_{HDC}}{L_{PerPass} \cdot \pi d_o} \tag{3.5}$$

The length of a tube in a long DC is assumed to be the total tube length divided by the number of passes. The mass flowrate into the DC can be estimated as follows:

$$m_{CDC} = m_{C0} \frac{n_{tDS}}{n_t} \tag{3.6}$$

- The DS has 2 sub-zones because the feedwater in the tubes running through the DC will be warmer than the balance of the feedwater not passing through the DC.
- Similarly the COND zone will also have 2 sub-zones: COND**R** is the condensing zone that contains the n_{tDC} tubes while the COND**C** is the condensing zone that contains the balance of the tubes. The heat transfer areas, making use of symmetry, are calculated as follows:

$$A_{HCONDC} = A_{HDC} \frac{n_{tDC}}{n_t - n_{tDC}} + \frac{n_t - n_{tDC}}{n_t} \left(A_{HCOND} - A_{HDC} \frac{n_{tDC}}{n_t - n_{tDC}} \right) \tag{3.7}$$

$$A_{HCONDR} = A_{HCOND} - A_{HCONDC} \tag{3.8}$$

- A more general formulation is derived below:

$$A_{HCONDR} = A_{HDC} \left(Passes - 1 \right) - \frac{n_{tDC}}{n_t} A_{HDS} \tag{3.9}$$

$$A_{HCONDC} = A_{HCOND} - A_{HCONDR} \tag{3.10}$$

- The model assumes that the steam exiting the DS is at T_{Hsat}.

Koehler and Weber claim that their long DC model provides accurate results based on several validation tests conducted with commissioning test data. This approach has therefore been adopted in the methodology of this model and the detail equations are presented in Appendix A.

3.2.3 Summary of *h* correlations used in other FWH models

The Fernández, Valdés and Tristán [50] model was developed to analyse the thermal performance of FWHs on nuclear power stations. They apply the LMTD method with an F-factor correction for deviation from counter current flow for the on-design validation and the effectiveness-NTU method for the off-design conditions. Xu, Yang and Sun [39] argued that the *Re* number in their

study was less than 1600 and therefore only considered gravity controlled condensation. A summary of the *h* correlations used in the four FWH models is presented in Table 3-6.

Table 3-6 Summary of the *h* correlations used in four FWH models

Parameter	**Antar** [38]	**Weber** [49]	**Fernández** [50]	**Xu** [39]
h_{in}	Dittus & Boelter	Dittus & Boelter	Rabas	Dittus & Boelter
h_o	McAdams/ Kern	vendor value	McAdams/ Kern	$0.27Re^{0.65}Pr^{0.36}$
h_{oCOND}	Nusselt	vendor value	Not specified	Nusselt
Surface area calc	Not specified	see Section 3.2.2	Not specified	Not specified

3.2.4 Proprietary software

ChemPlant Technology, Ltd. developed a 3 zone FWH rating model that outputs TTD, DCA and *h* performance parameters [51]. The model applies the LMTD method and it is assumed that the steam exits the DS at saturated steam conditions while the condensed liquid that enters the DC is at saturated liquid conditions.

The HEXTRAN simulation program, developed by SimSci, is an application that was intended as a complete heat exchanger design package [52]. This program also contains add-ons that can only be accessed by Heat Transfer Research, Inc. (HTRI) and Aspentech® HTFS members. HTRI and Aspentech® HTFS have their own software packages that can perform a performance evaluation of a heat exchanger. Chemstations CC-THERM software [53] also enables the design or performance evaluation of a heat exchangers.

Eskom does not have a license for any of these software packages, and will most likely not acquire a license in the future. That makes this current study very applicable to Eskom.

3.3 Standards and codes

The thermal and pressure drop calculations determines the heat transfer, operating conditions and minimum geometry requirements. These models are not explicitly described in any specific standard but are typically developed by the vendor. However, there is some guidance in the standards that is in-line with the general theory.

After completing the thermal design, the next step in the design process is to perform the mechanical design. The designer primarily looks at specifying the wall thickness of the shell, tube, tube sheet and water box. The mechanical design procedure and limits, such as flow induced vibration, are well documented in standards and codes namely:

- Heat Exchanger Institute (HEI) Closed Feedwater Heaters standard 8th Edition [9]
- Standards of the Tubular Manufacturers Association (TEMA) [11]

- ASME VIII – Boiler and pressure vessel code
- EN 13445 – Unfired pressure vessel code
- BS 5500 - Specification for unfired fusion welded pressure vessels

The performance of a FWH during commissioning or during routine performance tests is evaluated in accordance with ASME PTC 12.1 [54] within the Eskom fleet. The thermal model used to evaluate the results from this performance test is presented in Figure 3-16 and agrees with the structure of other models using the NTU method.

3.3.1 HEI

The Heat Exchanger Institute (HEI) Closed Feedwater Heaters standard 8th Edition provides detailed mechanical design guidelines for a FWH. It does not provide any thermal design guidelines but mentions a temperature safety margin that should be respected to avoid rapid erosion of tubes at the exit of the DS. This is termed the DWA temperature, and is described in Section 3.1.3.

3.3.2 TEMA

TEMA is an American general heat exchanger mechanical design standard and does not provide any thermal guidelines for designing a FWH. Most of the FWHs in the Eskom fleet were manufactured by European vendors that do not conform to the TEMA standard. The TEMA standard provides mechanical design guidelines for general STHE, which is sometimes referenced in the absence FWH specifications.

Several Eskom FWH specification sheets do not report the transverse pitch (P_T) and therefore standard pitch sizes were adopted. TEMA recommends a P_T of $1.25d_o$.

3.3.3 EPRI - Classical Heat Exchanger Analysis

The EPRI report [19], Classical Heat Exchanger Analysis, describes the thermal model used for the rating of a single phase steady state STHE. It also discusses the uncertainty analysis associated with the thermal model including the contributing uncertainty of measurement instruments, which is not the focus of this study because vendors do not report an uncertainty in their specification sheet.

The selection of the *h* correlations, used in the EPRI report, will be discussed including the distribution of uncertainty in the model calculation.

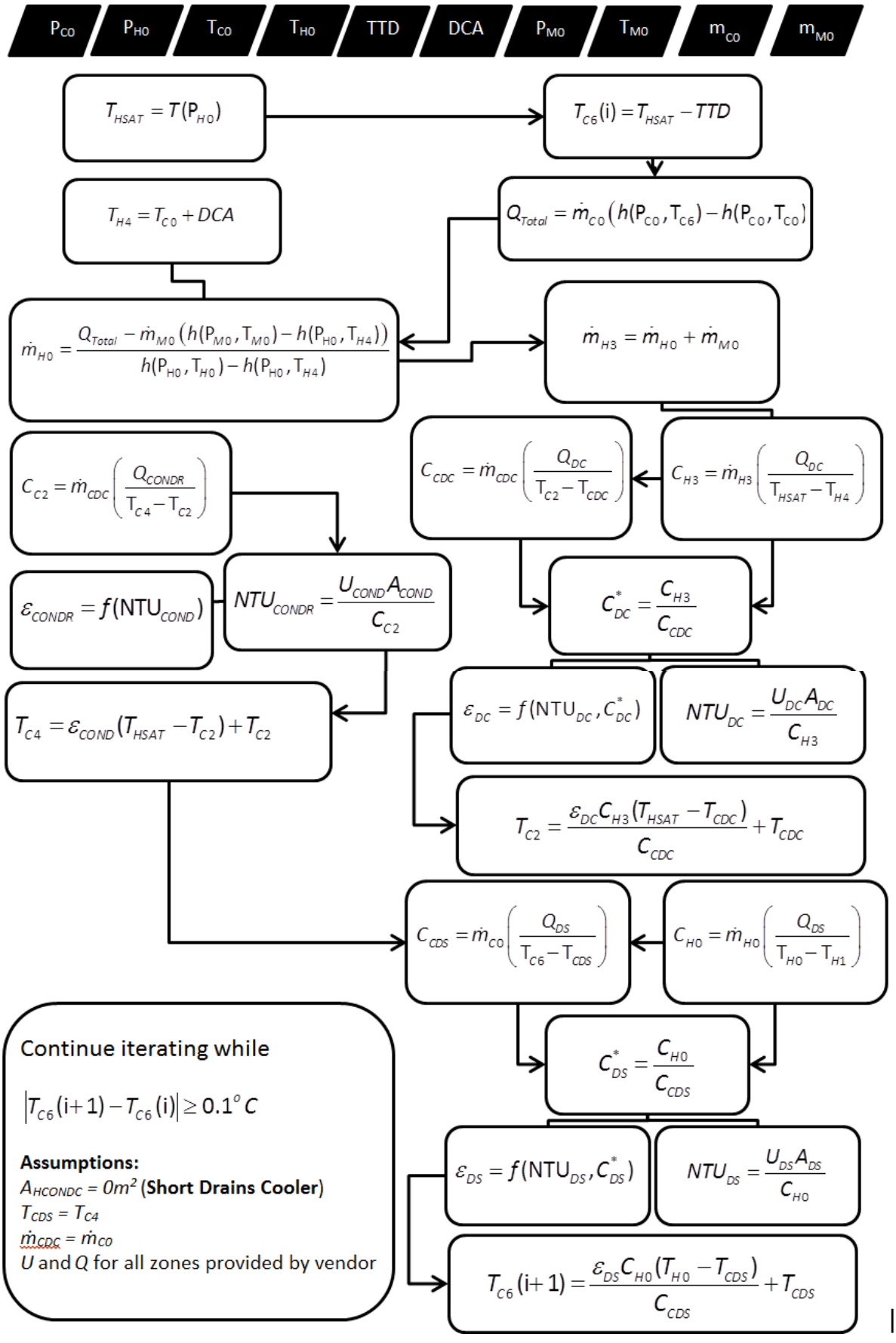

Figure 3-16. Overview of ASME PTC 12.1 FWH thermal model

h correlations

EPRI recommends the use of the Petukhov correlation, Equation (2.38), for the tube side. EPRI discusses the Stream Analysis and Bell Delaware method for estimating the shell side *h* and states that the uncertainty associated with the latter method ranges between ±20% to ±50%. The report provides guidelines for performing performance monitoring and hence relies on the *h* reported by the designer, as was the case with the Koehler and Weber model. EPRI discusses a simple method for estimating *h* on the shell side for off-design conditions and recommends the following correlation:

$$h = a\mathrm{Re}^{0.6}\,\mathrm{Pr}^{1/3} \tag{3.11}$$

The correlation is similar to the McAdams/ Kern correlation where the exponent of the *Re* number is 0.55 and the coefficient is 0.36.

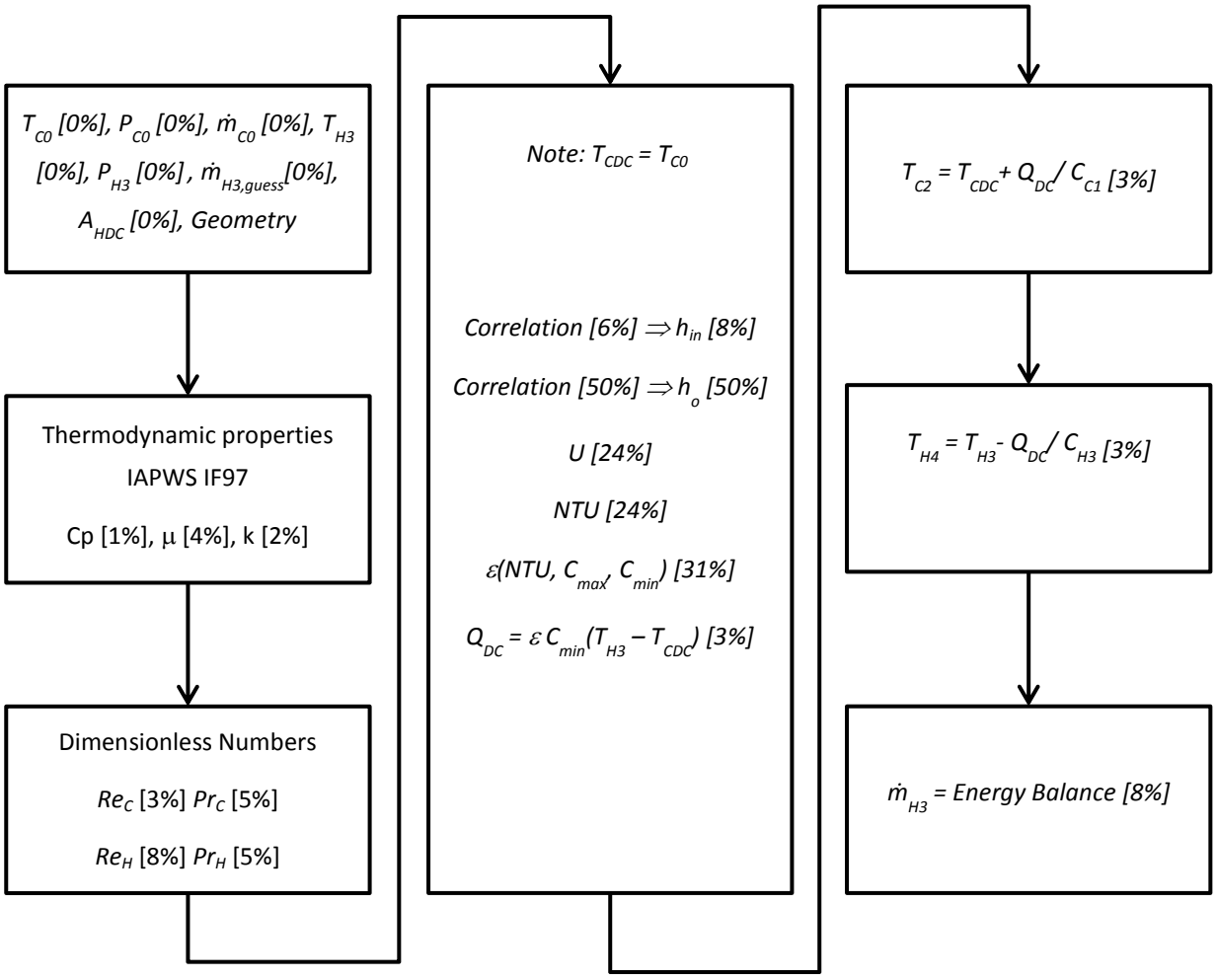

Figure 3-17. Analytical heat transfer uncertainty values extracted from Example 9.8 in the EPRI report [19] applied to a single phase residual heat removal heat exchanger

Uncertainty

The current study ignores measurement uncertainty or the uncertainty associated with the thermodynamic properties. However, the EPRI case studies incorporate all these uncertainties and discuss their effect on the terminal temperature calculation. An in-depth discussion of uncertainty analysis associated with error propagation is discussed in the report. The relative uncertainties associated with each calculation step, for Example 9.8 in the report, are presented in Figure 3-17.

The largest relative uncertainty is associated with the estimation of the external or shell side *h* values, which may be as high as 50% for the single phase heat transfer. However, this relative uncertainty does not necessarily generate a similar order of magnitude uncertainty in the output parameters such as *Q*, $\dot{m}_{H3}$, TTD or DCA. It is observed from Figure 3-17 that the consequential distribution of uncertainty is 3%, 8%, 3% and 3%, respectively.

The current study does not require measurements and hence no measurement uncertainties had to be incorporated into to the model. The uncertainties associated with the thermodynamic properties using the formulations from IAPWS-IF97 is also relatively small i.e. less than 4% for viscosity. This only leaves the uncertainty of *h* for both the shell and tube side. Hence, it was prudent to analyse the sensitivity of the model using the relative uncertainty of several correlations.

The dominant uncertainty introduced at this stage is the uncertainty associated with the heat transfer coefficients (*h*) correlation selected. There are a range of correlations and the client is not privy to this information. The use of more than one correlation per zone or sub-zone was therefore a consideration in the development of a FWH thermal model.

4. Methodology

The model was developed by applying the theory presented in Chapter 2 and building on existing thermal models that was reviewed in Chapter 3. The thermal model requires the user to input the overall geometry of the FWH in order to select the applicable correlations. The general stream identification for a 3 zone FWH was presented in Figure 3-12 but will be expanded due to the addition of a sub-zone called COND**S** and the consideration of other FWH variations.

4.1 Model development

The primary outputs of the elementary 3 zone model are the exit temperatures for each zone and sub-zone (*COND**C*** and *COND**R***). The steps associated with performing a heat transfer analysis for a single zone (DC in this case) is presented in Figure 4-1 and each step is summarised afterwards.

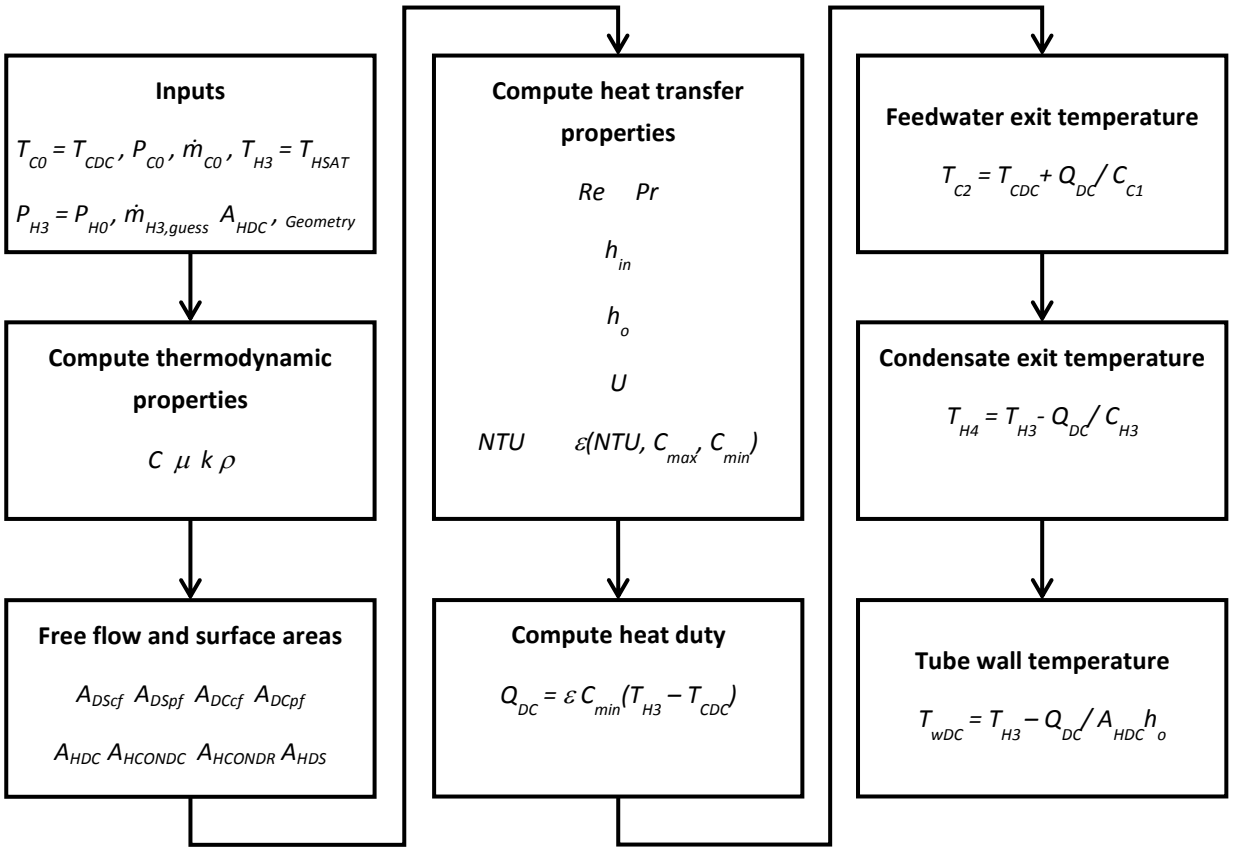

Figure 4-1. Analytical heat transfer calculation for the DC

- **Inputs**: This is the inlet temperatures, pressures, mass flow rates and geometry of the FWH.
- **Compute thermodynamic properties**: Use inlet stream temperature if the average temperature is not known.
- **Compute free flow and surface areas**: The correlations selected for this study determines the method for calculating the free flow areas. The symmetry of the tube bundle in the FWH determines the manner in which the surface areas of the sub-zones are calculated.
- **Compute heat transfer parameters**: The dimensionless parameters are then calculated in order to calculate *h* and *U* values. The NTU method is then used to compute the ε of the particular STHE using the capacity rates (*C*) of the two streams, surface area (*A*) and *U* that was calculated in the earlier steps.
- **Heat duty (*Q*):** The heat transferred in each zone and sub-zone is calculated using the ε together with the maximum possible heat that can be transferred in that particular zone.
- **Exit temperatures:** The exit and average tube wall temperatures are then calculated by using the energy balance and external convective heat transfer equation, respectively.

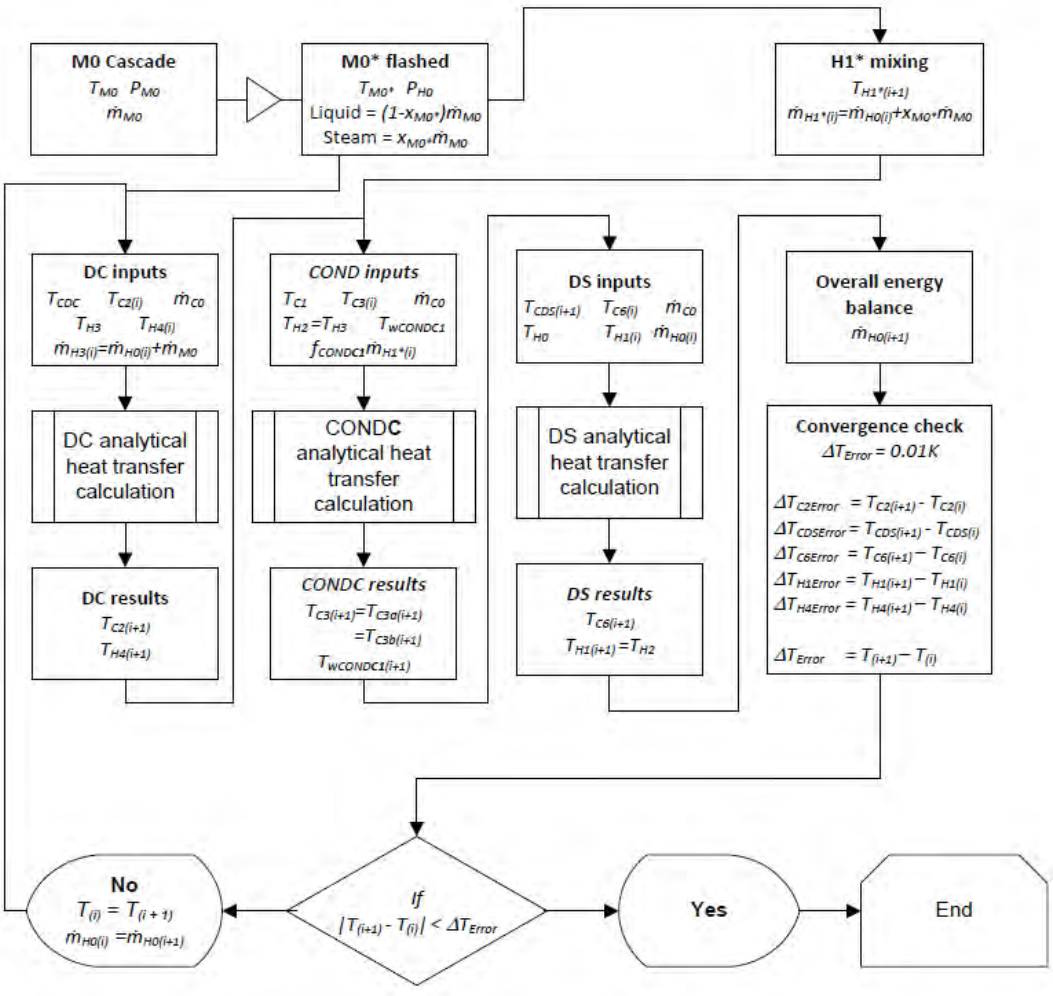

Figure 4-2. Flow diagram of a iterative solver for a 3 zone FWH

The overall sequence of calculations in a basic 3 zone FWH is illustrated in Figure 4-2. An initialisation step precedes the iterative solver step. In the initialisation step the thermodynamic properties of each stream are calculated using the inlet temperatures to the zones and sub-zones. The bled steam flowrate ($\dot{m}_{H0,guess}$) is not known but is an input and therefore a calculated guess has to be made, which is presented later as Equation (4.11). This value gets updated after each iterative step when an overall energy balance is performed. A crude heat transfer analysis of the FWH can now be performed.

The iterative solver then uses the average temperature that can now be calculated after the initialisation step, to calculate the thermodynamic properties. The solver converges when the exit temperatures, between successive iterative steps, do not change by more than a specified tolerance.

Thermodynamic properties of water in the steam are calculated with aid of the formulations proposed in IAPWS-IF97.

The estimation of the free flow and surface areas of the zones and sub-zones is a critical calculation step. Guidance for calculating the free flow area is normally provided by the original developer of the *h* correlation, which was discussed in Chapter 2. The surface area of the sub-zones is calculated by making use of geometric symmetry and some simplifying assumptions inside the FWH, which was outlined by Koehler and Weber [46] in Section 3.2.2. (Remember that detail geometrical data is not available to the user of the model). The distribution of surface area amongst the zones and sub-zones also determines the mass flow rate distribution, on both the tube side and shell side, of these zones.

The previous FWH models apply the Nusselt correlation for the condensation zone (COND**R** and COND**C**) which is independent of the bled steam mass flow ($\dot{m}_{H2a}$ and $\dot{m}_{H2b}$) to each sub-zone. However, the turbulent correlations require the bled steam mass flow distribution. This is also not known and an initial guess of a 50:50 ($f_{COND\mathbf{R}}$:$f_{COND\mathbf{C}}$) split is assumed between COND**R** and COND**C**. This ratio gets updated after each iterative step when the heat duty of each zone is compared to the total heat duty in the COND i.e. $Q_{COND\mathbf{C}}/Q_{COND}$ and $Q_{COND\mathbf{R}}/Q_{COND}$. This will be described in more detail in Section 4.1.3.

The addition of a new sub-zone in the COND zone will be discussed in the next section. This sub-zone does not remove latent heat and therefore must be deducted from total heat load of the COND zone when computing the bled steam mass flow distribution (*f*) described earlier.

4.1.1 Addition of COND**S** sub-zone to current thermal model

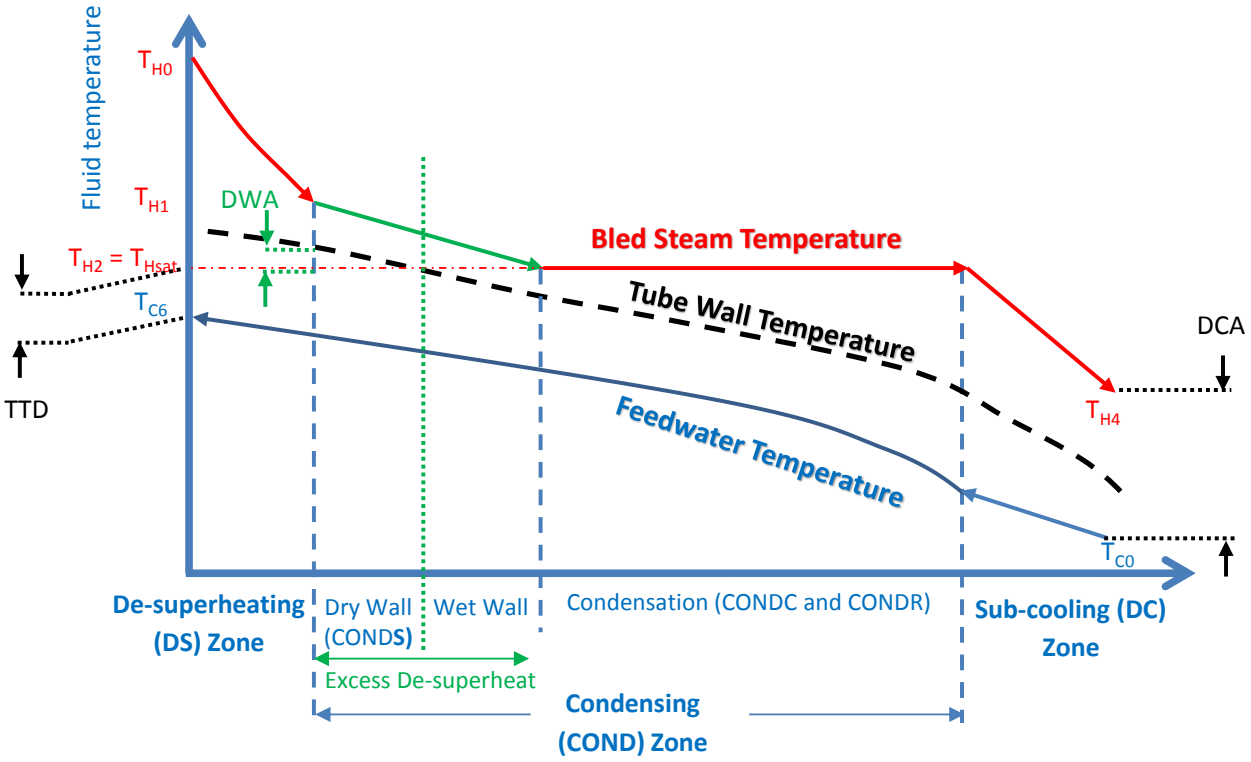

Figure 4-3. Dry wall de-superheating indicated on 3 zone FWH temperature profile

The existence of COND**S** was briefly mentioned in Section 3.1.1. This sub-zone will only be present if steam exiting the DS contains excess superheat or if steam entering the COND directly contains excess superheat. This sub-zone is not included in any previous thermal models reviewed in this study. Traditionally all FWH models assume that the steam exiting the DS is saturation steam, i.e. any superheat is ignored. However, FWHs that are fitted with a DS are typically designed such that the steam exits with excess superheat. This is to avoid erosion of the tubes in the DS that will be caused by fast moving entrained water droplets. Hewitt, Shires and Bott [47] states that condensation will occur while the steam is superheated if $T_w < T_{Hsat}$, where T_w is the tube wall temperature. A DWA margin is required to avoid rapid erosion, which could exceed the recommended margin 1°C. Single phase de-superheating will occur when $T_w > T_{Hsat}$ and is called dry wall de-superheating. Two phase de-superheating will occur when $T_w < T_{Hsat}$ and is called wet wall de-superheating, which is illustrated in Figure 4-3.

In this study excess superheat is removed in the COND zone assuming a dry wall de-superheating method. This implies that single phase heat transfer correlations will be applied which predicts significantly lower values than two phase heat transfer. The Colburn j correlation and Zukauskas correlations may be applied in the COND**S** sub-zone.

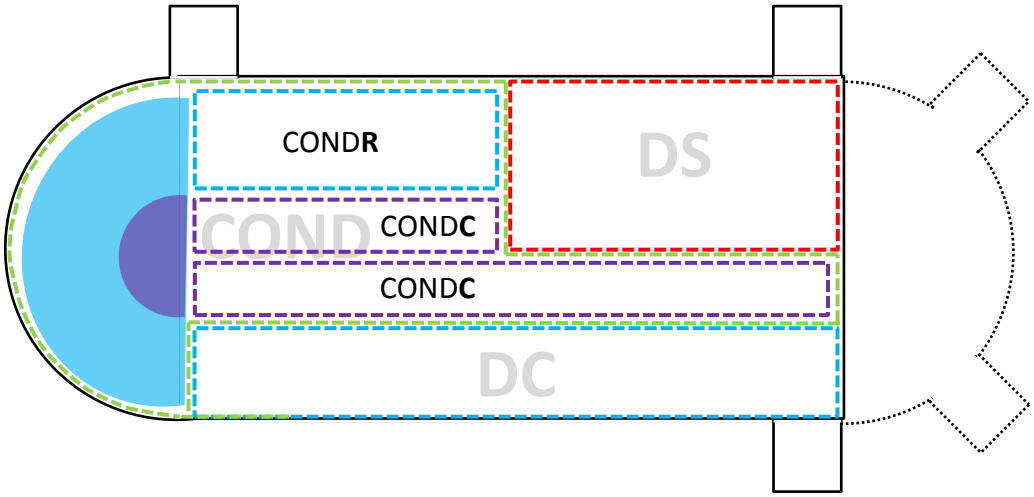

Figure 4-4. Designation of the COND zone and sub-zones for a 3 zone tube plate type FWH

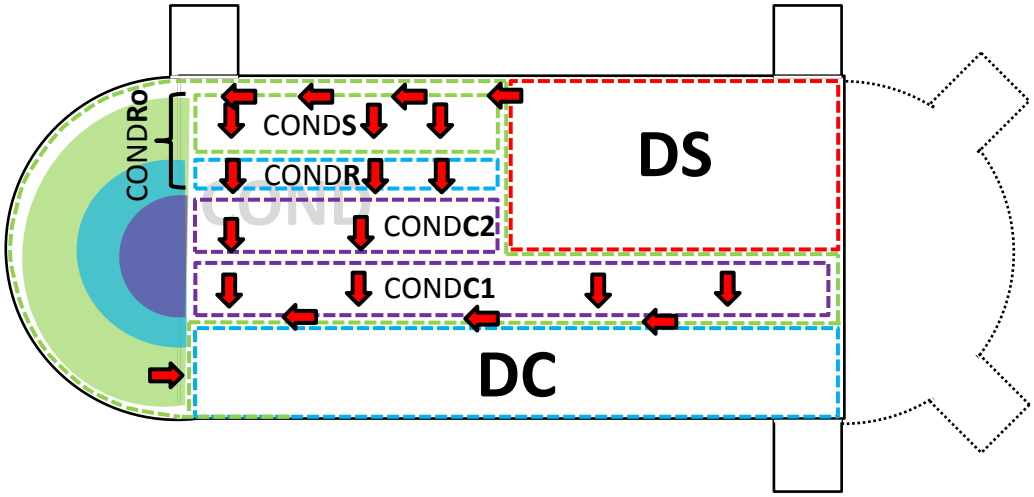

Figure 4-5. Location of the COND**S** sub-zone and logical allocation to be part of the COND**R** sub-zone

The sub-zones of the COND zone

The COND zone may be broken down into several sub-zones as was discussed in Section 3.1.1. Koehler and Weber [46] and Jestin [23] splits the COND zone into two sub-zones designated in this study as COND**R** and COND**C**. The total number of tubes on a single pass is n_t. The tubes routed through COND**R** (n_{tDC}) initially passed through the DC while the remainder of the tubes passes directly through COND**C** ($n_{tC} = n_t - n_{tDC}$) i.e. there is no prior feedwater heating as is the case with COND**R**. The allocation of the sub-zones in a tube plate FWH is illustrated in Figure 4-4.

CONDS zone

The COND**S** sub-zone would theoretically be located at the top of the shell. As it is assumed that the steam that exits the DS will distribute across the length of the COND zone before flowing in a cross flow manner across the tube bundle, see Figure 4-5. The COND**S** sub-zone will therefore

consume surface area made available for condensation in COND**R**. The initial total area is identified as COND**Ro**. When COND**S** = 0, then COND**R** = COND**Ro**, but as COND**S** is increased to remove the excess superheat, COND**R** reduces such that COND**R**+COND**S** = COND**Ro**.

It soon became apparent that a general model for all FWH configurations could not be developed with this allocation of COND**S**, as not all FWHs are fitted with a DC zone (i.e. COND**R** sub-zone). Hence, only the COND**S** sub-zone **surface area calculation** was formulated such that it would be deducted from the area in the last pass of the COND**C** sub-zone. The arrangement of the CONDC subzones for a FWH not fitted with a DC is illustrated in Figure 4-6. The arrangement of the CONDC subzones for a FWH fitted with a DC is illustrated in Figure 4-7.

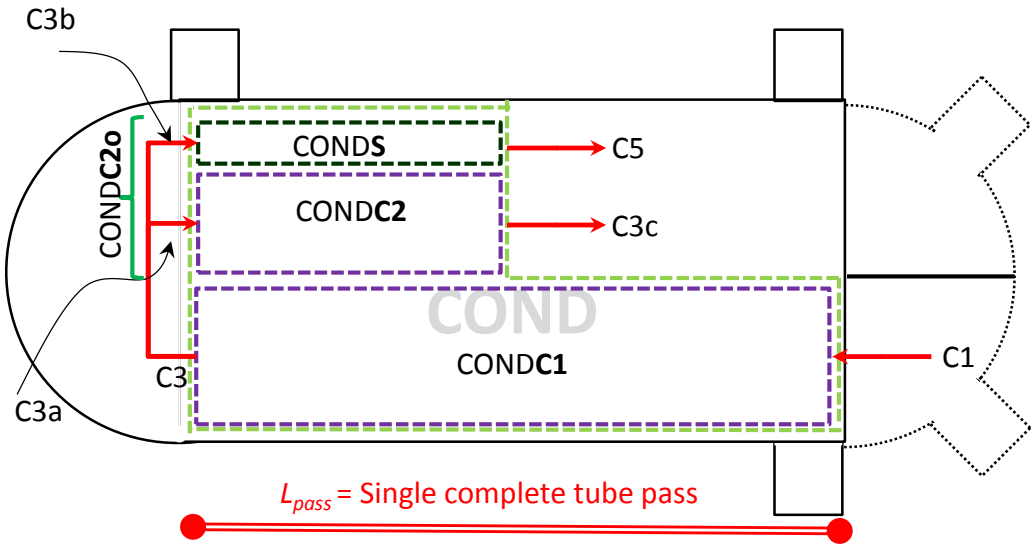

Figure 4-6. Designation and the location of CONDS sub-zone and associated feedwater streams for a FWH with no DC

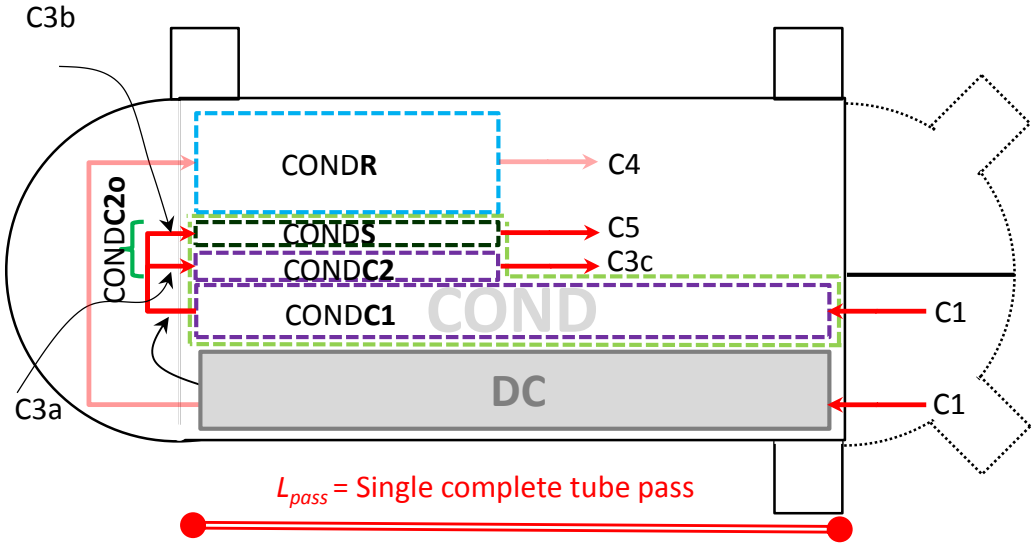

Figure 4-7. Designation and the location of CONDS sub-zone and associated feedwater streams for a FWH with a DC

The shell side stream configuration is still consistent with Figure 4-5 but the surface area is deducted from COND**C**, which is illustrated in Figure 4-7. The COND**S** is only assumed to be present in the last pass of the COND**C**. The surface area in the last pass is designated as (COND**C2o**), it comprises of COND**C2** and COND**S**.

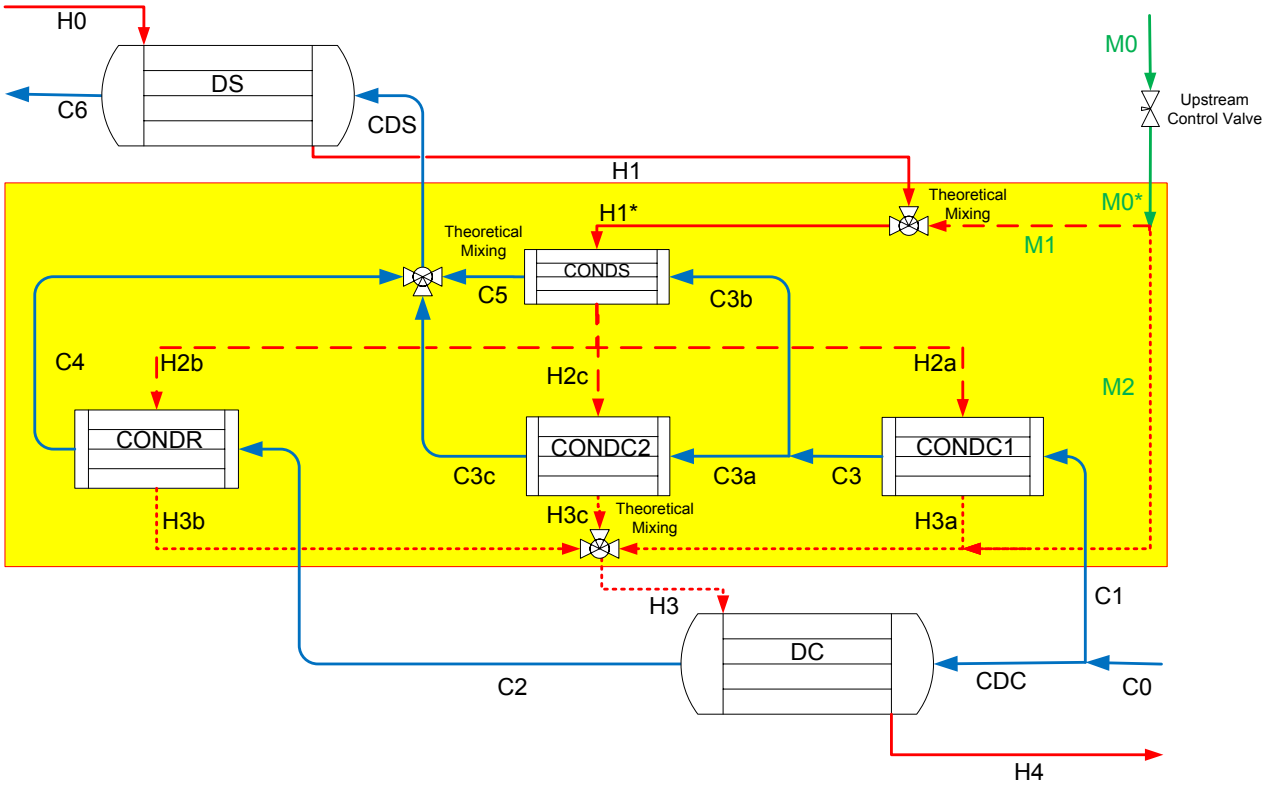

Figure 4-8. Designation of streams based on zone and subzone designation adopted in this study

Table 4-1 Stream assignment for the process flow diagram describing a 3 zone FWH

Stream	Description	Stream	Description
C0	Inlet feedwater	**H0**	Inlet bled steam extraction
CDC	Portion of *C0* entering DC	**H1**	Steam at exit of DS
C1	Portion of *C0* entering COND**C**	**H1***	Steam mixture of H1 and M1
C2	Exit of DC	**H2**	Saturated steam
C3	Feedwater exiting COND**C1**	**H2a/b/c**	Saturated steam
C3a	Feedwater entering COND**C2**	**H3**	Condensate exit from DC
C3b	Feedwater entering COND**S**	**H3a/b/c**	Saturated water
C3c	Feedwater exiting COND**C2**	**H4**	Condensate exit from DC
C4	Feedwater exiting COND**R**	**M0**	Cascading stream inlet
C5	Feedwater exiting COND**S**	**M0***	M0 that is depressurised in FWH
CDS	Feedwater exiting COND	**M1**	M0 that is saturated steam
C6	Feedwater exiting DS	**M2**	M0 that is saturated water

The limitation with the COND**S** subzone area allocation is that it can only be as large as COND**C2o**. If this is still insufficient to remove the excess superheat, the calculation will continue to progress with the assumption that all the excess superheat is removed in this zone. Ideally there should not be a large degree of excess superheat, as the consumption of COND area will drastically reduce the FWH's performance. This is illustrated in Section 5.4.

To conclude, the COND**C** region can be divided into the COND**C1** and COND**C2o** sub-zones. The COND**C1** sub-zone represents the tubes in COND**C** that complete the first and subsequent complete passes (for header-type heaters). The COND**C2o** sub-zone represents the total area in the last pass. The COND**C2o** area allocated for dry wall de-superheating and condensation is split between COND**S** and COND**C2**, respectively.

The amended process flow diagram now incorporates the COND**S** sub-zone and is illustrated in Figure 4-8 with the stream descriptions provided in Table 4-1. Note that the tube side streams entering the DS are modelled as a single mixed stream identified by subscript *CDS* (refer to section 3.1.2 for a discussion about this choice).

4.1.2 Heat transfer correlation selection

The heat transfer coefficient *h* is the parameter associated with the largest uncertainty in the heat transfer analytical calculation. The choice of correlation and its uncertainty may affect the magnitude of the performance parameters (Q, TTD and DCA) as was discussed in Section 3.3.3. In this study the user may compare the results using different correlation options listed in Table 4-2.

Table 4-2 Heat transfer correlations *h* implemented in the current study

Name	Geometry,Option	Correlation	Equation number	Uncertainty
Tube-side h_{in}	in,0	Petukhov	(2.38)	±6%
	in,1	Dittus & Boelter	Table 2-5	±25%
Shell-side single phase h_o	SEG,0	McAdams/ Kern	(2.57)	±25%
	SEG,1	Jestin	(2.62)	±25%
	SEG,2	Bell Delaware	(2.69)	±25%
	GRID,0	Modified Donohue	(2.56)	±25%
	GRID,1	Gentry	(2.49)	±25%
Shell-side condensing h_{oCOND}	Horizontal,0	Shekriladze	(2.88)	±47%
	Horizontal,1	McNaught	(2.93)	±27%
	Horizontal,2	Butterworth	(2.91)	±25%
	Vertical,0	Kutateladze	(2.79)	±7%
	Vertical,1	Kirkbride and Badger	(2.81)	±7%
	Vertical,2	Lubuntsov	(2.82)	±4%
Ideal cross flow h_{oCF}	CF,0	Colburn j (Bell)	(2.70)	±15%
	CF,1	Zukauskas	(2.73)	±15%

4.1.3 Mass flow distribution calculations

The results from the free flow area calculations are required for input into the correlations mentioned above. The cross and parallel flow areas are calculated based on the method employed by the original developer of the correlation or the internal geometry of the FWH. The details of the method used to calculate these free flow areas are presented in Appendix A.

The equations used to calculate the surface area of the sub-zones is also described in Appendix A. The methodology used in this section is similar to that adopted by Koehler and Weber [46] and has been extended to header type FWHs.

The mass distribution through a particular zone or sub-zone is proportional to the surface area distribution in that particular zone or sub-zone. Please refer to the process flow diagram of Figure 4-8 for reference to the various stream definitions.

The feedwater enters the FWH with a mass flow rate of $\dot{m}_{C0}$. If a DC is installed the mass flow rate distributes proportionally to the number of tube located in the DC and is formulated as follows:

$$\dot{m}_{C2} = \frac{n_{tDC}}{n_t}\dot{m}_{C0} \tag{4.1}$$

The number of tubes n_{tDC} is based on an area ratio using Equation (A.8) in Appendix A. Hence, the mass flow rate that enters the COND zone directly, $\dot{m}_{C1}$, is calculated as follows:

$$\dot{m}_{C1} = \frac{n_{tC}}{n_t}\dot{m}_{C0} = \dot{m}_{C0} - \dot{m}_{C2} \tag{4.2}$$

The mass flow rate $\dot{m}_{C1}$ will split in the last pass between the tubes located in A_{HCONDS} and $A_{HCONDC2}$. The mass flow distribution is again assumed to be proportional to the number of tubes in each sub-zone, which in turn is proportional to the associated heat transfer area.

$$\dot{m}_{C3b} = \dot{m}_{C1}\frac{A_{HCONDS}}{A_{HCONDC2o}} = \dot{m}_{C5} \tag{4.3}$$

where $\dot{m}_{C3b}$ is the mass flow rate that passes through the single phase cross flow sub-zone (COND**S**) and $\dot{m}_{C3a}$ is the balance of the mass flow rate that passes through the purely condensing zone in the last pass (COND**C2**).

$$\dot{m}_{C3a} = \dot{m}_{C3} - \dot{m}_{C3b} = \dot{m}_{C3c} \tag{4.4}$$

The feedwater is then assumed to mix before entry into the DS:

$$\dot{m}_{CDS} = \dot{m}_{C3c} + \dot{m}_{C4} + \dot{m}_{C5} \tag{4.5}$$

The flow of bled steam in the COND zone was illustrated in Figure 4-5 and is designated as $\dot{m}_{H1*}$. The bled or extraction steam enters at a mass flow rate of $\dot{m}_{H0}$, which is typically an unknown, and mixes with the cascading flow (if present) that flashes partly to steam ($x_{M0*}\dot{m}_{M0}$).

$$\dot{m}_{H1*} = \dot{m}_{H0} + x_{M0*}\dot{m}_{M0} \tag{4.6}$$

The split of the steam mass flow through the CONDC1, CONDC2 and CONDR sub-zones can be calculated from the heat transferred in each zone as follows:

$$f_{CONDC1} = \frac{Q_{CONDC1}}{Q_{CONDC1} + Q_{CONDC2} + Q_{CONDR}} \tag{4.7}$$

$$f_{CONDC2} = \frac{Q_{CONDC2}}{Q_{CONDC1} + Q_{CONDC2} + Q_{CONDR}} \tag{4.8}$$

$$f_{CONDR} = \frac{Q_{CONDR}}{Q_{CONDC1} + Q_{CONDC2} + Q_{CONDR}} \tag{4.9}$$

where *f* represents the fraction of $\dot{m}_{H1*}$ steam that is condensed in each sub-zone heat exchanger.

The distribution is not known at the initialisation step but is required as an input. Hence, an initial distribution of 50:50:0 (f_{CONDR}:f_{CONDC1}:f_{CONDC2}) is assumed between COND**R**, COND**C1** and COND**C2**. This ratio gets updated after each iterative step when the heat duty of each sub-zone is compared to the total heat duty in the COND zone minus the heat duty of the CONDS sub-zone, see Equations (4.7) to (4.9).

4.2 Model Initialisation

Only the inlet conditions to the FWH (except the bled steam mass flow) are known at the start. It is therefore necessary to perform an initialisation of the process conditions and mass flows of all the streams in order to solve the complete system. One way would be to simply assume/guess a temperature for each stream, and trust that the iterative loop will adjust the guesses towards the correct results. An alternative is to calculate the exit conditions of each successive heat exchanger from the inlet to the outlet (as seen from the feedwater flow direction). The advantage of the latter method is that the iterative solver starts with a calculated guess for the outlet conditions.

Literature recommends using the average temperature between the inlet and outlet of a stream, to calculate the thermodynamic properties of the fluids inside a heat exchanger. Since the outlet temperatures are not known at the start, the fluid properties can only be calculated using the inlet temperatures. The next iteration can then use a better average temperature.

The initial guess for the bled steam flow is calculated assuming that there is no need for de-superheating and that the terminal hot and cold stream temperatures coincide i.e. $T_{C6} = T_{H2} = T_{Hsat}$ and $T_{H4} = T_{C0}$. Hence, the overall heat transfer (Q_{TOTAL}) with reference to the tube side is computed as follows:

$$Q_{TOTAL} = \dot{m}_{C0}\left(\hbar(\mathrm{P}_{C0}, \mathrm{T}_{Hsat}) - \hbar(\mathrm{P}_{C0}, \mathrm{T}_{C0})\right) \tag{4.10}$$

and therefore the bled steam mass flow rate using the overall energy balance on the shell side is calculated as follows:

$$\dot{m}_{H0,\mathrm{guess}} = \frac{Q_{TOTAL} - \dot{m}_{M0}\left[\hbar(\mathrm{P}_{M0}, \mathrm{T}_{M0}) - \hbar(\mathrm{P}_{H0}, \mathrm{T}_{C0})\right]}{\left[\hbar(\mathrm{P}_{H0}, x_{H0} = 1) - \hbar(\mathrm{P}_{H0}, \mathrm{T}_{C0})\right]} \tag{4.11}$$

This estimate of $\dot{m}_{H0}$ will be used as the initial guess to complete the first calculation run. At the end of the initialization, the next value for $\dot{m}_{H0}$ using the overall energy balance and the updated temperatures can be calculated:

$$\dot{m}_{H0} = \frac{\dot{m}_{C0}\left(\hbar(\mathrm{P}_{C0}, \mathrm{T}_{C6}) - \hbar(\mathrm{P}_{C0}, \mathrm{T}_{C0})\right) - \dot{m}_{M0}\left(\hbar(\mathrm{P}_{M0}, \mathrm{T}_{M0}) - \hbar(\mathrm{P}_{H0}, \mathrm{T}_{H4})\right)}{\hbar(\mathrm{P}_{H0}, \mathrm{T}_{H0}) - \hbar(\mathrm{P}_{H0}, \mathrm{T}_{H4})} \tag{4.12}$$

The size of $\mathrm{A_{HCONDS}}$ is also not known hence it is initially set to 0 m^2. After calculating all the temperatures, the degree of superheat entering the COND zone is known as T_{H1*}. One can now make an informed estimate of the size of A_{HCONDS} in order to remove all superheat. This is done by assuming that CONDS behaves like a single-stream heat exchanger, with the steam side being the only stream experiencing a temperature change, and the water side staying constant. This is a reasonable approximation, given that there should normally not be a very large degree of superheat, hence the water would not heat up significantly. The general sequence for re-calculating A_{HCONDS} is presented in Figure 4-9.

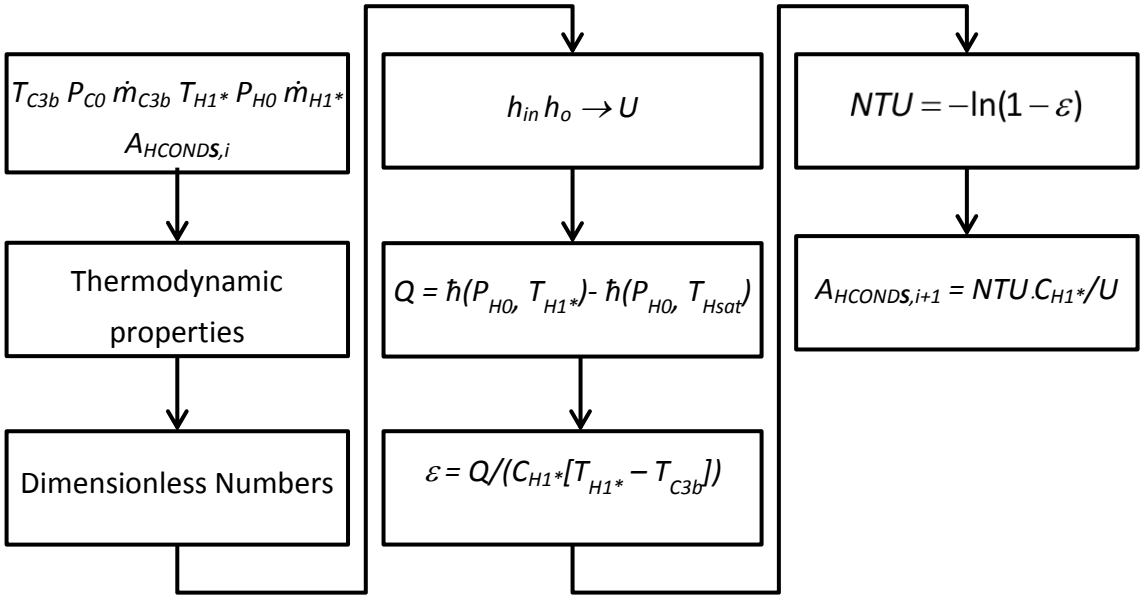

Figure 4-9. General calculation sequence for estimating the heat transfer area of the COND**S** subzone

The average tube wall temperatures in the COND zone ($T_{wCOND\mathbf{C1}}$, $T_{wCOND\mathbf{C2}}$ and $T_{wCOND\mathbf{R}}$) are required for the condensing heat transfer correlations, h_{oCOND}. As a start, the temperature is set to be equal to T_{HSAT} - 1^oC. The updated tube wall temperature for each condensing sub-zone may be calculated after the heat duty for that particular zone is calculated. The average tube wall temperatures can be calculated using Newton's law of cooling equation with reference to the outer boundary layer:

$$T_w = \frac{(T_{H0} + T_{H1})}{2} - \frac{Q}{A_H h_o} \tag{4.13}$$

The HP6 FWH of station PS16 is used as an example to illustrate how the calculation progresses through each zone. The known inputs are populated in the **start** column of Table 4-3. The following values are also automatically estimated:

- The shell side temperature in the COND zone (T_{H2} and T_{H3}) corresponds to the saturation temperature, T_{Hsat}, which is calculated from inlet shell side pressure.
- The initial guess for $A_{HCONDS} = 0\ m^2$ forces the shell side DS zone exit temperature, T_{H1}, and T_{H1*} to be equal to T_{Hsat} until the heat transfer calculations are performed around the DS.
- The initial guess for $\dot{m}_{H0,guess}$ and the bled steam mass distribution in COND is estimated.

The general calculation sequence for each zone and sub-zone, is then executed from left to right in Table 4-3. The last column represents the inputs into the first iterative step. In this next step the average temperatures across each zone and sub-zone heat exchanger will be used to obtain the thermodynamic properties.

Table 4-3 The terminal temperatures of zone and sub-zone heat exchangers of the HP6 FWH of station PS16 populated from left to right

Stream	**Start**	**DC**	COND**C1**	COND**C2**	COND**R**	COND**S(T_{C5})**	**Mix_{CDS}**	**DS**	**Mix_{CONDS}**	**$\dot{m}_{H0}$**	**A_{CONDS}**
$T_{C0,CDC,C1}$	**228.8°C**	228.8°C	228.8°C	228.8°C	228.8°C	228.8°C	228.8°C	228.8°C	228.8°C	228.8°C	228.8°C
T_{C2}		**238.6°C**	238.6°C	238.6°C	238.6°C	238.6°C	238.6°C	238.6°C	238.6°C	238.6°C	238.6°C
$T_{C3, C3a}$			**265.1°C**	265.1°C	265.1°C	265.1°C	265.1°C	265.1°C	265.1°C	265.1°C	265.1°C
$T_{wCONDC1}$	**267.6°C**	267.6°C	**264.5°C**	264.5°C	264.5°C	264.5°C	264.5°C	264.5°C	264.5°C	264.5°C	264.5°C
T_{C3b}						**265.1°C**	265.1°C	265.1°C	265.1°C	265.1°C	265.1°C
T_{C3c}				**267.0°C**	267.0°C	267.0°C	267.0°C	267.0°C	267.0°C	267.0°C	267.0°C
$T_{wCONDC2}$	**267.6°C**	267.6°C	267.6°C	**268.0°C**	268.0°C	268.0°C	268.0°C	268.0°C	268.0°C	268.0°C	268.0°C
T_{C4}					**264.8°C**	264.8°C	264.8°C	264.8°C	264.8°C	264.8°C	264.8°C
T_{wCONDR}	**267.6°C**	267.6°C	267.6°C	267.6°C	**265.3°C**	265.3°C	265.3°C	265.3°C	265.3°C	265.3°C	265.3°C
T_{C5}						**265.1°C**	265.1°C	265.1°C	265.1°C	265.1°C	265.1°C
T_{CDS}							**266.2°C**	266.2°C	266.2°C	266.2°C	266.2°C
T_{C6}								**268.6°C**	268.6°C	268.6°C	268.6°C
T_{H0}	**334.2°C**	334.2°C	334.2°C	334.2°C	334.2°C	334.2°C	334.2°C	334.2°C	334.2°C	334.2°C	334.2°C
T_{H1}	**268.6°C**	268.6°C	268.6°C	268.6°C	268.6°C	268.6°C	268.6°C	**300.7°C**	300.7°C	300.7°C	300.7°C
T_{H1*}	**268.6°C**	268.6°C	268.6°C	268.6°C	268.6°C	268.6°C	268.6°C	268.6°C	**300.7°C**	300.7°C	300.7°C
$T_{H2,H2a,H2b}$	**268.6°C**	268.6°C	268.6°C	268.6°C	268.6°C	268.6°C	268.6°C	268.6°C	268.6°C	268.6°C	268.6°C
$T_{H3,H3a,H3b}$	**268.6°C**	268.6°C	268.6°C	268.6°C	268.6°C	268.6°C	268.6°C	268.6°C	268.6°C	268.6°C	268.6°C
T_{H4}		**236.9°C**	236.9°C	236.9°C	236.9°C	236.9°C	236.9°C	236.9°C	236.9°C	236.9°C	236.9°C
$\dot{m}_{H0}$	**31.7 kg/s**	31.7 kg/s	31.7 kg/s	31.7 kg/s	31.7 kg/s	31.7 kg/s	31.7 kg/s	31.7 kg/s	31.7 kg/s	**28.7 kg/s**	31.7 kg/s
A_{HCONDS}	**0 m^2**	0 m^2	0 m^2	0 m^2	0 m^2	0 m^2	0 m^2	0 m^2	0 m^2	148.4 m^2	**148.4 m^2**

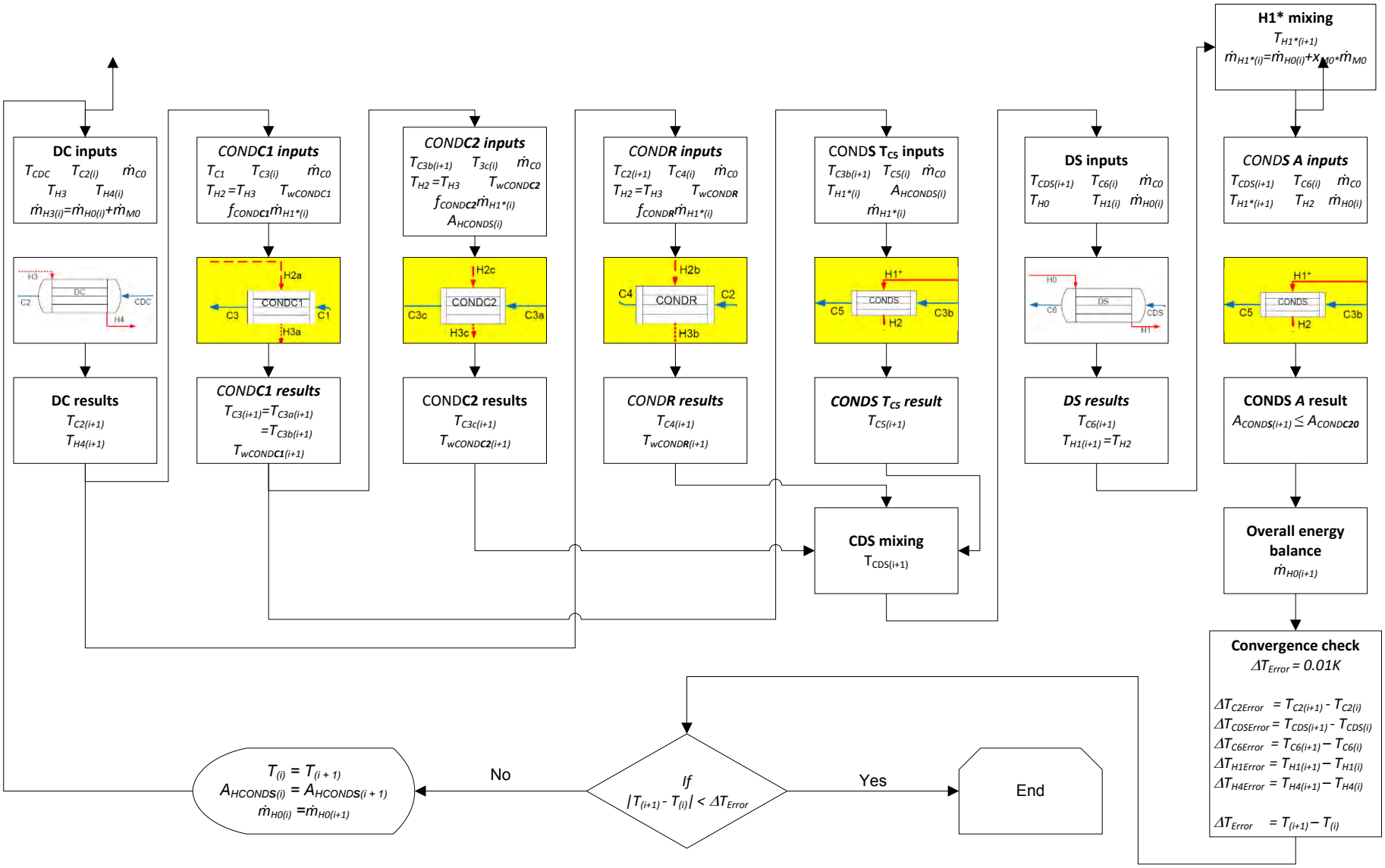

Figure 4-10. Graphic representation of the iterative solver for a 3 zone FWH

4.3 Iterative solver

An overview of the iterative solver is presented in Figure 4-10. The exit temperatures from the initialisation step will be used as the initial values into the iterative solver that will run until the exit temperatures converges within a specified tolerance described in Equation (4.14). The tolerance is defined as the difference between successive values:

$$tolerance = \Delta T_{Error} = T_{i+1} - T_i \leq 0.1K \tag{4.14}$$

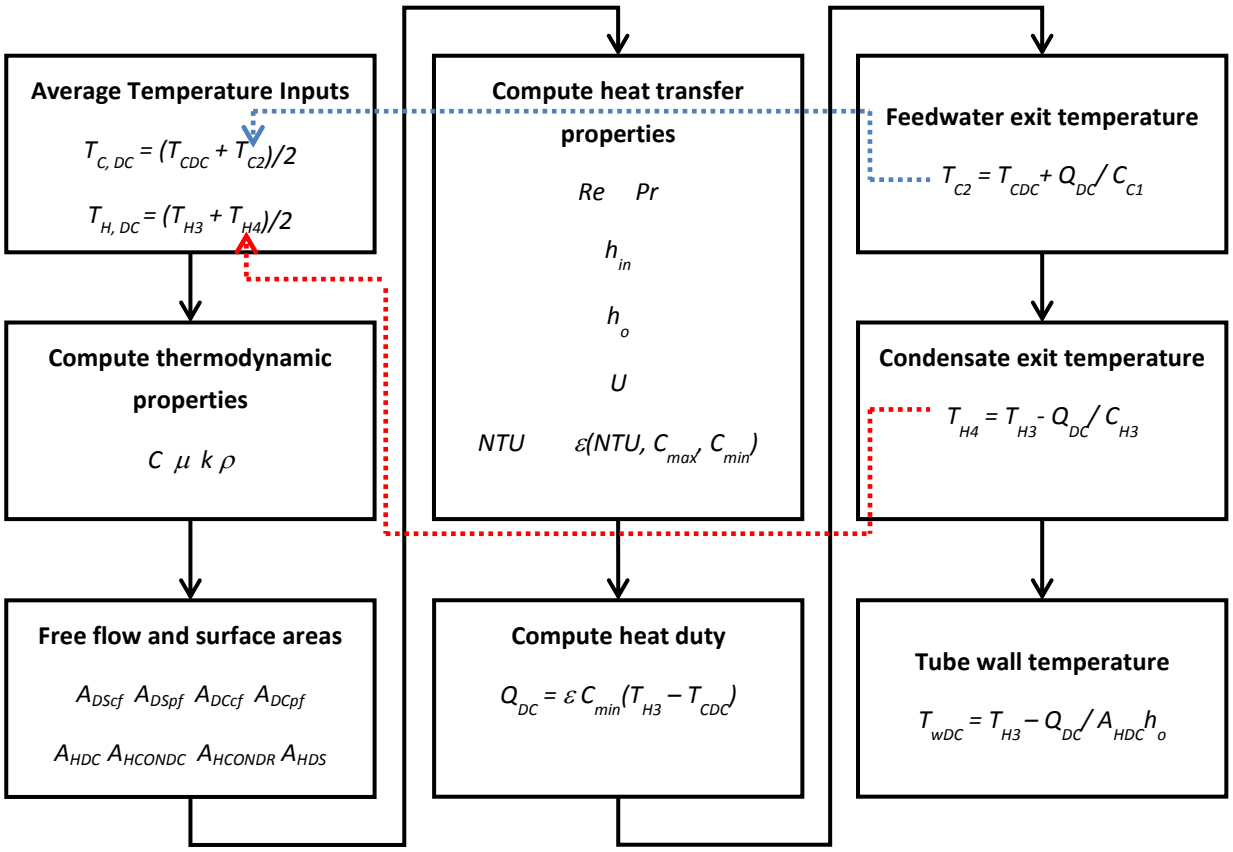

Figure 4-11. Analytical heat transfer calculation for the DC

The analytical calculation starts at the DC and the average stream temperature is calculated. This average temperature of the cold and hot stream is used to calculate the thermodynamic properties. The analytical calculation progresses until the exit temperatures are calculated for each zone and sub-zone in the FWH, see Figure 4-10. All the updated exit temperatures, $\dot{m}_{H0}$ and A_{HCONDS} are then compared to their previous values to verify if convergence has been achieved. If convergence was not achieved the updated values becomes the input for the next iteration, see Figure 4-11. This elementary method has proven to be effective with convergence being achieved within 6 iterations.

The limitation with this model is that A_{HCONDS} is only calculated in the last pass. Hence, the model will indicate that the DS zone is inefficiently sized if the heat transfer area required to remove the excess superheat is greater than the area available ($A_{HCONDC2o}$) in the last pass.

The progress of the iterative loop for the HP6 FWH from station PS00 is presented in Figure 4-12. The x- axis is designated as *i*, which represented the iteration number. Note how each performance parameter converges within 10 iterations. The convergence tolerance is set to 0.1K.

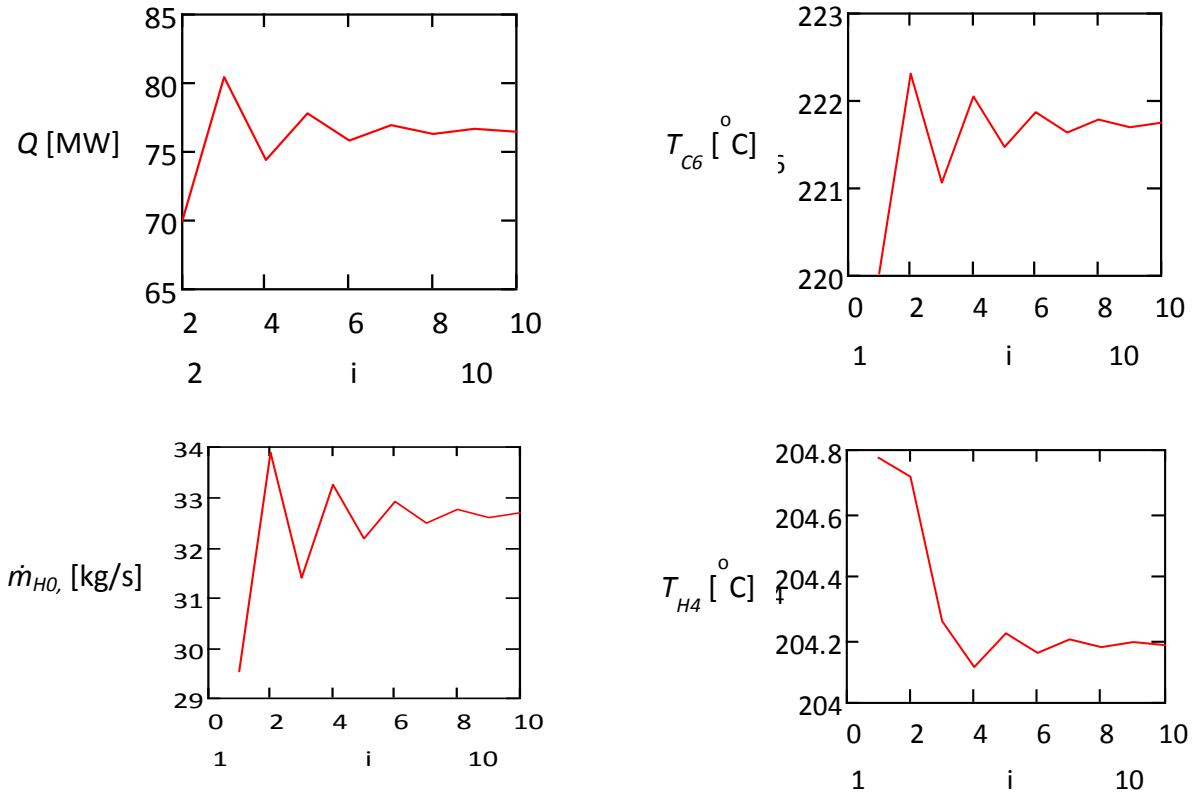

Figure 4-12. The progress of the iterative loop for the HP6 FWH from station PS00

4.4 Definition of inputs

The inputs of the model are grouped into two portions, namely overall geometry and detail stream and dimensional inputs. These two portions are elaborated below.

4.4.1 Overall geometry or dimensional inputs

The overall geometry inputs define the general layout and type of FWH. It affects the stream definitions and set of correlations to be used. These inputs can be obtained visually on site and by consulting the vendor specification sheets and layout drawings if available. Figure 4-13 presents a graphical view of the inputs and a hypothetical input sheet is illustrated in Figure 4-14.

- **Orientation and type:** This was discussed in Section 3.1 but suffice to say that there are two types of FWHs. The LP heaters are of the tube plate type while the HP heaters are either of the tube plate or header types. Header type FWHs may have multiple passes on the tube side while tube plate type FWHs only has two passes. This will influence the number of tubes in the vertical column that is used to calculate the effect of condensate inundation has on *h* for condensation for a horizontally orientated FWH. The vertical or horizontal orientation of the FWH determines which correlations will be utilised for the COND zone.
- **Zone allocation:** The number of zones (1/2/3) present in the FWH must be identified by populating their respective heat transfer areas. These areas are identified as A_{HDS}, A_{HCOND} and A_{HDC}. An area of zero implies that the zone does not exist.
- **Baffle arrangement:** Segmented or grid baffles must be identified.
- **Short or long DC:** Either a short or long DC design philosophy may be adopted. The long DC is common in horizontal tube plate or header type FWHs while the short DC is common in vertically orientated FWHs. The shortcoming of a short DC is that there may be a portion of tubes in the COND zone, that will be submerged and therefore not participate in any significant heat transfer. Hence, the surface area of the submerged tubes must be specified, which will be deducted from the area allocated to CONDC1.
- **Overall dimensions:**
  - The available surface areas for each zone is required (A_{HCOND}, A_{HDC}, A_{HDS}) in [m^2]
  - Internal diameter of the shell (D_{shell}) in [m]
  - The total number of U-shaped or snake-like tubes per pass (n_t)
  - Outside tube diameter (d_o) in [mm]
  - Tube thickness (t) in [mm]
  - Thermal conductivity of the tube (k_{tube}) in W/mK. The tube conductivity for a LP and HP FWHs is typically 17 and 50 W/mK, respectively.

- The number of tube passes (*Passes*)
- The tube arrangement (*Layout*) can be specified as either 30^o, 60^o, 45^o or 90^o
- The baffle spacing for the DC or DS ($L_{B,DC}$ or $L_{B,DS}$) in [mm]. In the absence of data, a default value of 500 mm and 300 mm for the DC and DS can be inputted, respectively.
- The baffle cut for the DC or DS ($B_{cut,DC}$ or $B_{cut,DS}$) in [%]. In the absence of data, a default value of 25% can be inputted, respectively.
- Transverse tube pitch (P_T) and longitudinal tube pitch (P_L) in [mm]. Only one of the pitches is required while the other pitch is calculated using the method proposed in Appendix A.
- The grid plate thickness (t_{grid}) in [mm]. A default value is 2.4 mm.
- The length of the grid plate in contact with the tube (L_{grid}) in [mm]. A default value is 50 mm.

4.4.2 Stream inputs

The inlet stream inputs and the surface areas for the zones that are required as inputs to the model are illustrated in Figure 4-14.

For the feedwater passing on the tube side, only the inlet temperature (T_{C0}) and pressure (P_{C0}) is required to define it fully. It is assumed that the water is subcooled liquid, hence the temperature has to be lower than the corresponding saturation temperature for the given pressure. The feedwater mass flow rate ($\dot{m}_{C0}$) is also a required input.

A single property is required if the bled steam enters as saturated steam (x=1 assumed), so either the inlet temperature (T_{H0}) or pressure (P_{H0}) must be specified. If the steam enters above saturated conditions i.e. superheated, then both the inlet temperature (T_{C0}) and pressure (P_{C0}) must be specified.

If a cascade stream exists, the mass flow rate ($\dot{m}_{M0}$) is required, alternatively is can be set to zero. The cascade stream is typically sub-cooled liquid, and hence the inlet temperature (T_{M0}) and pressure (P_{M0}) must be specified. This is only needed if the mass flow is not zero.

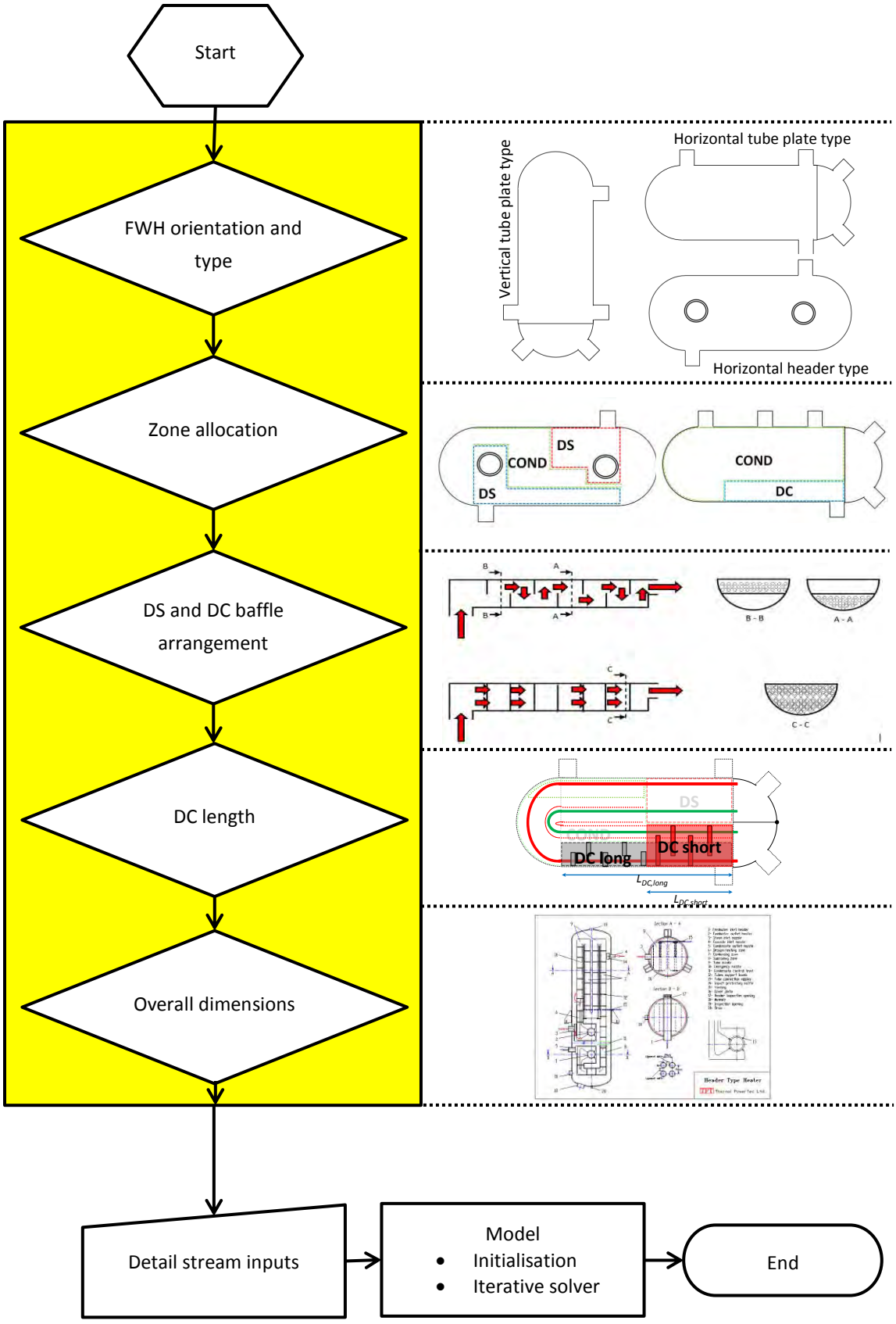

Figure 4-13. Overview of the FWH thermal model with a focus on the overall geometry inputs

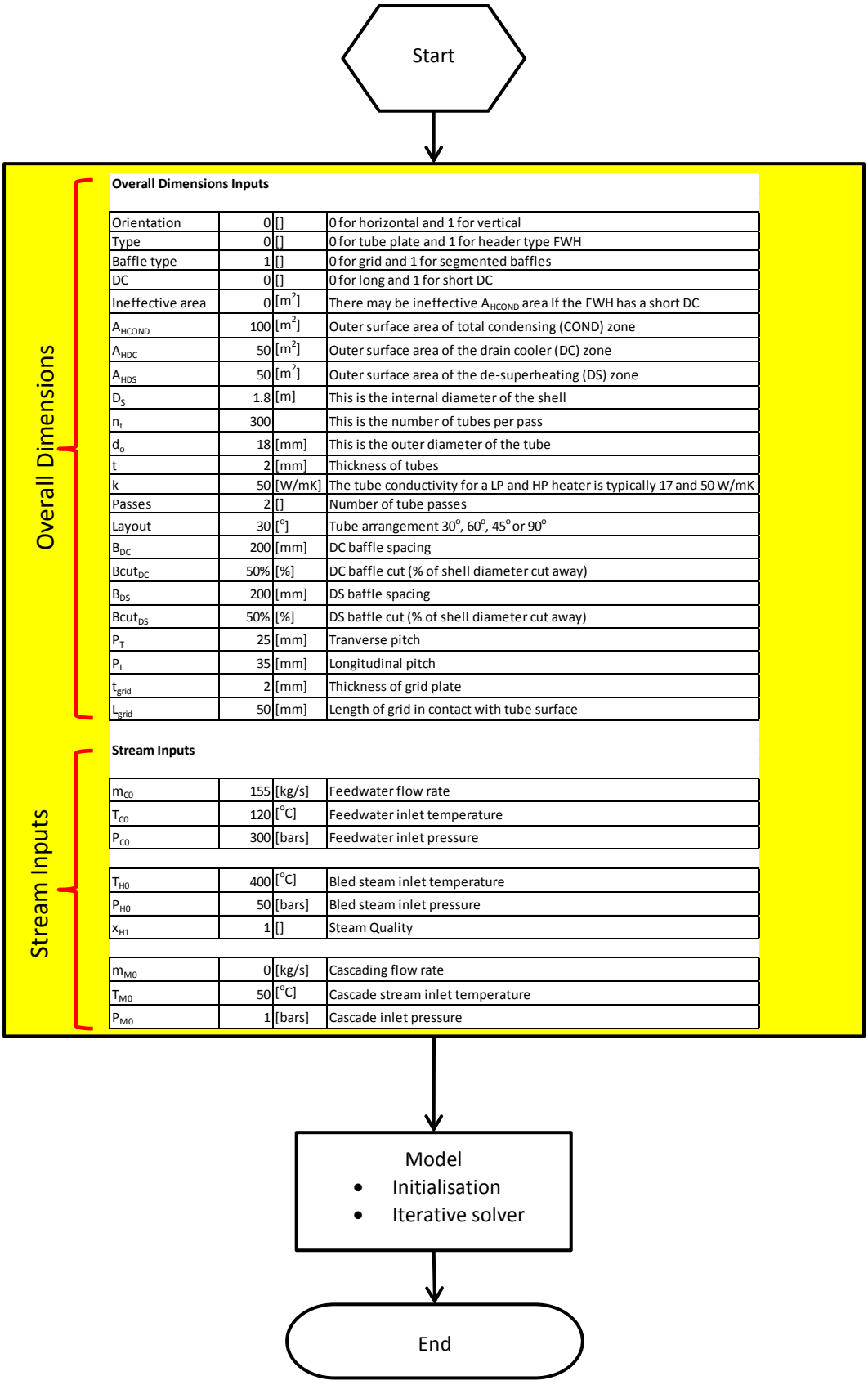

Figure 4-14. Overview of the FWH thermal model with a populated list of the stream and overall dimensional inputs

4.4.3 Solver settings

Convergence tolerance

The convergence tolerance (ΔT_{Error}) was set to 0.1°C as this is recommended by ASME [54]. However, the user may improve the tolerance that will consequently increase the number of iterations required to achieve convergence, see Table 4-4.

Table 4-4 Sensitivity of solver convergence tolerance on speed of convergence and accuracy of results for the HP FWH from station PS00

ΔT_{Error} [°C]	Iterations	T_{C6} [°C]	T_{H4} [°C]
1.000	5	221.4775	204.2213
0.100	10	221.7521	204.1837
0.010	14	221.7358	204.1868
0.001	18	221.7339	204.1872

Choice of correlations and uncertainty

There is a list of 15 correlations based on Table 4-2. The selection of the correlation applicable to a zone and sub-zone depends on the number of zones, orientation and type of baffle fitted.

The selection of option 0 correlations will be illustrated for a hypothetical 3 zone FWH that is orientated horizontally and fitted with segmented baffles, see Table 4-5. Note that the nominal result from each correlation was selected by selecting an uncertainty of 0%. The user can select any applicable option listed in Table 4-5 and the upper or lower uncertainty.

Table 4-5 Option 0 correlations selected for a hypothetical 3 zone FWH orientated horizontally and fitted with segmented baffles

Name	Geometry,Option	Correlation	Option Selection	Uncertainty
Tube-side h_{in}	in,0	Petukhov	in,0	0%
	in,1	Dittus & Boelter		0%
Shell-side single phase h_o	SEG,0	McAdams/ Kern	SEG,0	0%
	SEG,1	Jestin		0%
	SEG,2	Bell Delaware		0%
	GRID,0	Modified Donohue		0%
	GRID,1	Gentry		0%
Shell-side condensing h_{oCOND}	Horizontal,0	Shekriladze	Horizontal,0	0%
	Horizontal,1	McNaught		0%
	Horizontal,2	Butterworth		0%
	Vertical,0	Kutateladze		0%
	Vertical,1	Kirkbride and Badger		0%
	Vertical,2	Lubuntsov		0%
Ideal cross flow h_{oCF}	CF,0	Colburn j (Bell)	CF,0	0%
	CF,1	Zukauskas		0%

4.5 Analysing all possible combinations

The purpose of this study was to develop a tool which can be used to evaluate the validity of tenders for new FWHs. The vendors do not disclose which correlations, of the range of different heat transfer correlations available in literature, they used for their design. It is not feasible to perform only one simulation and compare that with the tender claims. Instead, one needs to perform the analysis with all possible combinations of heat transfer correlations. Furthermore, a vendor might apply in-house correction factors to take into account the potential over or under-estimation of the correlations. This needs to be taken into account as well.

The range of possible combinations used in this study is presented in Figure 4-15 and illustrates that several combinations of *h* can be selected for a single model run. There are a total of 24 combinations for a 3 zone FWH. The *h* values generated from these correlations are identified as the nominal values because the uncertainty corresponds to 0%.

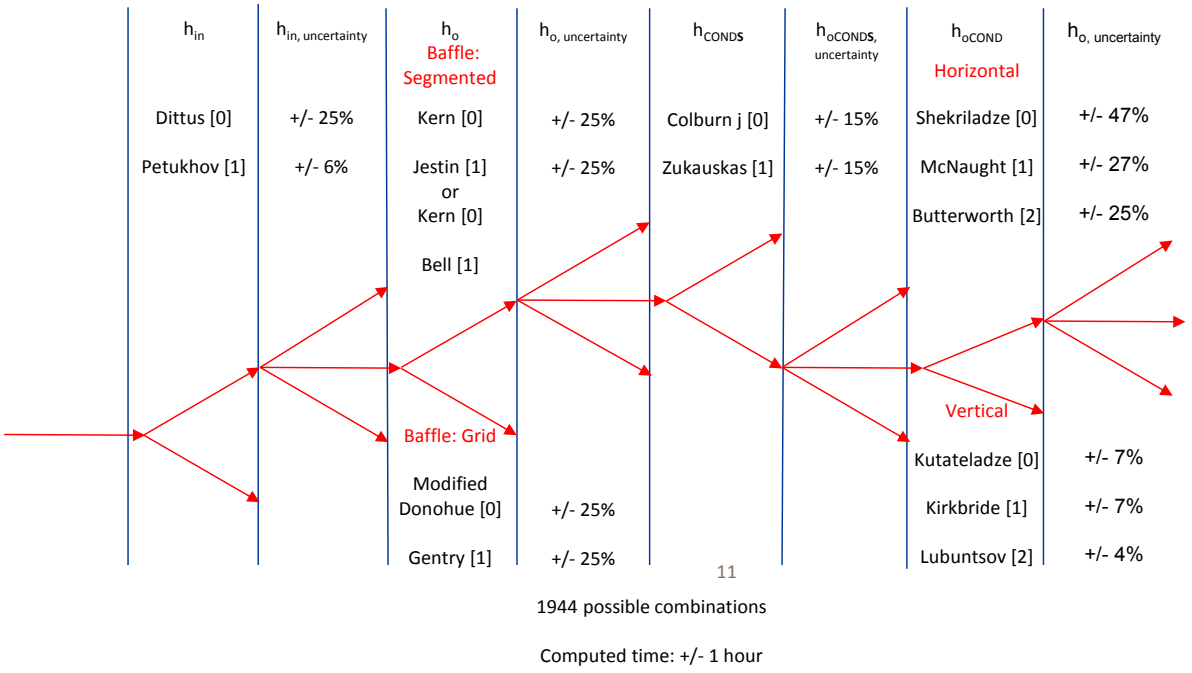

Figure 4-15. List of correlations and their associated uncertainty used in thermal model of which there are 1944 combinations in a heat transfer calculation for a 3 zone FWH

However, each correlation has an uncertainty that implies that there is a maximum and minimum value for each *h* computation. The model allows the user to select the applicable correlation and the uncertainty. Thus 3 values for *h* may be computed for each boundary layer in the three zones: a nominal, maximum and minimum value. This results in a total of 1944 combinations for a 3-zone FWH.

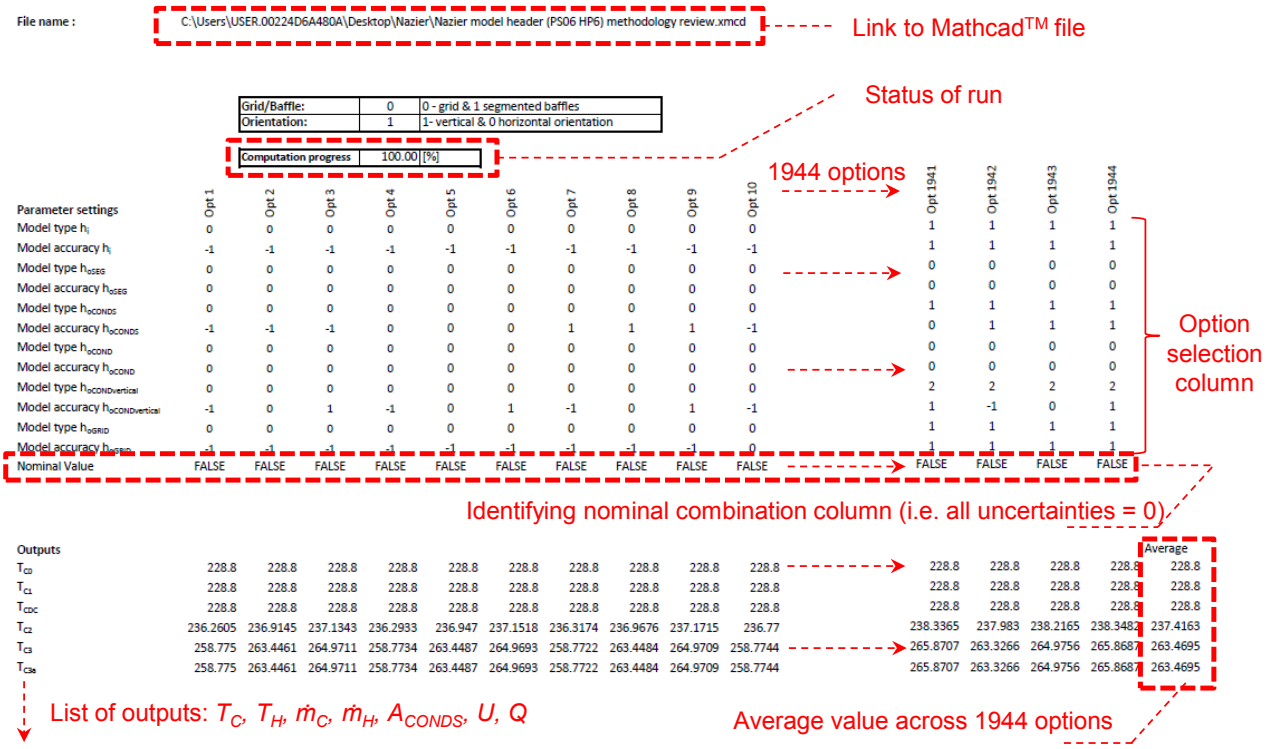

Figure 4-16. Screenshot of the Excel programme used to generate the results for the 1944 calculation

The complete model was developed in Mathcad. It makes use of input tables and flag settings to enable the user to choose different correlations and uncertainty. The Mathcad code produces a set of temperatures and other results for one specific set of user choices. To solve for all possible combinations, an Excel table was used. The table was generated using a script such that each column represents a new but unique combination of options (see Figure 4-16). The Mathcad model was then executed from within Excel using a script for each column in the table. Each time the new set of options was passed to Mathcad, and the results were sent back and stored in the table.

The outcome of solving for all possible combinations is that one can with reasonable confidence identify a min/max window in which the vendor claims should fall to be credible. Furthermore, from the statistics one can identify a most probable true answer, which can also be compared to the vendor's claims. The results of such a comparison will be showed in the next chapter.

5. Application of model, results and discussion

The credibility of the thermal model had to be verified by applying it to the following test cases:

- Evaluate the differences between the predictions of different film heat transfer coefficient (*h*) correlations. Two stations were selected in order to utilise all the correlations listed for this study.
  Station PS15 HP6 is a 3 zone FWH that is orientated horizontally and is fitted with grid baffles.
  Station PS00 HP6 is a 2 zone FWH that is orientated vertically and is fitted with segmented baffles.
- The previous thermal models, reviewed in Section 3.2, assume that the steam exits the DS as saturated steam. The current model calculates the exit steam temperature based on the geometry of the DS. The current model also accounts for single phase heat transfer of this steam (excess de-superheating) in the COND zone i.e. dry wall de-superheating.
  A test case is used to demonstrate that the exit steam temperature is sensitive to the size of the DS and that the effect of excess superheat in the exiting steam, from the DS, is captured in the current thermal model.
- Case studies, using FWH specifications from several Eskom stations, are used to demonstrate the robustness of the model and that there is acceptable agreement of the model results with vendor specifications.

5.1 Source of data

The performance of several FWHs in the Eskom fleet will be analysed with the aid of the thermal model to confirm its trend and versatility.

Eskom is the largest utility in South Africa and produces 95% of the electricity used in the country. The utility maintains and operates 24 stations, with a combined capacity of 44GW. The utility is engaged with 3 new build projects that include the construction of two (2) coal power stations and one (1) hydro-electric power station. There are a total of thirteen (13) coal power stations and a single nuclear power station in the fleet that utilise FWHs [5].

Plant visits were arranged to several power stations with the intention of the visits being to obtain the following data:

- **Heat balance sheet:** It specifies the operating conditions of important streams in the thermodynamic cycle at 100%MCR (maximum continuous rating) at original commissioning

conditions. It allows the heat duty (Q) to be calculated for each FWH by performing an energy balance on the feedwater line.

- **FWH specification sheet:** This sheet contains the mechanical design requirements of the FWH and may also specify the original operating conditions.
- **FWH drawings:** The vendor does not document mechanical design requirements of the baffle arrangement in the specification sheet. Hence, cross section drawings of the FWH needed to be viewed in order to confirm the type of baffles used.

The following power stations were visited with the intention of collecting data for their FWHs while data for station PS16 was obtained via the EPPEI centre:

- PS05 Power Station
- PS08 Power Station
- PS12 Power Station
- PS00 Power Station
- PS06 Power Station

Stations PS04 and PS09 Power Station were also visited but no data could be obtained from these sites. Factory visits to 3 local manufactures of FWHs was arranged and FWH related construction activities were witnessed at each of these sites.

5.2 Effect of different *h* correlations on model results

The correlations applicable to FWH thermal modelling was selected based on an extensive theory and literature review. More than one correlation is available for selection per heat transfer mode. In this section the effect of similar correlations are evaluated and the effect they have on the performance parameters are evaluated.

The two phase correlations, for both vertical and horizontal tubes, have shown good agreement. However, this is not the case with other heat transfer modes and can be demonstrated when the performance parameters are compared using an option *h[0]* and option *h[1]* or option *h[2]* correlation. Two case studies are used to compare the differences but note that a different case study may result in a slightly different factor of change.

The HP6 FWH from station PS16 is used as the case study to perform this comparison. This FWH is a 3 zone header type FWH that is orientated horizontally and is fitted with grid baffles, see Appendix C. The HP6 FWH from station PS00 will be used to evaluate the effect of the vertical condensation and segmented baffle correlations. This FWH is a 2 zone FWH that is orientated vertically and is fitted with segmented baffles.

The performance parameters for the reference case is generated by running the model with all the correlations selected to option 0. The model is then run again after one correlation is changed from option 0 to option 1 e.g. select h_{in} and use Petukhov correlation $h_{in}[1]$ instead of the Dittus and Boelter correlation $h_{in}[0]$. The performance parameter results from this run are compared to the reference case, $h_{in}[0]$, using the ratio of the two results. A relative change of around 1, for the performance parameters, implies that the variable is not sensitive to the change in correlation selection.

5.2.1 HP6 FWH from station PS16 (3 zone horizontal FWH with grid baffles)

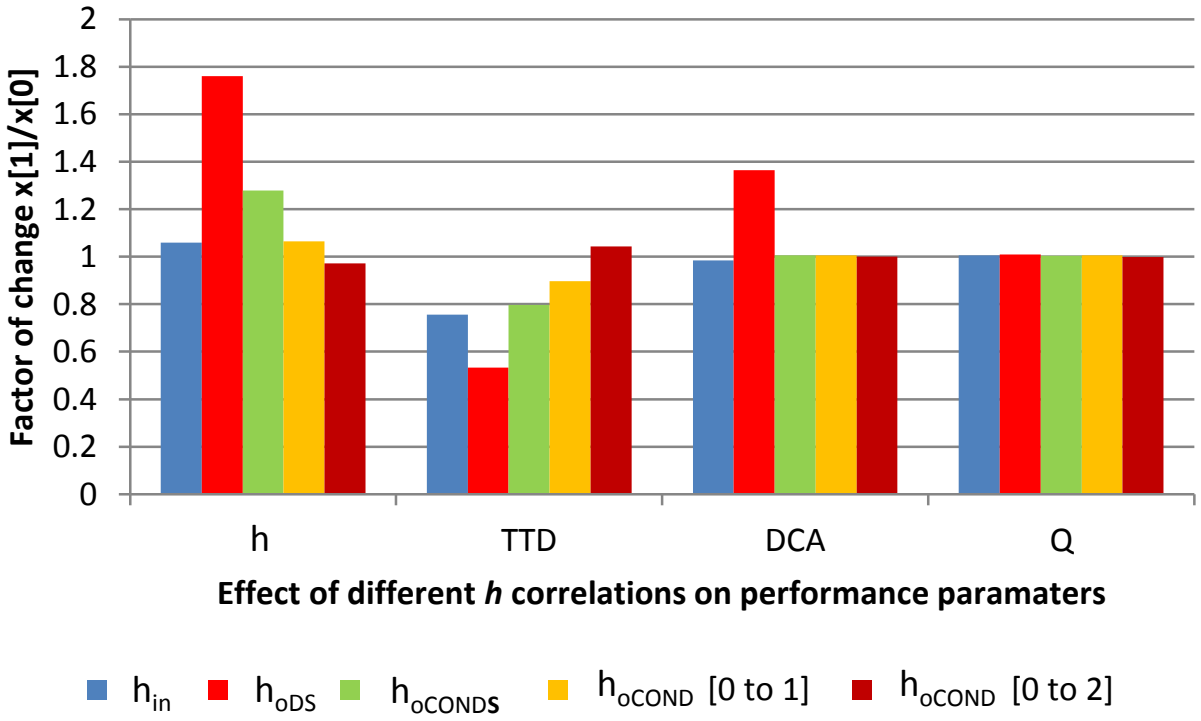

Figure 5-1. Effect of the option 1 or option 2 correlation on the performance parameters relative to the results from the option 0 correlation (PS16 HP6 case study)

Single phase heat transfer (h_{in}) comparison

The Petukhov correlation $h_{in}[1]$ is predicted to be marginally larger than the Dittus and Boelter correlation $h_{in}[0]$. The TTD and DCA improved because a 6% larger value for h_{in} is predicted with the option 1 correlation. The TTD dropped by 0.2°C and the DCA dropped by 0.1°C. There is no significant change in *Q*.

Single phase heat transfer (h_o) comparison (grid baffles)

There is a larger variation of h_o in the DC and DS zones. The Gentry correlation predicts an 80% larger h_o for the DS in comparison to the modified Donohue correlation for the DS see Figure 5-1.

The effect on the DC is not illustrated on Figure 5-1, but h_o for the DC drops by 20% and a detailed comparison is illustrated in Table 5-1. This drop in h_o adversely affects the DCA causing an increase of almost 40%.

Table 5-1 Comparison of option 0 and 1 correlations used to predict h_{oDC} and h_{oDS} for Medupi HP6

Option 0: Modified Donohue (Equation (2.56))	**Option 1:** Gentry (Equation (2.49))
$\frac{hD_e}{k}=\left(1+\frac{B_{grid}}{B}\left(2\left\lfloor\frac{A_{unitgrid}}{A_{unit}}\right\rfloor-1\right)\right)1.16\mathrm{D}_e^{0.6}\mathrm{Re}_{D_e}{}^{0.6}\mathrm{Pr}^{0.3}$	$\frac{hD_e}{k}=C_{RB}\mathrm{Re}_{D_e}{}^{0.8}\mathrm{Pr}^{0.4}$
$h_{sDC}=\left(70\frac{W}{m^2K}\right)(0.07)\mathrm{Re}_{D_e}{}^{0.6}\mathrm{Pr}^{0.33}=2952\frac{W}{m^2K}$	$h_{sDC}=\left(70\frac{W}{m^2K}\right)(0.009)\mathrm{Re}_{D_e}{}^{0.8}\mathrm{Pr}^{0.4}=2338\frac{W}{m^2K}$
$h_{sDS}=\left(6\frac{W}{m^2K}\right)(0.07)\mathrm{Re}_{D_e}{}^{0.6}\mathrm{Pr}^{0.33}=625\frac{W}{m^2K}$	$h_{sDS}=\left(6\frac{W}{m^2K}\right)(0.025)\mathrm{Re}_{D_e}{}^{0.8}\mathrm{Pr}^{0.4}=1100\frac{W}{m^2K}$

Cross-flow heat transfer (h_{oCF}) comparison

The cross-flow h_{oCF} predicted by the Colburn j-factor $h_{oCF[0]}$ correlation is almost 20% lower than that predicted by the Zukauskas correlation $h_{oCF[1]}$, see Figure 5-1.

Condensing heat transfer (h_{oCOND}) comparison

There is good agreement between the condensing zone correlations for a horizontally orientated tube bundle (option 0, option 1 and option 2), see Figure 5-1. The variation of h_{oCOND}, only affects TTD and not DCA because the assumption is that the DC shroud is always submerged with saturated water at the correct water level i.e. saturated water always enters the DC.

5.2.2 HP6 FWH from station PS00 (2 zone vertical FWH with segmented baffles)

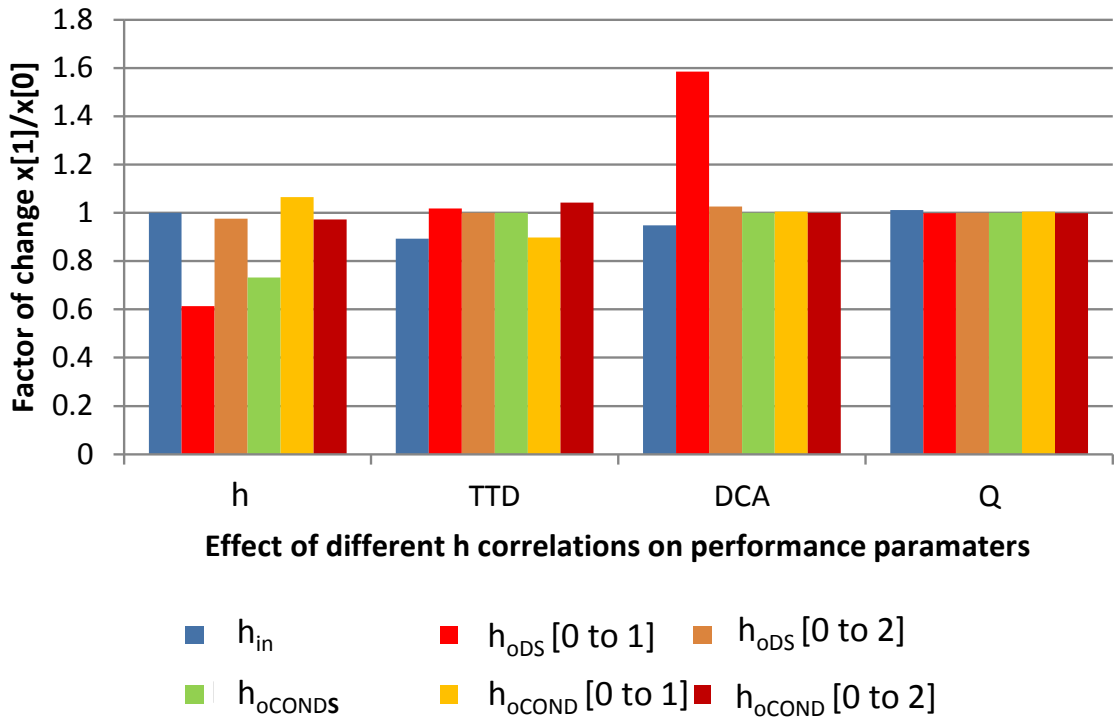

Figure 5-2. Effect of the option 1 or option 2 correlation on the performance parameters relative to the results from the option 0 correlation (PS00 HP6 case study)

Single phase heat transfer (h_{in}) comparison

A 20% change is also observed between the Petukhov correlation $h_{in}[1]$ Dittus and Boelter correlation $h_{in}[0]$ for this case study.

Single phase heat transfer (h_o) comparison (segmented baffles)

The option 1 and 2 correlations predict a smaller value with a reduction of 40% and 2%, respectively. The effect of the different correlations had a negligible effect on the total heat duty (Q), see Figure 5-2. There was almost no change in TTD because this FWH does not have a DS zone. The effect of the different h_o correlations were therefore only noticeable when comparing the DCA values. Option 1 predicts a smaller h_o which adversely affects DCA and results in an increase of almost 60%. There is almost no change in the Bell-Delaware model (option 2) prediction compared to that of option 0, which would imply no change in the DCA and is observed in Figure 5-2.

Cross-flow heat transfer (h_{oCF}) comparison

The cross-flow h_{oCF} predicted by the Colburn j-factor $h_{oCF}[0]$ correlation is almost 30% lower than that predicted by the Zukauskas correlation $h_{oCF}[1]$, see Figure 5-2. However, this does not affect any performance parameters because the steam enters at saturated conditions and therefore does not require excess de-superheating.

Condensing heat transfer (h_{oCOND}) comparison

There is also good agreement between the condensing zone correlations for vertically orientated FWHs. The *h* values predicted by the option 1 and option 2 correlations where compared to the value predicted by the Kutateladze correlation (option 0), see Figure 5-2. There is very little impact on the performance parameters because of this good agreement between the correlations.

5.3 Effect of DS heat transfer area on FWH performance

The model presented in this study incorporates the effect of excess superheat entering the COND zone with the inclusion of a COND**S** sub-zone, which essentially consumes a portion of the heat transfer surface available for condensation. A poorly designed (i.e. undersized) DS zone would therefore result in a large COND**S** zone, and negatively affect the performance of the FWH.

The LP3 FWH from station PS16 was used to confirm that the thermal model captures the effect of reducing the DS surface area on the performance parameters. The FWH is illustrated in Figure 5-3. Here the DS zone area is decreased but the total area is maintained constant (A_{HCOND} + A_{HDS}) by adding the deducted DS area to the COND zone.

The DS surface area was reported to be 157 m^2, see Appendix C. The FWH thermal model was run each time the DS area was reduced by 20%. The results at each increment is compared to the corresponding results at the reference case i.e. $A_{HDS(0)}$ = *157* m^2 or *100%*. The relative change in each parameter is then plotted as a function of the percentage reduction in A_{HDS}.

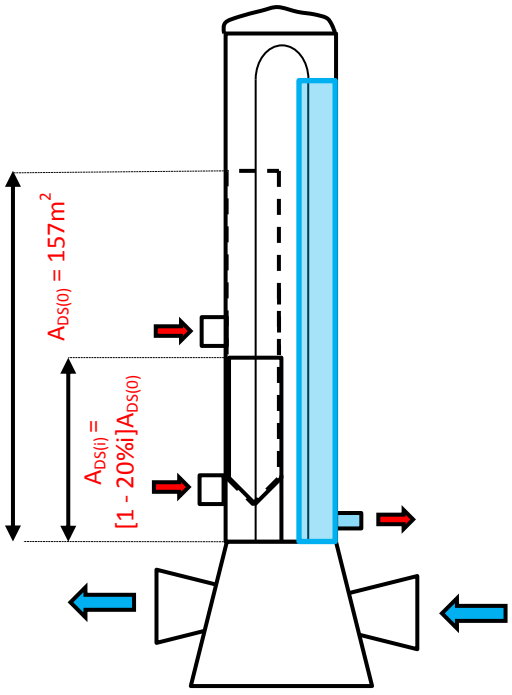

Figure 5-3. Station PS16 LP3 FWH

The option 0 correlations were used for all zones and sub-zones, except for estimating h_o where the Bell-Delaware correlation (option 2) was used.

An increase in TTD is undesirable because it implies that the feedwater exit temperature drifts away from T_{Hsat}. An increase in TTD was in fact observed for each incremental drop in A_{HDS} surface area, see Figure 5-4. This drop in feedwater exit temperature implies that the heat transfer calculated from an energy balance, on the feedwater side, will also drop as is observed from Figure 5-4. The four-fold increase in TTD results in a drop in heat transfer ability from 100% to 90%.

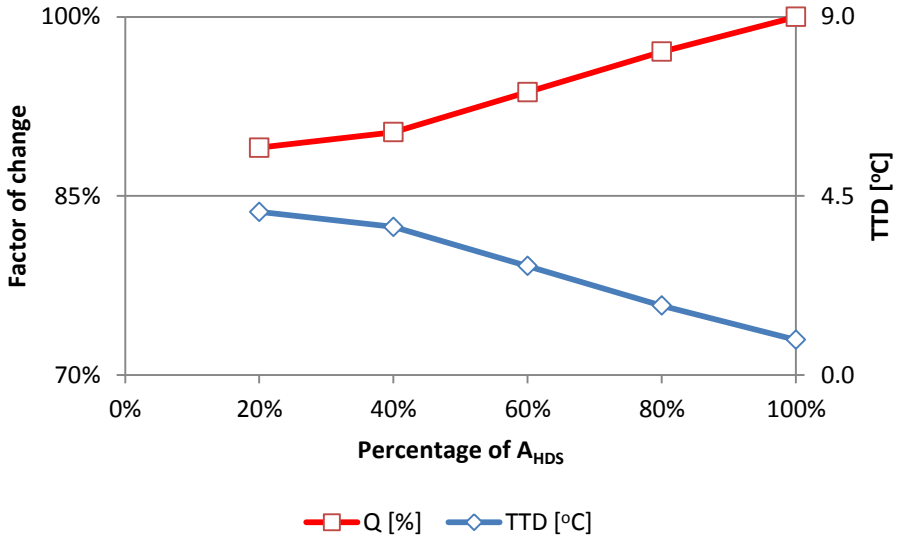

Figure 5-4. TTD and Q as a function of A_{HDS}

Recall that only the surface area in the COND**C2o** sub-zone, located in the last pass, is available for excess superheat removal (due to the model choices made, see 4.1.1). The portion of this area that is used for excess superheat removal is A_{HCONDS} while the remainder of this area will be used for latent heat transfer ($A_{HCONDC2}$), see Figure 4-7. It is therefore insightful to monitor the ratio of $A_{HCONDS}/A_{HCONDC2o}$ as a value of 1 will imply that all the available surface area in the last pass has been consumed for excess superheat removal, see Figure 5-5. This is the limit which the model can accommodate, after which all remaining superheat will be ignored.

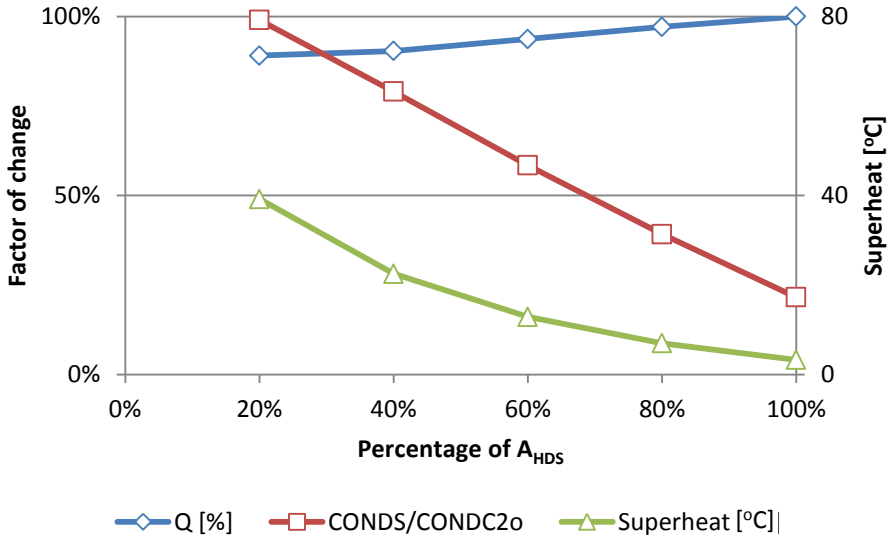

Figure 5-5. Q and COND**S** as a function of A_{HDS}

The drop in the *Q* and increase in excess superheat is observed in Figure 5-5 as more tubes are consumed for sensible heat removal. The available surface area in the last pass (COND**C2o**) was consumed when A_{HDS} was reduced by 80% (20%A_{HDS}). In fact, there is insufficient heat transfer surface available when A_{HDS} was reduced by 80%, resulting in the model ignoring any remaining superheat. This can be seen in the kink in the normally linear trends in Figure 5-4.

In a similar manner, it can be shown how operating a FWH at a higher bled steam inlet temperature, will result in a reduced performance because the DS has not been designed to remove the additional excess superheat.

5.4 Effect of DS heat transfer area on FWH size

The drop in TTD, caused by the incremenatal drop in DS area, can be improved by increasing the size of the COND zone. However, this implies that the FWH size needs to increase. If one assumes that the number of tubes remain constant then the FWH needs to become longer (L_{pass}).

Figure 5-6 shows the effect of maintaining the original TTD of $0.88^{o}C$ for all incremental increases in COND zone surface area. The COND zone surface area must be increased by 60% to maintain the original TTD if the DS area is dropped by 80%. The single pass length (L_{pass}) increases by 40% for this drop in surface area.

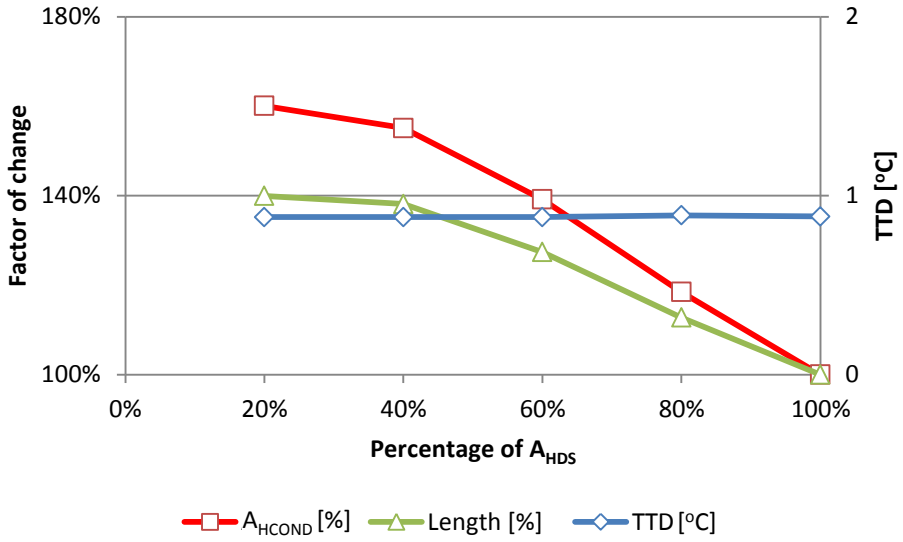

Figure 5-6. COND zone area and FWH length as a function of A_{HDS} if TTD is kept constant at 0.88°C

This analysis demonstrates the importance of designing the DS correctly such that only the minimum amount of excess superheat remains. This minimum is determined by the DWA margin selected for the particular design.

5.5 Model application to various FWHs

Accurate and complete thermal performance measurements of new FWHs are not available for any of the Eskom heaters. Hence, a validation test of the model is not possible. The compromise is to apply the model to a range of FWHs, which are already in service, where confidence has been established in the specification sheets based on its operating measurements. It is then assumed that these FWHs are performing as specified. Hence, if the model predicts a performance range that envelopes the vendor's claims, one can state that the model produces valid results.

To properly test the model, a range of various types of FWHs will be considered, shown in the table below. The detailed set of input parameters used for each FWH is presented in Appendix C.

Table 5-2 Variation of FWH designs analysed in this study

Station	Heater	Type	Zones	Orientation	Baffle type
PS00	LP2	Tube plate	COND + DC long	Horizontal	Segmented
	LP3	Tube plate	COND + DC long	Horizontal	Segmented
	LP4	Tube plate	COND	Horizontal	N/A
	HP5	Tube plate	COND + DC long	Vertical	Segmented
	HP6	Tube plate	COND + DC long	Vertical	Segmented
PS05	HP3	Tube plate	COND	Vertical	N/A
	HP4	Tube plate	COND	Vertical	N/A
	HP5	Tube plate	DS + COND	Vertical	Segmented
	HP6	Tube plate	DS + COND	Vertical	Segmented
PS06	LP1	Tube plate	COND	Horizontal	N/A
	LP2	Tube plate	COND	Horizontal	N/A
	LP3	Tube plate	DS + COND	Horizontal	Segmented
	LP4	Tube plate	DS + COND	Horizontal	Segmented
	HP6	Header	DS + COND + DC short	Vertical	Grid
	HP7	Header	DS + COND + DC short	Vertical	Grid
PS08	LP1	Tube plate	COND	Horizontal	N/A
	LP2	Tube plate	COND	Horizontal	N/A
	LP3	Tube plate	COND	Horizontal	N/A
	HP5	Header	DS + COND + DC long	Horizontal	Grid
	HP6	Header	DS + COND + DC long	Horizontal	Grid
PS12	LP1	Tube plate	COND	Horizontal	N/A
	LP2	Tube plate	COND	Horizontal	N/A
	LP3	Tube plate	COND + DC long	Horizontal	Grid
	HP5	Header	DS + COND + DC short	Vertical	Grid
	HP6	Header	DS + COND + DC short	Vertical	Grid
PS16	LP1	Tube plate	COND	Horizontal	N/A
	LP2	Tube plate	COND	Horizontal	N/A
	LP3	Tube plate	DS + COND + DC long	Horizontal	Grid
	HP5	Header	DS + COND + DC long	Horizontal	Grid
	HP6	Header	DS + COND + DC long	Horizontal	Grid

5.5.1 Metrics for interpreting the results

Since the model can produce results for all combinations of *h* options, some statistical metric is needed to properly interpret the results. Two metrics will be used: the first will compare a mean value to the vendor's claim; while the second metric verifies if the vendor's claim lies within the bounds of all possible values.

The arithmetic mean of a performance parameter is calculated from the model runs where the nominal h correlations are used i.e where the uncertainty is selected to zero for all the correlations. The absolute deviation (Δ_1) is calculated by subtracting the vendor's claim from this mean value predicted by the model, see Equation (5.1). It is desired to have Δ_1 equal to zero as it indicates that the vendor's claim coincides with the most probable solution considering all possible correlation choices.

$$\Delta_1 = mean(x_{\text{Model,Nominal}}) - x_{\text{Contract}} \tag{5.1}$$

The second comparison technique, Δ_2, verifies if the vendor's claim lies within the bounds of all possible results predicted by the model. It is a normalized metric since the difference from the mean is divided by the difference between the maximum and minimum value predicted by the model. The range is computed using all the permutations in the thermal model that will arise due to the selection of the specified *h* correlations together with their associated uncertainty. There are a total of 1944 permutations for a 3 zone FWH, which includes the 24 nominal cases. This metric is an indication of how significant the deviation is from the total range of expected result. This is because a large absolute deviationΔ_1 could be acceptable if the possible range is also very large. This is demonstrated by Figure 5-7.

$$\Delta_2 = \frac{\left| mean(x_{\text{Model,Nominal}}) - x_{\text{Contract}} \right|}{x_{\text{Model,Max}} - x_{\text{Model,Min}}} \tag{5.2}$$

The ideal results would correspond to the following:

- Δ_1 to be close to 0
- Δ_2 to be close to 0
- $x_{Min} < x_{Contract} < x_{Max}$

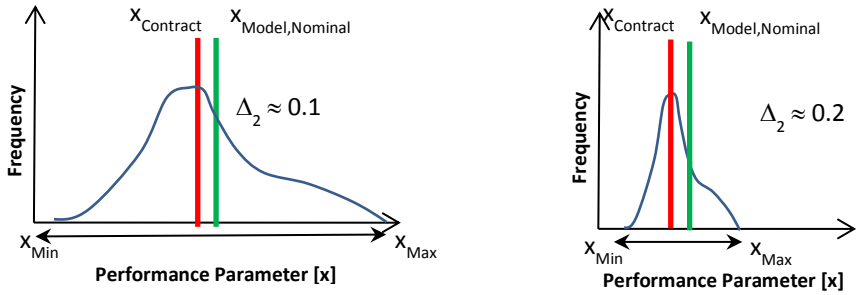

Figure 5-7. Graphic representation of Δ_2 for large and small ranges

It should also be noted that the model does not consider fouling on either side of the tube since this is not disclosed in the specification sheets. The allowance for plugging is only included if it is disclosed in the specification sheets, which only applies to the FWHs of station PS16. These are factors of conservatism added by the vendor, which could result in the model predicting better performance than claimed.

5.5.2 Example of results for one FWH

This section presents the detail results obtained for one FWH as an example. The way in which the inputs were generated, as well as the post processing and interpretation of the results, will be presented. The FWH of this example is a 3-zone horizontally orientated header type with grid supports.

- **Data from FWH specification sheets and drawings used as inputs to model**

  Data from the specification sheet and basic cross section drawing was extracted and summarised in a single input sheet as illustrated in Figure 5-8 (The input sheets of all the FWHs used in this study is provided in Appendix C.). The data from the input sheet is a direct entry into the thermal model. The contracted values documented by the vendor are also illustrated in Figure 5-8. The operational data used to generate the performance parameters is obtained from the heat balance in the absence of commissioning data.

  The HP6 FWH from station PS16 is not fitted with segmented baffles but an arbitrary input for the baffle cut (B_{cut}) is required in order for the programme to initiate even though it has no impact on the results. The baffle spacing (L_B) is applicable for both segmented or grid type baffles. Similarly, the steam quality for the bled steam and cascading streams may be required if the conditions of these streams are at saturation conditions. A value must be entered even if these streams are not at saturation conditions and default values are suggested. A value of 0 kg/s must be entered if no cascade flow is present.

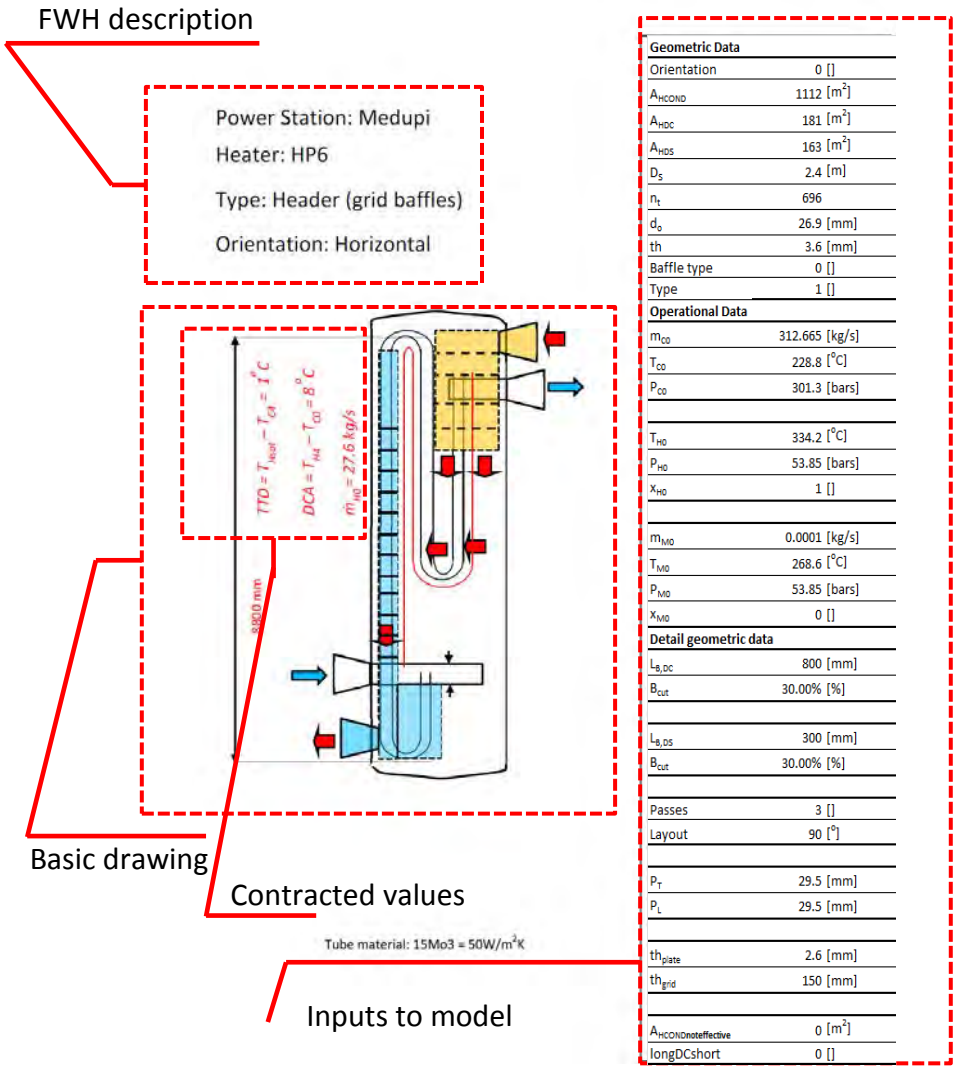

Figure 5-8. Extract from Appendix C illustrating input sheet for the HP6 FWH from station PS16

- **Results**

The results of each performance parameter for all the options can be plotted on a frequency plot to get an indication of the spread of solutions. This is shown in Figure 5-9 and similar graphs are presented in Appendix E for remaining FWHs investigated in this study. The red vertical bar represents the contracted value. Note that the shape of the frequency plot is not expected to fit a normal distribution; hence a standard statistical analysis has not been applied. This is very evident in Figure 5-9(b) and clearly indicates the jumps from one heat transfer correlation option to another.

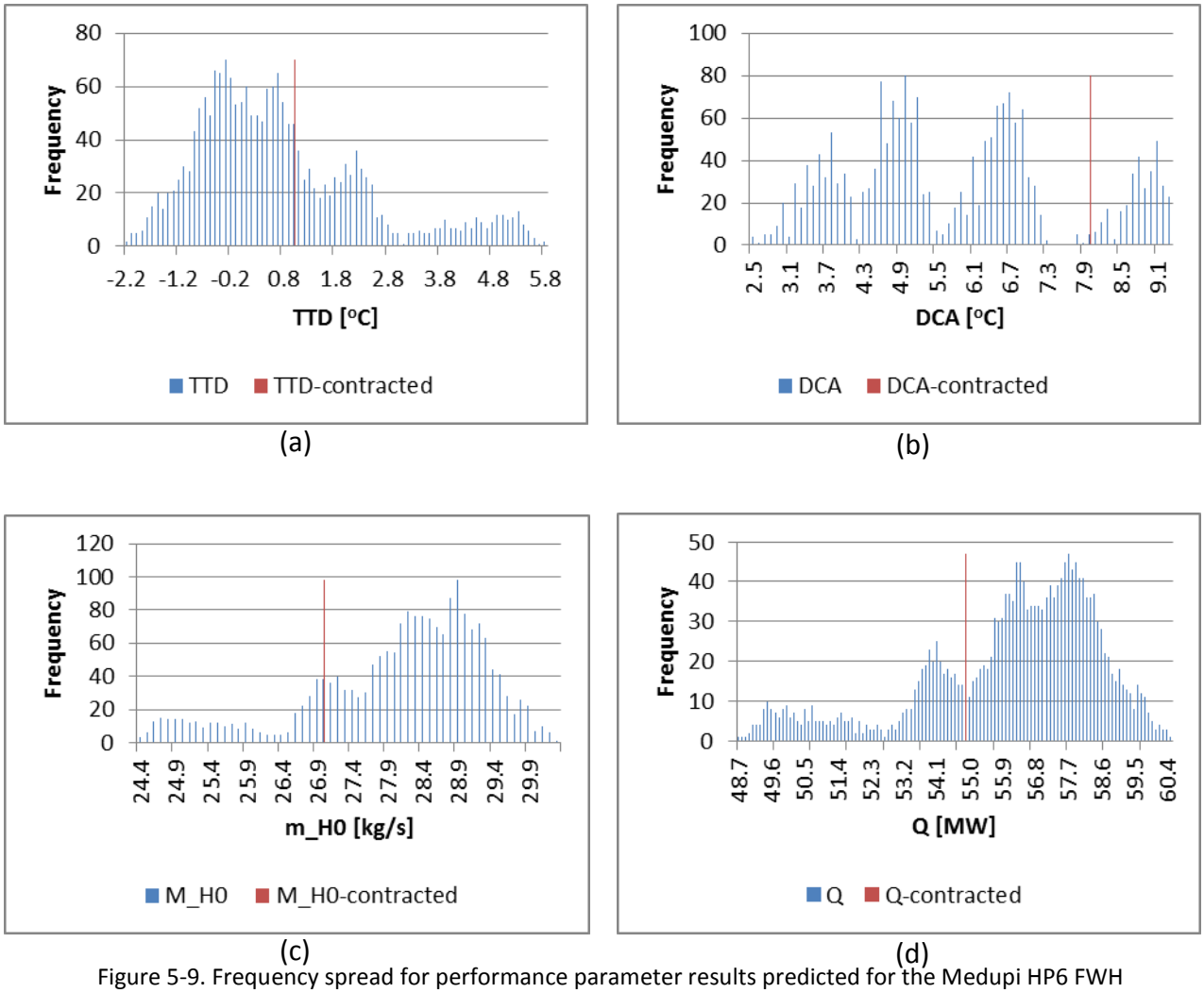

Figure 5-9. Frequency spread for performance parameter results predicted for the Medupi HP6 FWH

The results from the model are presented in the table below and display both the arithmetic mean, minimum and maximum value of the particular performance parameter. This is compared to the contractors claim using the two deviation metrics defined previously.

The average value for TTD produced by the model predicts that the FWH will perform better than the claim made by the vendor. This is also the case with the DCA and the deviation falls within the range of possible values predicted by the model, see Figure 5-9(a) and Figure 5-9(b). The thermal design limit of achieving a DWA greater than 1°C was confirmed and was calculated to be 1.4°C.

Table 5-3 Medupi HP6 FWH model results compared with contracted values

Medupi HP6 FWH								
	Units	**Min**	**Mean**	**Max**	**Claim**[55]	Δ_1	Δ_2	**Range**
TTD	[^oC]	-2.3	0.2	5.8	**1**	-0.85	10%	Yes
DCA	[^oC]	2.4	5.5	9.3	**8**	-2.5	36%	Yes
DWA	[^oC]	-3.3	1.4	4.4	**1**	0.4	5%	Yes
$\dot{m}_{H0}$	[kg/s]	24.3	28.4	30.3	**27**	1.4	23%	Yes
U_{DC}	[W/m^{2}K]	1193.6	1785.3	2405.2	**1340**	445.3	37%	Yes
U_{CONDC1}	[W/m^{2}K]	2173.1	3404.5	4453.1	**2980**	424.5	19%	Yes
U_{CONDR}	[W/m^{2}K]	2318.1	3556.6	4662.6	**2980**	576.6	25%	Yes
U_{DS}	[W/m^{2}K]	396.7	745.2	1189.5	**720**	25.2	3%	Yes
Q_{TOTAL}	[MW]	48.6	56.9	60.5	**54.9**	2	16%	Yes
A_{HCONDS}	[m^2]	69.8	200.8	202.2				

The estimation of the average bled steam mass flowrate, $\dot{m}_{H0}$, is slightly larger than the vendor's claim. Since all the steam is condensed in the heater, one would expect the total heat transfer rate (Q) to increase as well. This is because latent heat transfer is the primary mechanism to heat the feedwater. The frequency distribution of the bled steam should therefore have a similar shape as the heat transfer, as is observed in Figure 5-9 (c) and (d).

The primary driver for the overall better performance is the larger mean U value for each of the zones. In other words, it is possible that the vendor has underestimated the heat transfer in the different zones or has built in a safety factor for plugging and fouling allowances. If Δ_2 was considerably large, say more than 50% for all the zones, one could suggest to the vendor to reduce the size of the FWH to achieve better cost optimization.

5.5.3 Summary of results for TTD

The Figure 5-10 presents the deviation between the model and vendor values for all the FWHs analysed in this study. A negative absolute deviation indicates that the model predication is more conservative. A positive deviation does not necessary mean a poorly designed FWH as the vendor's value may still lie in the range of values calculated with the full selection of correlations, and their associated uncertainties. The TTD values reported by all the vendors ranges between -2^{o}C to 4^{o}C. The absolute TTD deviation or Δ_1 varies between -3 ^{o}C and 2^{o}C over the range of FWHs analysed in this study. The model runs predicts that almost 60% of the 30 FWHs would perform better ($\Delta_1 < 0$) than that reported by the vendors, while 20% of the FWHs exhibit a marginal difference.

The remaining FWHs exhibit $\Delta_1 > 0$, which infers that the vendor over estimates the performance of their FWHs. The user may therefore challenge the vendor about their design but should also bear in mind that the thermal model does not consider wet de-superheating. Wet de-superheating is prevalent on the lower order FWHs where steam enters the FWH with up to 50°C of superheat. A DS is not used in this application because the tube wall temperature is lower than saturation temperature, which results in condensation of the superheated steam.

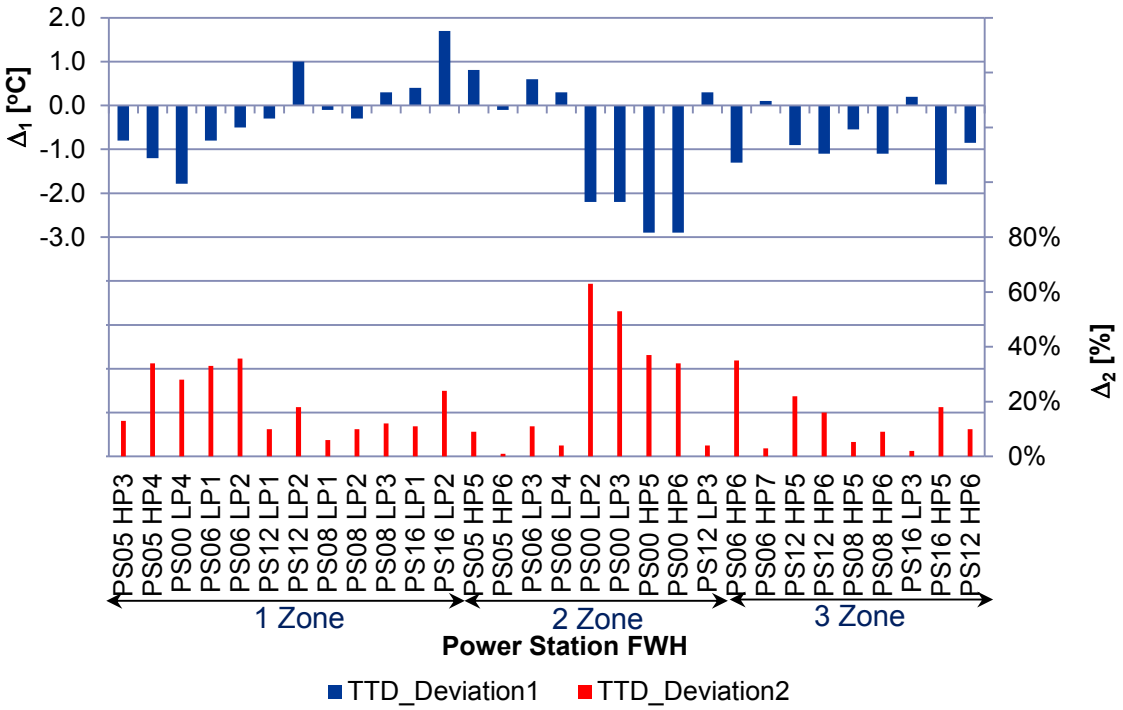

Figure 5-10. Prediction of TTD deviations for FWHs analysed in this study

The Δ_2, which compares this absolute deviation to the range of all possible results, varies between 1% and 60%. However, even with this large deviation only the vendor's claim for Koeberg HP5 and Koeberg HP6 lies outside the range of results predicted by all model permutations (see Appendix E-21). The vendor's claim is in fact more conservative, which implies that the model predicts a better performing FWH.

5.5.4 Summary of results for DCA

The DCA does not apply to FWHs not fitted with a DC zone. Hence, the DCA deviations are not displayed for these FWHs in Figure 5-11.

The DCA values reported by the vendors range between 5°C to 12°C. The absolute DCA deviation or Δ_1 varies between -6°C and 5°C, where a negative value indicates that the model predicts a better performing DC.

The Δ_2 results indicate that the Kriel HP7 vendor value is significantly higher than the model result and it also lies outside the range of results predicted by the model (see Appendix E-11). Hence, the performance of this FWH may require further evaluation. The original data for this FWH was extracted from a tender evaluation and no detailed drawing was available to confirm the values in this document.

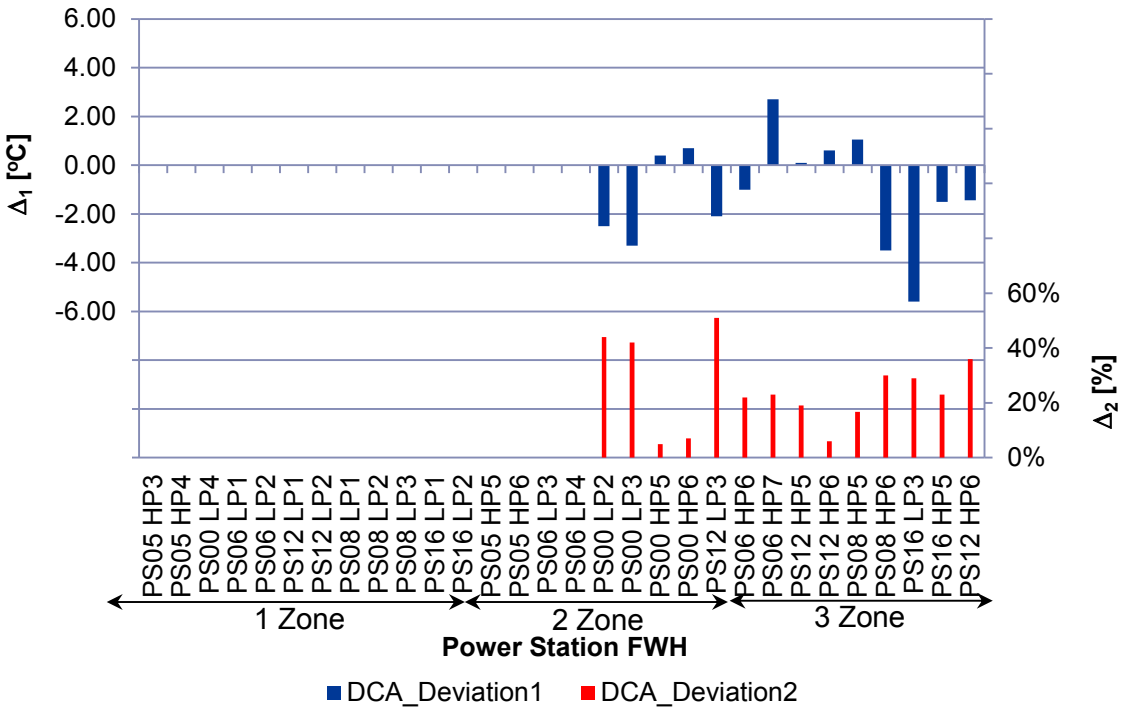

Figure 5-11. Prediction of DCA deviations for FWHs analysed in this study

5.5.5 Summary of results for *Q*

The trend followed by the bled steam mass flow rate ($\dot{m}_{H0}$) and heat duty (Q) is very similar, hence only the model results for Q will be discussed. However, the results for both $\dot{m}_{H0}$ and Q are presented in Figure 5-12 and Figure 5-13, respectively.

The absolute deviation of Q or Δ_1 varies between -3 MW and 4 MW, where a positive value indicates a more conservative model prediction.

Even though there are cases (almost 40% of the FWHs in study) where the vendor reports a larger prediction of Q it still lies within the range of possible results predicted by the model. The maximum value for Δ_2 is 60%, which implies that the Δ_1 encompasses 60% of the possible model answer range.

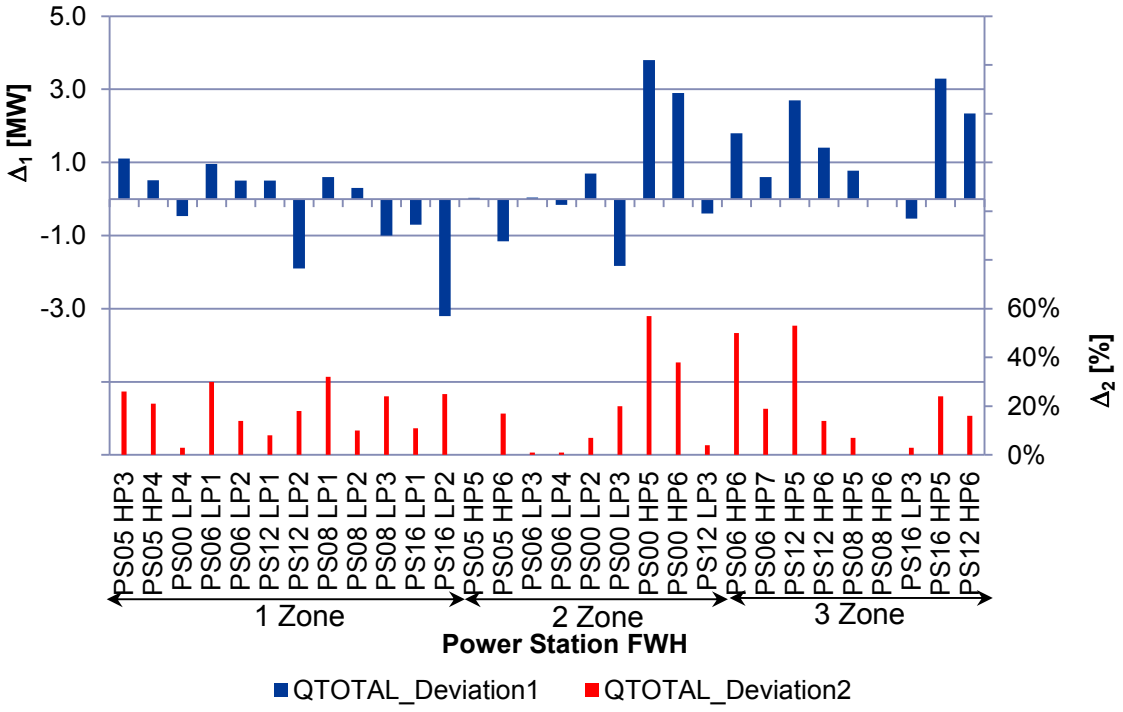

Figure 5-12. Prediction of deviations in *Q* for FWHs analysed in this study

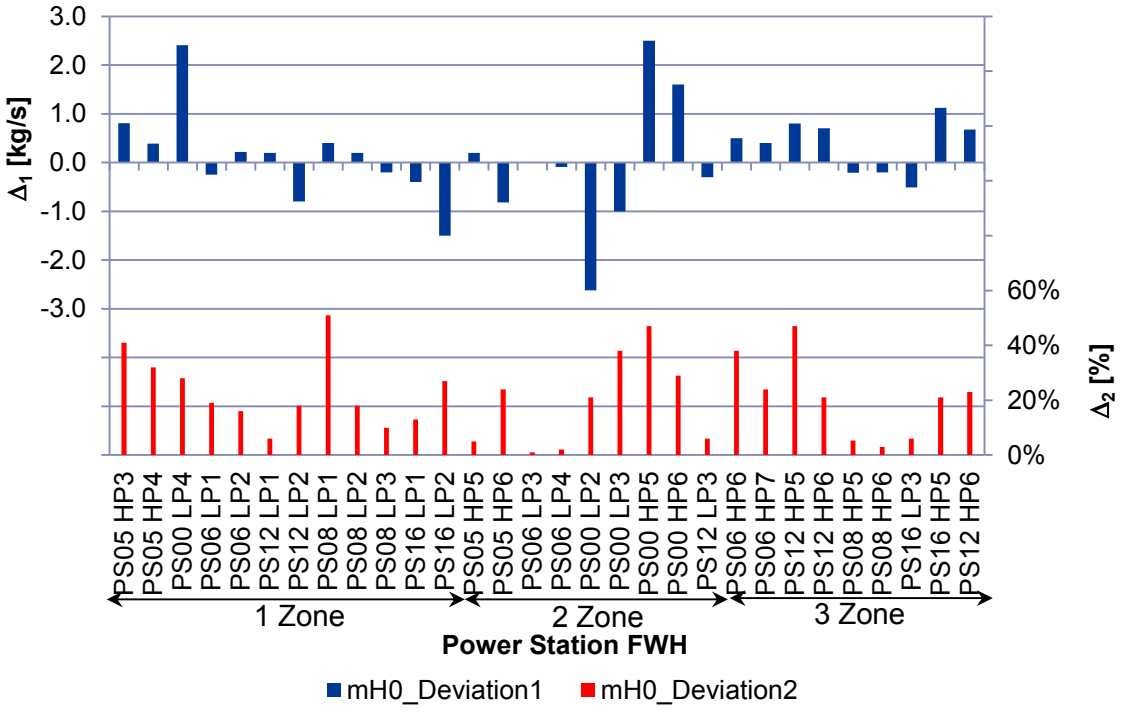

Figure 5-13. Prediction of deviations in m_{H0} for FWHs analysed in this study

5.5.6 Summary of results for DWA

The FWHs highlighted in Figure 5-14 are all fitted with a DS zone. It is imperative that the DWA of greater than 1°C is maintained to avoid tube erosion that affects the longevity of the tube bundle. The deviation from this limit is presented in Figure 5-14. The HP5 and HP6 FWH from the new station PS16 complies with this limit and indicates that designers are now considering DWA as a critical design limitation for FWHs fitted with DS zones.

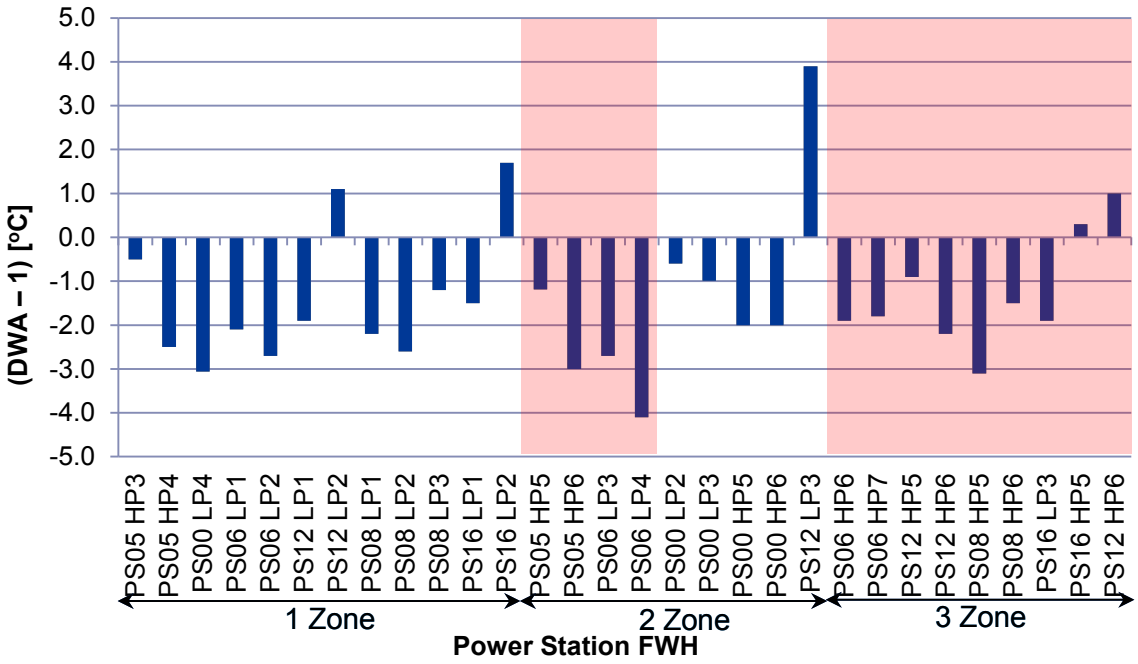

Figure 5-14. Prediction of DWA deviations from HEI standard limit of 1°C for FWHs analysed in this study

5.5.7 Summary of results for A_{CONDS} consumption

The available area in the last pass (CON**C2o**) of CONC was allocated for excess superheat removal. A single phase external heat transfer mode was adopted in this study even though tube wall temperatures at the exit of the DS or at the inlet nozzle may be less than the saturation temperature ($T_w < T_{Hsat}$). The model allows COND**S** to be between 1% and 99% of the CON**C2o** sub-zone area. The calculation will progress even if the maximum area is consumed and it will be assumed that all the excess superheat is removed in this region.

The FWHs highlighted in Figure 5-15 are fitted with a DS zone, but still many of them consume the total available area in the last pass. It was found that the actual required surface area for complete excess superheat removal may vary between 1 to 3 times the available area in the last pass (COND**C2o**).

The 1 zone LP FWHs that receive extraction steam with excess superheat also consumes COND**C2o** surface area. The application of dry wall de-superheating may be a model shortcoming in this particular type of FWH but is nevertheless a conservative approach.

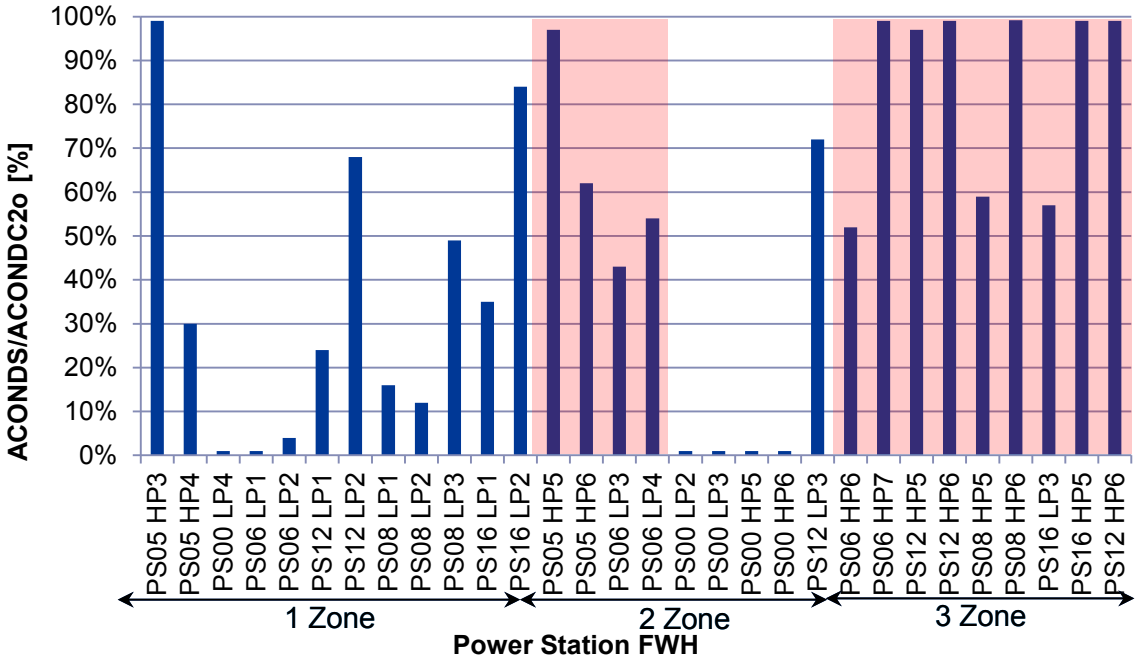

Figure 5-15. Consumption of COND zone surface area in the last pass (COND**C2o**) for excess superheat removal (COND**S**) for FWHs analysed in this study

The thermal model predicts an over estimate for *Q*, for 50% of the stations fitted with a DS, even with this conservative assumption of only dry de-superheating in the COND**S** sub-zone.

However, the remaining 50% of the stations consume all the allocated area in the last pass. This could be a genuine concern or could be attributed to the assumption that only single phase heat transfer occurs in this region. The model can be improved by incorporating the following conditions:

- Extend the COND**C2o** (COND**C2 +** COND**S**) sub-zone into the bottom COND**C1** pass or passes.
- Include wet de-superheating in the COND**S** sub-zone that requires a continuous update of the tube wall temperature in this region.

6. Conclusions and recommendations

6.1 Conclusions

The purpose of this study was to develop a FWH thermal model that predicts the performance parameters of a particular FWH, which has been achieved. The model assumes that there is no fouling and is therefore ideally suited for evaluating an existing FWH against it original contractual specification. It may also be used to evaluate a new FWH during a technical tender. Vendors do not disclose their complete design, which made it important to identify the minimum number of inputs for the model that would produce meaningful results. Due to the lack of commissioning data, the model results were compared to contractual specifications. The thermal model's validity was verified by executing the following secondary objectives:

- Identify applicable heat transfer correlations for the thermal modelling of FWHs.
- What internal zone definitions are needed to allow the model to properly capture the heater performance? This is specifically important for the condensing zone where most models assume that saturated steam exits the DS zone, though in practice this is not the case.
- Do the results from case studies demonstrate the robustness of the model and is there acceptable agreement of the model results with vendor specifications on existing power stations?

An account of how each of these objectives was met is presented in the following sections.

6.1.1 Selection of *h* correlations applicable to FWHs

The heat transfer mode determines which heat transfer correlations are applicable. The list of correlations applicable to FWH thermal modelling was selected from the heat transfer theory and other FWH thermal models published in open literature. The selection of these correlations is further complicated by the fact that there is more than one accepted correlation for a particular heat transfer mode.

The user of the model therefore has the functionality to select a correlation from a list of possible correlations, refer to Table 4-2 for the list. The model run can be repeated with an alternative correlation in order to compare the results from two or more model runs. There are a total of 4 heat transfer modes with at least 2 selections in each mode. Any combination may be selected resulting in a total of 24 possible combinations for a 3 zone FWH. Additionally the min/max tolerance of each correlation may also be activated, allowing one to evaluate the most optimistic or conservative result.

6.1.2 Inclusion of the COND**S** zone

An additional sub-zone was added to the general FWH model, employed in previous studies, to account for excess superheat entering the COND zone. In previous studies, the DS exit steam temperature is assumed to correspond to the saturation temperature. However, this is not the case as vendors deliberately design the DS such that the steam exits above the saturation temperature. This implies that previous thermal models may have overestimated the performance of a FWH. The COND**S** region is modelled as a single phase heat transfer region and therefore has a substantially lower *h* compared to the COND zone. The inclusion of this zone will therefore provide a more conservative analysis.

The model was tested on a FWH, from station PS16, where the size of the DS was decreased in 20% increments. The model was able to predict the drop in performance of the FWH due to the increase in superheat of the DS exiting steam. The same test case was used to determine the additional COND zone surface area required to absorb the drop in performance of the FWH. The model predicted that the FWH length would have to increase by almost 40% to absorb a drop in A_{HDS} of 60%. The effect of a further drop in A_{HDS} could not be accurately evaluated because the available surface area for the COND**S** region was consumed when A_{HDS} was reduced by 80%.

6.1.3 Case studies

A total of 30 FWHs of different types have been analysed with the aid of this thermal model. The results closely match the FWH performance predicted by the vendor. The exceptions that were noted could be explained, though others may in fact be inaccuracies by the vendor.

The deviation ($\Delta_1 < 0$) in *Q,* for the 30 FWHs, varied between 8% and -5%. This corresponds to 1.2 MW and -3.2 MW, respectively. The TTD varied between 2^{o}C and -3^{o}C. The TTD results indicate that 80% of the FWHs are over designed while the design of the remaining FWHs should be challenged after evaluating the impact of wet de-superheating. It was observed that only the HP heaters of the new power stations would report a DWA that exceeds the safe design limitation of 1^{o}C. This indicates that DWA was considered in this tender.

Although no detail commissioning data was available for proper model validation, it was proven that the consistent results produced from the case studies has added credibility to the thermal model.

6.2 Limitations and other applications

The treatment of the last pass as the only region (COND**S**) allocated for the removal of excess superheat is a model limitation. This limitation could be eliminated in a future study by including wet de-superheating in the COND**S** and to increase available area beyond the last tube pass.

The lack of directly applicable *h* correlations for grid baffles has identified a niche for further research. The theoretical development of the modified Donohue correlation (Equation (2.56)) requires further experimental testing but has shown good correlation for estimating *h* for the DS but dramatically lower values for the DC.

Although the main purpose of the model is to be used to evaluate tenders for new heaters, it is also suitable for performance evaluation of existing heaters, provided that the heater has been recently cleaned, and plugged pipes are taken into account.

The internal arrangement of several FWHs could not be determined because of the lack of detailed drawings. Hence, the arrangements of the vessels were assumed based on the observations made on other FWHs.

6.3 Recommendations for future work

A complete run of the 1944 correlation permutations, using the Excel interface with Mathcad®, takes on average 1 hour with a standard desktop PC. It is also cumbersome because the Mathcad® file address must be verified for each case study. Further work is required to incorporate the Excel functionality in the Mathcad® file, or translate the model into a seamless executable program.

The treatment of the last pass as the only region (COND**S**) allocated for the removal of excess superheat is a model limitation. This limitation could be eliminated in a future study by including wet de-superheating in the COND**S** and to increase available area beyond the last tube pass.

The hydraulic analysis of the FWH may be added in a future study. The computed pressure drops will feed into the thermal model and will drive and adjustment of the thermal conditions.

The thermal model can be extended to incorporate fouling and tube plugging. An additional study, that analyses these considerations may be evaluated in the future in order to extend the model's application to FWHs in operation.

7. List of References

[1] T. Terranova and I. Gibbard, *Power plant feedwater heaters*, no. 0. Power Plant Enginering, 2006.

[2] BiLFINGER Power Systems (Steinmuller Africa), “High pressure feed water heater Process design,” *BiLFINGER Power Syst. (Steinmuller Africa) Tech. Man.*, pp. 199–205, 2014.

[3] HEI, “Tech sheet #127: Basics of closed feedwater heaters,” 2007.

[4] L. Jestin, “EPPEI course: Power plant basic design presentation,” 2013.

[5] B. Maccoll, D. Morawiak, and A. Hesom, *Eskom Power Plant Engineering Institute: 2012-2013 Programme*. 2013.

[6] Eskom, “Koeberg Process Animation,” 2014. [Online]. Available: http://www.eskom.co.za/Whatweredoing/ElectricityGeneration/KoebergNuclearPowerStation/Pages/Operating_Method.aspx.

[7] P. Stephan, H. Martin, S. Kabelac, D. Mewes, M. Kind, and K. Schaber, *VDI Heat Atlas*. Springer, 2010, p. 696.

[8] S. Kakac and H. Liu, *Heat Exchangers Selection, Rating, and Thermal Design*, 2nd ed. New York: CRC Press, 2002, p. 308.

[9] Heat Exchanger Institute, “HEI Closed Feedwater Heaters 8th Edition,” *Stand. closed Feed. heaters*, no. 8th Edition, 2009.

[10] J. R. Welty, C. E. Wicks, R. E. Wilson, and G. L. Rorrer, *Fundamentals of Momentum, Heat, and Mass Transfer*, 5th ed. Wiley, 2008.

[11] I. TUBULAR EXCHANGER MANUFACTURERS ASSOCIATION, *Standards of the Tubular Exchangers Manufacturers Association*, 8th ed. 1999.

[12] K. Thulukkanam, *Heat Exchanger Design Handbook*, 2nd ed. 2013, p. 1260.

[13] A. Bejan, *Convection heat transfer*. John Wiley & Sons, 2013, p. 379.

[14] C. C. Gentry, M. C. Gentry, and G. E. Scanlon, “Shell and tube heat exchanger applications,” *Pet. Technol. Quart.*, pp. 95–101, 1999.

[15] W. H. McAdams, *Heat transmission*, 1st ed. New York McGraw-Hill Book Company, Inc, 1942.

[16] B. S. Petukhov, “Heat Transfer and Friction in Turbulent Pipe Flow with Variable Physical Properties,” vol. 6, pp. 503–564, 1970.

[17] J. P. Holman, *Heat Transfer*, 6th ed. McGraw-Hill, 1986, p. 277.

[18] D. Q. Kern, *Process Heat Transfer*, 1st ed. McGraw-Hill, 1950.

[19] EPRI, “Classical Heat Exchanger Analysis,” 2013.

[20] Bronswerk(R) Heat Transfer, “EM Baffle,” 2015. [Online]. Available: http://www.bronswerk.com/en/EM-Baffle/SA80/. [Accessed: 13-Apr-2015].

[21] D. A. Donohue, “Heat Transfer and Pressure Drop in Heat Exchangers,” *Ind. Eng. Chem.*, vol. 41, no. 11, pp. 2499–2511, 1949.

[22] K. Shiina, S. Nakamura, and S. Matsumura, “Shell Side Heat Transfer Characteristics to Water Flowing Parallel with an Eggcrate Support Plate for Water in Parallel Flow,” *Trans. Japan Soc. Mech. Eng. Ser. B*, vol. 64, no. 620, pp. 1187–1195, 1998.

[23] L. Jestin, “personal communication,” 2015.

[24] K. J. Bell, “Final Report of the Cooperative Research Program on Shell and Tube Heat Exchangers (Bulletin No. 5, University of Delaware Engineering Experimental Station Network),” 1963.

[25] A. D. Kraus and A. Bejan, “Heat Exchangers,” in *Heat Transfer Handbook*, John Wiley & Sons, 2003.

[26] R. Mukherjee, “S H E L L- A N D - T U B E H E AT E X C H A N G E R S,” *Chem. Eng. Prog.*, no. February, 1998.

[27] M. Harsha, “Heat exchanger sectional view,” 2012. [Online]. Available: https://grabcad.com/library/shell-and-tube-heat-exchanger--1.

[28] M. V. Holloway, T. a. Conover, H. L. McClusky, D. E. Beasley, and M. E. Conner, “The Effect of Support Grid Design on Azimuthal Variation in Heat Transfer Coefficient for Rod Bundles,” *J. Heat Transfer*, vol. 127, no. 6, p. 598, 2005.

[29] O. Augustyn, “personal communication with Eskom assistant engineer that performs FWH performance assessments,” 2014.

[30] K. J. Bell and A. C. Meuller, “Delaware rating for shell-side rating of shell and tube heat exchangers,” in *Wolverine tube heat transfer book*, Wolverine Tube Inc., 2001.

[31] Y. Ali Kara and Ö. Güraras, “A computer program for designing of shell-and-tube heat exchangers,” *Appl. Therm. Eng.*, vol. 24, no. 13, pp. 1797–1805, Sep. 2004.

[32] Wolverine Tube Inc., “Engineering Data Book III,” 2000.

[33] R. Laskowski and K. Wawrzyk, “Comparison of two simple mathematical models for feed water heaters,” vol. 91, no. 1, pp. 14–22, 2011.

[34] E. Cao, *Heat Transfer in Process Engineering*, 6th ed. 2009.

[35] Yunus A. Cengel and A. J. Ghajar, *Heat and Mass Transfer Fundamentals and Applications*, 5th ed. McGraw-Hill, 2011, p. 901.

[36] W. L. McCabe, J. C. Smith, and P. Harriott, *Unit operations of chemical engineering*, 5th ed. McGraw-Hill, 1993.

[37] M.-H. Chun and K.-T. Kim, “A new natural convection heat transfer correlation for laminar and turbulent ilm condensation derived from a statistical analysis of existing models and data,” *J. Korean Nucl. Soc.*, vol. 23, no. 2, 1991.

[38] M. a. Antar and S. M. Zubair, “The impact of fouling on performance evaluation of multi-zone feedwater heaters,” *Appl. Therm. Eng.*, vol. 27, no. 14–15, pp. 2505–2513, Oct. 2007.

[39] J. Xu, T. Yang, Y. Sun, K. Zhou, and Y. Sh, “Research on varying condition characteristic of feedwater heater.pdf,” *Appl. Therm. Eng.*, vol. 67, pp. 179–189, 2014.

[40] M. Kubin, J. Hirs, and J. Plasek, “Experimental analysis of steam condensation in vertical tube with small diameters,” *Int. J. Heat Mass Transf.*, vol. 94, pp. 403–410, 2016.

[41] J. R. Thome, “Condensation on External Surfaces,” *Eng. Data B. III*, no. 1983, pp. 1–52, 2007.

[42] A. Briggs, “Theoretical and Experimental Studies,” in *6th International Conference on Heat Transfer, Fluid Mechanics and Thermodynamics*, 2008, no. July, p. K2.

[43] Alstom, “THE WORLD ’ S HEAT EXCHANGER SPECIALISTS Welcome to Alstom Power,” 2012. [Online]. Available: www.alstom.com/power.

[44] Blacke Durr (an SPX Company), “HEADER-TYPE HEATERS,” *Product brochure*, 2013. .

[45] James Brown and Hamer Ltd, “Duvha HP FWH cross section drawings,” 1970.

[46] D. Koehler and G. Weber, “Using PEPSE to analyse feedwater heaters with long drain coolers,” 1992.

[47] Geoffrey Frederick Hewitt, G. L. Shires, and T. R. Bott, *Process heat transfer*. CRC Press, 1994, p. 1042.

[48] I. S. Hussaini, S. M. Zubair, and M. a. Antar, “Area allocation in multi-zone feedwater heaters,” *Energy Convers. Manag.*, vol. 48, no. 2, pp. 568–575, Feb. 2007.

[49] G. Minner and J. Weber, “PTC 12 . 1 Calculations Using PEPSE – Beta Testing,” 2000.

[50] M. Álvarez-Fernández, L. Del Portillo-Valdés, and C. Alonso-Tristán, “Thermal analysis of closed feedwater heaters in nuclear power plants,” *Appl. Therm. Eng.*, vol. 68, no. 1–2, pp. 45–58, Jul. 2014.

[51] F. Madron, “Modeling a 3-zone Feedwater Heater,” 2013.

[52] SimSci (Simulation Sciences Inc.), “HEXTRAN Getting Started Guide,” 2002.

[53] B. J. E. Edwards, “Design and Rating Shell and Tube Heat Exchangers,” Chemstation Inc., 2008.

[54] ASME, “PTCC 12.1 - 2000 Closed Feedwater Heaters,” 2000.

[55] Alstom, “Medupi HP FWH specification sheet,” 2014.

[56] Eskom - Duvha PS, “Duvha FWH acceptance test.pdf,” 1980.

[57] Alstom Power, “Koeberg NPS - Set of heat balances,” 2010.

[58] EPRI, “2007 EPRI Feedwater Heater Conference Proceedings,” in *Memphis, Tennessee, August 22-23, 2007. EPRI, Palo Alto, CA: 2007. 1014165.*, vol. 3, no. 3.

Appendix A. Area calculations

The primary reason for calculating the flow area is to calculate the *Re* number for the cross flow and parallel flow on the shell side. The *Re* number is then used as an input to the specific *h* correlation.

A-1. Bundle Diameter

The bundle diameter (D_{bundle}) or tube plate diameter can be obtained from the detailed FWH drawings but because this information is not necessary available on all the Eskom stations a more general method [8] had to be selected. This method uses the tube count and an assumed uniform distribution of tubes, with some additional correction factors.

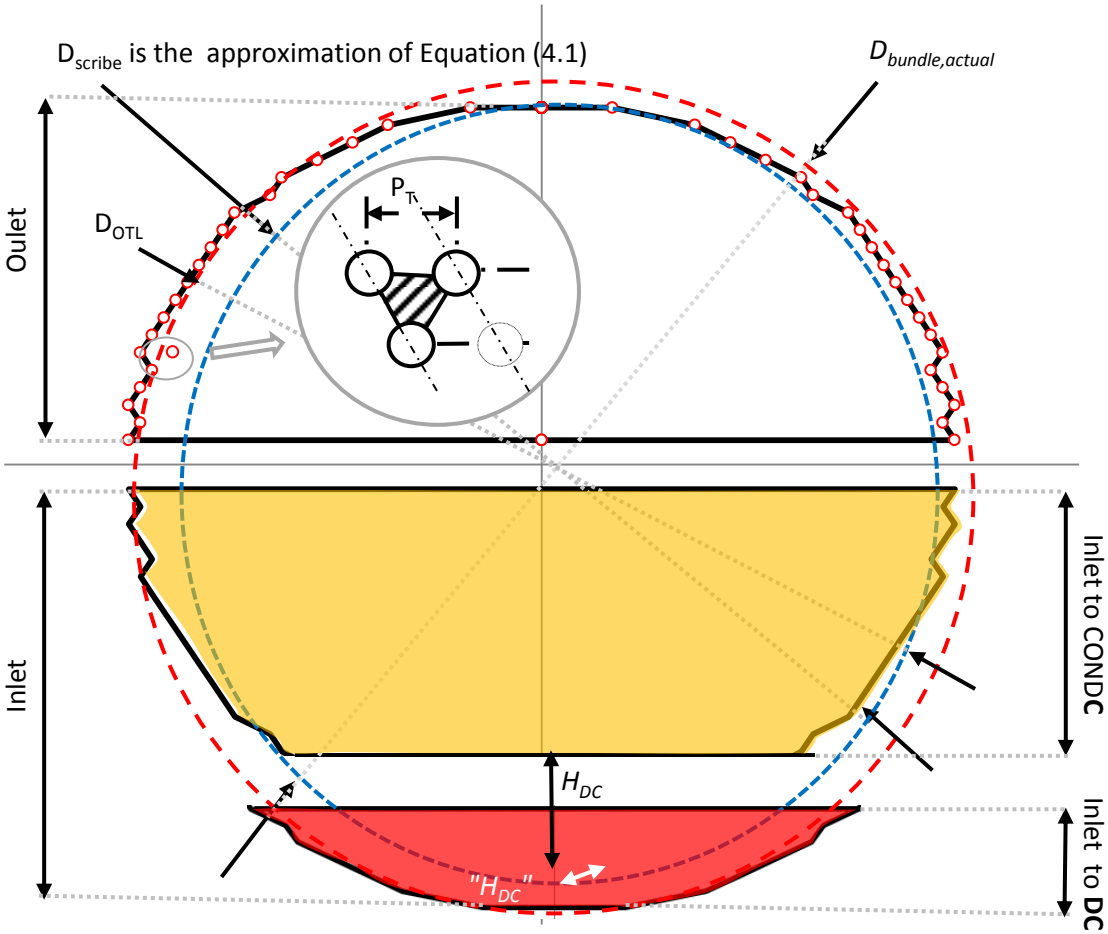

Figure A-1. Tube plate arrangement with offset DC tubes

The bundle diameter (D_{bundle}) that results from the arrangement of n_t number of tubes on a tube plate with a set P_T pitch may be approximated as follows:

$$D_{bundle} = \sqrt{\frac{n_t 4 A_T}{(\mathrm{CTP})\pi}} \tag{A.1}$$

where *CTP* is the tube count calculation constant that accounts for the unused tube plate area at the pass lanes and the clearance between the D_{OTL} and D_{shell}.

The *CTP* values are dependent on the tube passes and are listed below:

- One tube pass: *CTP = 0.93*
- Two tube pass: *CTP = 0.90*
- Three tube pass: *CTP = 0.85*
- Four tube pass: *CTP = 0.80 (This has been assumed)*

The pitch area (A_T) is calculated for a square pitch and then corrected for a staggered pitch using the tube layout correction factor (*CL*):

$$A_T = (\mathrm{CL})\mathrm{P}_T^2 \tag{A.2}$$

The *CL* values are dependent on the layout and are listed below:

- 90^o or 45^o: *CL = 1*
- 30^o or 60^o: *CL = 0.87*

A-2. Tube lengths

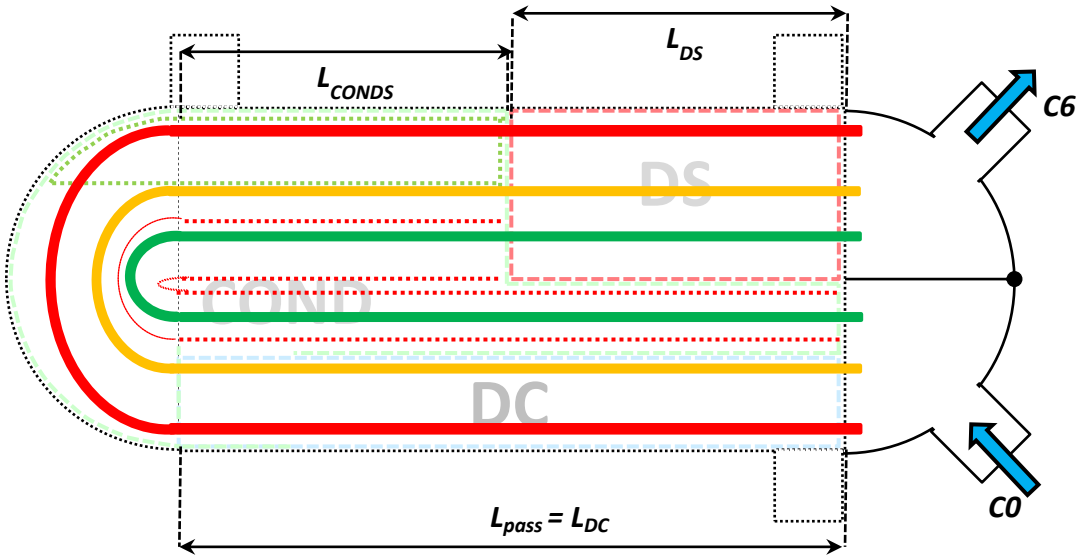

Figure A-2. Designation of tube lengths

The lengths of the bends are incorporated into the straight length. Hence, the length of the tube per pass is calculated as follows:

$$L_{pass} = \frac{A_{HDC} + A_{HCOND} + A_{HDS}}{Passes \cdot \pi d_o n_t} \tag{A.3}$$

However, this equation is not valid for a 3 zone vertically orientated header type FWH because the DC is not located in a single pass region, see Figure A-7.

$$L_{pass} = \frac{A_{HCOND} + A_{HDS}}{Passes \cdot \pi d_o n_t} \tag{A.4}$$

The tube length of the tubes in a long DC will coincidentally be equal to L_{pass} and can be confirmed using the following formula:

$$L_{DC} = \frac{A_{HDC}}{\pi d_o n_{tDC}} \tag{A.5}$$

The tube length in a short DC will be calculated by dividing A_{HDC} by the total number of tubes (n_t) in a single pass.

The tube length in the DS can estimated using a similar formula:

$$L_{DS} = \frac{A_{HDS}}{\pi d_o n_t} \tag{A.6}$$

These tube lengths will be required for a 3 zone FWH to calculate the residual tube length in the last pass that does not run through the DS. This tube length referred to as L_{CONDS} is mathematically described below and illustrated in Figure A-2:

$$L_{CONDS} = L_{\text{pass}} - L_{DS} \tag{A.7}$$

A-3. Drains Cooler (DC)

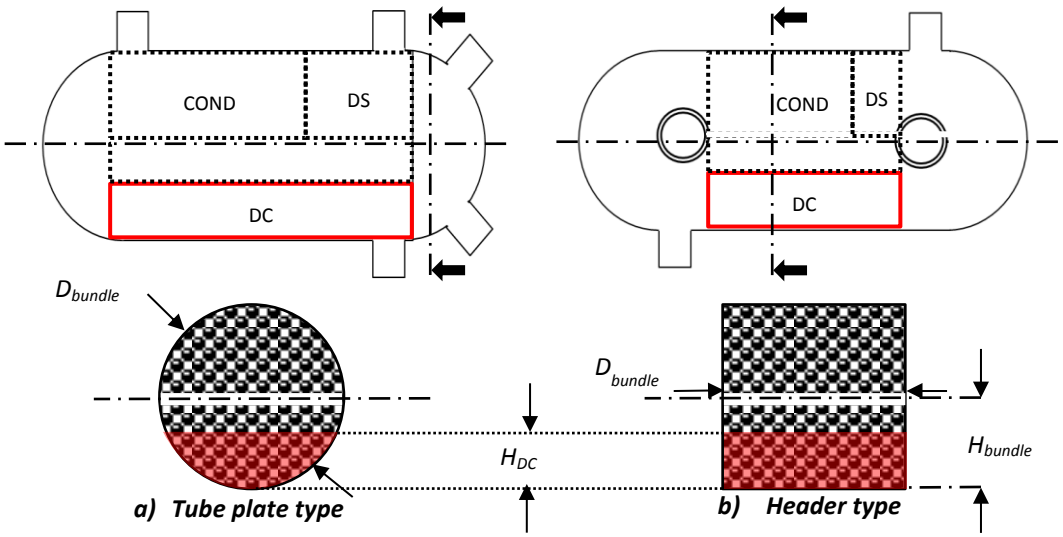

Figure A-3. Distribution of heat transfer area about a symmetrical axis for a two pass 3 zone FHW and the associated tubes located in the DC

Surface area calculation in the DC

The number of tubes (n_t) participating in sub-cooling is calculated by utilising the heat transfer surface areas. These areas are known inputs and are visualised diving the FWH into equal or symmetrical regions, as indicated in Figure A-3. This equation is only applicable for a long DC for both tube plate and header types FWH. In the event of a short DC, $n_{tDC} = n_t$ as all the tubes runs through it.

$$n_{tDC} = \left(n_t \frac{Passes \cdot A_{HDC}}{A_{HDC} + A_{HCOND} + A_{HDS}} \right) \tag{A.8}$$

In the event of a long DC the number of tubes that does not pass through the DC is simply:

$$n_{tC} = n_t - n_{tDC} \tag{A.9}$$

Height of the DC region

The cross section area of the DC is illustrated by the shaded region of the tube plate type FWH in Figure A-3. The height is calculated by assuming the ratio of number of tubes in the DC vs the total number of tubes in the circular cross section is the same as the area ratio it occupies. Using Equation (2.67) one can write:

$$\frac{n_{tDC}}{Passes \cdot n_t} = \frac{\cos^{-1}\left(\frac{R_{bundle} - H_{DC}}{R_{bundle}}\right) R^2{}_{bundle} - \left(R_{bundle} - H_{DC}\right)\left(\sqrt{2R_{bundle}H_{DC} - H_{DC}{}^2}\right)}{\pi R^2_{bundle}} \quad \text{(A.10)}$$

This is an implicit equation, and H_{DC} must be solved numerically. An initial guess is needed to initialize the solver, which can be estimated using the following equation:

$$H_{DC} \approx \left(\frac{A_{HDC}}{A_{HDC} + A_{HCOND} + A_{HDS}}\right) D_{bundle} \quad \text{(A.11)}$$

A cross section view through a header type FWH reveals that the layout is almost rectangular, see Figure A-3. The horizontal length is assumed to be equal to the D_{bundle} calculated using Equations (A.1) and (A.2), while the vertical height is calculated as follows:

$$n_{tDC\_H} = \frac{D_{bundle}}{P_T} \quad \text{(A.12)}$$

$$n_{tDC\_V} = \frac{n_t}{n_{tDC\_H}} \quad \text{(A.13)}$$

$$H_{DC} = n_{tDC\_V} P_L \quad \text{(A.14)}$$

where n_{tDC_H} is the number of tubes located along the axis of D_{bundle}, n_{tDC_V} is the number of tubes located perpendicular to the axis of D_{bundle}.

Free flow area calculation applied to segmented baffles

The cross flow and longitudinal flow can now be calculated for a FWH fitted with segmented baffles. The cross flow area (A_{DCcf}) is computed using Equation (2.61) as the basis and re-formulated as Equation (A.15).

$$A_{DCcf} = B_{DC}(\mathrm{P}_T - \mathrm{d}_o)\left(\frac{2\sqrt{2R_{bundle}H_{DC} - H_{DC}^2}}{P_T}\right) \quad \text{(A.15)}$$

The longitudinal or parallel flow area varies between two areas depending on the baffle cut (B_{cutDC}). Hence, the average value of the two longitudinal areas is used for further computation.

The baffle cut is seldom disclosed by the vendor but a value of 25% or 30% was identified after studying available drawing. It is defined as H_{cutDC}/H_{DC}, see Figure A-4.

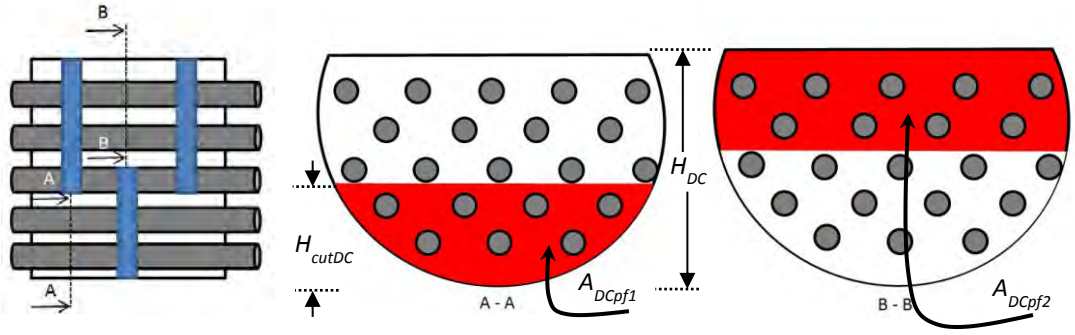

Figure A-4. Illustration of two longitudinal free flow areas in a tube plate FWH

The bottom cross section or parallel flow area (A_{DCpf1}) in Figure A-4 will first be computed using an equation similar to Equation (A.10) and formulated as follows:

$$A_{DCpf1} = R_{bundle}^2 \cos^{-1}\left(\frac{R_{bundle} - B_{DCcut}H_{DC}}{R_{bundle}}\right) - \left[R_{bundle} - B_{DCcut}H_{DC}\right]\left[\sqrt{2R_{bundle}B_{DCcut}H_{DC} - (B_{DCcut}H_{DC})^2}\right] \quad \text{(A.16)}$$

The next step is to compute the number of tubes located in this shaded region (n_{tDCpf1}) in order that the tube cross section area may be subtracted from the bottom cross section area. The ratio of the cross section area is utilised to compute n_{tDCpf1} and the associated longitudinal or parallel area for the bottom region is calculated as follows:

$$n_{tDCpf1} = n_{tDC}\frac{A_{DCpf1}}{A_{DC}} \quad \text{(A.17)}$$

$$A_{DCpf1\,freeflow} = A_{DCpf1} - n_{tDCpf1}\left(\frac{\pi d_o^2}{4}\right) \quad \text{(A.18)}$$

The cross section area for the top shaded region is calculated as follows:

$$A_{DCpf2} = A_{DC} - A_{DCpf1} \quad \text{(A.19)}$$

The number of tubes located in the top shaded region (n_{tDCpf2}) is calculated as follows:

$$n_{tDCpf2} = n_{tDC} - n_{tDCpf1} \tag{A.20}$$

$$A_{DCpf2\,freeflow} = A_{DCpf2} - n_{tDCpf2}\left(\frac{\pi \mathrm{d}_o^2}{4}\right) \tag{A.21}$$

The average value of the two longitudinal areas can now be computed:

$$A_{DCpf} = \frac{A_{DCpf1\,freeflow} + A_{DCpf2\,freeflow}}{2} \tag{A.22}$$

There is only a single longitudinal or parallel free flow area for a header type heater and it is calculated using the results from Equations (A.12) to (A.14) and is computed as follows:

$$A_{DCpf} = H_{DC} D_{bundle} - n_{tDC}\frac{\pi d_o^2}{4} \tag{A.23}$$

The free flow area in a cross flow orientation is calculated as follows:

$$A_{DCcf} = L_{B,DC}\left(H_{DC} D_{bundle} - n_{tDC}\left(\frac{\pi \mathrm{d}_o^2}{4}\right)\right) \tag{A.24}$$

The classical *Re* number (Equation (2.27)) for both the cross and parallel flow regions can now be formulated using the mass flow rate and geometric areas as follows:

$$\mathrm{Re}_{DCcf} = (\rho v)_{cf}\frac{D_e}{\mu} = \frac{\dot{m}}{A_{DCcf}}\frac{D_e}{\mu} \tag{A.25}$$

$$\mathrm{Re}_{DCpf} = (\rho v)_{pf}\frac{d_o}{\mu} = \frac{\dot{m}}{A_{DCpf}}\frac{d_o}{\mu} \tag{A.26}$$

where the (ρv) term is called as the shell-side mass velocity.

Free flow area calculation applied to grid baffles

Shiina, Nakamura and Matsumura [22] and Gentry, Gentry and Scanlon [14] requires the length of the plate (L_r) used in the manufacture of a single baffle. This specified length is multiplied by the

grid's thickness in order to compute the area obstructing free flow. There will be a single longitudinal flow area for both a tube plate and header type FWH. Equations (A.21) and (A.23) will be applicable but across the entire cross section of the DC. The grid area obstructing free flow will be subtracted from this area to arrive at the free flow area. However, the value for L_r is typically not known and a more convenient method had to be developed to calculate the obstructed free flow area due to the grid.

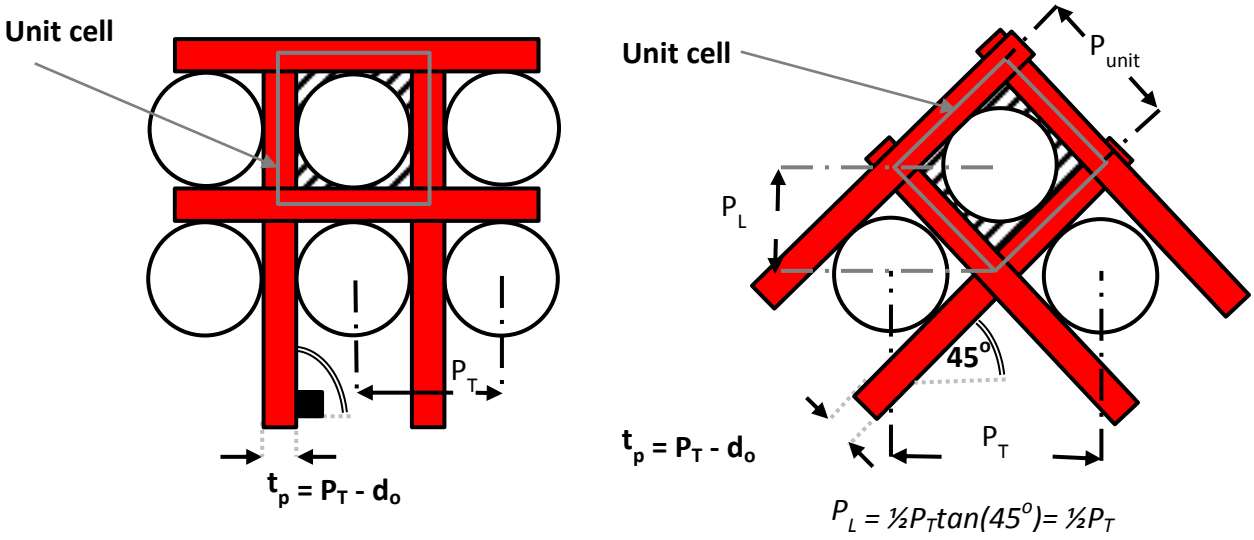

Figure A-5. Grid arrangement for a 90° and 45° layout

A method was developed to compare the obstructed free flow area to the unobstructed free flow area ($A_{unitgrid}/A_{unit}$). A convenient approximation is to identify a unit cell, which is a building block for an idealised square tube arrangement in a square duct as is illustrated in Figure A-5. It will also be applied to a circular tube plate. The P_T for a grid baffle is determined from the thickness of the grid plate as can be seen from Figure A-5. It can be deduced that the thickness of the plate must be predefined in order to ensure a secure fit of the tube, which is indicated in Figure A-5. The unit cell for a square arrangement is given in Equation (A.28) and for a 45° staggered in Equation (A.29).

$$A_{unit} = \left(d_o + t_p\right)^2 - \pi\frac{d_o^2}{4} = \left(d_o + \left(P_T - d_o\right)\right)^2 - \pi\frac{d_o^2}{4} = P_T^2 - \pi\frac{d_o^2}{4} \qquad \text{(A.27)}$$

$$A_{unitgrid.sq} = A_{unit} - \frac{t_p}{2}\left[2\left(d_o + t_p\right) + 2d_o\right] \qquad \text{(A.28)}$$

$$A_{unitgrid.45} = A_{unit} - \frac{t_p}{2}\left[4\sqrt{\left(\frac{1}{2}P_T\right)^2 + \left(\frac{1}{2}P_T\right)^2} - 2t_p\right] = A_{unit} - \frac{t_p}{2}\left[4\sqrt{\frac{1}{2}P_T^2} - 2t_p\right] \qquad \text{(A.29)}$$

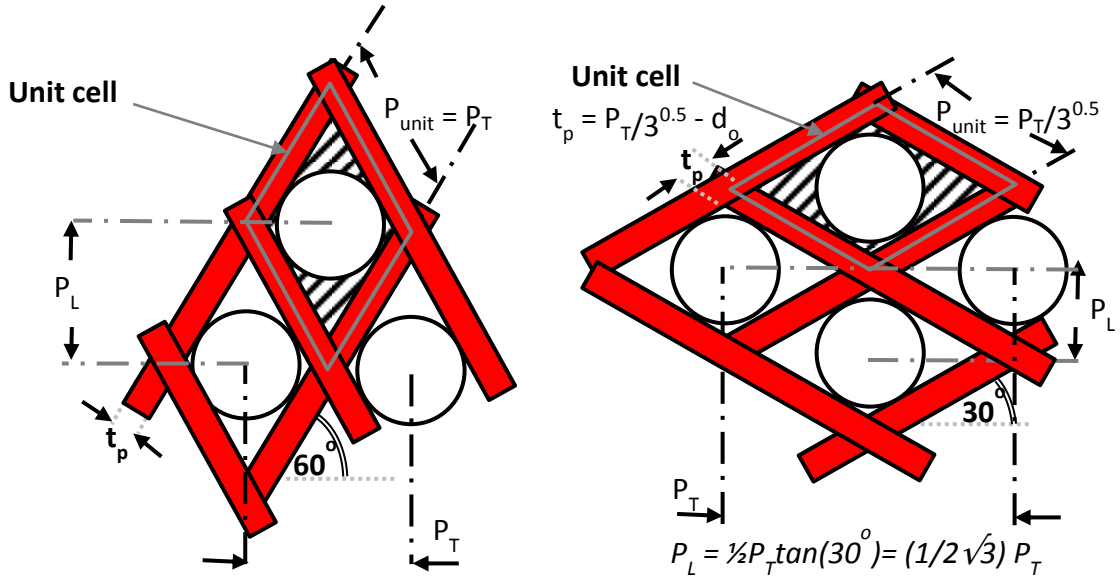

Figure A-6. Grid arrangement for a 60° and 30° layout

The 60° tube layout provides the smallest area for cross flow and is illustrated in Figure A-6. The unit cell for this arrangement is not a square but a rhombus and hence A_{unit} will differ to that of the 90° and 45° tube layout.

The rhombus consists of two equilateral triangles and hence half the area of the rhombus is equated to the area of the equilateral triangle.

$$A_{unit.60} = 2\left(\frac{1}{2}P_T\frac{P_T}{2\sqrt{3}}\right) - \pi\frac{d_o^2}{4} = 2\left(\frac{P_T^2}{4\sqrt{3}}\right) - \pi\frac{d_o^2}{4} = \frac{P_T^2}{2\sqrt{3}} - \pi\frac{d_o^2}{4} \qquad \text{(A.30)}$$

$$A_{unitgrid.60} = A_{unit.60} - \frac{t_p}{2}\left[4\frac{P_T}{\sqrt{3}} - 2t_p\right] \qquad \text{(A.31)}$$

A 30° tube layout staggered tube arrangement is also illustrated in Figure A-6 and the unit area is calculated as follows:

$$A_{unit.30} = \left(\frac{P_T \sqrt{3} P_T}{2} \right) - \pi \frac{d_o^2}{4} = \left(\frac{\sqrt{3} P_T^2}{2} \right) - \pi \frac{d_o^2}{4} = \frac{\sqrt{3} P_T^2}{2} - \pi \frac{d_o^2}{4} \tag{A.32}$$

$$A_{unitgrid.30} = A_{unit.30} - \frac{t_p}{2} \left[4P_T - 2t_p \right] \tag{A.33}$$

The ratio of $A_{unitgrid}/A_{unit}$ represented the obstructed free flow area to the unobstructed free flow area. This factor is multiplied by the unobstructed free flow area calculated using Equations (A.21) and (A.23). The obstructed free flow area for a grid baffle is required by Shiina, Nakamura and Matsumura [22] and Gentry, Gentry and Scanlon [14] correlations.

A grid baffle does not cut the parallel flow region into two regions. Hence, there is only a single free flow area for the tube plate and header type header using grid baffles. The formula for the tube plate type FWH is presented in Equation (A.34).

$$A_{DCpf\_ob} = A_{DCpf} \left\lfloor \frac{A_{unitgrid}}{A_{unit}} \right\rfloor = \left(A_{DCpf} - n_{tDCpf} \left(\frac{\pi \mathrm{d}_o^2}{4} \right) \right) \left\lfloor \frac{A_{unitgrid}}{A_{unit}} \right\rfloor \tag{A.34}$$

The formula for the header type FWH is presented in Equation (A.35) and relies on the earlier computation from Equation (A.23):

$$A_{DCpf\_ob} = A_{DCpf} \left\lfloor \frac{A_{unitgrid}}{A_{unitgrid}} \right\rfloor = B_{DCcut} \left(H_{DC} D_{bundle} - n_{tDC} \left(\frac{\pi \mathrm{d}_o^2}{4} \right) \right) \left\lfloor \frac{A_{unitgrid}}{A_{unitgrid}} \right\rfloor \tag{A.35}$$

where the subscript *DCpf_ob* indicates the obstructed free flow area.

A-4. De-superheater zone (DS)

The same method described for the DC is also applicable for the DS but only the subscript in the equations will change from DC to DS.

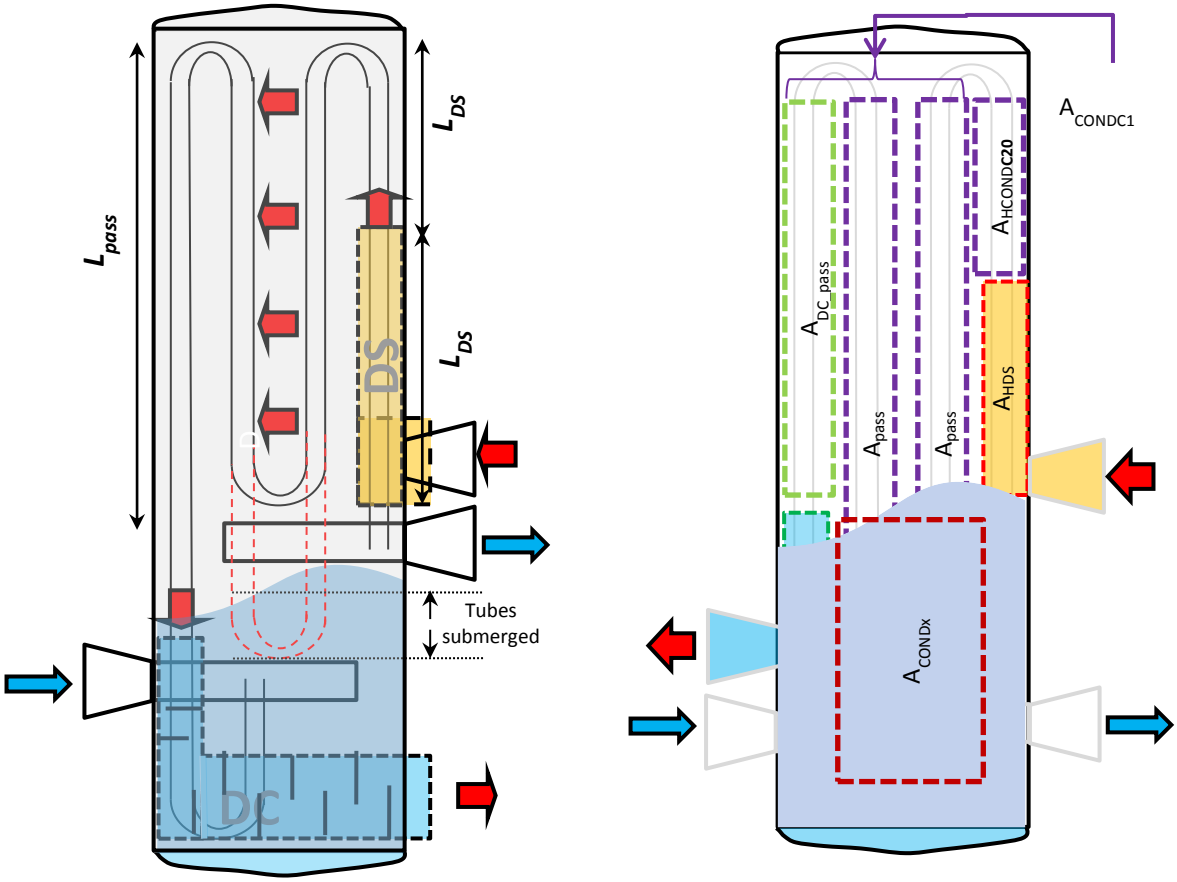

Figure A-7. Designation of tube lengths and area allocation in a 3 zone vertically orientated header type FWH

A-5. Condensing zone (COND = CONDC1 + CONDC2 + CONDR)

Cross flow area calculations

The flow arrangement in COND is modelled as cross flow and hence the cross flow area is required to compute *h*. The COND**R** cross flow area for a tube plate type FWH is calculated similar to the cross flow areas calculated earlier for the DC zone but here the tube length in the last pass is used instead of the baffle spacing. The diameter used in this calculation corresponds to the diameter calculated for the DC because they are symmetrical. The thickness of the baffles has been ignored.

$$A_{CONDRcf} = L_{CONDS}\left[(\mathrm{P}_T - \mathrm{d}_o)\left(\frac{2\sqrt{2R_{bundle}H_{DC} - H_{DC}^2}}{P_T}\right)\right] \qquad \text{(A.36)}$$

The header type FWHs has a more rectangular tube arrangement, refer to Figure A-3, and hence is calculated as follows:

$$A_{CONDRcf} = L_{\mathrm{CONDS}}\left[(\mathrm{P}_T - \mathrm{d}_o)\left(\frac{D_{bundle}}{P_T}\right)\right] \qquad \text{(A.37)}$$

The COND**C1** cross flow area for both a tube plate type and header type FWH is calculated using Equation (A.38).

$$A_{CONDC1cf} = L_{\mathrm{pass}}\left[(\mathrm{P}_T - \mathrm{d}_o)\left(\frac{D_{bundle}}{P_T}\right)\right] \qquad \text{(A.38)}$$

The COND**C2** cross flow area for both types of FWHs is calculated as follows:

$$A_{CONDC2cf} = L_{\mathrm{CONDS}}\left[(\mathrm{P}_T - \mathrm{d}_o)\left(\frac{D_{bundle}}{P_T}\right)\right] \qquad \text{(A.39)}$$

The cross flow areas are required for the correlations applicable both the vertical and horizontal condensing zones.

The external *Re* number (Equation (2.27)) for the different regions is defined in terms of the ρv term, and equivalent diameter:

$$\mathrm{Re}_{COND\_} = (\rho v)_{COND\_} \frac{D_e}{\mu} \tag{A.40}$$

The ρv term is calculated from the mass flow and cross flow area per zone:

$$(\rho v)_{CONDC1} = f_{CONDC1} \frac{\dot{m}_{H1*}}{A_{CONDC1cf}} \tag{A.41}$$

$$(\rho v)_{CONDC2} = f_{CONDC2} \frac{\dot{m}_{H1*}}{A_{CONDC2cf}} \tag{A.42}$$

$$(\rho v)_{CONDR} = f_{CONDR} \frac{\dot{m}_{H1*}}{A_{CONDRcf}} \tag{A.43}$$

where *f* represents the fraction of $\dot{m}_{H1*}$ steam that is condensed in each sub-zone heat exchanger (see section 4.1.3)

Surface area calculations

The surface areas associated with the COND zone component areas is required to compute the ε of the particular COND sub-zone. The COND zone arrangement used in this study was illustrated in Figure 4-7 and in the amended process flow diagram (Figure 4-8), which incorporates the COND**S** dry de-superheating zone.

The total heat transfer area in the COND zone comprises of the following components:

$$A_{HCOND} = A_{HCONDR} + A_{HCONDCo} \tag{A.44}$$

where the "*H*" in the subscript indicates that it is the heat transfer surface area, and the "o" in $A_{HCONDCo}$ indicates that it is the total area of the COND**C** sub-zone, which is constant independent of the distribution of the component areas.

The total area of the COND**C** sub-zone or $A_{HCONDCo}$ is calculated as follows:

$$A_{HCONDCo} = A_{HCONDC1} + A_{HCONDC2o} \tag{A.45}$$

where $A_{HCONDC1}$ represents the area in the 1st pass or the total complete single passes illustrated in Figure A-2 and $A_{HCONDC2o}$ represents the area in the last pass. The tube length, L_{CONDS}, is shorter in the last pass and was calculated earlier using Equation (A.6).

The area in the 1st pass is constant and $A_{HCONDC1}$ for any number of tube passes is calculated as follows:

$$A_{HCONDC1} = \left(Passes - 1\right) L_{\text{pass}} n_{tC} \left(\pi d_o\right) \tag{A.46}$$

For a FWH fitted with a short DC which is oriented vertically, Equation (A.47) applies.

$$A_{HCONDC1} = \frac{A_{HCONDC0} + A_{HDS} - A_{HCONDx}}{Passes}\left(Passes - 1\right) \tag{A.47}$$

A_{HCONDx} represents the COND surface area that is submerged and does not participate in significant heat transfer, see Figure A-7.

There are no horizontally orientated FWHs in the Eskom fleet, fitted with a shortDC, but the area calculation is provided for completeness in Equation (A.48):

$$A_{HCONDC1} = L_{DC}\left(n_t \pi d_o\right) + L_{\text{pass}}\left(n_t \pi d_o\right)\left(Passes - 2\right) \tag{A.48}$$

In the event that a short DC is present, the DC will be connected to CONDC instead of CONDR because the model is designed with CONDS being part of CONDC. The inlet temperature to CONDC1 will therefore be T_{C2} and not T_{C1}.

The area is the last pass $A_{HCONDC2o}$ comprises of A_{HCONDS} and A_{HCOND2}. The surface area required to remove the excess superheat, A_{HCONDS}, is a result from the iterative solver and hence $A_{HCOND\mathbf{C2}}$ is calculated as follows:

$$A_{HCONDC2} = A_{HCONDC2o} - A_{HCONDS} \tag{A.49}$$

As was discussed earlier, the limitation with this approach is that it is assumed that the excess superheat is only removed in the last pass i.e. $A_{HCONDC2o}$. Once the upper limit has been the reached, the model will continue to run with $A_{HCONDS} = 0.99\, A_{HCONDC2o}$, while the energy balance will assume that all the excess superheat is removed.

Appendix B. Program code

The model was compiled in the Mathcad 15.0 software package and consists of 78 pages of code. It was therefore not included in the Appendix but may be obtained from the Specialisation Centre for Energy Efficiency, based in the Department of Mechanical Engineering at the University of Cape Town (UCT). It is also loaded on the Vula website under the Energy Efficiency course.

The Mathcad 15.0 file was loaded on a CD and submitted together with the thesis.

Appendix C. Feedwater heater specifications

Power Station: PS05
Heater: HP3

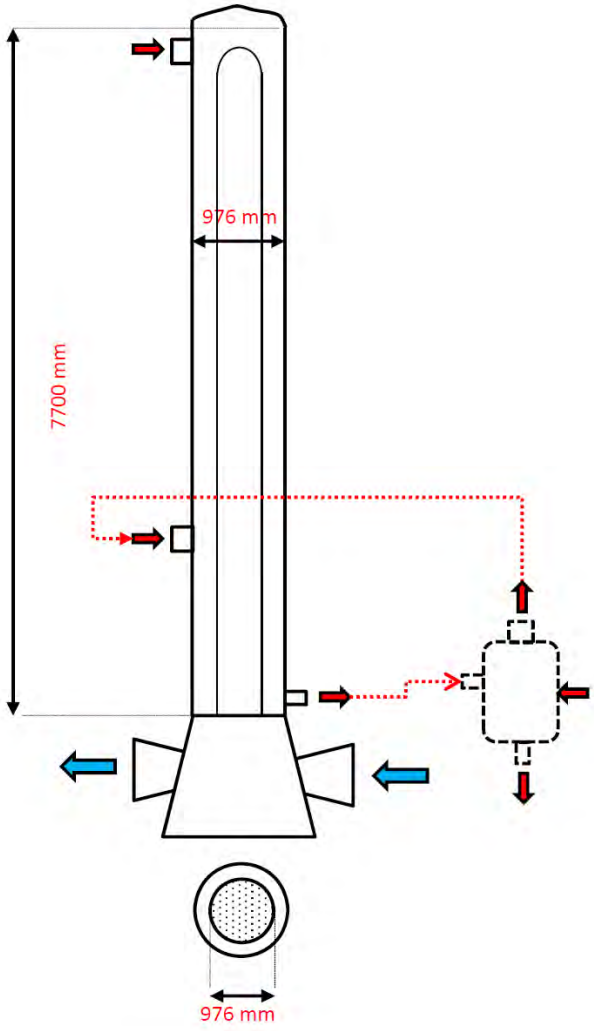

Tube material: 16Mo6 = 50W/m^{2}K

Geometric Data		
Orientation	1	[]
A_{HCOND}	335	[m^2]
A_{HDC}	0	[m^2]
A_{HDS}	0	[m^2]
D_S	1	[m^2]
n_t	370	[m]
d_o	20	
th	1.5	[mm]
Baffle type	1	[]
FWH Type	0	[]
Operational Data		@350MW
m_{C0}	159	[kg/s]
T_{C0}	122	[°C]
P_{C0}	200	[bars]
T_{H0}	228	[°C]
P_{H0}	5	[bars]
x_{H0}	1	[]
m_{M0}	32.8	[kg/s]
T_{M0}	176	[°C]
P_{M0}	10.13	[bars]
x_{M0}	0	[]
B	500	[mm]
Bc	25.00%	[%]
B	500	[mm]
Bc	25.00%	[%]
Passes	2	[]
Layout	60	[°]
P_T	25.0	[mm]
P_L	43.30	[mm]
th_{plate}	2.4	[mm]
th_{grid}	25	[mm]
A_{CONDif}	0	[m^2]
DC	0	[]

Power Station: PS05
Heater: HP4

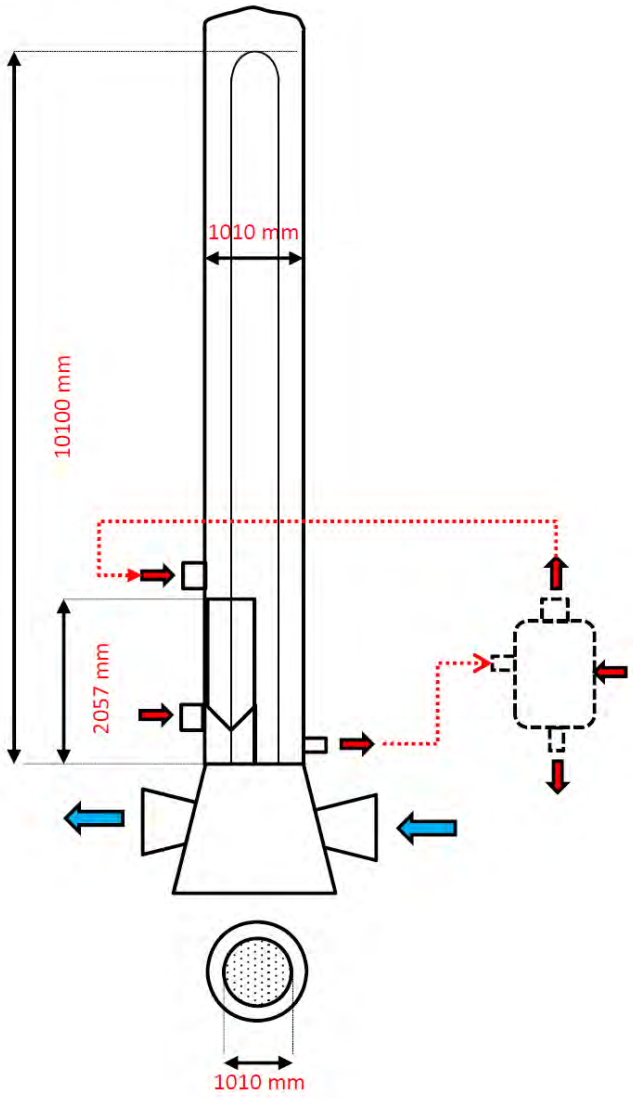

Tube material: 16Mo6 = 50W/mK

Geometric Data		
Orientation	1	[]
A_{HCOND}	345	[m^2]
A_{HDC}	0	[m^2]
A_{HDS}	0	[m^2]
D_S	1	[m^2]
n_t	380	[m]
d_o	20	
th	1.5	[mm]
Baffle type	1	[]
FWH Type	0	[]
Operational Data		@350MW
m_{C0}	159	[kg/s]
T_{C0}	143	[°C]
P_{C0}	200	[bars]
T_{H0}	181	[°C]
P_{H0}	9.13	[bars]
x_{H0}	1	[]
m_{M0}	25.5	[kg/s]
T_{M0}	212	[°C]
P_{M0}	21	[bars]
x_{M0}	0	[]
B	500	[mm]
Bc	25.00%	[%]
B	500	[mm]
Bc	25.00%	[%]
Passes	2	[]
Layout	60	[°]
P_T	25.0	[mm]
P_L	43.30	[mm]
th_{plate}	2.4	[mm]
th_{grid}	25	[mm]
A_{CONDif}	0	[m^2]
DC	0	[]

Power Station: PS05
Heater: HP5

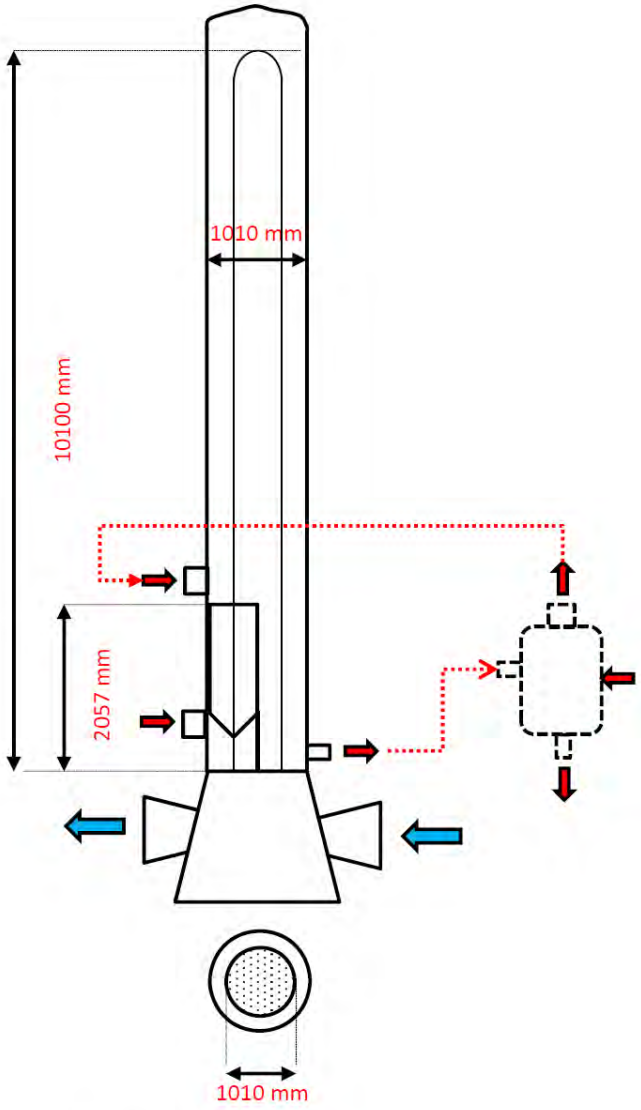

Tube material: 16Mo6 = 50W/mK

Geometric Data		
Orientation	1	[]
A_{HCOND}	410	[m^2]
A_{HDC}	0	[m^2]
A_{HDS}	70	[m^2]
D_S	1	[m^2]
n_t	402	[m]
d_o	20	
th	1.5	[mm]
Baffle type	1	[]
FWH Type	0	[]
Operational Data		@350MW
m_{C0}	159	[kg/s]
T_{C0}	171	[°C]
P_{C0}	200	[bars]
T_{H0}	414	[°C]
P_{H0}	21	[bars]
x_{H0}	1	[]
m_{M0}	13.8	[kg/s]
T_{M0}	253	[°C]
P_{M0}	43	[bars]
x_{M0}	0	[]
B	500	[mm]
Bc	25.00%	[%]
B	500	[mm]
Bc	25.00%	[%]
Passes	2	[]
Layout	60	[°]
P_T	25.0	[mm]
P_L	43.3012702	[mm]
th_{plate}	2.4	[mm]
th_{grid}	25	[mm]
A_{CONDif}	0	[m^2]
DC	0	[]

Power Station: PS05
Heater: HP6

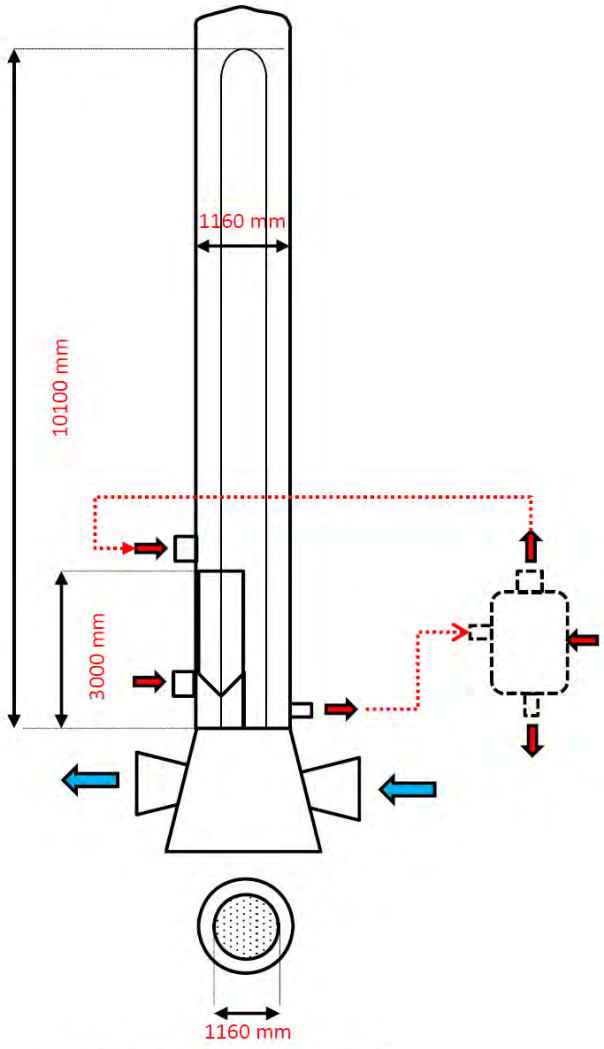

Tube material: 16Mo6 = 50W/mK

Geometric Data		
Orientation	1	[]
A_{HCOND}	347	[m^2]
A_{HDC}	0	[m^2]
A_{HDS}	73	[m^2]
D_S	1	[m^2]
n_t	415	[m]
d_o	20	
th	1.5	[mm]
Baffle type	1	[]
FWH Type	0	[]
Operational Data		@350MW
m_{C0}	159	[kg/s]
T_{C0}	215	[°C]
P_{C0}	200	[bars]
T_{H0}	325	[°C]
P_{H0}	42	[bars]
x_{H0}	1	[]
m_{M0}	0.0001	[kg/s]
T_{M0}	253.267	[°C]
P_{M0}	42	[bars]
x_{M0}	0	[]
B	500	[mm]
Bc	25.00%	[%]
B	500	[mm]
Bc	25.00%	[%]
Passes	2	[]
Layout	60	[°]
P_T	25.0	[mm]
P_L	43.30	[mm]
th_{plate}	2.4	[mm]
th_{grid}	25	[mm]
A_{CONDif}	0	[m^2]
DC	0	[]

Power Station: PS00
Heater: LP2

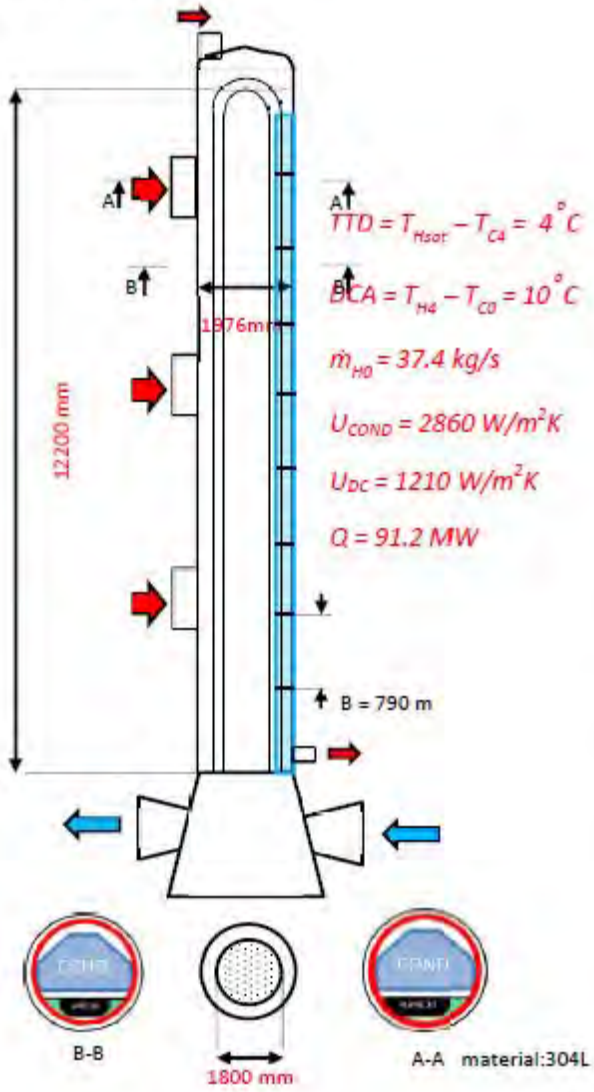

Geometric Data		
Orientation	0	[]
A_{HCOND}	1690	[m^2]
A_{HDC}	380	[m^2]
A_{HDS}	0	[m^2]
D_S	1.976	[m^2]
n_t	1711	[m]
d_c	16	
th	1.2	[mm]
Baffle type	1	[]
FWH Type	0	[]

Operational Data		@930MW
m_{C0}	521.5	[kg/s]
T_{C0}	52.6	[°C]
P_{C0}	40	[bars]
T_{H0}	98.5	[°C]
P_{H0}	0.9603	[bars]
x_{H0}	0.936	[]
m_{M0}	37.8	[kg/s]
T_{M0}	104.5	[°C]
P_{M0}	3.371	[bars]
x_{M0}	0	[]
B	790	[mm]
Bc	30.00%	[%]
B	300	[mm]
Bc	30.00%	[%]
Passes	2	[]
Layout	30	[°]
P_T	22.5	[mm]
P_L	22.5	[mm]
th_{plate}	2.4	[mm]
th_{grid}	50	[mm]
A_{CONDif}	0	[m^2]
DC	0	[]

Power Station: PS00
Heater: LP3

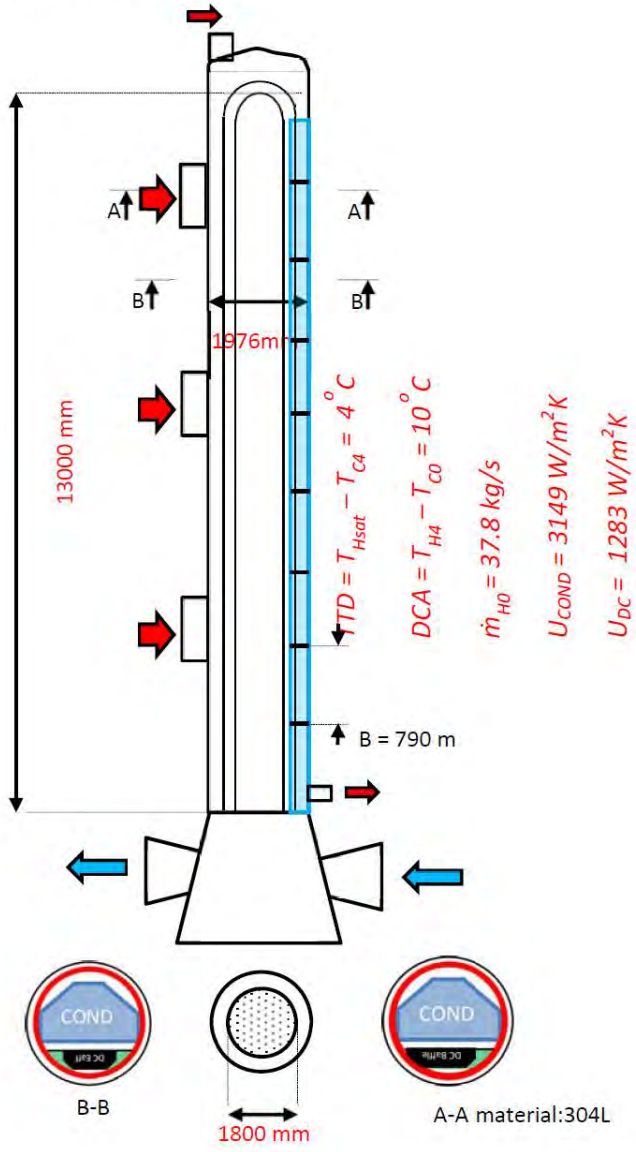

Geometric Data		
Orientation	0	[]
A_{HCOND}	1640	[m^2]
A_{HDC}	200	[m^2]
A_{HDS}	0	[m^2]
D_S	1.8	[m^2]
n_t	1711	[m]
d_o	16	
th	1.2	[mm]
Baffle type	1	[]
FWH Type	0	[]
Operational Data		@930MW
m_{C0}	521.5	[kg/s]
T_{C0}	94.2	[°C]
P_{C0}	40	[bars]
T_{H0}	137.6	[°C]
P_{H0}	3.371	[bars]
x_{H0}	0.997	[]
m_{M0}	0.00001	[kg/s]
T_{M0}	137.6	[°C]
P_{M0}	3.371	[bars]
x_{M0}	0	[]
B	700	[mm]
Bc	30.00%	[%]
B	300	[mm]
Bc	30.00%	[%]
Passes	2	[]
Layout	30	[°]
P_T	22.5	[mm]
P_L	22.5	[mm]
th_{plate}	2.4	[mm]
th_{grid}	50	[mm]
A_{CONDif}	0	[m^2]
DC	0	[]

Power Station: PS00
Heater: LP4

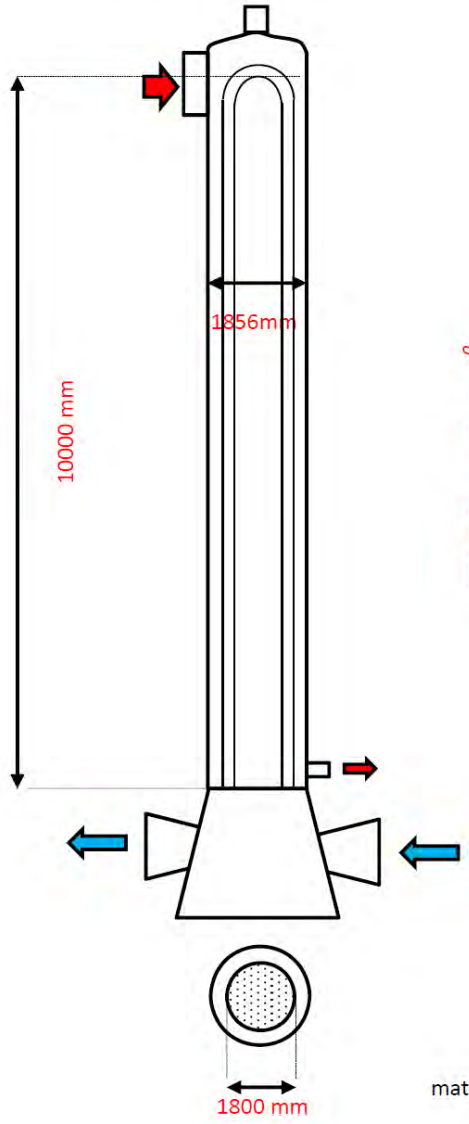

material:304L

$TTD = T_{Hsat} - T_{C4} = 4\ ^{o}C$

$\dot{m}_{H0} = 57.8\ kg/s$

$U_{COND} = 3144\ W/m^2K$

Geometric Data		
Orientation	0	[]
A_{HCOND}	1770	[m^2]
A_{HDC}	0	[m^2]
A_{HDS}	0	[m^2]
D_S	1.856	[m^2]
n_t	1769	[m]
d_o	16	
th	1.2	[mm]
Baffle type	1	[]
FWH Type	0	[]
Operational Data		@930MW
m_{C0}	521.5	[kg/s]
T_{C0}	133.2	[^{o}C]
P_{C0}	40	[bars]
T_{H0}	183.9	[^{o}C]
P_{H0}	10.95	[bars]
x_{H0}	0.889	[]
m_{M0}	0.00001	[kg/s]
T_{M0}	183.9	[^{o}C]
P_{M0}	10.95	[bars]
x_{M0}	0	[]
B	700	[mm]
Bc	30.00%	[%]
B	300	[mm]
Bc	30.00%	[%]
Passes	2	[]
Layout	30	[^{o}]
P_T	22.5	[mm]
P_L	22.5	[mm]
th_{plate}	2.4	[mm]
th_{grid}	50	[mm]
A_{CONDif}	0	[m^2]
DC	0	[]

Power Station: PS00
Heater: HP5

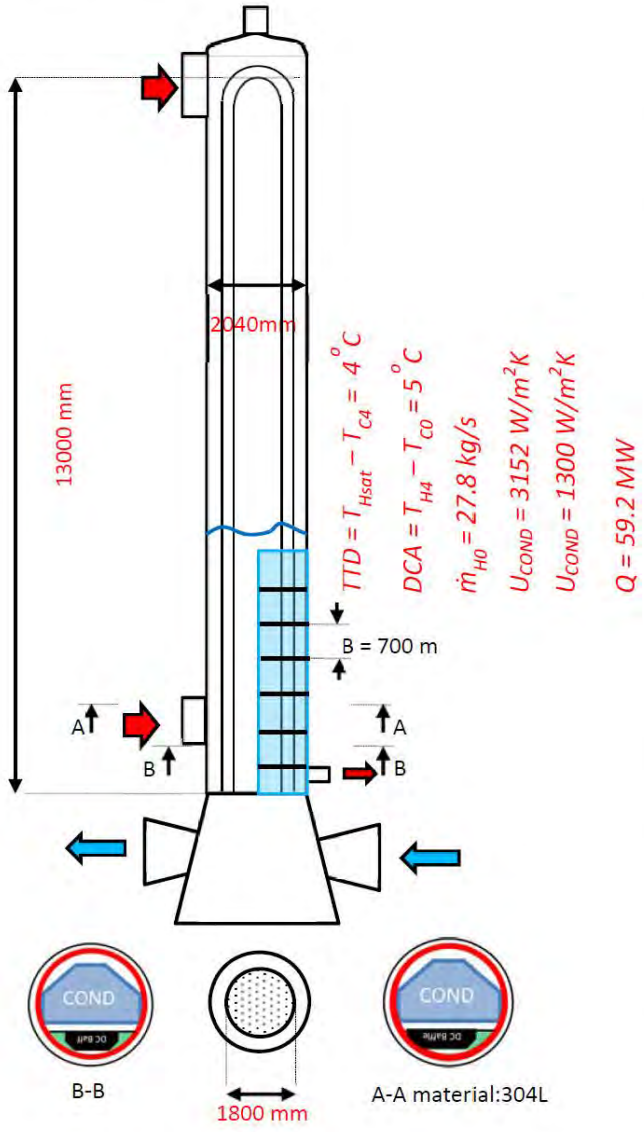

Geometric Data		
Orientation	1	[]
A_{HCOND}	2371	[m^2]
A_{HDC}	647	[m^2]
A_{HDS}	0	[m^2]
D_S	2.1	[m^2]
n_t	1789	[m]
d_c	21	
th	2	[mm]
Baffle type	1	[]
FWH Type	0	[]
Operational Data		@930MW
m_{C0}	755.135	[kg/s]
T_{C0}	181.5	[°C]
P_{C0}	73	[bars]
T_{H0}	203.3	[°C]
P_{H0}	16.64	[bars]
x_{H0}	0.909	[]
m_{M0}	87.5	[kg/s]
T_{M0}	209.3	[°C]
P_{M0}	24.7	[bars]
x_{M0}	0	[]
B	630	[mm]
Bc	30.00%	[%]
B	300	[mm]
Bc	30.00%	[%]
Passes	2	[]
Layout	30	[°]
P_T	28	[mm]
P_L	28	[mm]
th_{plate}	2.4	[mm]
th_{grid}	50	[mm]
A_{CONDif}	703	[m^2]
DC	1	[]

Power Station: PS00
Heater: HP6

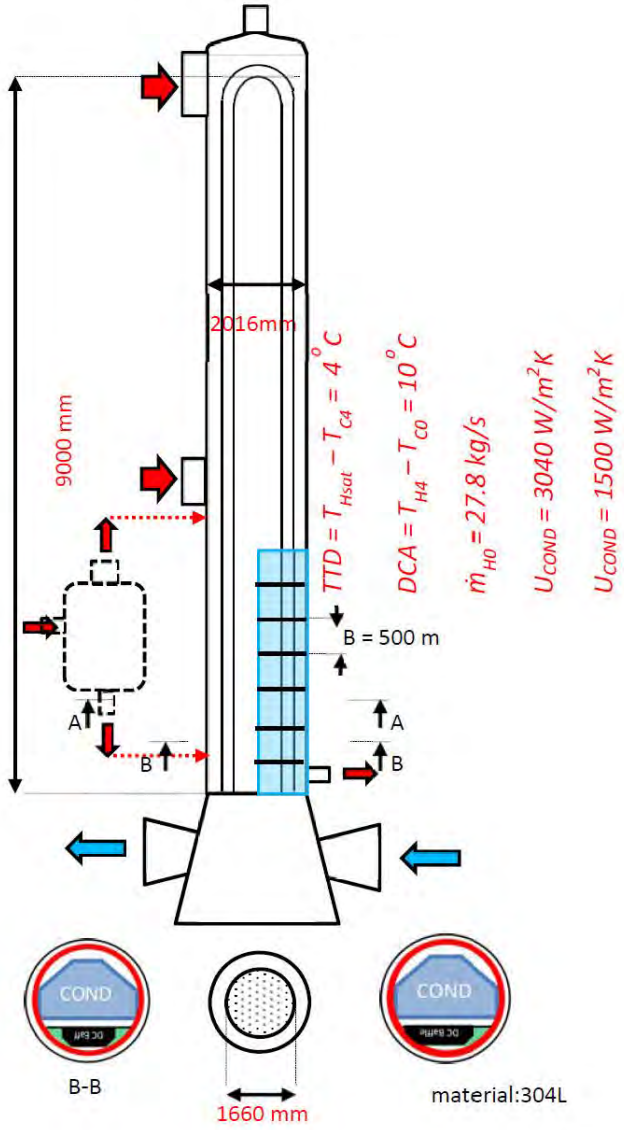

Geometric Data		
Orientation	1	[]
A_{HCOND}	2227	[m^2]
A_{HDC}	251	[m^2]
A_{HDS}	0	[m^2]
D_S	2.4	[m^2]
n_t	1789	[m]
d_o	21	
th	2	[mm]
Baffle type	1	[]
FWH Type	0	[]
Operational Data		@930MW
m_{C0}	755.135	[kg/s]
T_{C0}	199.3	[°C]
P_{C0}	73	[bars]
T_{H0}	223.3	[°C]
P_{H0}	24.7	[bars]
x_{H0}	0.934	[]
m_{M0}	60.163	[kg/s]
T_{M0}	265.4	[°C]
P_{M0}	51.24	[bars]
x_{M0}	0.029	[]
B	630	[mm]
Bc	30.00%	[%]
B	300	[mm]
Bc	30.00%	[%]
Passes	2	[]
Layout	30	[°]
P_T	28	[mm]
P_L	28	[mm]
th_{plate}	2.4	[mm]
th_{grid}	50	[mm]
A_{CONDif}	297	[m^2]
DC	1	[]

Power Station PS06
Heater: LP1

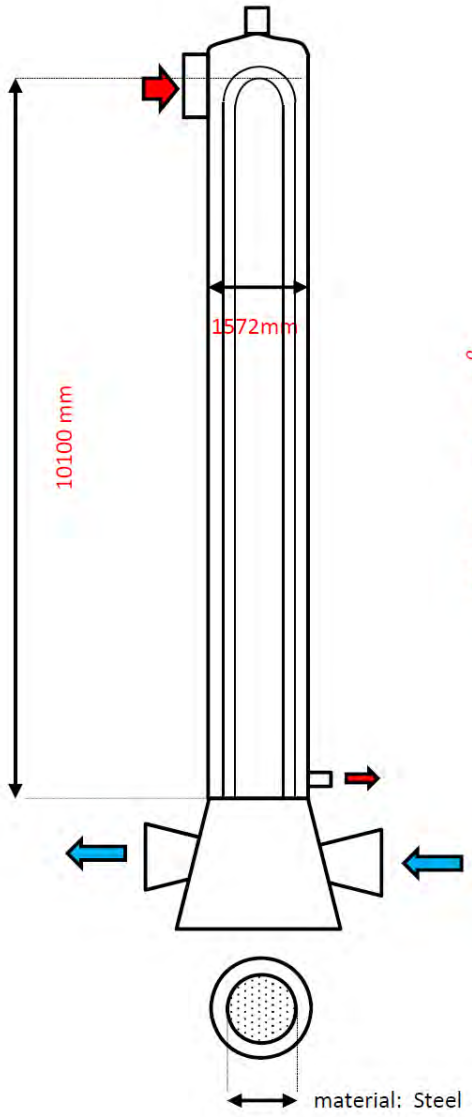

$TTD = T_{Hsat} - T_{C4} = 2\,^{\circ}C$

$\dot{m}_{H0} = 15.3\ kg/s$

$Q = 35.7\ MW$

Geometric Data		
Orientation	0	[]
A_{HCOND}	1020	[m^2]
A_{HDC}	0	[m^2]
A_{HDS}	0	[m^2]
D_S	1.6	[m^2]
n_t	1080	[m]
d_o	15	
th	1	[mm]
Baffle type	1	[]
FWH Type	0	[]

Operational Data		@930MW
m_{C0}	319.736	[kg/s]
T_{C0}	41.6	[°C]
P_{C0}	23.878	[bars]
T_{H0}	68.6	[°C]
P_{H0}	0.293	[bars]
x_{H0}	0.983	[]
m_{M0}	0.0001	[kg/s]
T_{M0}	68.6	[°C]
P_{M0}	0.293	[bars]
x_{M0}	0	[]
B	550	[mm]
Bc	30.00%	[%]
B	400	[mm]
Bc	30.00%	[%]
Passes	2	[]
Layout	30	[°]
P_T	20.4	[mm]
P_L	20.4	[mm]
th_{plate}	5	[mm]
th_{grid}	50	[mm]
A_{CONDif}	0	[m^2]
DC	0	[]

Power Station: PS06
Heater: LP2

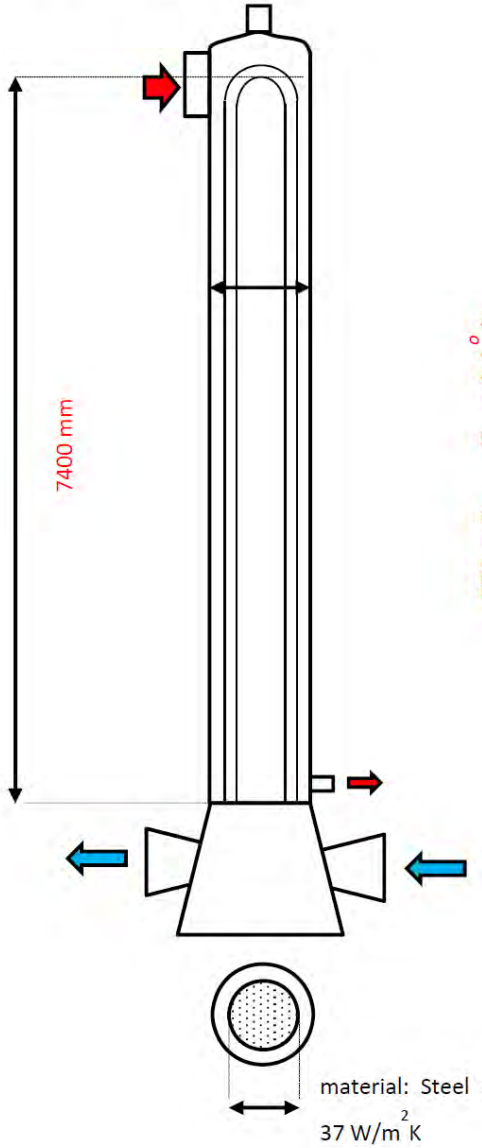

Geometric Data		
Orientation	0	[]
A_{HCOND}	742	[m^2]
A_{HDC}	0	[m^2]
A_{HDS}	0	[m^2]
D_S	1.6	[m^2]
n_t	1080	[m]
d_o	17	
th	1	[mm]
Baffle type	1	[]
FWH Type	0	[]
Operational Data		@930MW
m_{C0}	319.736	[kg/s]
T_{C0}	66.7	[°C]
P_{C0}	23.878	[bars]
T_{H0}	86.6	[°C]
P_{H0}	0.616	[bars]
x_{H0}	0.983	[]
m_{M0}	18.244	[kg/s]
T_{M0}	115.5	[°C]
P_{M0}	1.757	[bars]
x_{M0}	0	[]
B	550	[mm]
Bc	30.00%	[%]
B	400	[mm]
Bc	30.00%	[%]
Passes	2	[]
Layout	30	[°]
P_T	20.4	[mm]
P_L	20.4	[mm]
th_{plate}	5	[mm]
th_{grid}	50	[mm]
A_{CONDif}	0	[m^2]
DC	0	[]

Power Station: PS06
Heater: LP3

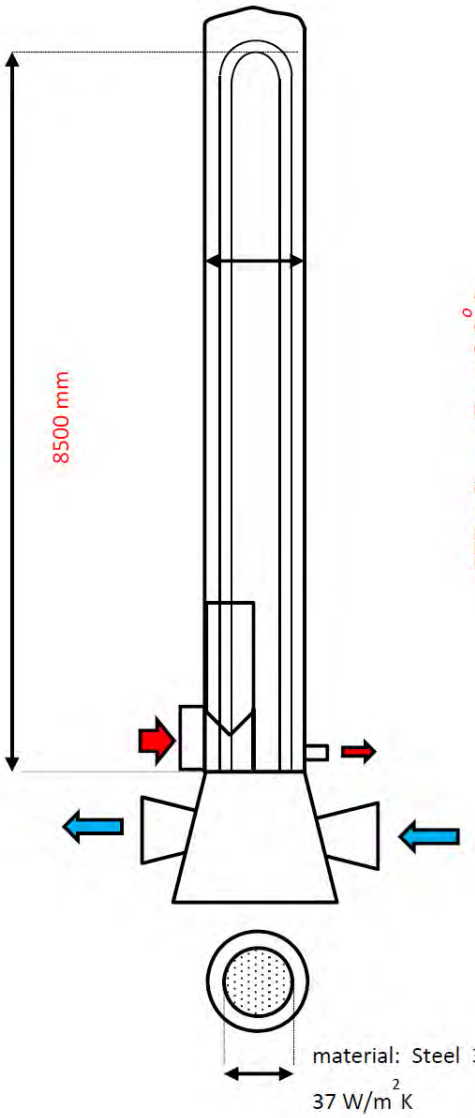

$TTD = T_{Hsat} - T_{C4} = 2.2\ ^{o}C$

$\dot{m}_{H0} = 17.88\ kg/s$

$Q = 40.9\ MW$

Geometric Data		
Orientation	0	[]
A_{HCOND}	788	[m^2]
A_{HDC}	0	[m^2]
A_{HDS}	70	[m^2]
D_S	1.6	[m^2]
n_t	1080	[m]
d_o	15	
th	1	[mm]
Baffle type	1	[]
FWH Type	0	[]
Operational Data		@930MW
m_{C0}	347.519	[kg/s]
T_{C0}	84.5	[°C]
P_{C0}	23.878	[bars]
T_{H0}	157.4	[°C]
P_{H0}	1.757	[bars]
x_{H0}	1	[]
m_{M0}	0.0001	[kg/s]
T_{M0}	116.164	[°C]
P_{M0}	1.757	[bars]
x_{M0}	0	[]
B	550	[mm]
Bc	30.00%	[%]
B	400	[mm]
Bc	30.00%	[%]
Passes	2	[]
Layout	30	[°]
P_T	18.75	[mm]
P_L	18.75	[mm]
th_{plate}	5	[mm]
th_{grid}	50	[mm]
A_{CONDif}	0	[m^2]
DC	0	[]

Power Station: PS06

Heater: LP4

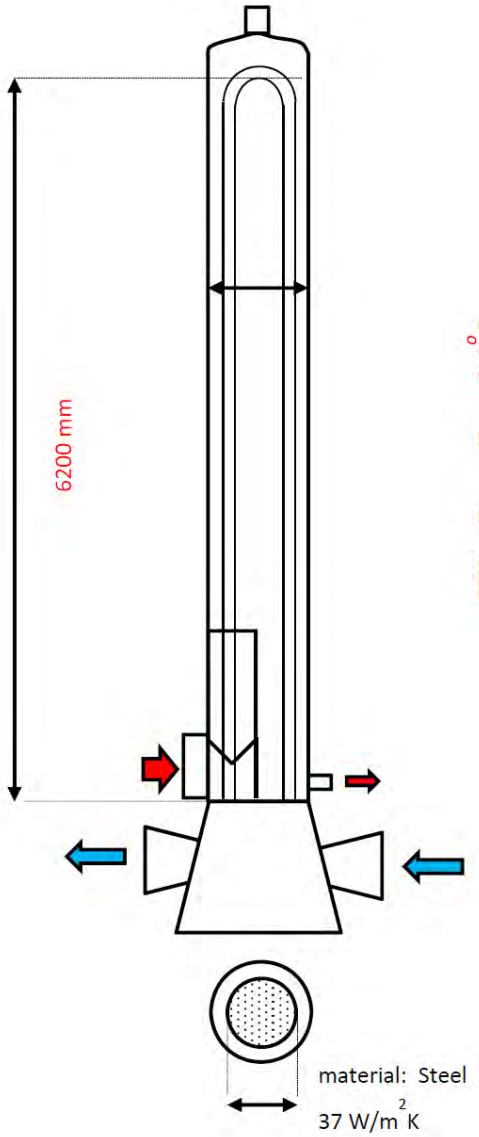

Geometric Data		
Orientation	0	[]
A_{HCOND}	627	[m^2]
A_{HDC}	0	[m^2]
A_{HDS}	75	[m^2]
D_S	1.6	[m^2]
n_t	1080	[m]
d_o	15	
th	1	[mm]
Baffle type	1	[]
FWH Type	0	[]
Operational Data		@930MW
m_{C0}	347.519	[kg/s]
T_{C0}	113.1	[^{o}C]
P_{C0}	23.878	[bars]
T_{H0}	245.5	[^{o}C]
P_{H0}	4.23	[bars]
x_{H0}	1	[]
m_{M0}	0.0001	[kg/s]
T_{M0}	145.639	[^{o}C]
P_{M0}	4.23	[bars]
x_{M0}	0	[]
B	550	[mm]
Bc	30.00%	[%]
B	400	[mm]
Bc	30.00%	[%]
Passes	2	[]
Layout	30	[^{o}]
P_T	18.75	[mm]
P_L	18.75	[mm]
th_{plate}	5	[mm]
th_{grid}	50	[mm]
A_{CONDif}	0	[m^2]
DC	0	[]

Power Station: PS06
Heater: HP6

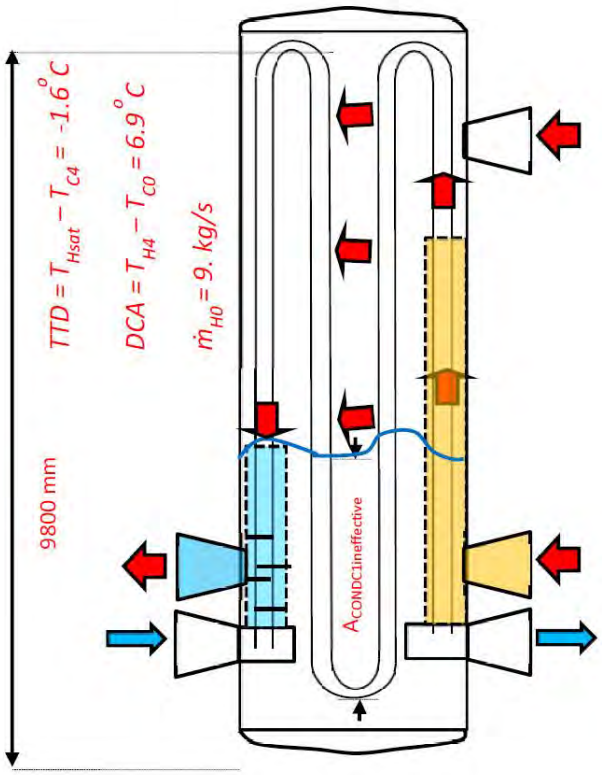

material: 15Mo3 1.541

50 W/m^{2}K

Geometric Data		
Orientation	1	[]
A_{HCOND}	573	[m^2]
A_{HDC}	63	[m^2]
A_{HDS}	97	[m^2]
D_S	1.7	[m^2]
n_t	347	[m]
d_c	25	
th	2.2	[mm]
Baffle type	1	[]
FWH Type	1	[]

Operational Data		@930MW
m_{C0}	212	[kg/s]
T_{C0}	178.1	[^{o}C]
P_{C0}	221.4	[bars]
T_{H0}	430.9	[^{o}C]
P_{H0}	17.7	[bars]
x_{H0}	1	[]
m_{M0}	15.02	[kg/s]
T_{M0}	241	[^{o}C]
P_{M0}	34.07	[bars]
x_{M0}	0	[]
B	550	[mm]
Bc	30.00%	[%]
B	400	[mm]
Bc	30.00%	[%]
Passes	4	[]
Layout	90	[^{o}]
P_T	30	[mm]
P_L	30	[mm]
th_{plate}	5	[mm]
th_{grid}	50	[mm]
A_{CONDif}	41	[m^2]
DC	1	[]

Power Station: PS06
Heater: HP7

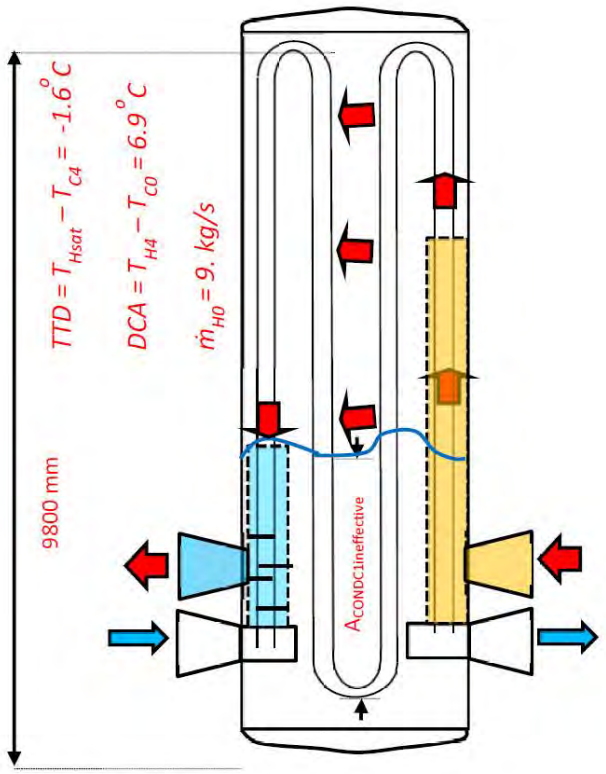

material: 15Mo3 1.541

50 W/m^{2}K

Geometric Data		
Orientation	1	[]
A_{HCOND}	712	[m^2]
A_{HDC}	48	[m^2]
A_{HDS}	70	[m^2]
D_S	1.7	[m^2]
n_t	347	[m]
d_c	25	
th	2.2	[mm]
Baffle type	0	[]
FWH Type	1	[]

Operational Data		@930MW
m_{CO}	212	[kg/s]
T_{CO}	207.8	[°C]
P_{CO}	221.4	[bars]
T_{H0}	296.6	[°C]
P_{H0}	34.07	[bars]
x_{H0}	1	[]
m_{M0}	0.00001	[kg/s]
T_{M0}	241.02	[°C]
P_{M0}	34.07	[bars]
x_{M0}	0	[]
B	300	[mm]
Bc	30.00%	[%]
B	300	[mm]
Bc	30.00%	[%]
Passes	4	[]
Layout	30	[°]
P_T	51.9	[mm]
P_L	30	[mm]
th_{plate}	2.4	[mm]
th_{grid}	50	[mm]
A_{CONDif}	41	[m^2]
DC	1	[]

Power Station: PS12

Heater: LP1

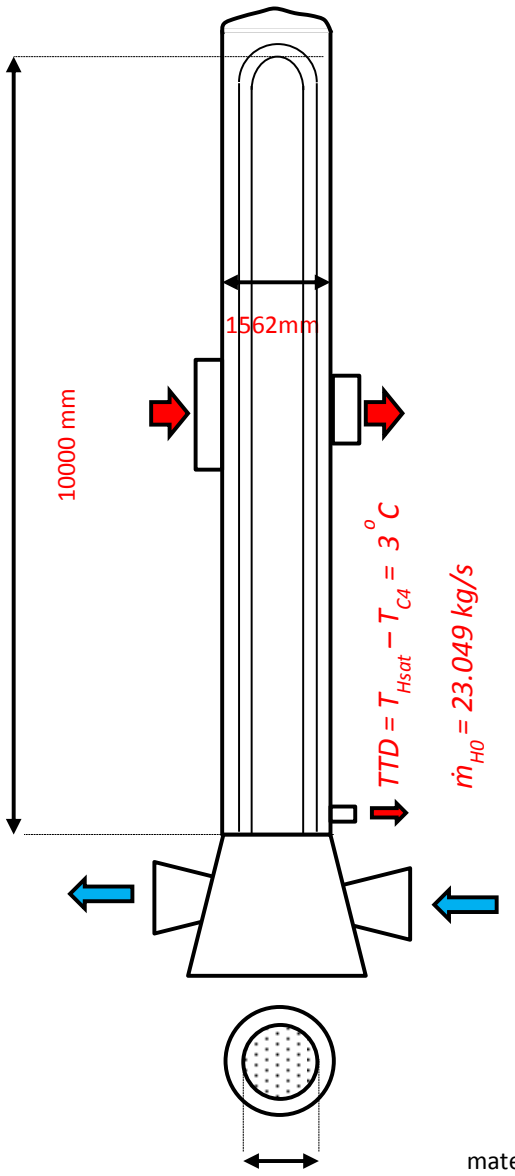

material: 1.4550

Geometric Data		
Orientation	0	[]
A_{HCOND}	1300	[m^2]
A_{HDC}	0	[m^2]
A_{HDS}	0	[m^2]
D_S	1.6	[m^2]
n_t	1449	[m]
d_o	17	
th	1	[mm]
Baffle type	0	[]
FWH Type	0	[]
Operational		@794MW
m_{CD}	429.358	[kg/s]
T_{CD}	61.2	[°C]
P_{CD}	11.6	[bars]
T_{H0}	99.3	[°C]
P_{H0}	0.7978	[bars]
x_{H0}	1	[]
m_{M0}	0.0001	[kg/s]
T_{M0}	93.4	[°C]
P_{M0}	0.7978	[bars]
x_{M0}	0	[]
B	300	[mm]
Bc	30.00%	[%]
B	300	[mm]
Bc	30.00%	[%]
Passes	2	[]
Layout	60	[°]
P_T	21.3	[mm]
P_L	36.8	[mm]
L_{plate}	2.1	[mm]
L_{grid}	50	[mm]
$A_{HCONDII}$	0	[m^2]
DC	0	[]

Power Station: PS06

Heater: LP2

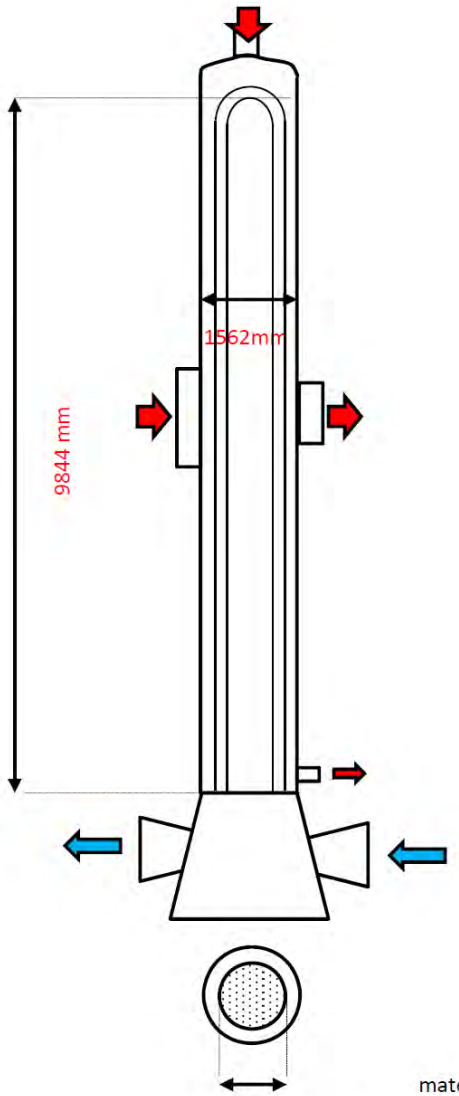

material: 1.4550

Geometric Data		
Orientation	0	[]
A_{HCOND}	1225	[m^2]
A_{HDC}	0	[m^2]
A_{HDS}	0	[m^2]
D_S	1.6	[m^2]
n_t	1449	[m]
d_o	17	
th	1	[mm]
Baffle type	0	[]
FWH Type	0	[]
Operational		@794MW
m_{C0}	429.358	[kg/s]
T_{C0}	90.4	[°C]
P_{C0}	11.1	[bars]
T_{H0}	183.3	[°C]
P_{H0}	2.1229	[bars]
x_{H0}	1	[]
m_{M0}	20.36	[kg/s]
T_{M0}	124.4	[°C]
P_{M0}	4.42	[bars]
x_{M0}	0	[]
B	300	[mm]
Bc	30.00%	[%]
B	300	[mm]
Bc	30.00%	[%]
Passes	2	[]
Layout	60	[°]
P_T	21.5	[mm]
P_L	36.8	[mm]
L_{plate}	2.4	[mm]
L_{grid}	50	[mm]
$A_{HCONDif}$	0	[m^2]
DC	0	[]

Power Station: PS12

Heater: LP3

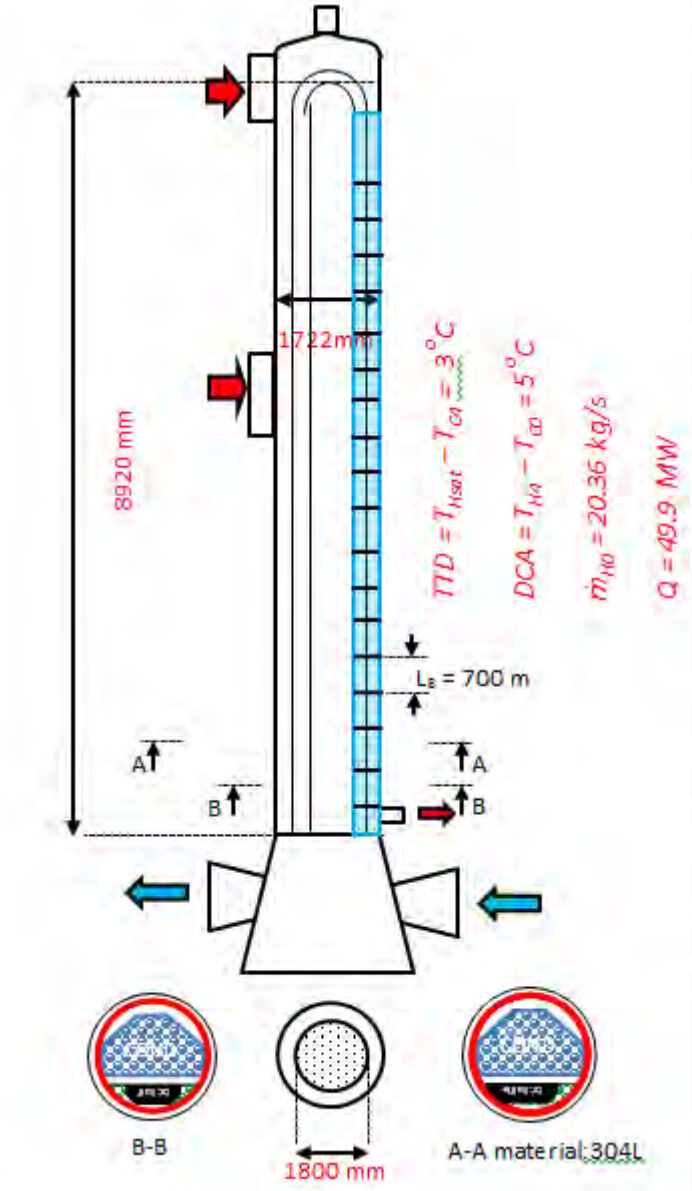

Geometric Data		
Orientation	0	[]
A_{HCOND}	1225	[m^2]
A_{HDC}	110	[m^2]
A_{HDS}	0	[m^2]
D_S	1.9	[m^2]
n_t	1621	[m]
d_o	17	
th	1	[mm]
Baffle type	0	[]
FWH Type	0	[]
Operational		@794MW
m_{C0}	471.997	[kg/s]
T_{C0}	119.4	[°C]
P_{C0}	10.6	[bars]
T_{H0}	256.2	[°C]
P_{H0}	4.4194	[bars]
x_{H0}	1	[]
m_{M0}	0.001	[kg/s]
T_{M0}	147.24	[°C]
P_{M0}	4.4194	[bars]
x_{M0}	0	[]
B	300	[mm]
Bc	30.00%	[%]
B	300	[mm]
Bc	30.00%	[%]
Passes	2	[]
Layout	60	[°]
P_T	21.5	[mm]
P_L	36.8	[mm]
L_{plate}	2.40	[mm]
L_{grid}	50	[mm]
$A_{HCONDif}$	0	[m^2]
DC	0	[]

Power Station: PS12

Heater: HP5

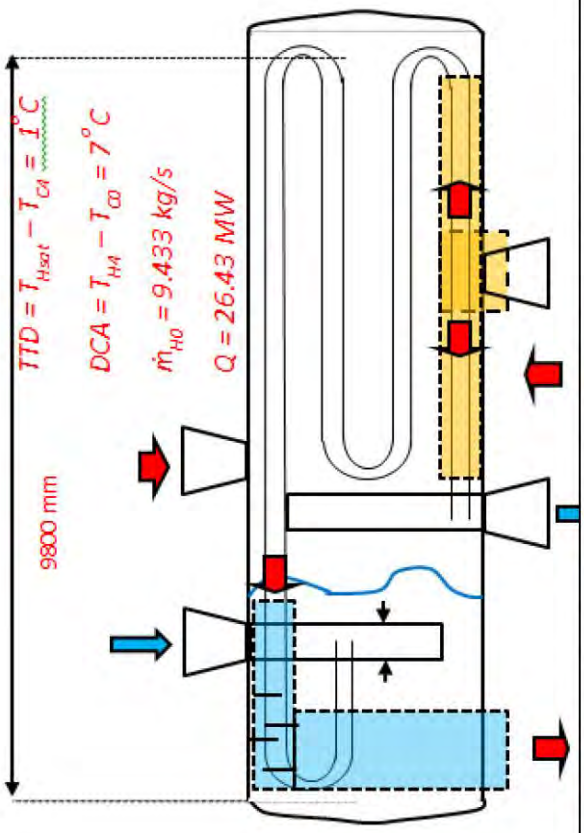

Material: 15Mo3 carbon steel 1.5415 50W/m^{2}K

Geometric Data		
Orientation	1	[]
A_{HCOND}	715	[m^2]
A_{HDC}	140	[m^2]
A_{HDS}	144	[m^2]
D_S	2.2	[m^2]
n_t	597	[m]
d_o	25	
th	2.9	[mm]
Baffle type	0	[]
FWH Type	1	[]
Operational		@794MW
m_{C0}	280	[kg/s]
T_{C0}	177.1	[°C]
P_{C0}	203	[bars]
T_{H0}	417.4	[°C]
P_{H0}	15.53	[bars]
x_{H0}	1	[]
m_{M0}	28.063	[kg/s]
T_{M0}	205.9	[°C]
P_{M0}	38.95	[bars]
x_{M0}	0	[]
B	800	[mm]
Bc	30.00%	[%]
B	700	[mm]
Bc	30.00%	[%]
Passes	4	[]
Layout	90	[°]
P_T	30	[mm]
P_L	30	[mm]
L_{plate}	5	[mm]
L_{grid}	50	[mm]
$A_{HCONDif}$	0	[m^2]
DC	1	[]

Power Station: PS12

Heater: HP6

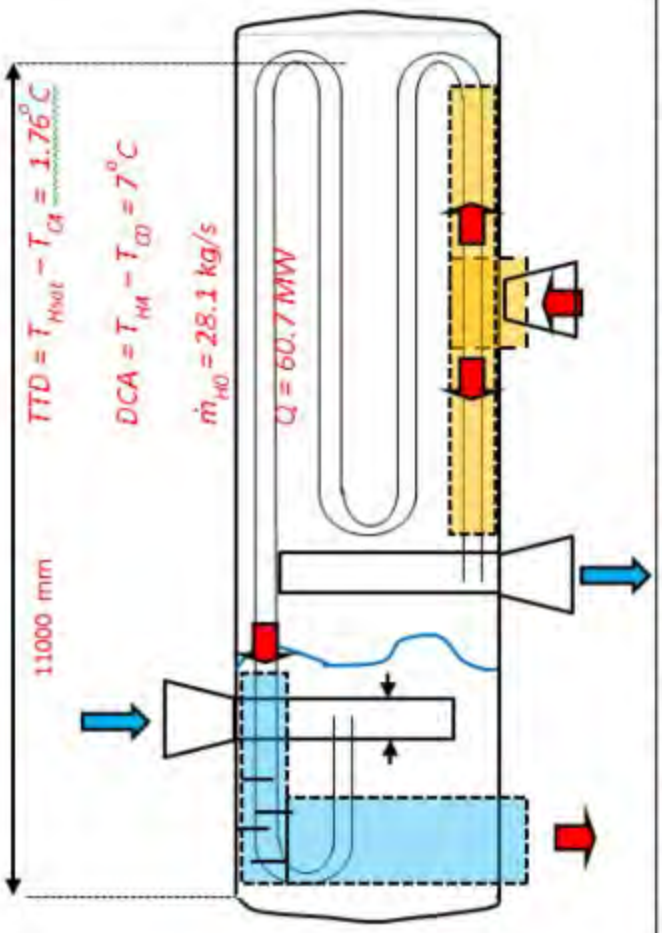

Geometric Data		
Orientation	1	[]
A_{HCOND}	832	[m^2]
A_{HDC}	207	[m^2]
A_{HDS}	145	[m^2]
D_s	2.3	[m^2]
n_t	628	[m]
d_o	25	
th	2.9	[mm]
Baffle type	0	[]
FWH Type	1	[]
Operational		@794MW
m_{CO}	280	[kg/s]
T_{CO}	198.9	[°C]
P_{CO}	202	[bars]
T_{HO}	329.1	[°C]
P_{HO}	38.95	[bars]
x_{HO}	1	[]
m_{MO}	0.0001	[kg/s]
T_{MO}	248.76	[°C]
P_{MO}	38.95	[bars]
x_{MO}	0	[]
B	800	[mm]
Bc	30.00%	[%]
B	700	[mm]
Bc	30.00%	[%]
Passes	4	[]
Layout	90	[°]
P_T	30	[mm]
P_L	30	[mm]
L_{plate}	5	[mm]
L_{grid}	50	[mm]
$A_{HCONDif}$	0	[m^2]
DC	1	[]

Power Station: PS08
Heater: LP1

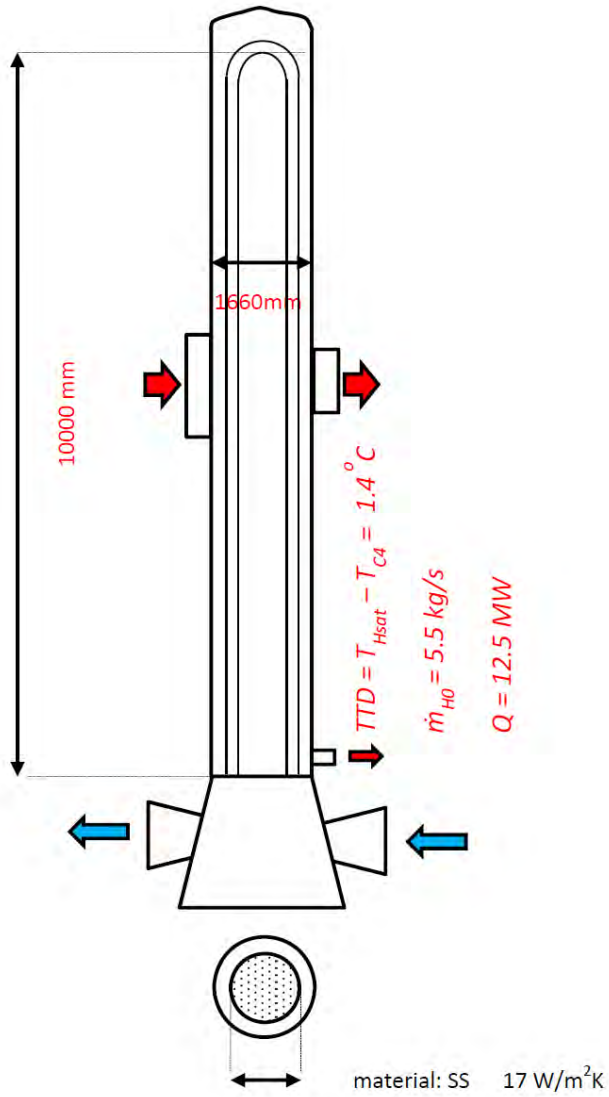

Geometric Data		
Orientation	0	[]
A_{HCOND}	752	[m^2]
A_{HDC}	0	[m^2]
A_{HDS}	0	[m^2]
D_S	1.7	[m^2]
n_t	788	[m]
d_o	19	
th	1.7	[mm]
Baffle type	1	[]
FWH Type	0	[]

Operational Data		@672MW
m_{C0}	193.53	[kg/s]
T_{C0}	41.4	[°C]
P_{C0}	16	[bars]
T_{H0}	58.841	[°C]
P_{H0}	0.189	[bars]
x_{H0}	0.938	[]
m_{M0}	0.0001	[kg/s]
T_{M0}	58.841	[°C]
P_{M0}	0.189	[bars]
x_{M0}	0	[]
B	630	[mm]
Bc	30.00%	[%]
B	300	[mm]
Bc	30.00%	[%]
Passes	2	[]
Layout	30	[°]
P_T	41.14	[mm]
P_L	23.75	[mm]
th_{plate}	2.4	[mm]
th_{grid}	50	[mm]
A_{CONDif}	0	[m^2]
DC	0	[]

Power Station: I PS08
Heater: LP2

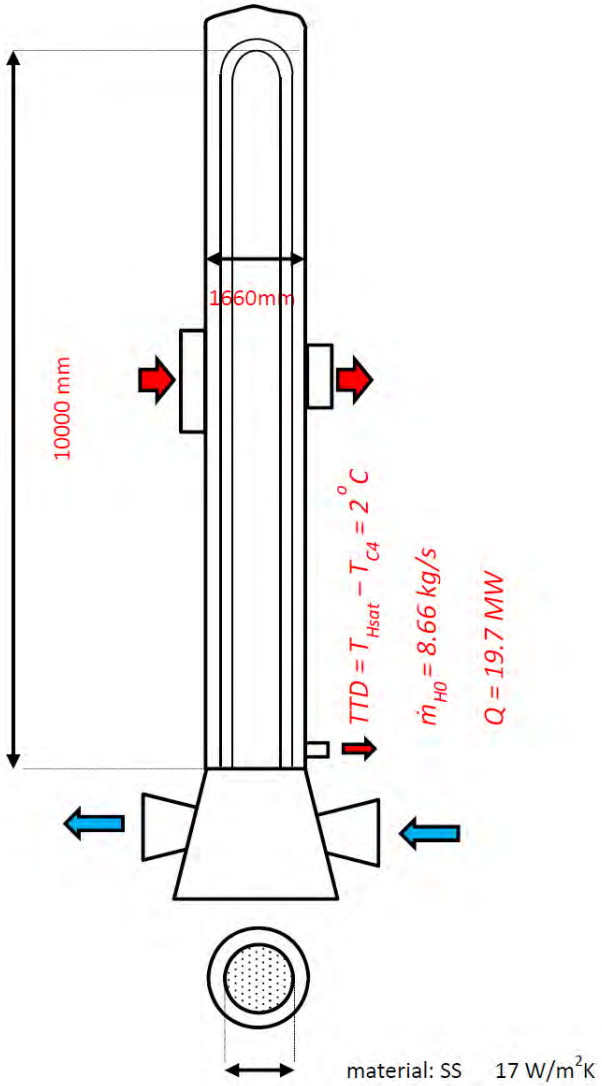

Geometric Data		
Orientation	0	[]
A_{HCOND}	750	[m²]
A_{HDC}	0	[m²]
A_{HDS}	0	[m²]
D_S	1.7	[m²]
n_t	786	[m]
d_o	19	
th	1.7	[mm]
Baffle type	1	[]
FWH Type	0	[]
Operational Data		@672MW
m_{C0}	193.53	[kg/s]
T_{C0}	57.4	[°C]
P_{C0}	16	[bars]
T_{H0}	83.7	[°C]
P_{H0}	0.55	[bars]
x_{H0}	0.979	[]
m_{M0}	0.0001	[kg/s]
T_{M0}	83.7	[°C]
P_{M0}	0.55	[bars]
x_{M0}	0	[]
B	630	[mm]
Bc	30.00%	[%]
B	300	[mm]
Bc	30.00%	[%]
Passes	2	[]
Layout	30	[°]
P_T	41.14	[mm]
P_L	23.75	[mm]
th_{plate}	2.4	[mm]
th_{grid}	50	[mm]
A_{CONDif}	0	[m²]
DC	0	[]

Power Station: PS08
Heater: LP3

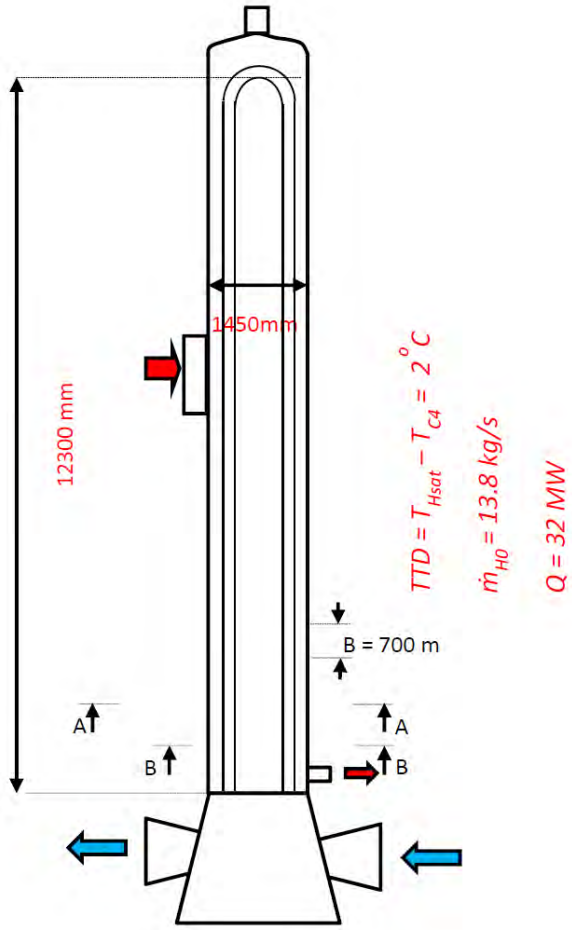

A-A material: SS 17 W/mK

Geometric Data		
Orientation	1	[]
A_{HCOND}	318	[m^2]
A_{HDC}	0	[m^2]
A_{HDS}	0	[m^2]
D_S	1	[m^2]
n_t	370	[m]
d_o	20	
th	1.5	[mm]
Baffle type	1	[]
FWH Type	0	[]
Operational Data		@672MW
m_{C0}	159	[kg/s]
T_{C0}	122	[°C]
P_{C0}	198	[bars]
T_{H0}	228	[°C]
P_{H0}	5.5	[bars]
x_{H0}	1	[]
m_{M0}	32.8	[kg/s]
T_{M0}	167.2	[°C]
P_{M0}	10.13	[bars]
x_{M0}	0	[]
B	500	[mm]
Bc	25.00%	[%]
B	500	[mm]
Bc	25.00%	[%]
Passes	2	[]
Layout	30	[°]
P_T	25	[mm]
P_L	25	[mm]
th_{plate}	2.4	[mm]
th_{grid}	25	[mm]
A_{CONDif}	0	[m^2]
DC	0	[]

Power Station: PS08

Heater: HP5 (previous design)

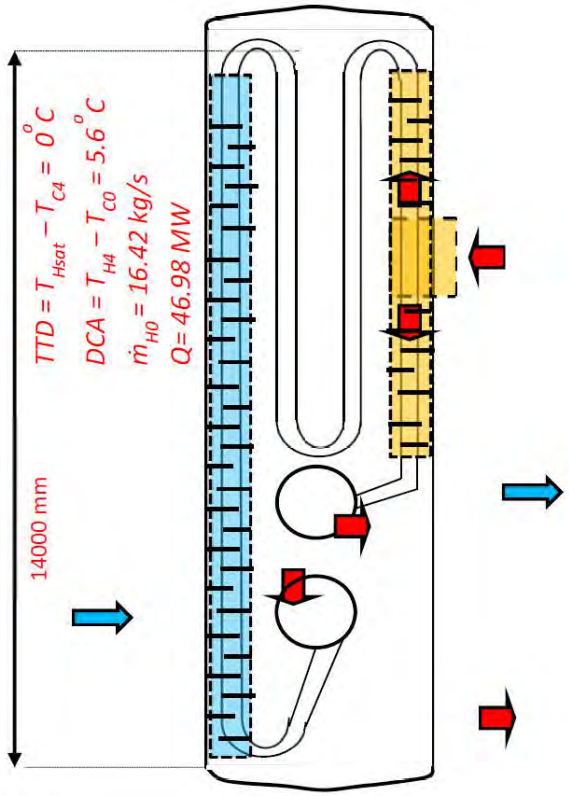

material: carbon steel 50 W/mK

Geometric Data		
Orientation	0	[]
A_{HCOND}	632	[m^2]
A_{HDC}	0	[m^2]
A_{HDS}	0	[m^2]
D_S	1.7	[m^2]
n_t	788	[m]
d_c	19	
th	1.7	[mm]
Baffle type	1	[]
FWH Type	0	[]

Operational Data		@672MW
m_{C0}	193.53	[kg/s]
T_{C0}	43.9	[°C]
P_{C0}	16	[bars]
T_{H0}	58.95	[°C]
P_{H0}	0.19	[bars]
x_{H0}	0.938	[]
m_{M0}	0.0001	[kg/s]
T_{M0}	265.4	[°C]
P_{M0}	51.24	[bars]
x_{M0}	0	[]
B	630	[mm]
Bc	30.00%	[%]
B	300	[mm]
Bc	30.00%	[%]
Passes	2	[]
Layout	30	[°]
P_T	22.5	[mm]
P_L	22.5	[mm]
th_{plate}	2.4	[mm]
th_{grid}	50	[mm]
A_{CONDif}	0	[m^2]
DC	0	[]

Power Station: PS08

Heater: HP6 (previous design)

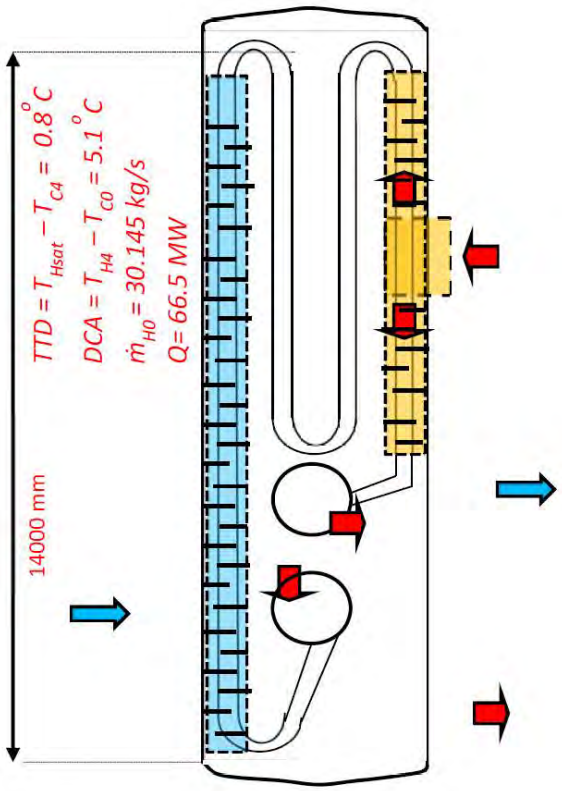

material: carbon steel 50 W/mK

Geometric Data		
Orientation	0	[]
A_{HCOND}	720	[m^2]
A_{HDC}	170	[m^2]
A_{HDS}	110	[m^2]
D_S	1.9	[m^2]
n_t	364	[m]
d_c	25	
th	2.9	[mm]
Baffle type	1	[]
FWH Type	1	[]
Operational Data		@672MW
m_{C0}	253.545	[kg/s]
T_{C0}	192.1	[°C]
P_{C0}	230	[bars]
T_{H0}	331.9	[°C]
P_{H0}	39.97	[bars]
x_{H0}	1	[]
m_{M0}	0.0001	[kg/s]
T_{M0}	250.313	[°C]
P_{M0}	39.97	[bars]
x_{M0}	0	[]
B	400	[mm]
Bc	25.00%	[%]
B	400	[mm]
Bc	25.00%	[%]
Passes	4	[]
Layout	90	[°]
P_T	31.25	[mm]
P_L	31.25	[mm]
th_{plate}	6.25	[mm]
th_{grid}	50	[mm]
A_{CONDif}	0	[m^2]
DC	0	[]

Power Station: PS16

Heater: LP1

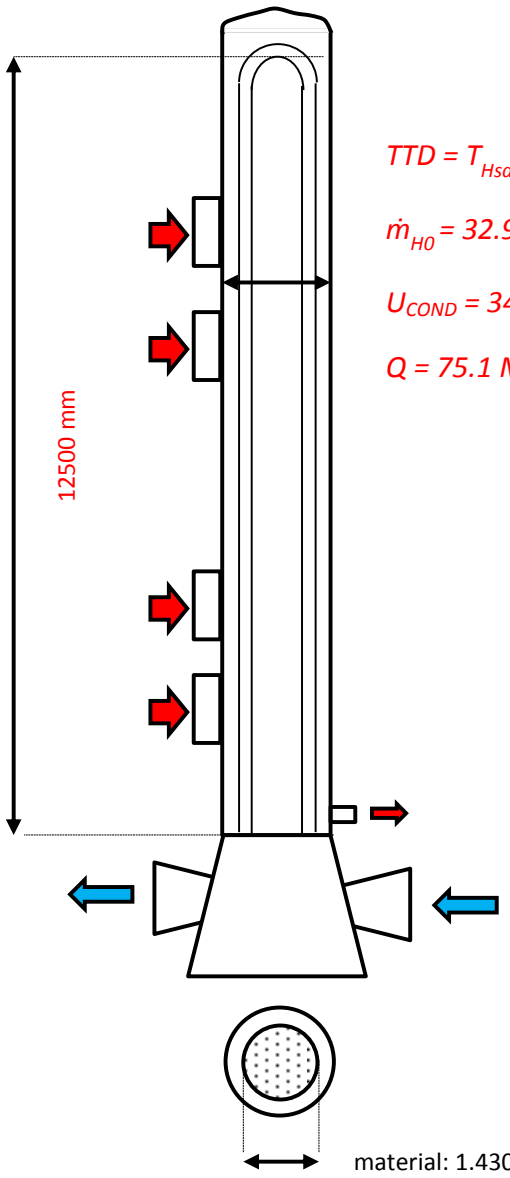

$TTD = T_{Hsat} - T_{C4} = 2\ ^{o}C$

$\dot{m}_{H0} = 32.94\ kg/s$

$U_{COND} = 3477\ W/m^2K$

$Q = 75.1\ MW$

Geometric Data		
Orientation	0	[]
A_{HCOND}	1572	[m^2]
A_{HDC}	0	[m^2]
A_{HDS}	0	[m^2]
D_S	1.8	[m^2]
n_t	1167	[m]
d_o	18	
th	0.8	[mm]
Baffle type	0	[]
FWH Type	0	[]

Operational Data		@794MW
m_{C0}	453.23	[kg/s]
T_{C0}	51.1	[^{o}C]
P_{C0}	25	[bars]
T_{H0}	97.53	[^{o}C]
P_{H0}	0.777	[bars]
x_{H0}	1	[]
m_{M0}	0.0001	[kg/s]
T_{M0}	92.7	[^{o}C]
P_{M0}	0.7777	[bars]
x_{M0}	0	[]
$L_{B,DC}$	300	[mm]
$B_{cut,DC}$	30.00%	[%]
$L_{B,DC}$	300	[mm]
$B_{cut,DC}$	30.00%	[%]
Passes	2	[]
Layout	30	[^{o}]
P_T	23.5	[mm]
P_L	23.5	[mm]
L_{plate}	5.5	[mm]
L_{grid}	100	[mm]
$A_{HCONDif}$	0	[m^2]
DC	0	[]

Power Station: PS16

Heater: LP2

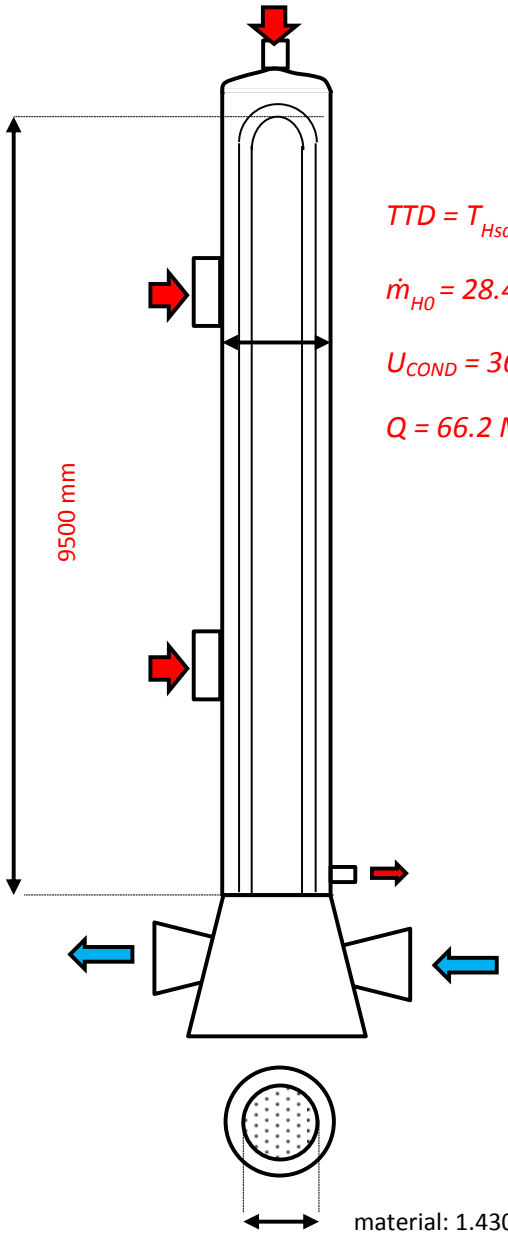

$TTD = T_{Hsat} - T_{C4} = 2\ ^{o}C$

$\dot{m}_{H0} = 28.46\ kg/s$

$U_{COND} = 3633\ W/m^2K$

$Q = 66.2\ MW$

material: 1.4306 17 W/m^{-1}K

Geometric Data

Orientation	0	[]
A_{HCOND}	1456	[m^2]
A_{HDC}	0	[m^2]
A_{HDS}	0	[m^2]
D_S	1.65	[m^2]
n_t	1184	[m]
d_o	18	
th	0.8	[mm]
Baffle type	0	[]
FWH Type	0	[]

Operational Data @794MW

m_{C0}	453.23	[kg/s]
T_{C0}	90.7	[^{o}C]
P_{C0}	25	[bars]
T_{H0}	192.28	[^{o}C]
P_{H0}	2.491	[bars]
x_{H0}	1	[]
m_{M0}	25.35	[kg/s]
T_{M0}	131.567	[^{o}C]
P_{M0}	5.588	[bars]
x_{M0}	0	[]
B	300	[mm]
Bc	30.00%	[%]
B	300	[mm]
Bc	30.00%	[%]
Passes	2	[]
Layout	30	[^{o}]
P_T	40.7	[mm]
P_L	23.5	[mm]
th_{plate}	5.5	[mm]
th_{grid}	100	[mm]

Power Station: PS16

Heater: LP3

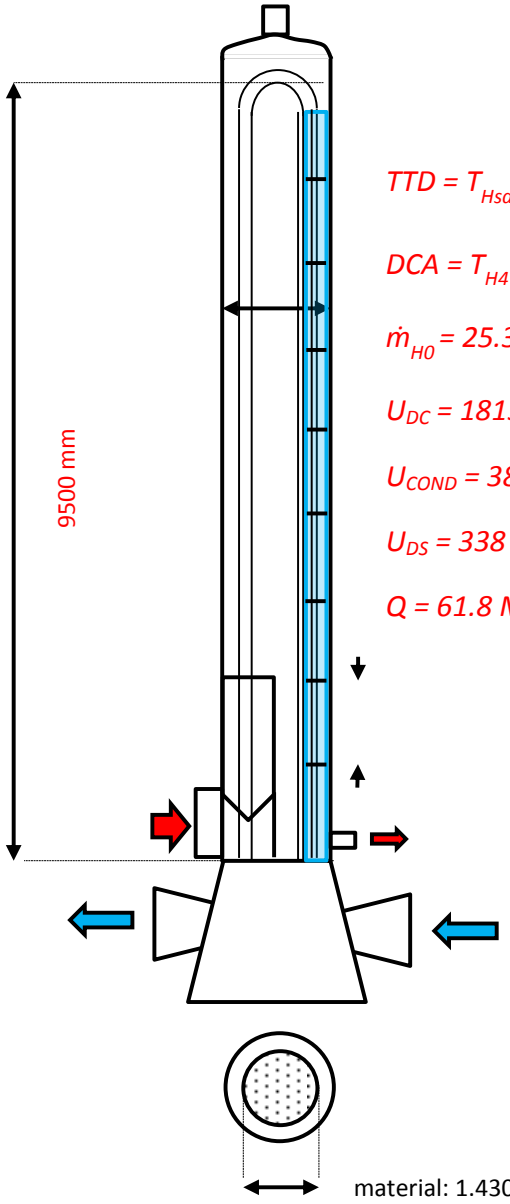

$TTD = T_{Hsat} - T_{C4} = 2\ ^{o}C$

$DCA = T_{H4} - T_{C0} = 6\ ^{o}C$

$\dot{m}_{H0} = 25.35\ kg/s$

$U_{DC} = 1815\ W/m^2K$

$U_{COND} = 3815\ W/m^2K$

$U_{DS} = 338\ W/m^2K$

$Q = 61.8\ MW$

material: 1.4306 17 W/m˚K

Geometric Data

Orientation	0	[]
A_{HCOND}	1110	[m^2]
A_{HDC}	110	[m^2]
A_{HDS}	149	[m^2]
D_S	1.7	[m^2]
n_t	1359	[m]
d_o	18	
th	0.8	[mm]
Baffle type	0	[]
FWH Type	0	[]

Operational Data @794MW

m_{C0}	507.04	[kg/s]
T_{C0}	125.6	[^{o}C]
P_{C0}	25	[bars]
T_{H0}	270.77	[^{o}C]
P_{H0}	5.588	[bars]
x_{H0}	1	[]
m_{M0}	0.0001	[kg/s]
T_{M0}	156.07	[^{o}C]
P_{M0}	5.588	[bars]
x_{M0}	0	[]
B	300	[mm]
Bc	30.00%	[%]
B	300	[mm]
Bc	30.00%	[%]
Passes	2	[]
Layout	30	[^{o}]
P_T	23.5	[mm]
P_L	23.5	[mm]
L_{plate}	5.5	[mm]
L_{grid}	100	[mm]

Power Station: PS16

Heater: HP5

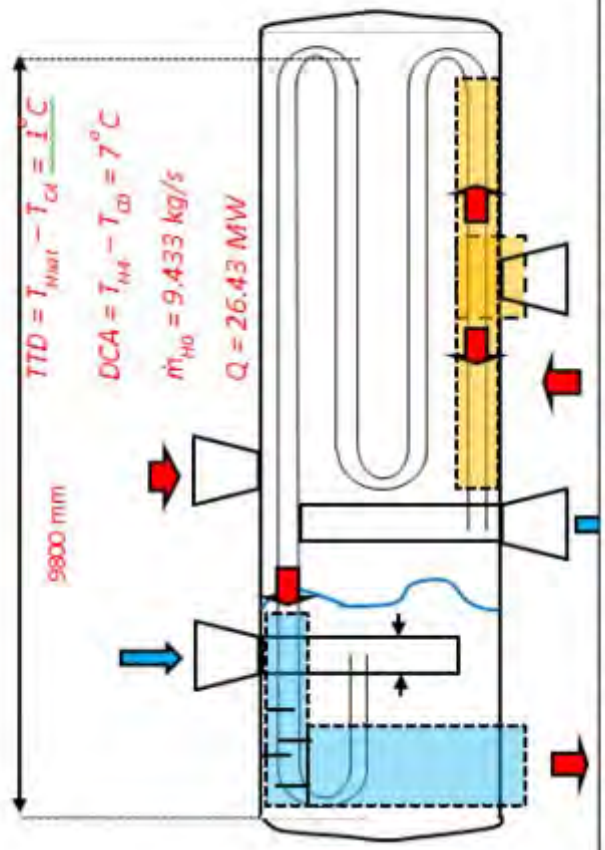

Material: 15Mo3 carbon steel 1.5415 50W/m K

Geometric Data		
Orientation	1	[]
A_{HCOND}	715	[m^2]
A_{HDC}	140	[m^2]
A_{HDS}	144	[m^2]
D_S	2.2	[m^2]
n_t	597	[m]
d_o	25	
th	2.9	[mm]
Baffle type	0	[]
FWH Type	1	[]
Operational		@794MW
m_{CD}	280	[kg/s]
T_{CD}	177.1	[°C]
P_{CD}	203	[bars]
T_{H0}	417.4	[°C]
P_{H0}	15.53	[bars]
x_{H0}	1	[]
m_{M0}	28.063	[kg/s]
T_{M0}	205.9	[°C]
P_{M0}	38.95	[bars]
x_{M0}	0	[]
B	800	[mm]
Bc	30.00%	[%]
B	700	[mm]
Bc	30.00%	[%]
Passes	4	[]
Layout	90	[°]
P_T	30	[mm]
P_L	30	[mm]
L_{plate}	5	[mm]
L_{grid}	50	[mm]
$A_{HCONDif}$	0	[m^2]
DC	1	[]

Power Station: PS16

Heater: HP6

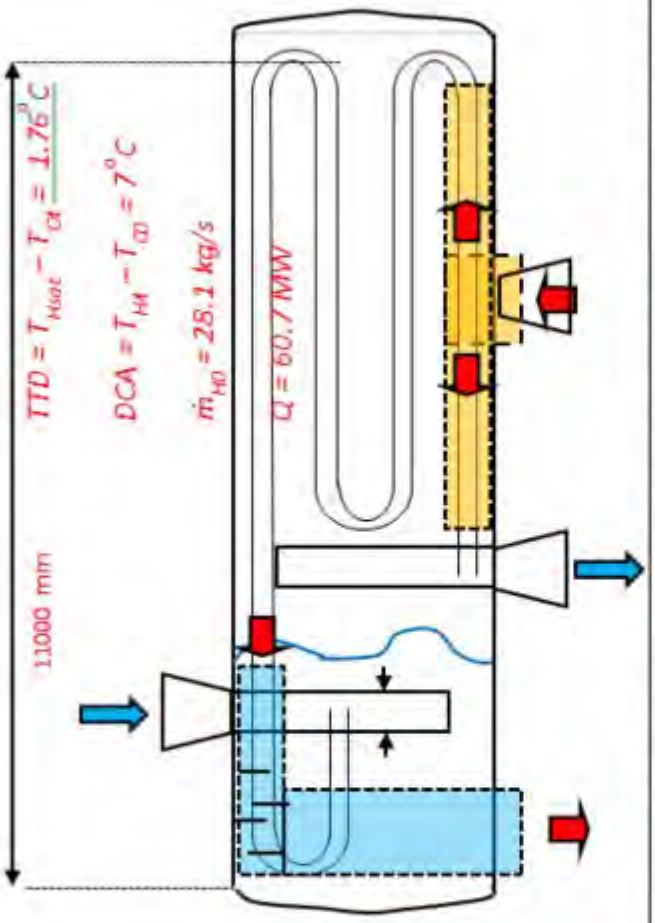

Geometric Data		
Orientation	1	[]
A_{HCOND}	832	[m^2]
A_{HDC}	207	[m^2]
A_{HDS}	145	[m^2]
D_S	2.3	[m^2]
n_t	628	[m]
d_o	25	
th	2.9	[mm]
Baffle type	0	[]
FWH Type	1	[]
Operational		@794MW
m_{CO}	280	[kg/s]
T_{CO}	198.9	[°C]
P_{CO}	202	[bars]
T_{HD}	329.1	[°C]
P_{HD}	38.95	[bars]
x_{HD}	1	[]
m_{MD}	0.0001	[kg/s]
T_{MD}	248.76	[°C]
P_{MD}	38.95	[bars]
x_{MD}	0	[]
B	800	[mm]
Bc	30.00%	[%]
B	700	[mm]
Bc	30.00%	[%]
Passes	4	[]
Layout	90	[°]
P_T	30	[mm]
P_L	30	[mm]
L_{plate}	5	[mm]
L_{grid}	50	[mm]
$A_{HCONDif}$	0	[m^2]
DC	1	[]

Appendix D. Feedwater heater configuration

PS05

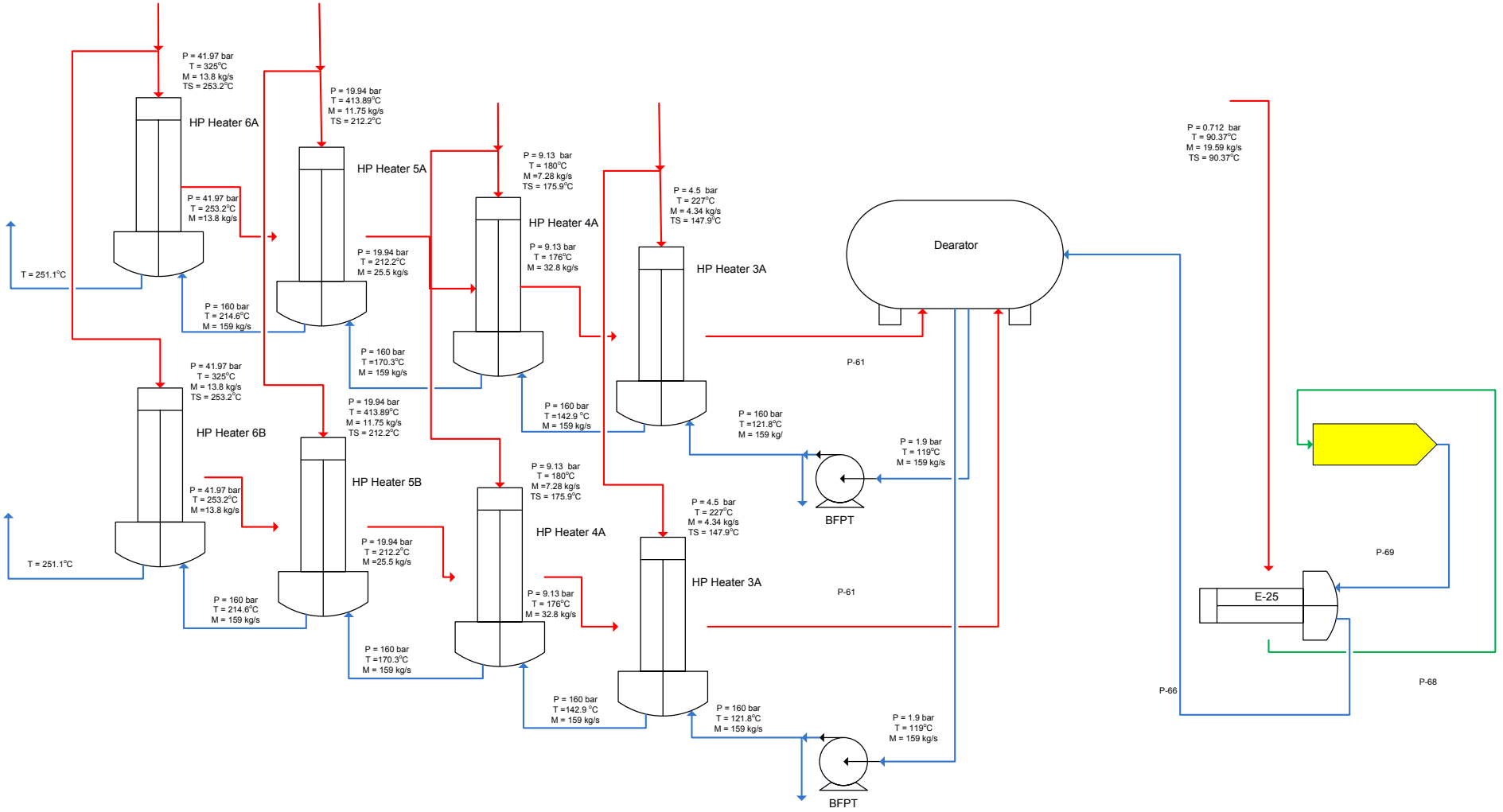

PS12

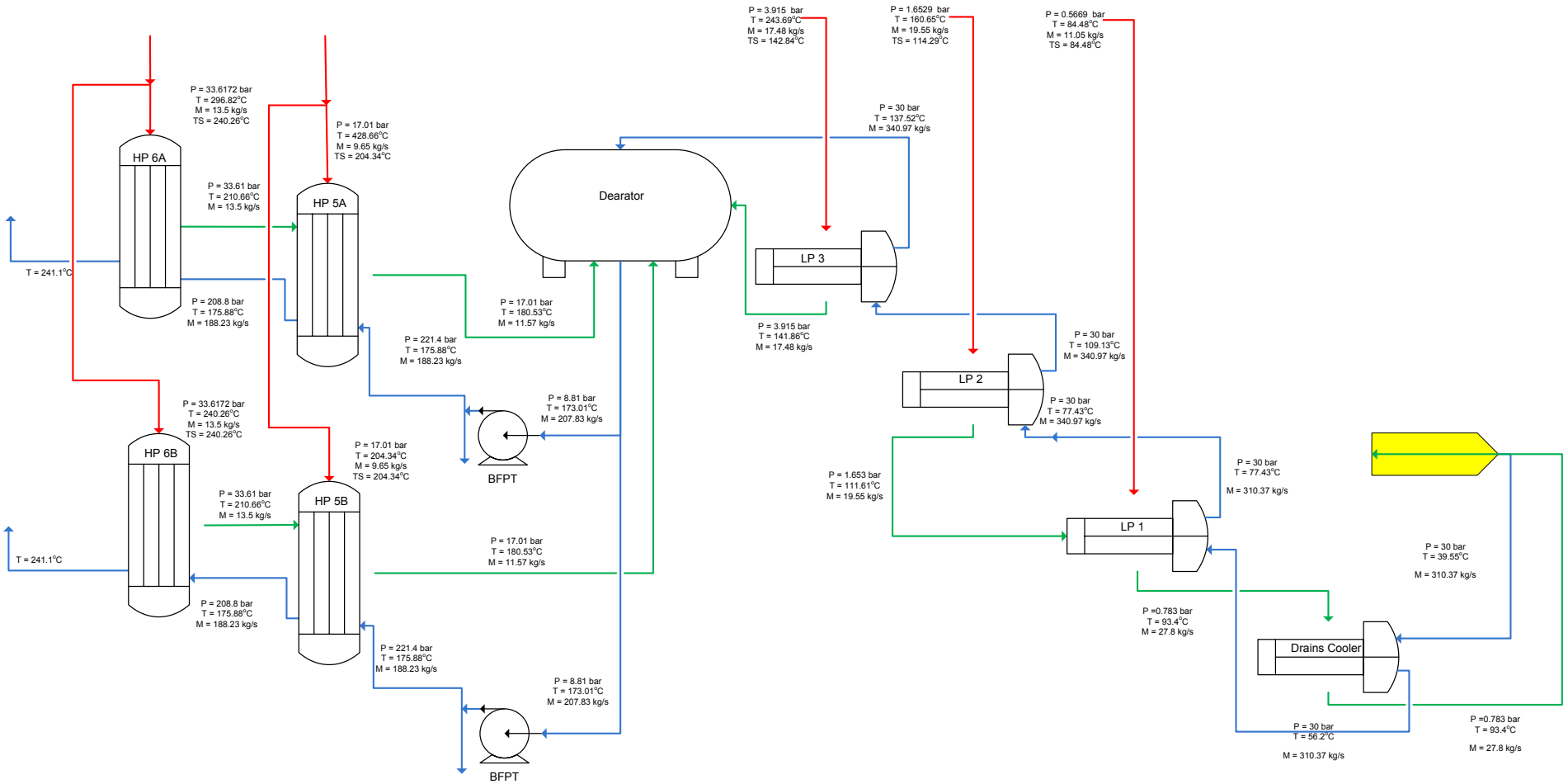
P = 3.915 bar
T = 243.69°C
M = 17.48 kg/s
TS = 142.84°C
P = 1.6529 bar
T = 160.65°C
M = 19.55 kg/s
TS = 114.29°C
P = 0.5669 bar
T = 84.48°C
M = 11.05 kg/s
TS = 84.48°C
P = 33.6172 bar
T = 296.82°C
M = 13.5 kg/s
TS = 240.26°C
P = 17.01 bar
T = 428.66°C
M = 9.65 kg/s
TS = 204.34°C
P = 30 bar
T = 137.52°C
M = 340.97 kg/s
HP 6A
HP 5A
Dearator
LP 3
P = 33.61 bar
T = 210.66°C
M = 13.5 kg/s
T = 241.1°C
P = 208.8 bar
T = 175.88°C
M = 188.23 kg/s
P = 17.01 bar
T = 180.53°C
M = 11.57 kg/s
P = 221.4 bar
T = 175.88°C
M = 188.23 kg/s
P = 3.915 bar
T = 141.86°C
M = 17.48 kg/s
P = 30 bar
T = 109.13°C
M = 340.97 kg/s
LP 2
P = 30 bar
T = 77.43°C
M = 340.97 kg/s
P = 33.6172 bar
T = 240.26°C
M = 13.5 kg/s
TS = 240.26°C
P = 8.81 bar
T = 173.01°C
M = 207.83 kg/s
BFPT
HP 6B
HP 5B
P = 17.01 bar
T = 204.34°C
M = 9.65 kg/s
TS = 204.34°C
P = 1.653 bar
T = 111.61°C
M = 19.55 kg/s
P = 30 bar
T = 77.43°C
M = 310.37 kg/s
LP 1
P = 33.61 bar
T = 210.66°C
M = 13.5 kg/s
T = 241.1°C
P = 17.01 bar
T = 180.53°C
M = 11.57 kg/s
P = 30 bar
T = 39.55°C
M = 310.37 kg/s
P =0.783 bar
T = 93.4°C
M = 27.8 kg/s
P = 208.8 bar
T = 175.88°C
M = 188.23 kg/s
Drains Cooler
P = 221.4 bar
T = 175.88°C
M = 188.23 kg/s
P = 8.81 bar
T = 173.01°C
M = 207.83 kg/s
BFPT
P = 30 bar
T = 56.2°C
M = 310.37 kg/s
P =0.783 bar
T = 93.4°C
M = 27.8 kg/s

PS00

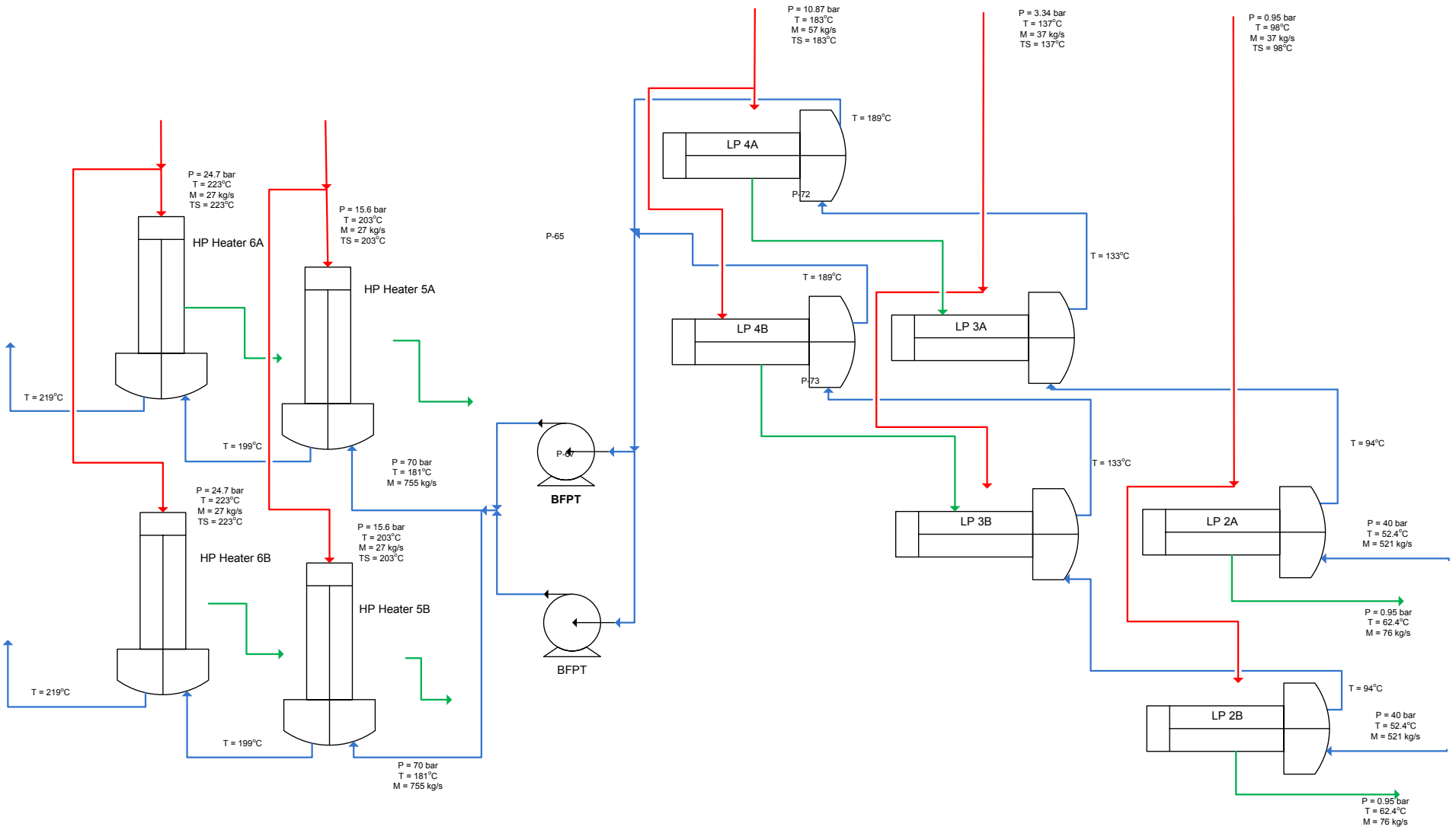
P = 10.87 bar
T = 183°C
M = 57 kg/s
TS = 183°C
P = 3.34 bar
T = 137°C
M = 37 kg/s
TS = 137°C
P = 0.95 bar
T = 98°C
M = 37 kg/s
TS = 98°C
T = 189°C
LP 4A
P-72
P-65
T = 189°C
LP 4B
P-73
LP 3A
T = 133°C
P = 24.7 bar
T = 223°C
M = 27 kg/s
TS = 223°C
HP Heater 6A
P = 15.6 bar
T = 203°C
M = 27 kg/s
TS = 203°C
HP Heater 5A
T = 219°C
T = 199°C
P = 70 bar
T = 181°C
M = 755 kg/s
P-67
BFPT
T = 133°C
T = 94°C
LP 3B
LP 2A
P = 40 bar
T = 52.4°C
M = 521 kg/s
P = 0.95 bar
T = 62.4°C
M = 76 kg/s
P = 24.7 bar
T = 223°C
M = 27 kg/s
TS = 223°C
HP Heater 6B
P = 15.6 bar
T = 203°C
M = 27 kg/s
TS = 203°C
HP Heater 5B
BFPT
T = 219°C
T = 199°C
P = 70 bar
T = 181°C
M = 755 kg/s
T = 94°C
LP 2B
P = 40 bar
T = 52.4°C
M = 521 kg/s
P = 0.95 bar
T = 62.4°C
M = 76 kg/s

PS06

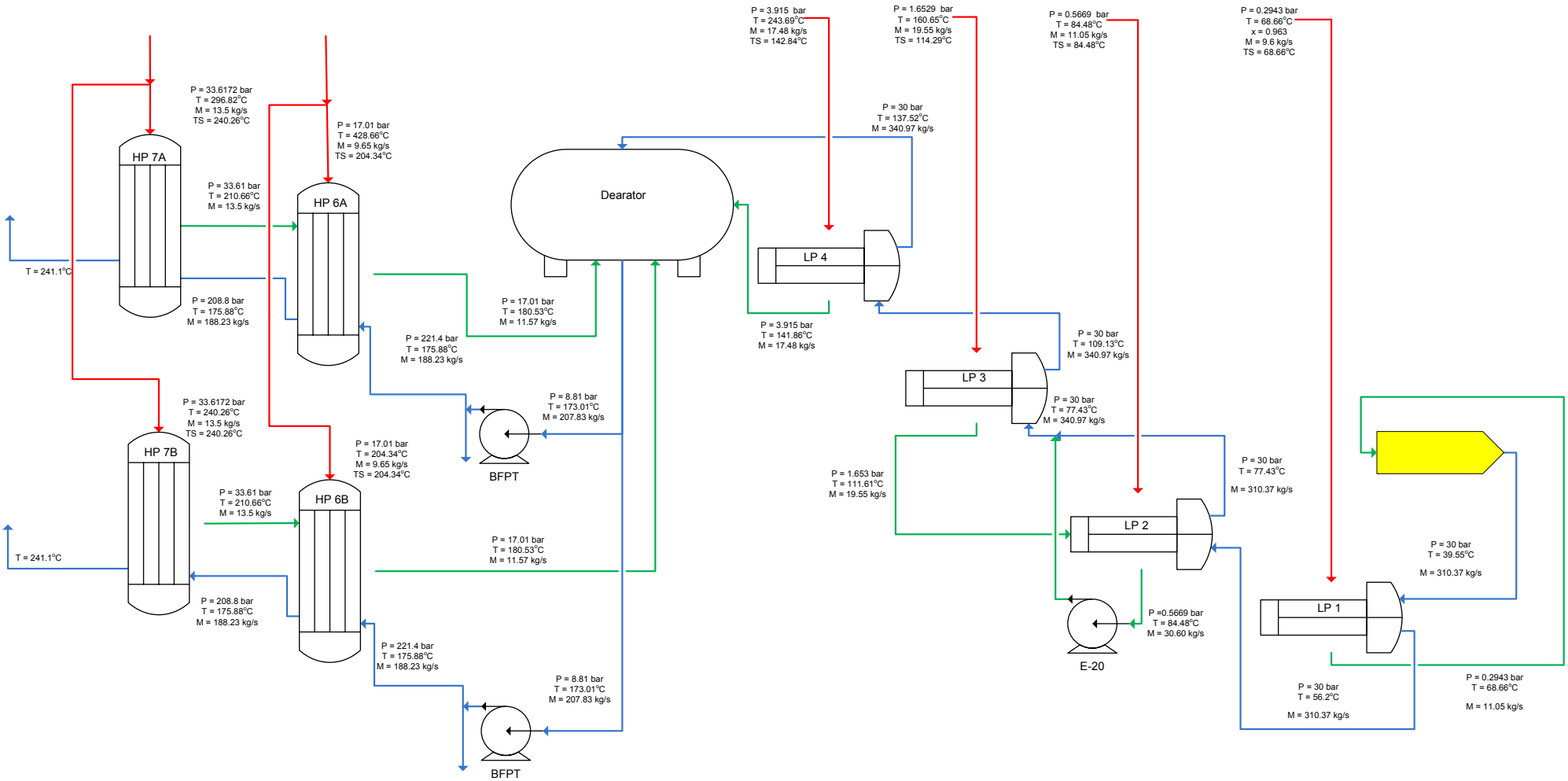
P = 33.6172 bar
T = 296.82°C
M = 13.5 kg/s
TS = 240.26°C
HP 7A
P = 33.61 bar
T = 210.66°C
M = 13.5 kg/s
T = 241.1°C
P = 208.8 bar
T = 175.88°C
M = 188.23 kg/s
P = 17.01 bar
T = 428.66°C
M = 9.65 kg/s
TS = 204.34°C
HP 6A
P = 17.01 bar
T = 180.53°C
M = 11.57 kg/s
P = 221.4 bar
T = 175.88°C
M = 188.23 kg/s
Dearator
P = 3.915 bar
T = 243.69°C
M = 17.48 kg/s
TS = 142.84°C
P = 1.6529 bar
T = 160.65°C
M = 19.55 kg/s
TS = 114.29°C
P = 0.5669 bar
T = 84.48°C
M = 11.05 kg/s
TS = 84.48°C
P = 0.2943 bar
T = 68.66°C
x = 0.963
M = 9.6 kg/s
TS = 68.66°C
P = 30 bar
T = 137.52°C
M = 340.97 kg/s
LP 4
P = 3.915 bar
T = 141.86°C
M = 17.48 kg/s
P = 30 bar
T = 109.13°C
M = 340.97 kg/s
LP 3
P = 30 bar
T = 77.43°C
M = 340.97 kg/s
P = 1.653 bar
T = 111.61°C
M = 19.55 kg/s
P = 30 bar
T = 77.43°C
M = 310.37 kg/s
LP 2
P =0.5669 bar
T = 84.48°C
M = 30.60 kg/s
E-20
P = 30 bar
T = 39.55°C
M = 310.37 kg/s
LP 1
P = 30 bar
T = 56.2°C
M = 310.37 kg/s
P = 0.2943 bar
T = 68.66°C
M = 11.05 kg/s
P = 8.81 bar
T = 173.01°C
M = 207.83 kg/s
BFPT
P = 33.6172 bar
T = 240.26°C
M = 13.5 kg/s
TS = 240.26°C
HP 7B
P = 33.61 bar
T = 210.66°C
M = 13.5 kg/s
T = 241.1°C
P = 208.8 bar
T = 175.88°C
M = 188.23 kg/s
P = 17.01 bar
T = 204.34°C
M = 9.65 kg/s
TS = 204.34°C
HP 6B
P = 17.01 bar
T = 180.53°C
M = 11.57 kg/s
P = 221.4 bar
T = 175.88°C
M = 188.23 kg/s
P = 8.81 bar
T = 173.01°C
M = 207.83 kg/s
BFPT

PS08

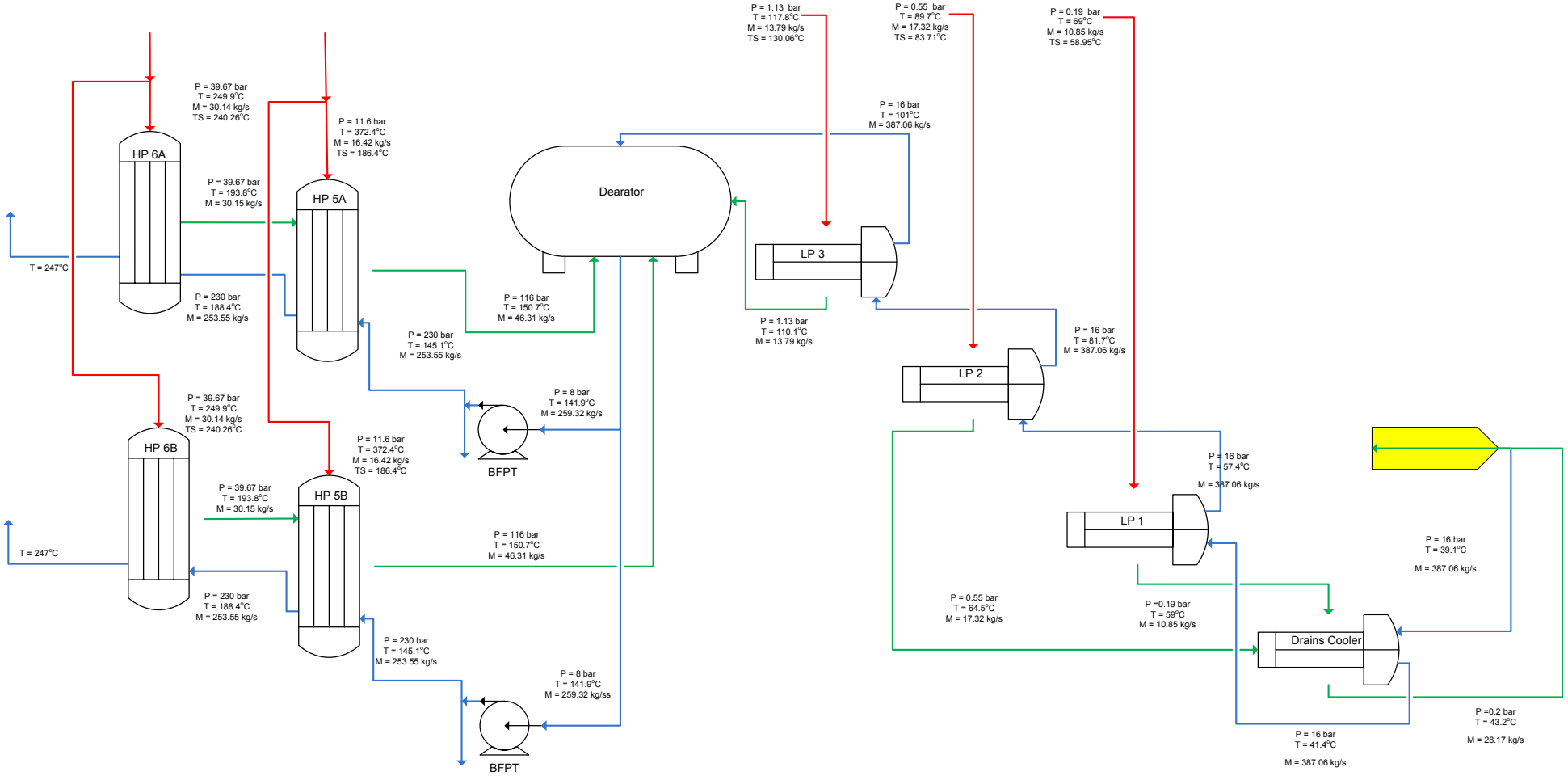
P = 1.13 bar
T = 117.8°C
M = 13.79 kg/s
TS = 130.06°C
P = 0.55 bar
T = 89.7°C
M = 17.32 kg/s
TS = 83.71°C
P = 0.19 bar
T = 69°C
M = 10.85 kg/s
TS = 58.95°C
P = 39.67 bar
T = 249.9°C
M = 30.14 kg/s
TS = 240.26°C
P = 11.6 bar
T = 372.4°C
M = 16.42 kg/s
TS = 186.4°C
P = 16 bar
T = 101°C
M = 387.06 kg/s
HP 6A
HP 5A
Dearator
LP 3
P = 39.67 bar
T = 193.8°C
M = 30.15 kg/s
T = 247°C
P = 230 bar
T = 188.4°C
M = 253.55 kg/s
P = 116 bar
T = 150.7°C
M = 46.31 kg/s
P = 230 bar
T = 145.1°C
M = 253.55 kg/s
P = 1.13 bar
T = 110.1°C
M = 13.79 kg/s
P = 16 bar
T = 81.7°C
M = 387.06 kg/s
LP 2
P = 39.67 bar
T = 249.9°C
M = 30.14 kg/s
TS = 240.26°C
P = 8 bar
T = 141.9°C
M = 259.32 kg/s
HP 6B
P = 11.6 bar
T = 372.4°C
M = 16.42 kg/s
TS = 186.4°C
BFPT
P = 16 bar
T = 57.4°C
M = 387.06 kg/s
HP 5B
P = 39.67 bar
T = 193.8°C
M = 30.15 kg/s
LP 1
T = 247°C
P = 116 bar
T = 150.7°C
M = 46.31 kg/s
P = 16 bar
T = 39.1°C
M = 387.06 kg/s
P = 0.55 bar
T = 64.5°C
M = 17.32 kg/s
P =0.19 bar
T = 59°C
M = 10.85 kg/s
P = 230 bar
T = 188.4°C
M = 253.55 kg/s
Drains Cooler
P = 230 bar
T = 145.1°C
M = 253.55 kg/s
P = 8 bar
T = 141.9°C
M = 259.32 kg/ss
BFPT
P =0.2 bar
T = 43.2°C
M = 28.17 kg/s
P = 16 bar
T = 41.4°C
M = 387.06 kg/s

PS16

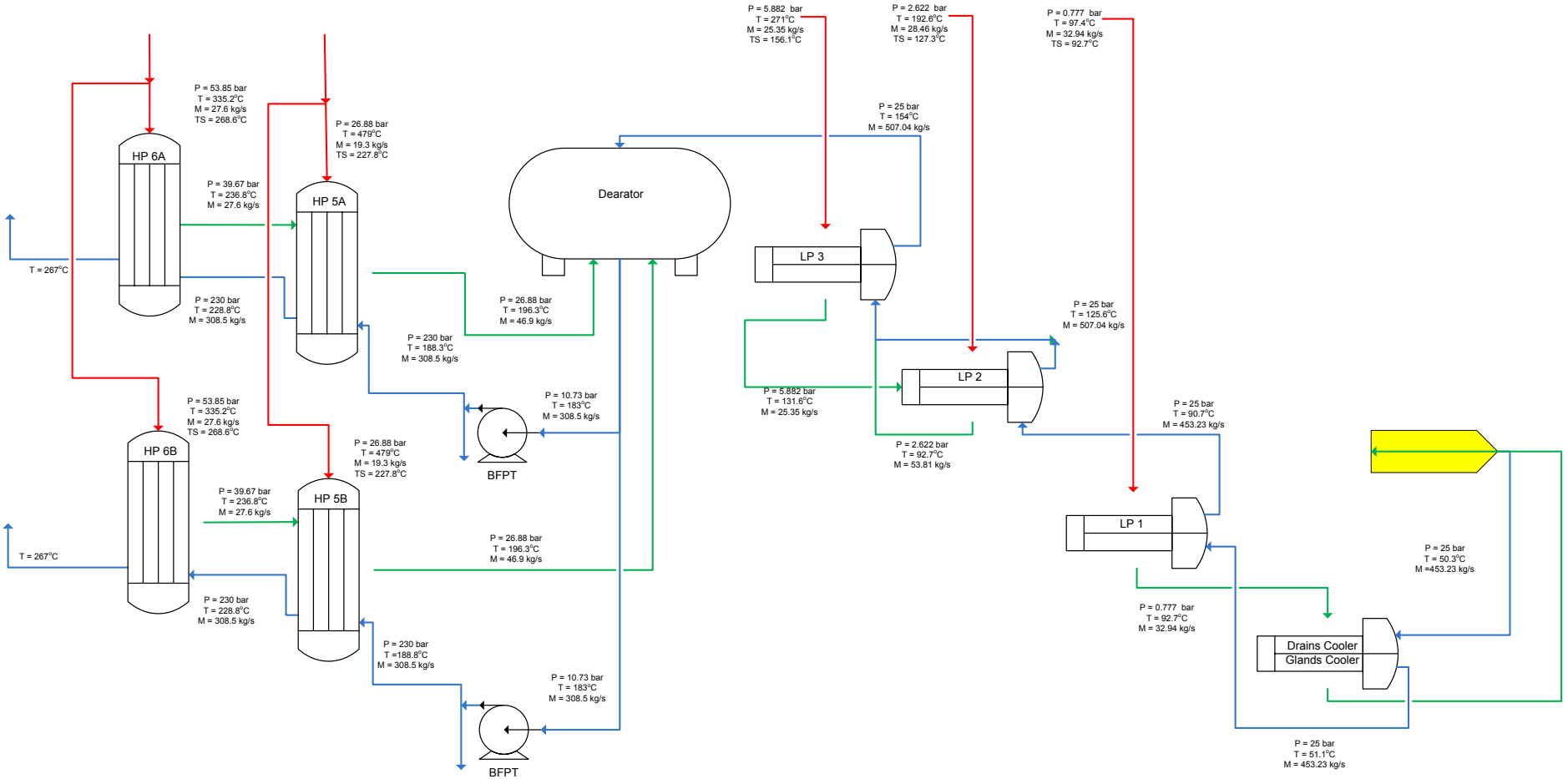
P = 5.882 bar
T = 271°C
M = 25.35 kg/s
TS = 156.1°C
P = 2.622 bar
T = 192.6°C
M = 28.46 kg/s
TS = 127.3°C
P = 0.777 bar
T = 97.4°C
M = 32.94 kg/s
TS = 92.7°C
P = 53.85 bar
T = 335.2°C
M = 27.6 kg/s
TS = 268.6°C
HP 6A
P = 26.88 bar
T = 479°C
M = 19.3 kg/s
TS = 227.8°C
HP 5A
P = 39.67 bar
T = 236.8°C
M = 27.6 kg/s
T = 267°C
P = 230 bar
T = 228.8°C
M = 308.5 kg/s
Dearator
P = 25 bar
T = 154°C
M = 507.04 kg/s
LP 3
P = 26.88 bar
T = 196.3°C
M = 46.9 kg/s
P = 230 bar
T = 188.3°C
M = 308.5 kg/s
P = 25 bar
T = 125.6°C
M = 507.04 kg/s
P = 5.882 bar
T = 131.6°C
M = 25.35 kg/s
LP 2
P = 10.73 bar
T = 183°C
M = 308.5 kg/s
BFPT
P = 2.622 bar
T = 92.7°C
M = 53.81 kg/s
P = 25 bar
T = 90.7°C
M = 453.23 kg/s
P = 53.85 bar
T = 335.2°C
M = 27.6 kg/s
TS = 268.6°C
HP 6B
P = 26.88 bar
T = 479°C
M = 19.3 kg/s
TS = 227.8°C
HP 5B
P = 39.67 bar
T = 236.8°C
M = 27.6 kg/s
T = 267°C
LP 1
P = 25 bar
T = 50.3°C
M =453.23 kg/s
P = 26.88 bar
T = 196.3°C
M = 46.9 kg/s
P = 0.777 bar
T = 92.7°C
M = 32.94 kg/s
P = 230 bar
T = 228.8°C
M = 308.5 kg/s
Drains Cooler
Glands Cooler
P = 230 bar
T =188.8°C
M = 308.5 kg/s
P = 10.73 bar
T = 183°C
M = 308.5 kg/s
BFPT
P = 25 bar
T = 51.1°C
M = 453.23 kg/s

Appendix E. Individual heater results

E-1. Tabular and graphical representation of results for the PS05 HP3 FWH

PS05 HP3 FWH								
	Units	**Min**	**Mean**	**Max**	**Claim**[56]	Δ_1	Δ_2	**Range**
TTD	[°C]	4.3	7.2	10.5	**8**	-10%	13%	Yes
DCA	[°C]							
DWA	[°C]	-1.1	0.5	1.5	**1**	-50%	19%	Yes
$\dot{m}_{H0}$	[kg/s]	4.2	5.2	6.0	**4.35**	19%	44%	Yes
U_{DC}	[W/m^{2}K]							
U_{CONC1}	[W/m^{2}K]							
U_{CONR}	[W/m^{2}K]							
U_{DS}	[W/m^{2}K]							
Q_{TOTAL}	[MW]	12.9	15.2	17.1	**14.08**	8%	26%	Yes
A_{CONDS}	[]	132.9	165.5	167.5				

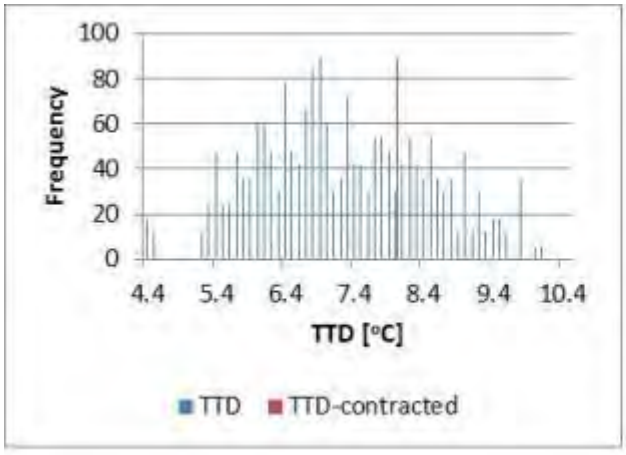

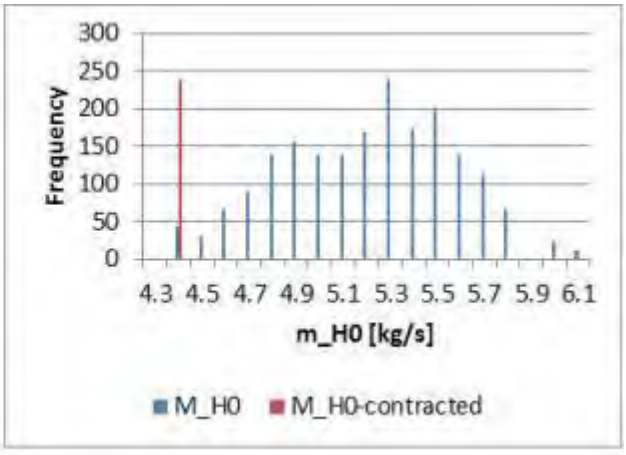

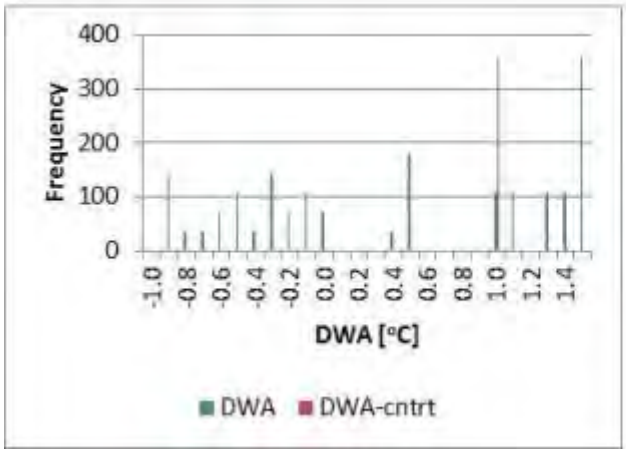

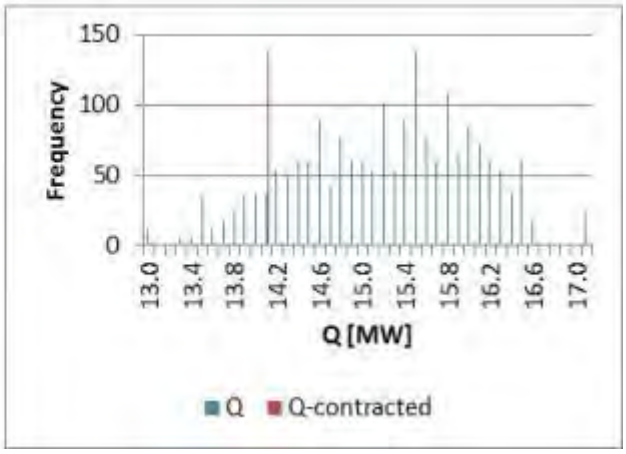

E-2. Tabular and graphical representation of results for the PS05 HP4 FWH

PS05 HP4 FWH								
	Units	**Min**	**Mean**	**Max**	**Claim**[56]	Δ_1	Δ_2	**Range**
TTD	[°C]	2.4	3.8	6.0	**5**	-1.2	34%	Yes
DCA	[°C]							
DWA	[°C]	-3.7	-1.5	-0.3	**1**	-2.5	75%	No
$\dot{m}_{H0}$	[kg/s]	6.9	7.7	8.1	**7.3**	5%	32%	Yes
U_{DC}	[W/m^{2}K]							
U_{CONC1}	[W/m^{2}K]							
U_{CONR}	[W/m^{2}K]							
U_{DS}	[W/m^{2}K]							
Q_{TOTAL}	[MW]	18.3	19.8	20.7	**19.3**	3%	21%	Yes
A_{CONDS}	[]	33.3	51.4	84.9				

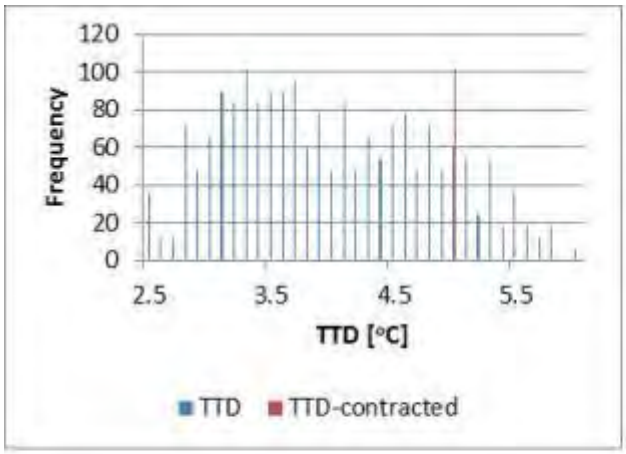

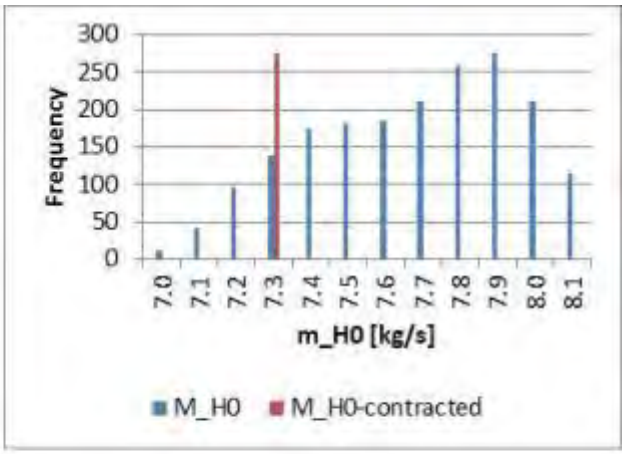

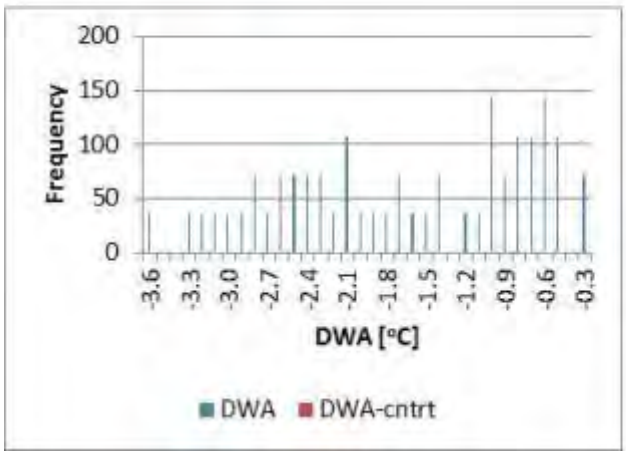

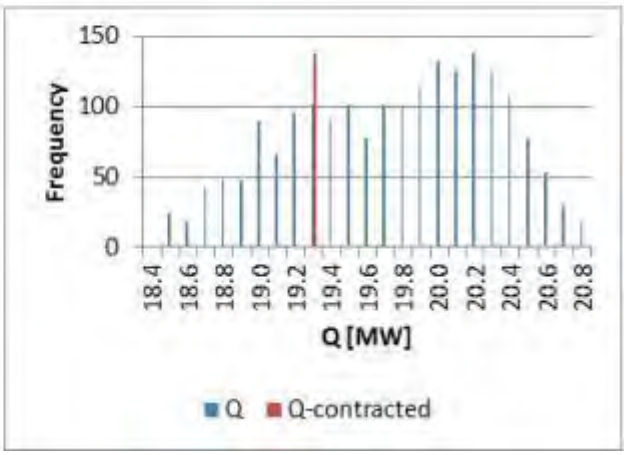

E-3. Tabular and graphical representation of results for the PS05 HP5 FWH

Heater: HP5 (original design segmented baffle design)

PS05 HP5 FWH								
	Units	**Min**	**Mean**	**Max**	**Claim**[56]	Δ_1	Δ_2	**Range**
TTD	[°C]	-4.6	-0.2	4.8	**-1**	-81%	9%	Yes
DCA	[°C]							
DWA	[°C]	-3.0	-0.2	1.7	**1**	-119%	25%	Yes
$\dot{m}_{H0}$	[kg/s]	10.4	11.9	13.3	**11.75**	2%	7%	Yes
U_{DC}	[W/m^{2}K]							
U_{CONC1}	[W/m^{2}K]							
U_{CONR}	[W/m^{2}K]							
U_{DS}	[W/m^{2}K]							
Q_{TOTAL}	[MW]	27.1	30.6	33.7	**30.6**	0%	0%	Yes
A_{CONDS}	[]	84.6	166.5	169.5				

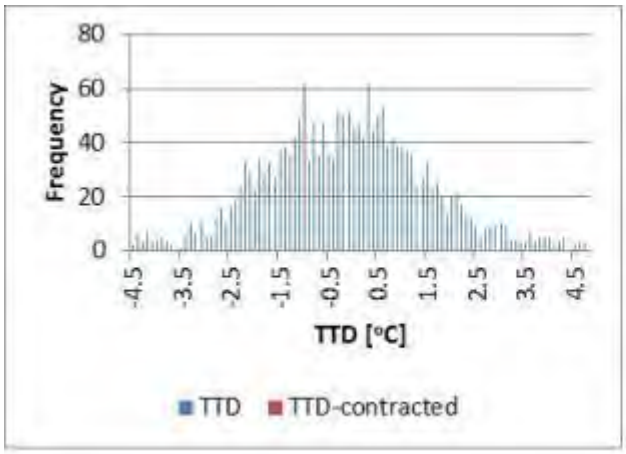

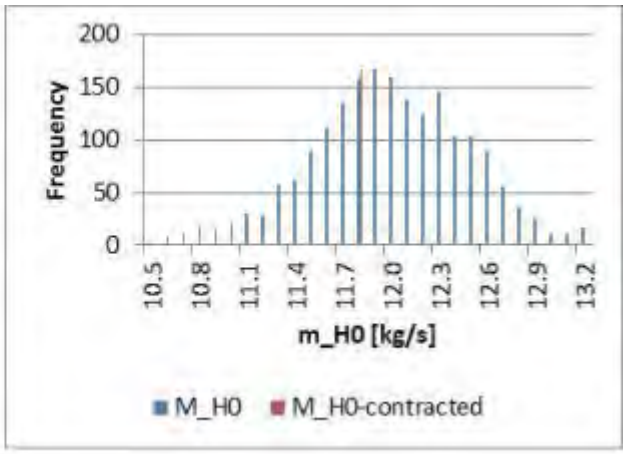

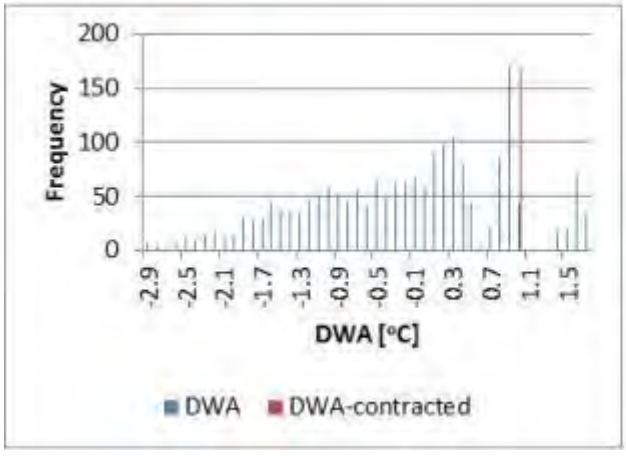

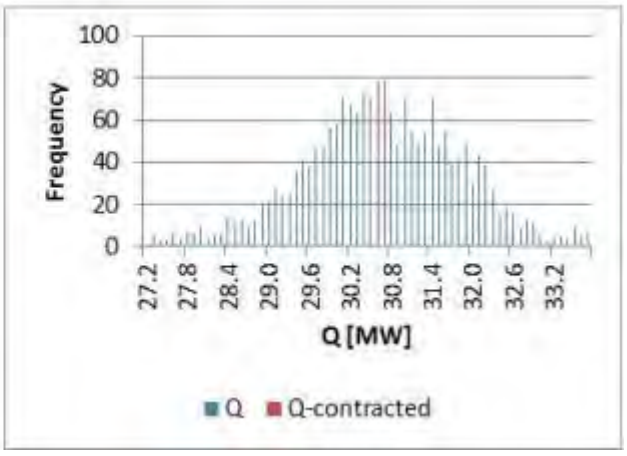

E-4. Tabular and graphical representation of results for the new PS05 HP5 FWH

Heater: HP5 (new design with grid baffle design)

PS05 HP5 FWH (new)								
	Units	**Min**	**Mean**	**Max**	**Claim**[57]	Δ_1	Δ_2	**Range**
TTD	[°C]	-4.8	1.2	10.1	**3**	-61%	12%	Yes
DCA	[°C]							
DWA	[°C]	-4.7	1.0	5.0	**1**	1%	0%	Yes
$\dot{m}_{H0}$	[kg/s]	9.2	12.1	14.1	**11.6**	5%	11%	Yes
U_{DC}	[W/m^{2}K]							
U_{CONC1}	[W/m^{2}K]	2117.8	3330.9	4782.8				
U_{CONR}	[W/m^{2}K]	3171.9	3997.4	4920.0				
U_{DS}	[W/m^{2}K]	119.4	274.2	503.5				
Q_{TOTAL}	[MW]	24.4	31.5	36.2	**30.3**	4%	10%	Yes
A_{HCONDS}	[m^2]	75.0	158.2	248.6				

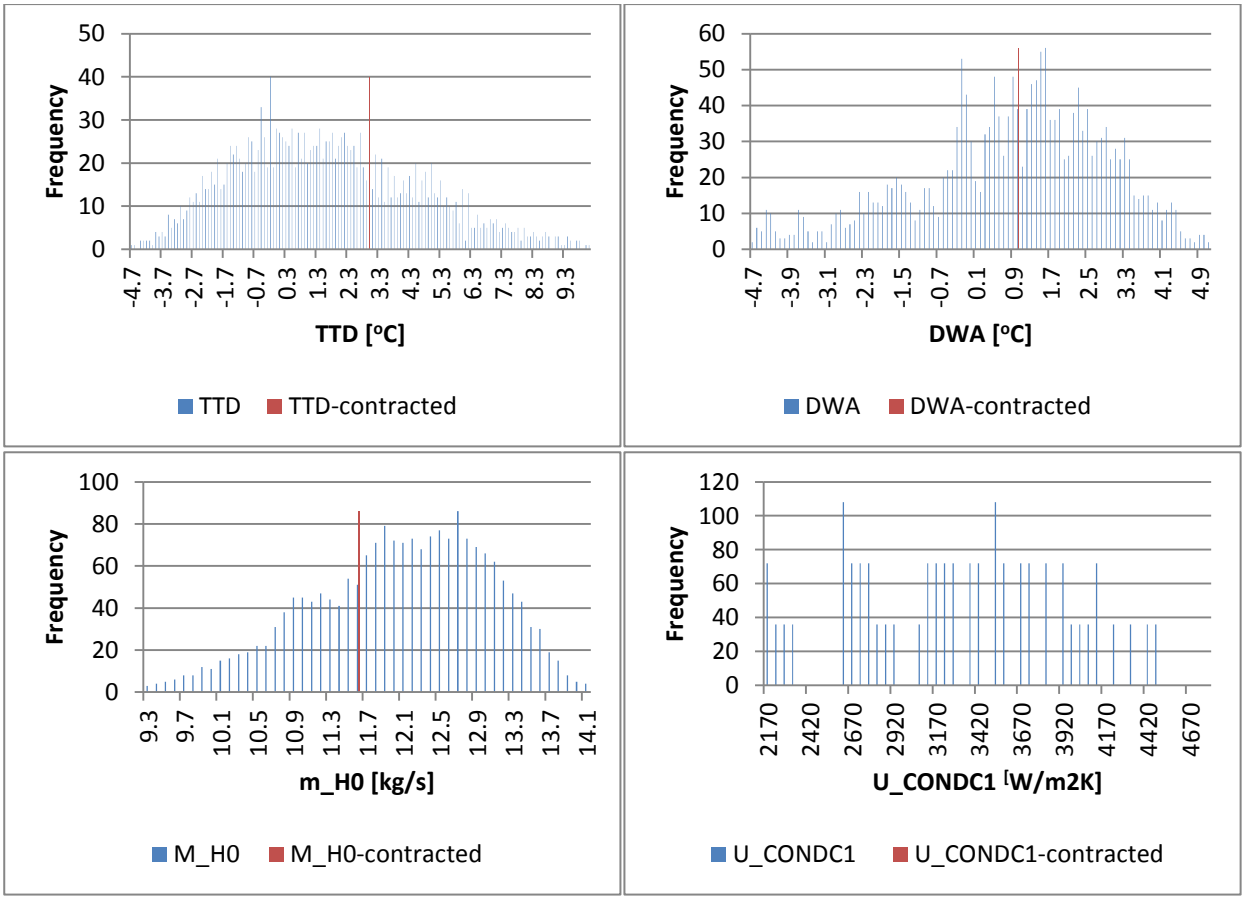

E-5. Tabular and graphical representation of results for the PS05 HP6 FWH

PS05 HP6 FWH								
	Units	**Min**	**Mean**	**Max**	**Claim**[56]	Δ_1	Δ_2	**Range**
TTD	[°C]	-0.1	3.9	8.9	**4**	-0.1	1%	Yes
DCA	[°C]							
DWA	[°C]	-5.0	-2.0	-0.1	**1**	-3.0	61%	No
$\dot{m}_{H0}$	[kg/s]	11.0	13.0	14.5	**13.8**	-6%	24%	Yes
U_{DC}	[W/m^{2}K]							
U_{CONC1}	[W/m^{2}K]							
U_{CONR}	[W/m^{2}K]							
U_{DS}	[W/m^{2}K]							
Q_{TOTAL}	[MW]	21.2	24.9	27.9	**26.1**	-4%	17%	Yes
A_{CONDS}	[]	30.3	107.8	137.0				

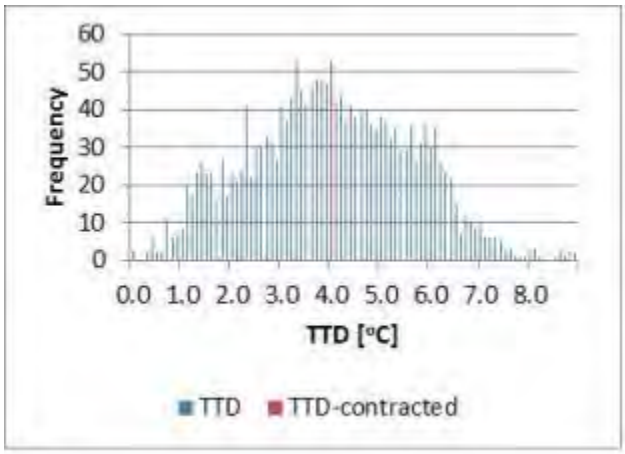

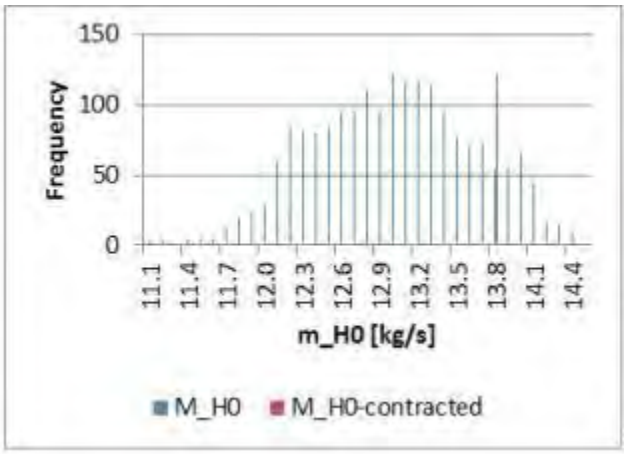

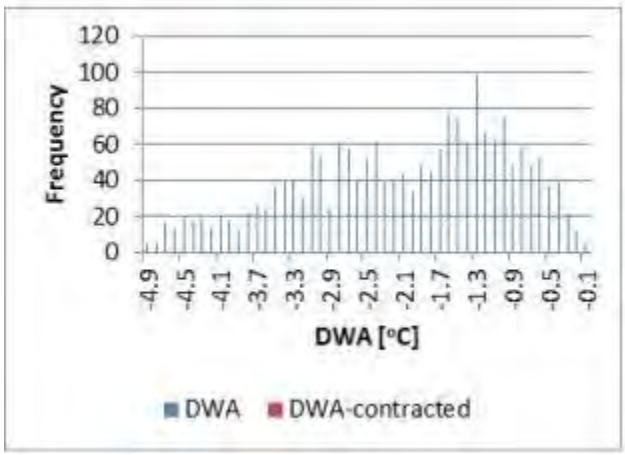

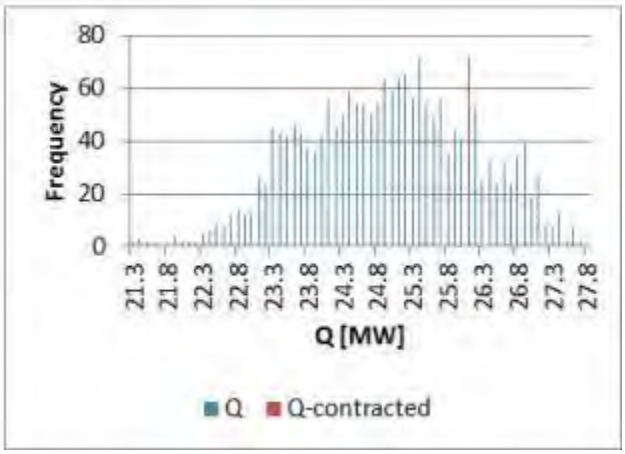

E-6. Tabular and graphical representation of results for the PS06 LP1 FWH

PS06 LP1 FWH								
	Units	**Min**	**Mean**	**Max**	**Claim**[56]	Δ_1	Δ_2	**Range**
TTD	[°C]	0.5	1.1	2.8	**1.9**	-0.8	33%	Yes
DCA	[°C]							
DWA	[°C]	-2.6	-1.1	-0.4	**1**	-2.1	94%	No
$\dot{m}_{H0}$	[kg/s]	13.8	14.8	15.1	**15**	-2%	19%	Yes
U_{DC}	[W/m^{2}K]							
U_{CONC1}	[W/m^{2}K]							
U_{CONR}	[W/m^{2}K]							
U_{DS}	[W/m^{2}K]							
Q_{TOTAL}	[MW]	32.2	34.5	35.4	**33.5**	3%	31%	Yes
A_{CONDS}	[]	1.1	2.1	3.8				

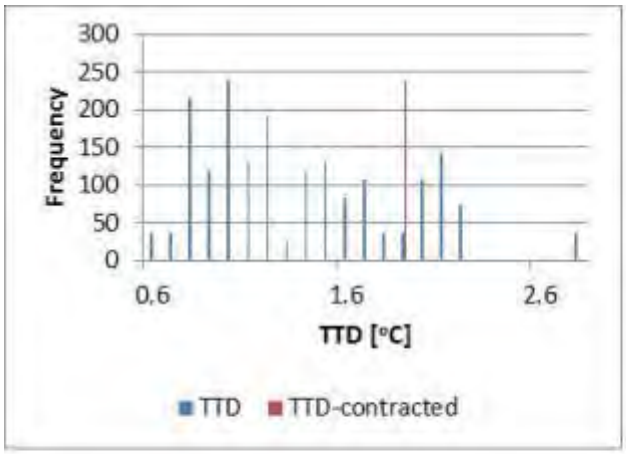

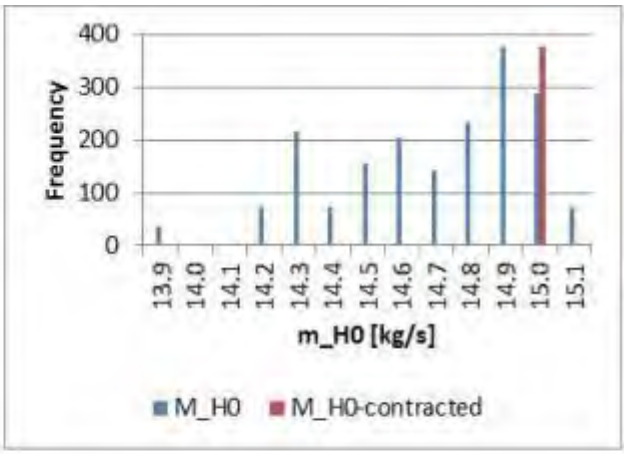

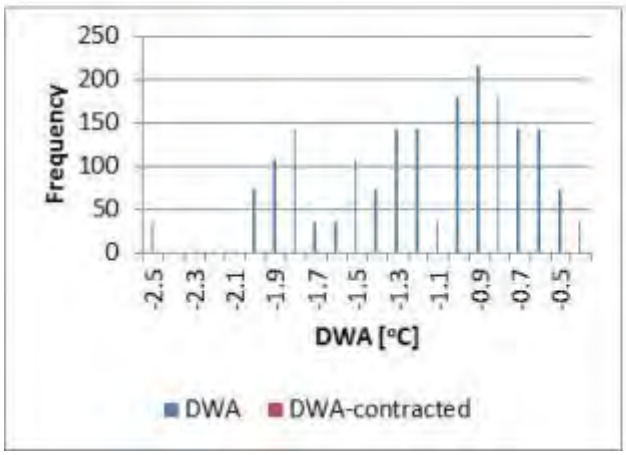

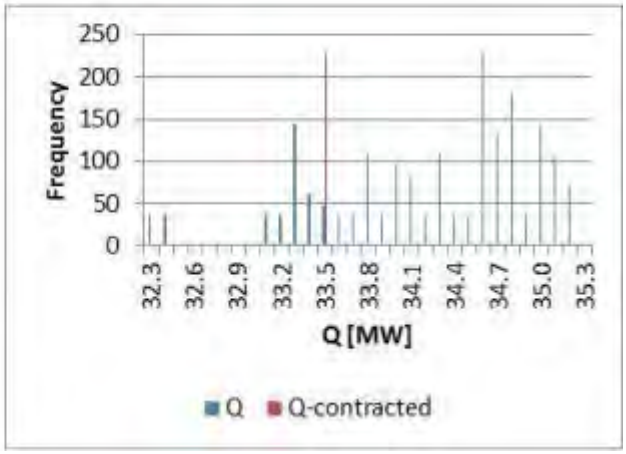

E-7. Tabular and graphical representation of results for the PS06 LP2 FWH

PS06 LP2 FWH								
	Units	**Min**	**Mean**	**Max**	**Claim**[57]	Δ_1	Δ_2	**Range**
TTD	[°C]	1.0	1.8	3.6	**2.3**	-0.5	18%	Yes
DCA	[°C]							
DWA	[°C]	-3.3	-1.7	-0.9	**1**	-2.7	109%	No
$\dot{m}_{H0}$	[kg/s]	8.7	9.8	10.3	**9.535**	2%	14%	Yes
U_{DC}	[W/m^{2}K]							
U_{CONC1}	[W/m^{2}K]	3201.7	4394.0	5613.7				
U_{CONR}	[W/m^{2}K]							
U_{DS}	[W/m^{2}K]							
Q_{TOTAL}	[MW]	21.8	24.2	25.4	**23.7**	2%	14%	Yes
A_{HCONDS}	[m^2]	7.4	7.4	7.4				

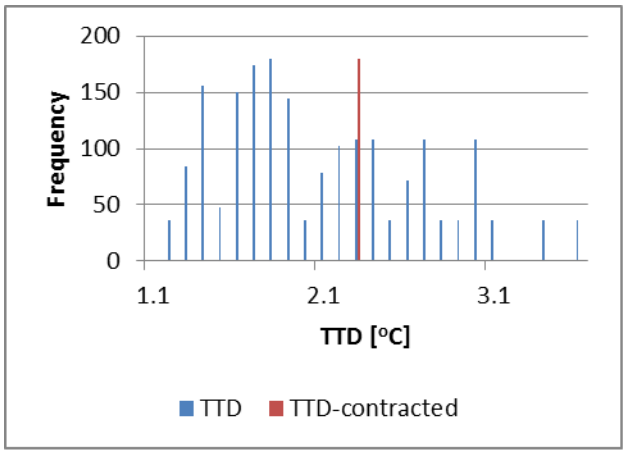

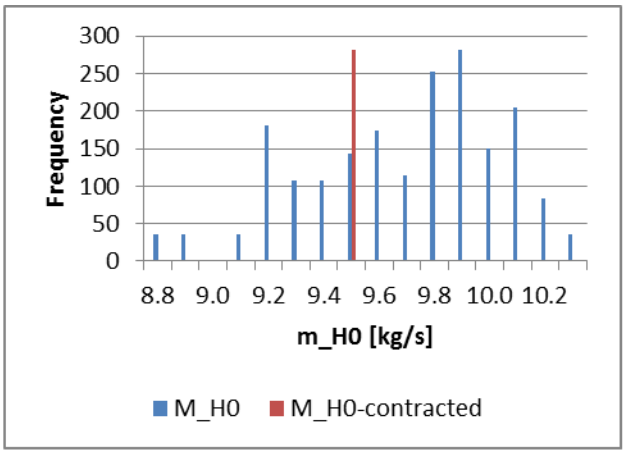

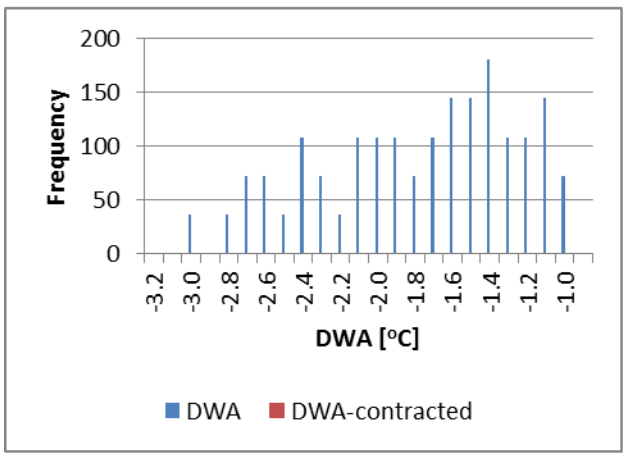

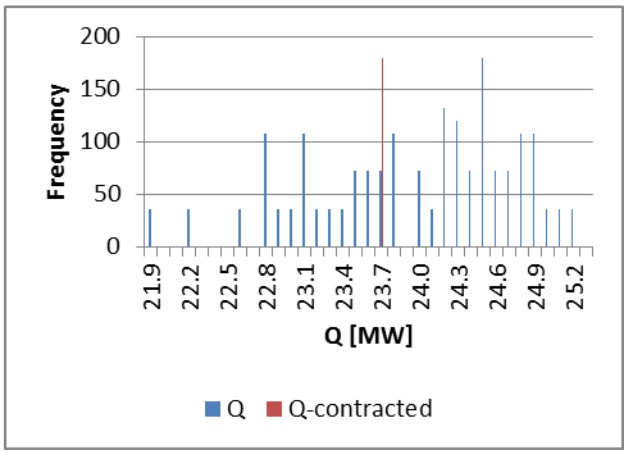

E-8. Tabular and graphical representation of results for the PS06 LP3 FWH

PS06 LP3 FWH								
	Units	**Min**	**Mean**	**Max**	**Claim**[57]	Δ_1	Δ_2	**Range**
TTD	[°C]	1.0	3.0	6.4	**2.4**	0.6	11%	Yes
DCA	[°C]							
DWA	[°C]	-4.6	-1.7	-0.4	**1**	-2.7	65%	No
$\dot{m}_{H0}$	[kg/s]	16.1	18.3	19.5	**18.244**	0%	0%	Yes
U_{DC}	[W/m^{2}K]							
U_{CONC1}	[W/m^{2}K]							
U_{CONR}	[W/m^{2}K]							
U_{DS}	[W/m^{2}K]							
Q_{TOTAL}	[MW]	36.9	41.9	44.8	**41.9**	0%	1%	Yes
A_{HCONDS}	[m^2]	22.0	137.5	316.4				

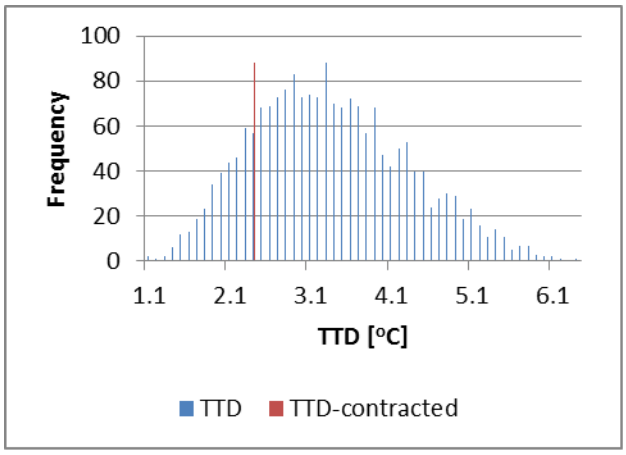

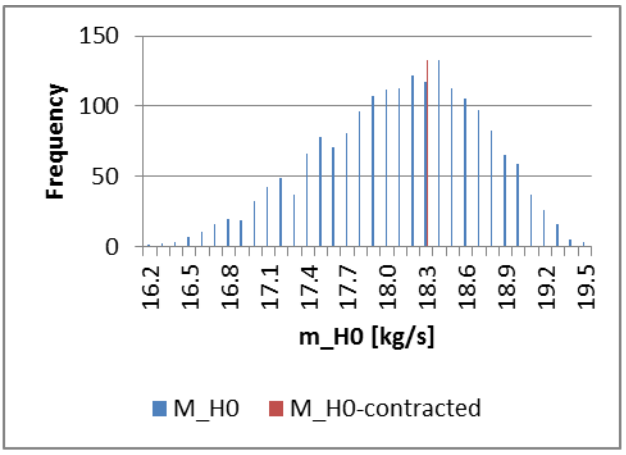

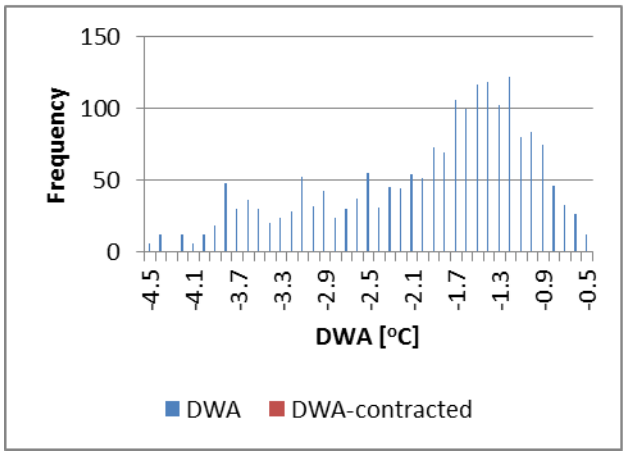

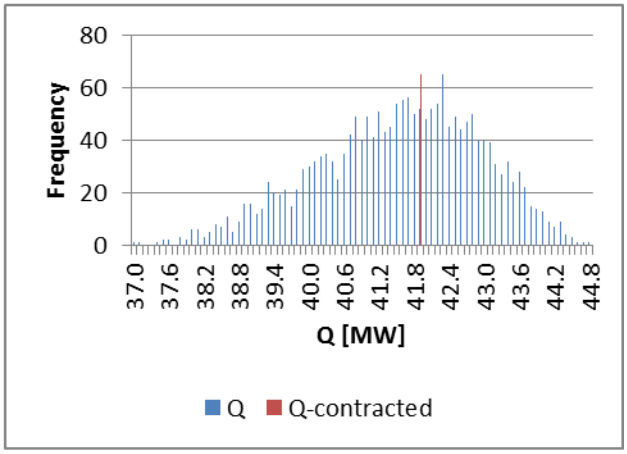

E-9. Tabular and graphical representation of results for the PS06 LP4 FWH

PS06 LP4 FWH								
	Units	**Min**	**Mean**	**Max**	**Claim**[57]	Δ_1	Δ_2	**Range**
TTD	[°C]	1.3	4.5	9.3	**4.2**	0.3	4%	Yes
DCA	[°C]							
DWA	[°C]	-7.2	-3.1	-1.0	**1**	-4.1	66%	No
$\dot{m}_{H0}$	[kg/s]	14.7	17.7	19.7	**17.8**	-1%	2%	Yes
U_{DC}	[W/m^{2}K]							
U_{CONC1}	[W/m^{2}K]							
U_{CONR}	[W/m^{2}K]							
U_{DS}	[W/m^{2}K]							
Q_{TOTAL}	[MW]	34.3	41.4	46.2	**41.6**	0%	1%	Yes
A_{HCONDS}	[m^2]	28.6	147.4	274.0				

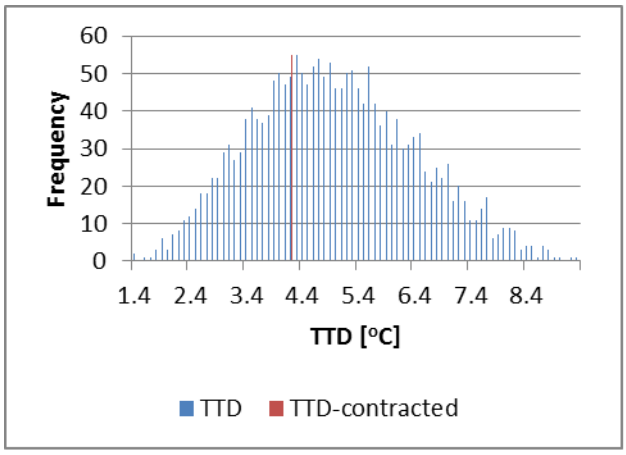

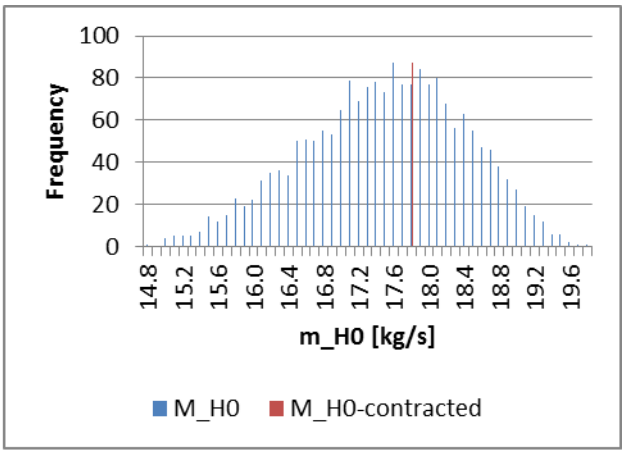

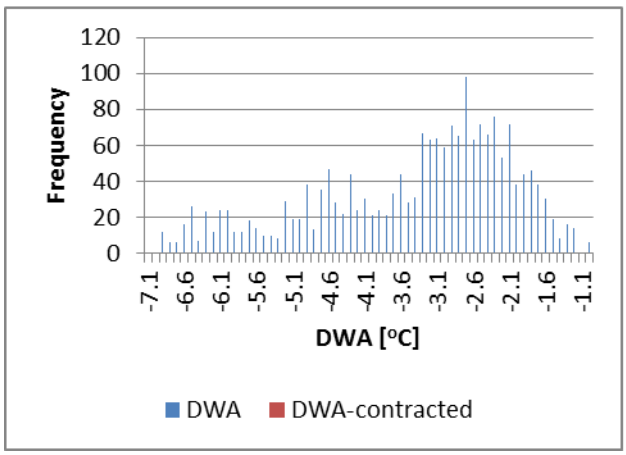

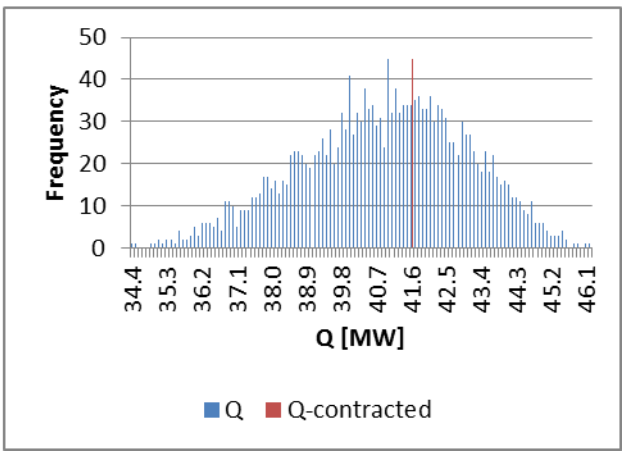

E-10. Tabular and graphical representation of results for the PS06 HP6 FWH (assuming segmented baffles)

PS06 HP6 FWH								
	Units	**Min**	**Mean**	**Max**	**Claim**[57]	Δ_1	Δ_2	**Range**
TTD	[°C]	-4.5	-2.9	-0.7	**-1.6**	-1.3	35%	Yes
DCA	[°C]	3.9	5.9	8.4	**6.9**	-1.0	22%	Yes
DWA	[°C]	-2.6	-0.9	0.3	**1**	-1.9	64%	No
$\dot{m}_{H0}$	[kg/s]	9.0	9.8	10.4	**9.3**	6%	38%	Yes
U_{DC}	[W/m^{2}K]	2233.6	2933.2	3715.4	**2560**	15%	25%	Yes
U_{CONC1}	[W/m^{2}K]	3663.4	4799.7	6277.7	**3965**	21%	32%	Yes
U_{CONR}	[W/m^{2}K]	4329.7	5556.4	7316.2	**3965**	40%	53%	No
U_{DS}	[W/m^{2}K]	440.2	626.7	832.2	**340**	84%	73%	No
Q_{TOTAL}	[MW]	26.7	28.8	30.2	**27**	7%	50%	Yes
A_{HCONDS}	[m^2]	50.7	60.0	60.1				

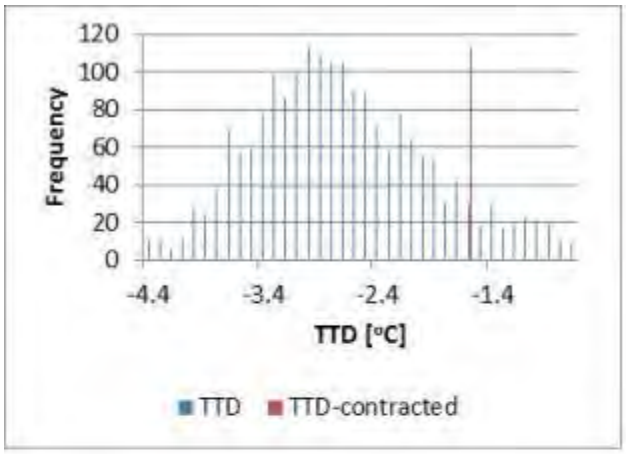

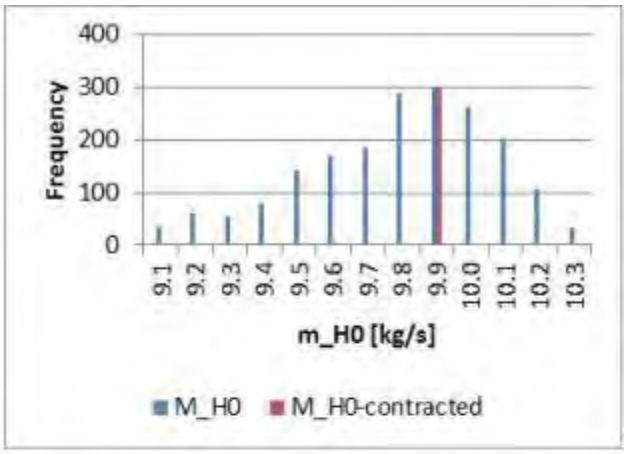

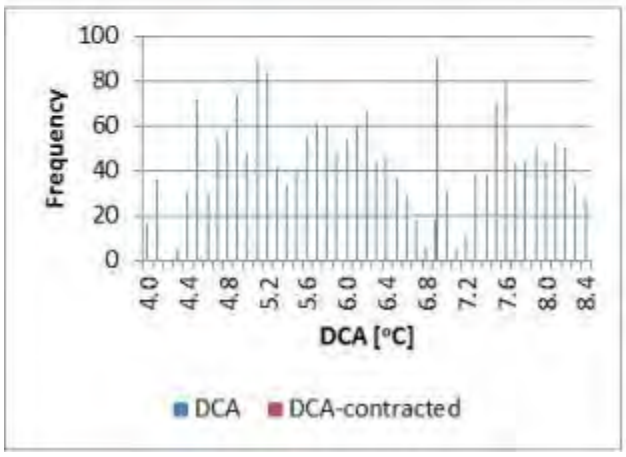

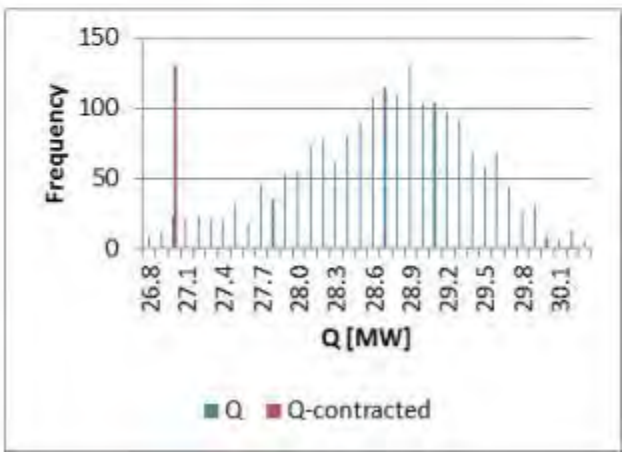

E-11. Tabular and graphical representation of results for the PS06 HP7 FWH (assuming grid baffles)

PS06 HP7 FWH								
	Units	**Min**	**Mean**	**Max**	**Claim**[57]	Δ_1	Δ_2	**Range**
TTD	[°C]	-1.1	0.3	2.1	**0.2**	0.1	3%	Yes
DCA	[°C]	8.3	8.9	9.4	**6.2**	2.7	230%	No
DWA	[°C]	-2.0	-0.8	-0.1	**1**	-1.8	93%	No
$\dot{m}_{H0}$	[kg/s]	14.5	15.4	16.0	**15.02**	2%	23%	Yes
U_{DC}	[W/m^{2}K]	1919.8	2035.4	2166.2	**2560**	-20%	213%	No
U_{CONC1}	[W/m^{2}K]	3569.8	4611.4	6199.8	**4235**	9%	14%	Yes
U_{CONR}	[W/m^{2}K]	4358.5	5548.8	7216.5	**4235**	31%	46%	No
U_{DS}	[W/m^{2}K]	590.0	614.3	636.2	**555**	11%	128%	No
Q_{TOTAL}	[MW]	29.6	31.4	32.7	**30.8**	2%	19%	Yes
A_{HCONDS}	[m^2]	114.5	114.5	114.5				

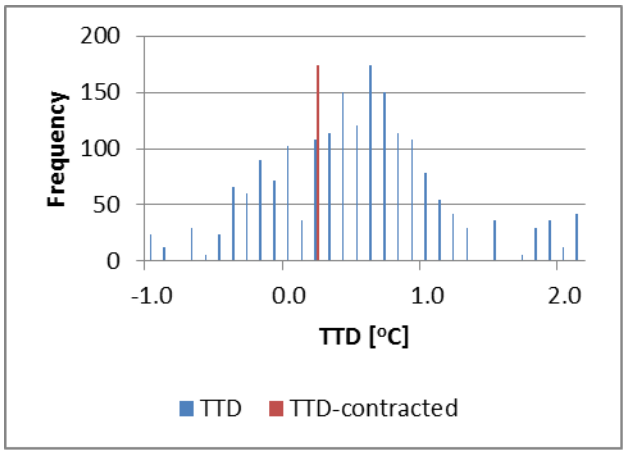

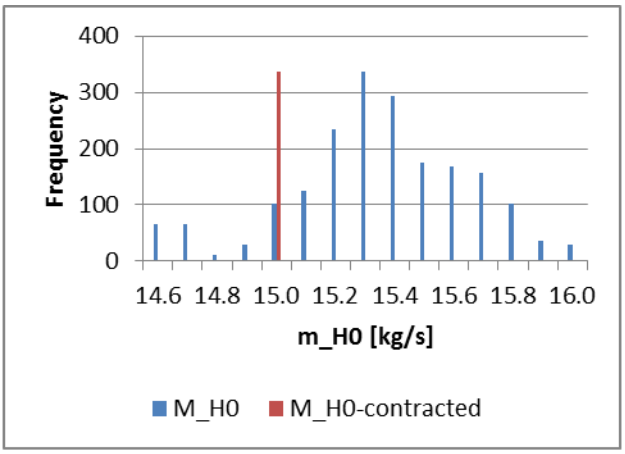

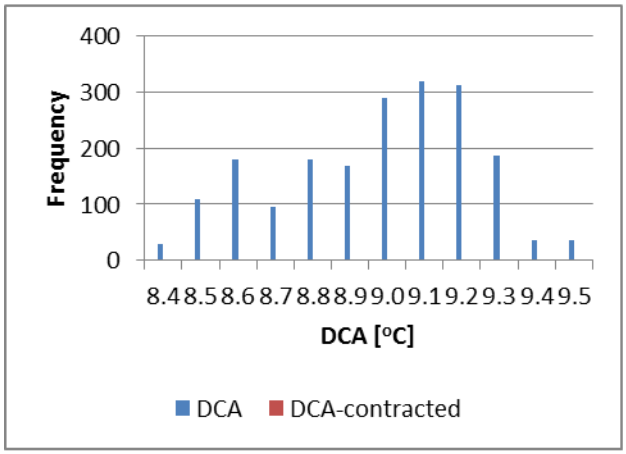

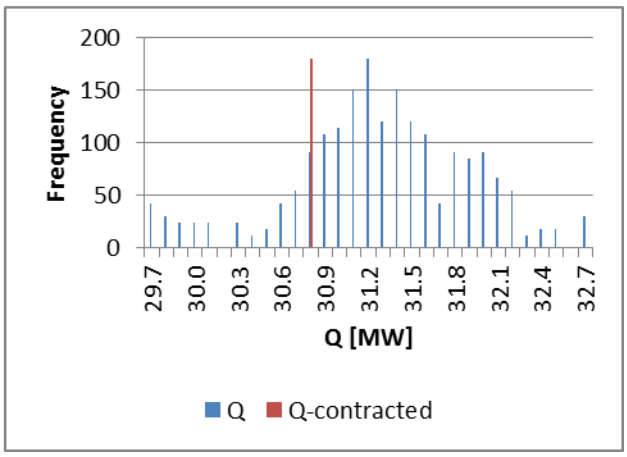

E-12. Tabular and graphical representation of results for the PS12 LP1 FWH

PS12 LP1 FWH								
	Units	**Min**	**Mean**	**Max**	**Claim**[56]	Δ_1	Δ_2	**Range**
TTD	[°C]	1.6	2.7	4.9	**3**	-0.3	10%	Yes
DCA	[°C]							
DWA	[°C]	-2.8	-0.9	-0.2	**1**	-1.9	74%	No
$\dot{m}_{H0}$	[kg/s]	21.5	23.3	24.1	**23.1**	1%	6%	Yes
U_{DC}	[W/m^{2}K]							
U_{CONC1}	[W/m^{2}K]	3129.2	4344.2	5590.7				
U_{CONR}	[W/m^{2}K]							
U_{DS}	[W/m^{2}K]							
Q_{TOTAL}	[MW]	49.1	53.2	55.1	**52.7**	1%	8%	Yes
A_{CONDS}	[]	109.1	174.8	273.8				

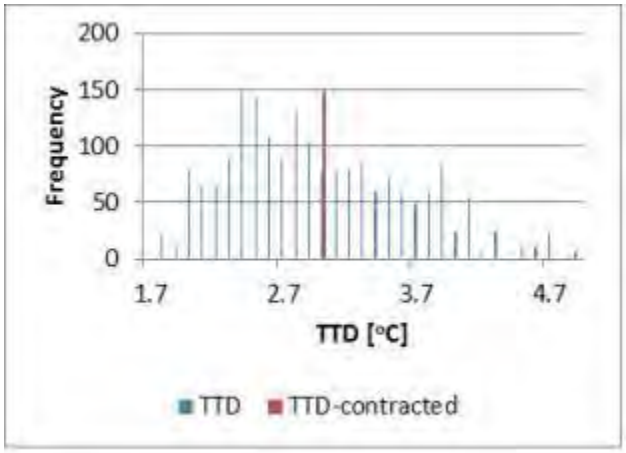

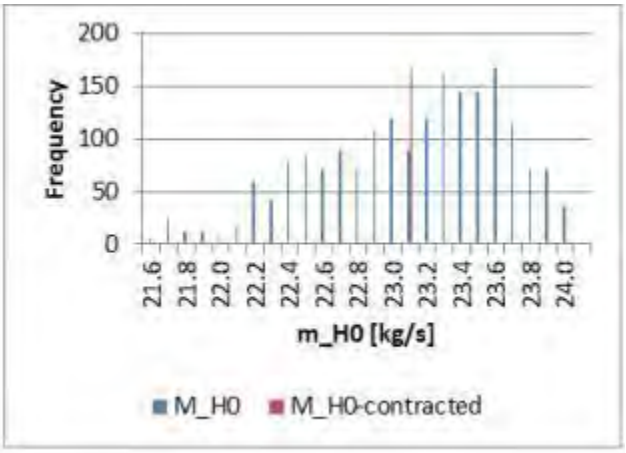

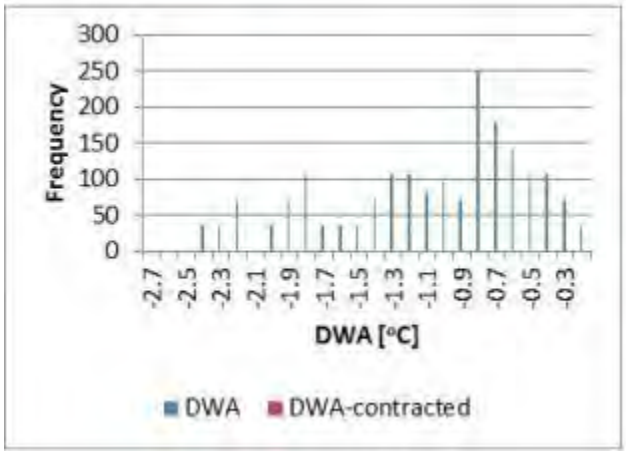

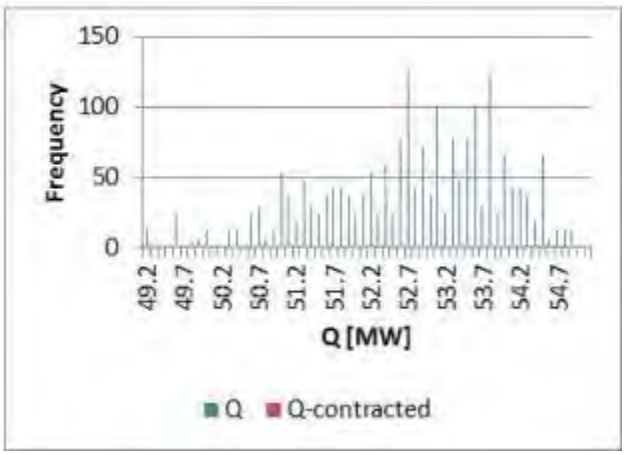

E-13. Tabular and graphical representation of results for the PS12 LP2 FWH

PS12 LP2 FWH								
	Units	**Min**	**Mean**	**Max**	**Claim**[56]	Δ_1	Δ_2	**Range**
TTD	[°C]	1.6	2.7	4.9	**3**	-0.3	10%	Yes
DCA	[°C]							
DWA	[°C]	-2.8	-0.9	-0.2	**1**	-1.9	74%	No
$\dot{m}_{H0}$	[kg/s]	21.5	23.3	24.1	**23.049**	1%	8%	Yes
U_{DC}	[W/m^{2}K]							
U_{CONC1}	[W/m^{2}K]	3129.2	4344.2	5590.7				
U_{CONR}	[W/m^{2}K]							
U_{DS}	[W/m^{2}K]							
Q_{TOTAL}	[MW]	49.1	53.2	55.1	**52.7**	1%	8%	Yes
A_{CONDS}	[]	109.1	174.8	273.8				

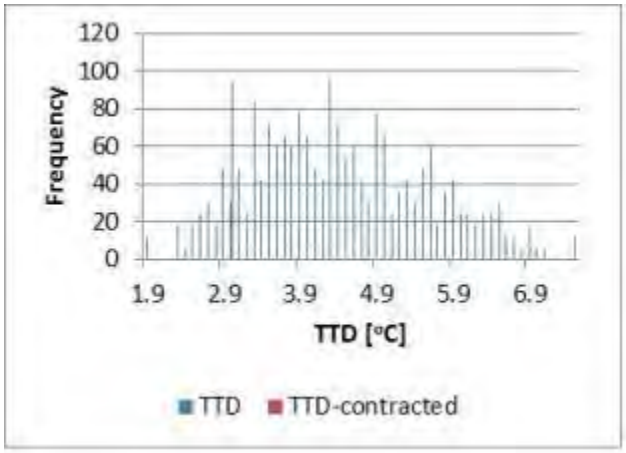

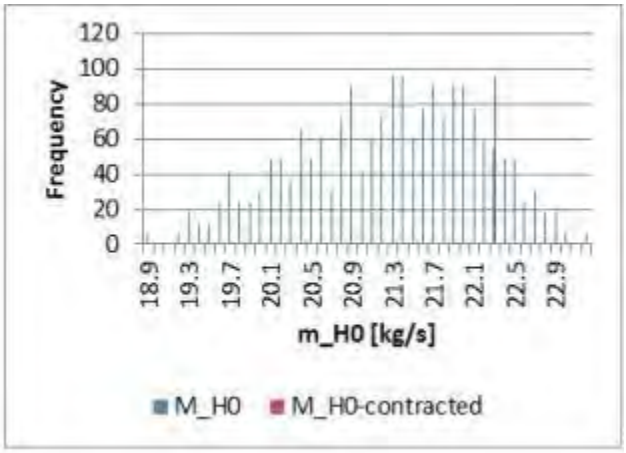

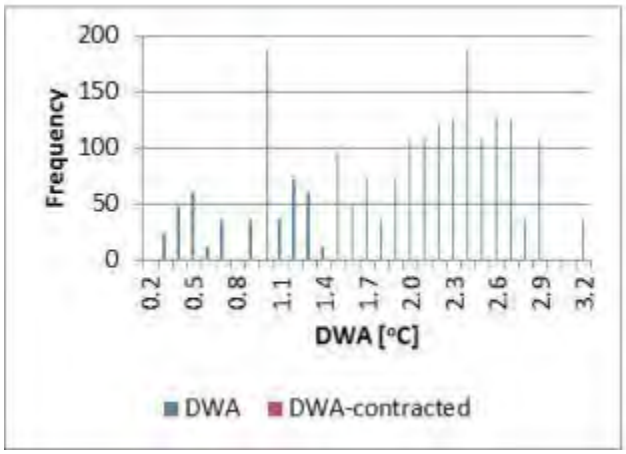

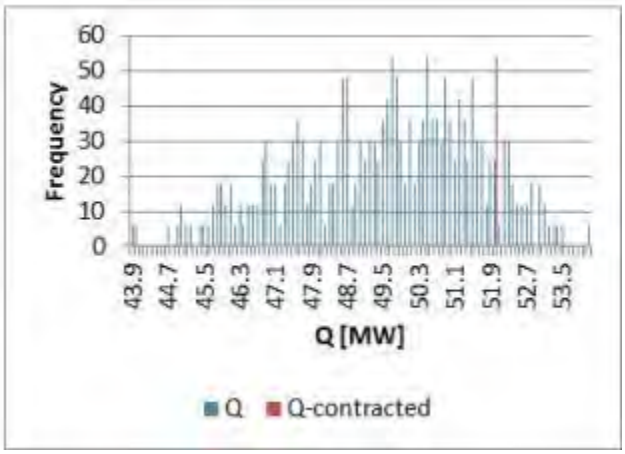

E-14. Tabular and graphical representation of results for the PS12 LP3 FWH (assuming grid baffles)

PS12 LP3 FWH								
	Units	**Min**	**Mean**	**Max**	**Claim**[56]	Δ_1	Δ_2	**Range**
TTD	[°C]	1.1	3.3	7.2	**3**	0.3	4%	Yes
DCA	[°C]	1.2	2.9	5.3	**5**	-0.4	51%	Yes
DWA	[°C]	2.0	4.9	6.5	**1**	3.9	87%	No
$\dot{m}_{H0}$	[kg/s]	16.9	20.1	22.0	**20.4**	-1%	6%	Yes
U_{DC}	[W/m^{2}K]							
U_{CONC1}	[W/m^{2}K]							
U_{CONR}	[W/m^{2}K]							
U_{DS}	[W/m^{2}K]							
Q_{TOTAL}	[MW]	41.6	49.5	53.9	**49.9**	-1%	4%	Yes
A_{CONDS}	[]	345.0	442.6	550.7				

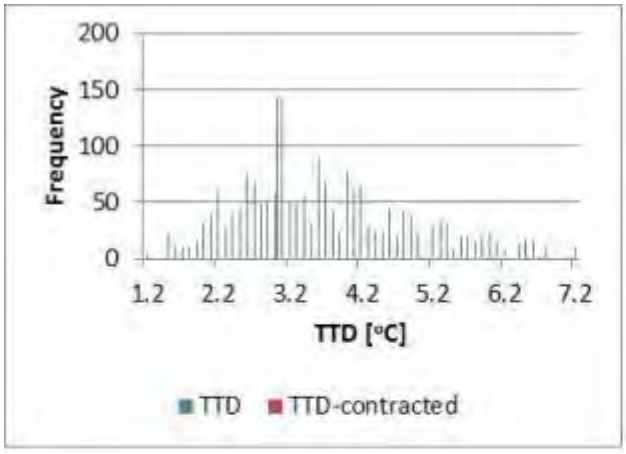

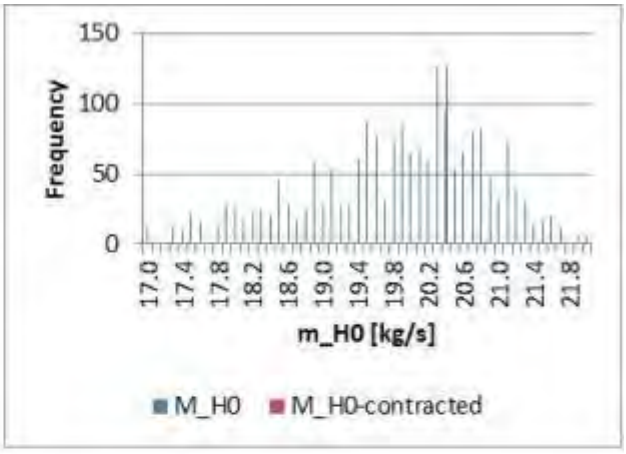

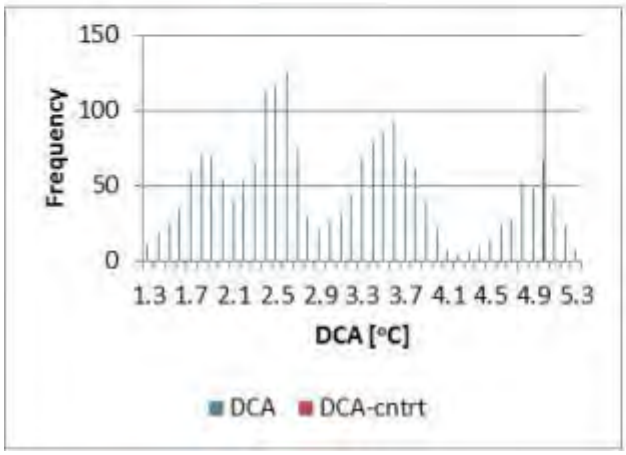

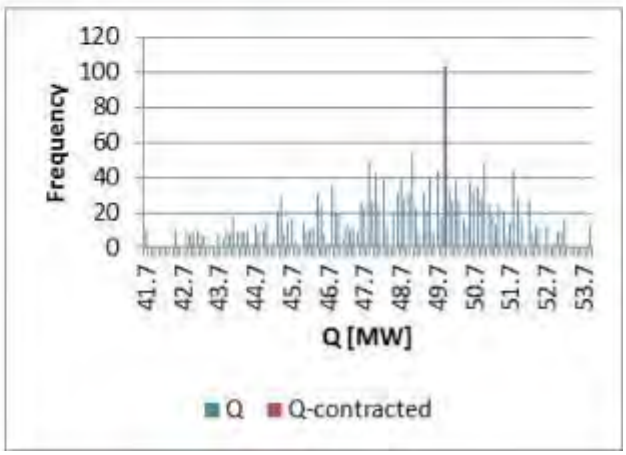

E-15. Tabular and graphical representation of results for the PS12 HP5 FWH (assuming grid baffles)

PS12 HP5 FWH								
	Units	**Min**	**Mean**	**Max**	**Claim**[56]	Δ_1	Δ_2	**Range**
TTD	[°C]	-3.7	-1.9	0.4	**-1**	-0.9	22%	Yes
DCA	[°C]	5.6	8.0	10.9	**7**	0.1	19%	Yes
DWA	[°C]	-1.6	0.1	1.8	**1**	-0.9	27%	Yes
$\dot{m}_{H0}$	[kg/s]	10.1	11.0	11.8	**10.1**	9%	53%	Yes
U_{DC}	[W/m^{2}K]	955.6	1385.1	1891.4				
U_{CONC1}	[W/m^{2}K]	3448.6	4753.3	6935.4				
U_{CONR}	[W/m^{2}K]	3826.0	4812.1	6267.8				
U_{DS}	[W/m^{2}K]	120.4	200.8	306.4				
Q_{TOTAL}	[MW]	27.4	30.2	32.4	**27.5**	10%	53%	Yes
A_{CONDS}	[]	70.0	70.0	70.0				

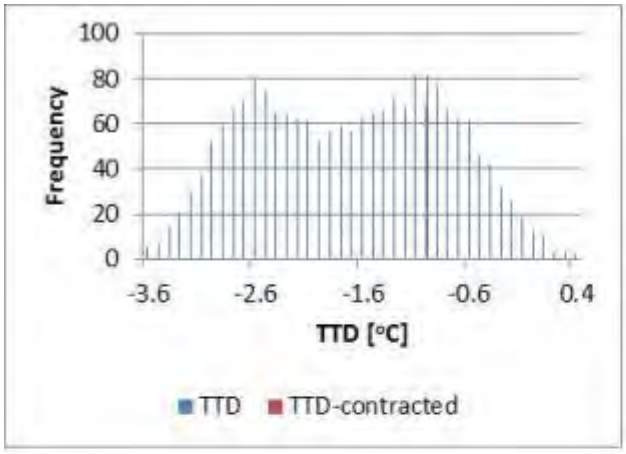

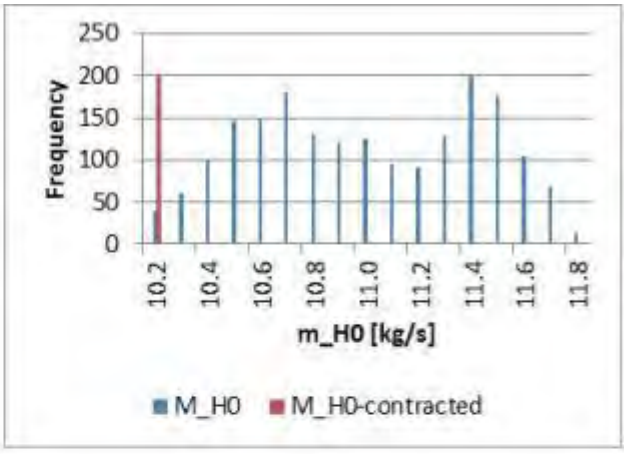

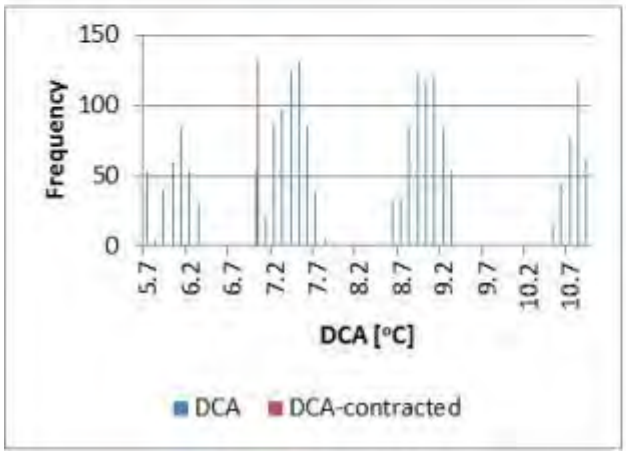

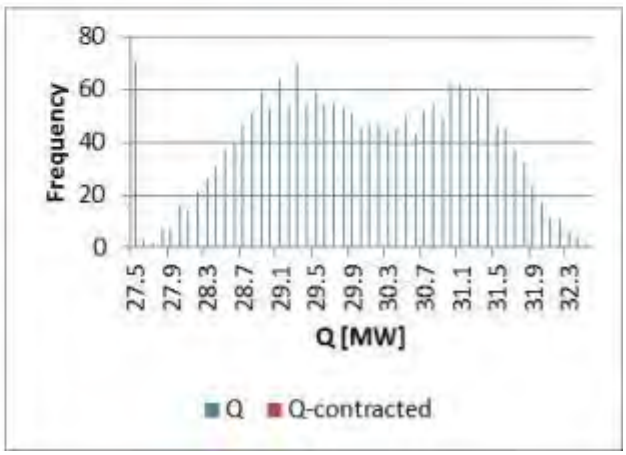

E-16. Tabular and graphical representation of results for the PS12 HP6 FWH (assuming grid baffles)

PS12 HP6 FWH								
	Units	**Min**	**Mean**	**Max**	**Claim**[56]	Δ_1	Δ_2	**Range**
TTD	[°C]	-2.5	0.7	4.5	**1.8**	-1.1	16%	Yes
DCA	[°C]	3.4	7.6	14.0	**7**	0.1	6%	Yes
DWA	[°C]	-4.3	-1.2	0.7	**1**	-2.2	44%	No
$\dot{m}_{H0}$	[kg/s]	26.8	28.8	30.5	**28**	3%	21%	Yes
U_{DC}	[W/m^{2}K]	846.4	1319.6	1916.7				
U_{CONC1}	[W/m^{2}K]	3052.9	3876.1	5131.3				
U_{CONR}	[W/m^{2}K]	3761.0	4698.1	6044.3				
U_{DS}	[W/m^{2}K]	237.4	487.5	840.5				
Q_{TOTAL}	[MW]	57.2	62.1	66.3	**60.8**	2%	14%	Yes
A_{CONDS}	[]	98.3	98.3	98.3				

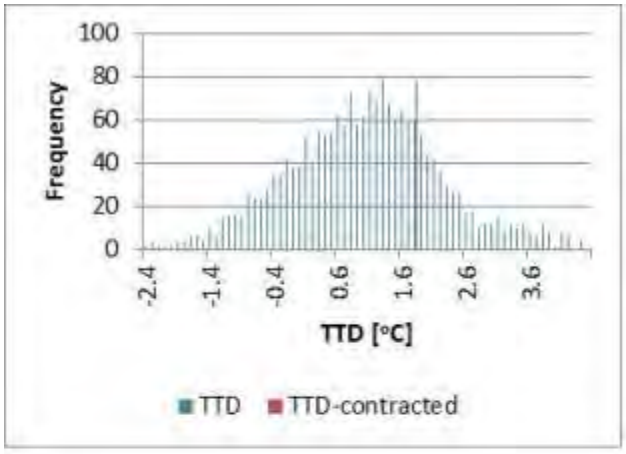

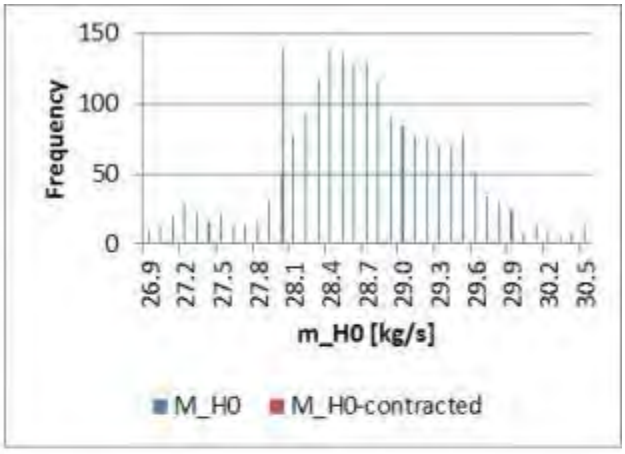

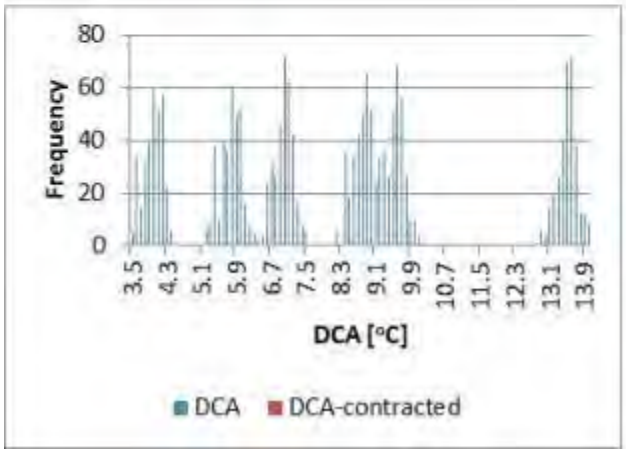

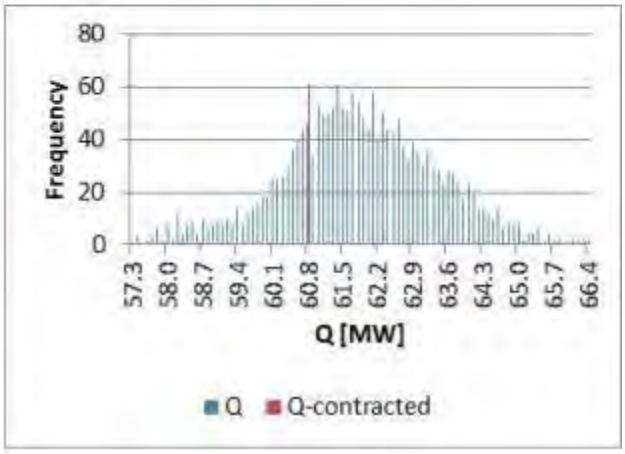

E-17. Tabular and graphical representation of results for the PS00 LP2 FWH

PS00 LP2 FWH								
	Units	**Min**	**Mean**	**Max**	**Claim**[56]	Δ_1	Δ_2	**Range**
TTD	[°C]	1.0	1.8	4.4	**4**	-2.2	63%	Yes
DCA	[°C]	5.3	7.5	10.8	**10**	-2.5	44%	Yes
DWA	[°C]	-2.3	-0.6	-0.2	**1**	-1.6	76%	No
$\dot{m}_{H0}$	[kg/s]	31.0	33.4	34.5	**34.1**	-2%	21%	Yes
U_{DC}	[W/m^{2}K]	1343.5	1784.8	2198.8	**1283**	39%	59%	No
U_{CONC1}	[W/m^{2}K]	2992.9	4150.7	5256.2	**3149**	32%	44%	Yes
U_{CONR}	[W/m^{2}K]	2859.5	4231.1	5280.8	**3149**	34%	45%	Yes
U_{DS}	[W/m^{2}K]							
Q_{TOTAL}	[MW]	80.4	86.0	87.9	**85.5**	1%	7%	Yes
A_{CONDS}	[]	0.0	9.3	13.1				

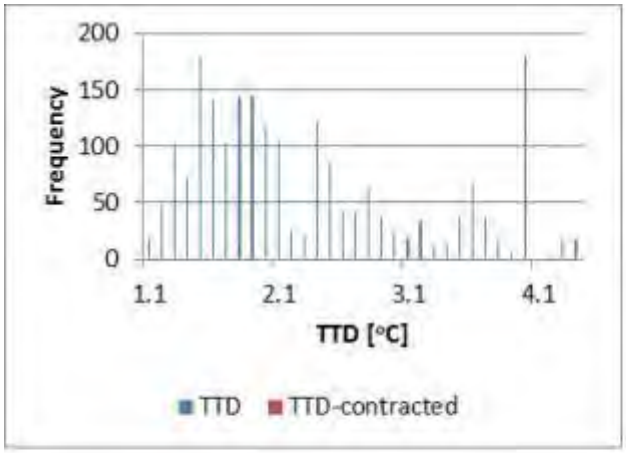

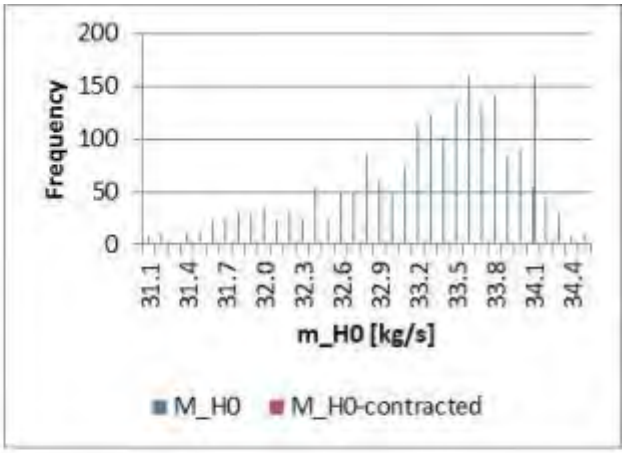

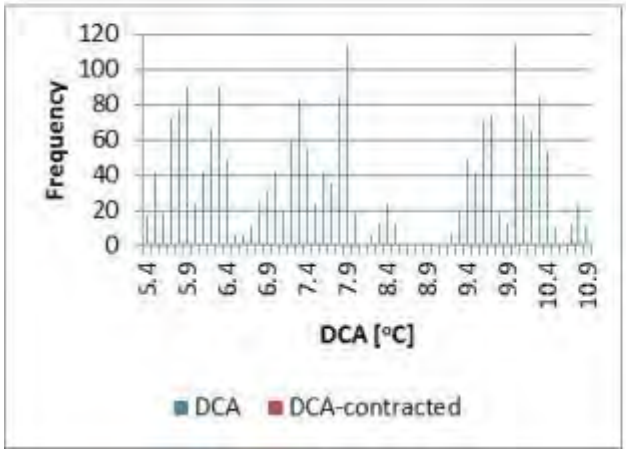

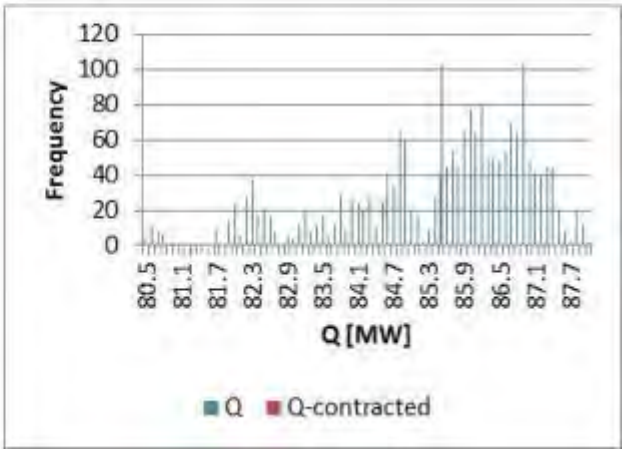

E-18. Tabular and graphical representation of results for the PS00 LP3 FWH

PS00 LP3 FWH								
	Units	**Min**	**Mean**	**Max**	**Claim**[56]	Δ_1	Δ_2	**Range**
TTD	[°C]	0.9	1.8	5.0	**4**	-2.2	53%	Yes
DCA	[°C]	3.4	6.7	11.3	**10**	-3.3	42%	Yes
DWA	[°C]	-3.6	-1.0	-0.3	**1**	-2.0	61%	No
$\dot{m}_{H0}$	[kg/s]	36.6	39.7	40.9	**40.8**	-3%	26%	Yes
U_{DC}	[W/m^{2}K]	1328.9	1996.6	2707.7	**1283**	56%	52%	No
U_{CONC1}	[W/m^{2}K]	2850.2	4188.1	5331.1	**3149**	33%	42%	Yes
U_{CONR}	[W/m^{2}K]	2981.0	4528.1	5684.1	**3149**	44%	51%	Yes
U_{DS}	[W/m^{2}K]							
Q_{TOTAL}	[MW]	84.5	91.6	93.6	**93.5**	-2%	21%	Yes
A_{CONDS}	[]	1.6	3.4	6.5				

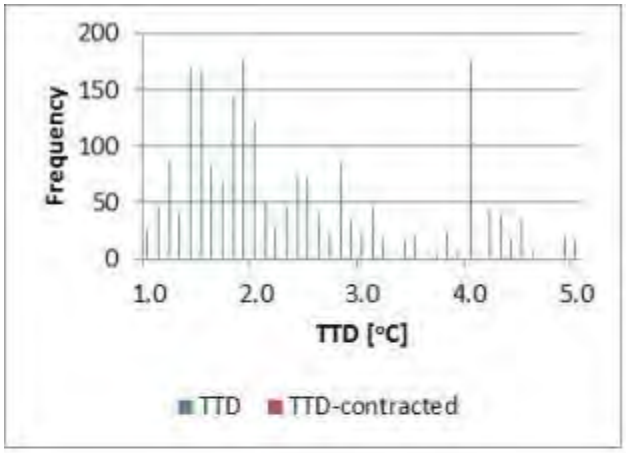

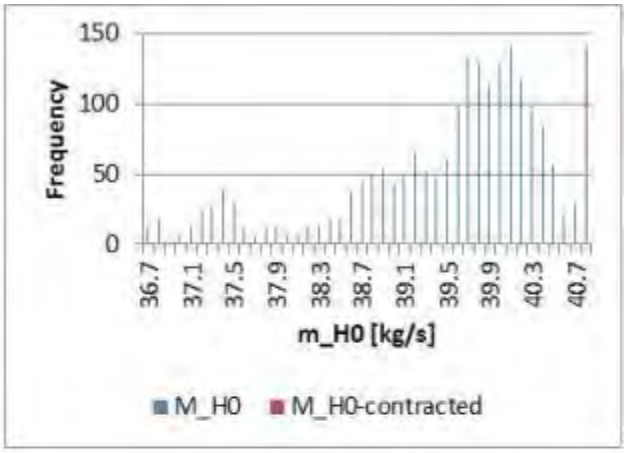

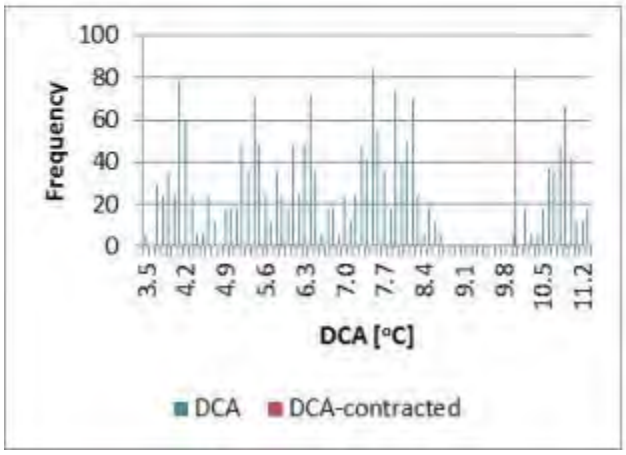

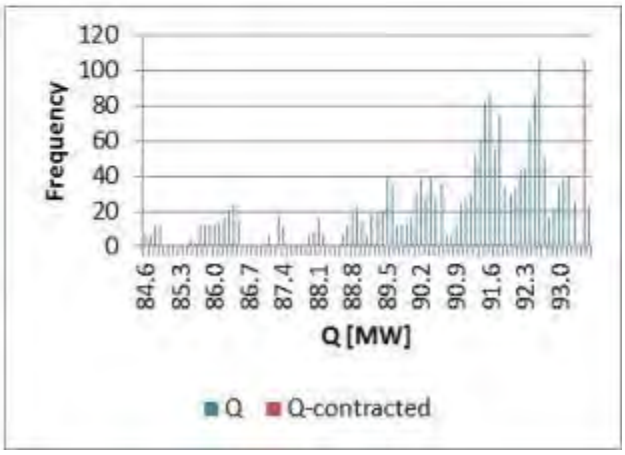

E-19. Tabular and graphical representation of results for the PS00 LP4 FWH

PS00 LP4 FWH								
	Units	**Min**	**Mean**	**Max**	**Claim**[56]	Δ_1	Δ_2	**Range**
TTD	[°C]	0.9	2.2	7.3	**4**	1.8	28%	Yes
DCA	[°C]							
DWA	[°C]	-7.0	-2.1	-0.8	**1**	-3.1	49%	No
$\dot{m}_{H0}$	[kg/s]	55.7	62.4	64.2	**60**	4%	28%	Yes
U_{DC}	[W/m^{2}K]							
U_{CONC1}	[W/m^{2}K]	2428.3	3908.2	5076.9	**3149**	24%	29%	Yes
U_{CONR}	[W/m^{2}K]							
U_{DS}	[W/m^{2}K]							
Q_{TOTAL}	[MW]	101.1	113.2	116.8	**113.7**	0%	3%	Yes
A_{CONDS}	[]	0.0	17.7	17.7				

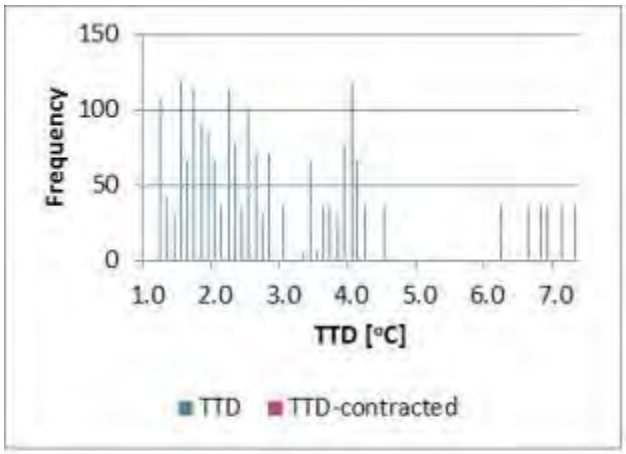

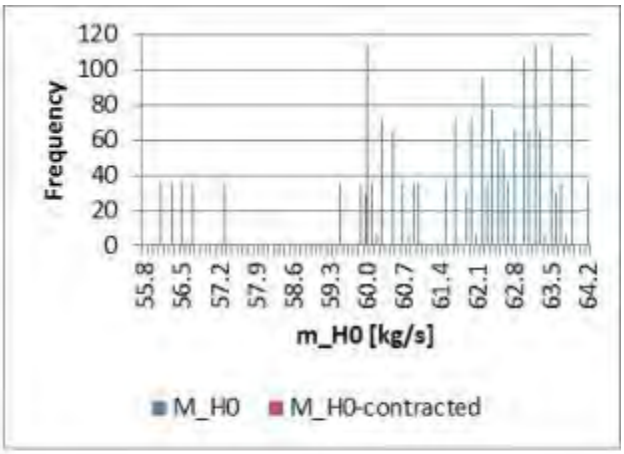

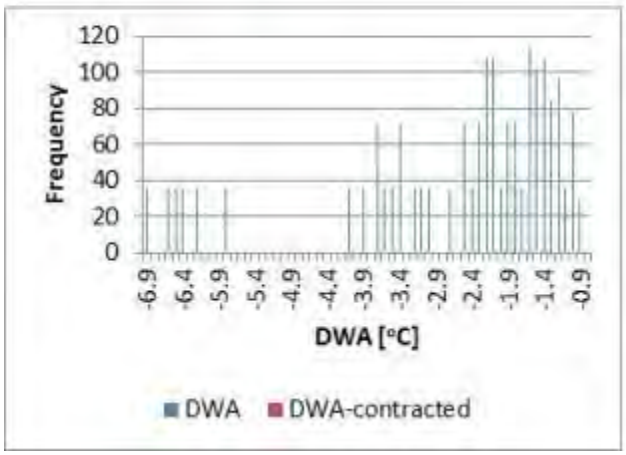

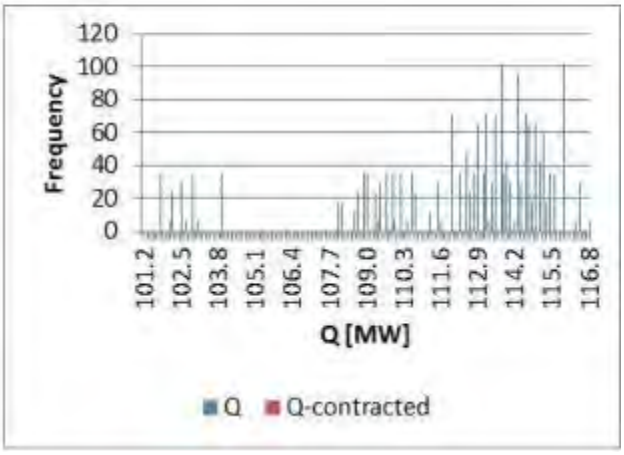

E-20. Tabular and graphical representation of results for the PS00 HP5 FWH

PS00 HP5 FWH								
	Units	**Min**	**Mean**	**Max**	**Claim**[56]	Δ_1	Δ_2	**Range**
TTD	[°C]	0.2	1.1	2.3	**4**	-74%	137%	No
DCA	[°C]	1.7	5.4	10.3	**5**	8%	5%	Yes
DWA	[°C]	-2.2	-1.0	-0.2	**1**	-198%	98%	No
$\dot{m}_{H0}$	[kg/s]	29.7	32.5	35.0	**30**	8%	47%	Yes
U_{DC}	[W/m^{2}K]	650.4	1324.0	2227.4	**1283**	3%	3%	Yes
U_{CONC1}	[W/m^{2}K]	3945.0	5428.9	7480.7	**3149**	72%	64%	No
U_{CONR}	[W/m^{2}K]	4640.3	6015.8	8281.5	**3149**	91%	79%	No
U_{DS}	[W/m^{2}K]							
Q_{TOTAL}	[MW]	65.1	69.1	71.8	**65.3**	6%	57%	Yes
A_{CONDS}	[]	0.0	15.3	16.7				

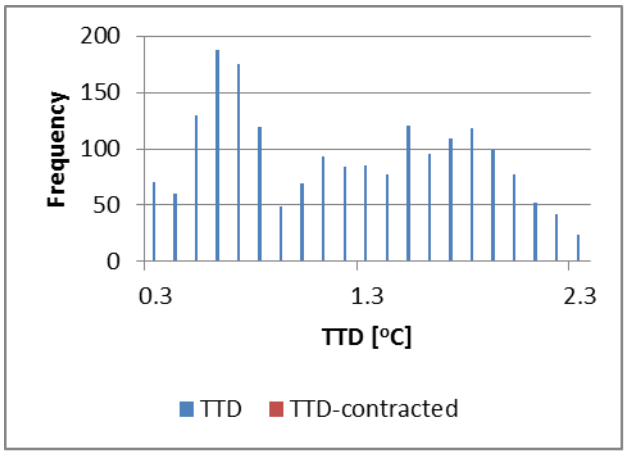

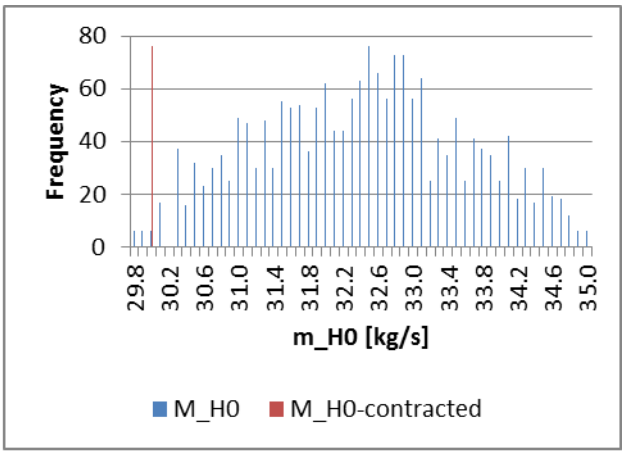

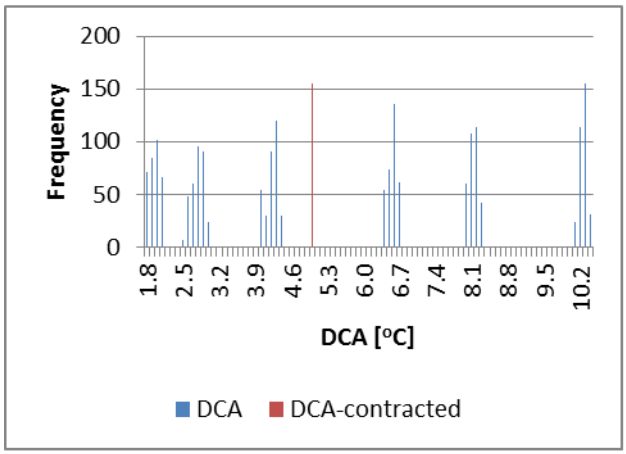

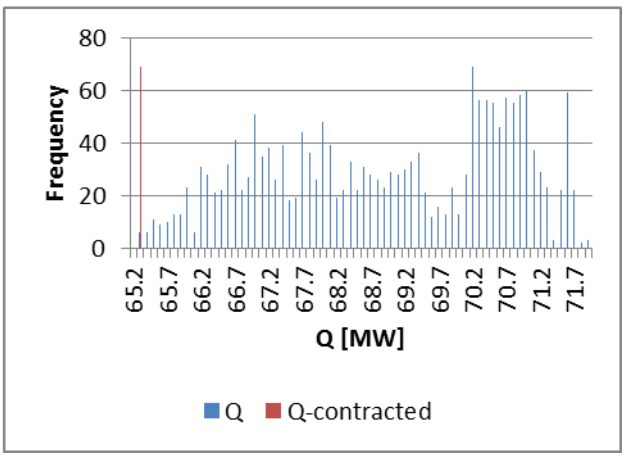

E-21. Tabular and graphical representation of results for the PS00 HP6 FWH

PS00 HP6 FWH								
	Units	**Min**	**Mean**	**Max**	**Claim**[56]	Δ_1	Δ_2	**Range**
TTD	[°C]	0.3	1.1	2.4	**4**	-2.9	134%	No
DCA	[°C]	5.9	10.7	15.6	**10**	0.7	7%	Yes
DWA	[°C]	-2.3	-1.0	-0.2	**1**	-2.0	97%	No
$\dot{m}_{H0}$	[kg/s]	28.4	31.6	34.0	**30**	5%	29%	Yes
U_{DC}	[W/m^{2}K]	665.6	1324.6	2201.5	**1283**	3%	3%	Yes
U_{CONC1}	[W/m^{2}K]	3777.9	4888.7	6495.1	**3149**	55%	64%	No
U_{CONR}	[W/m^{2}K]	4636.6	5980.0	8035.0	**3149**	90%	83%	No
U_{DS}	[W/m^{2}K]							
Q_{TOTAL}	[MW]	74.1	78.9	81.7	**76**	4%	38%	Yes
A_{CONDS}	[]	0.0	16.1	19.3				

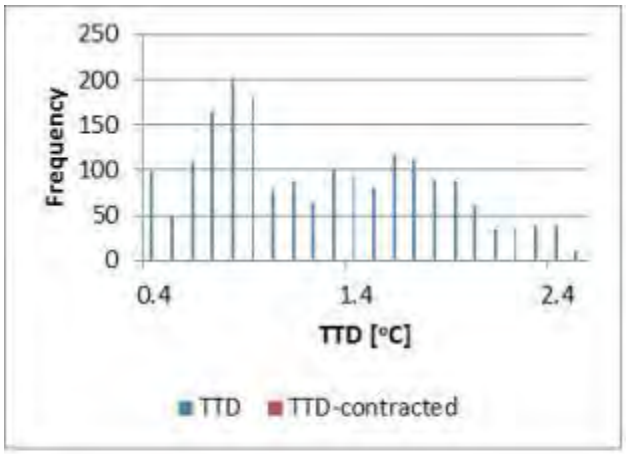

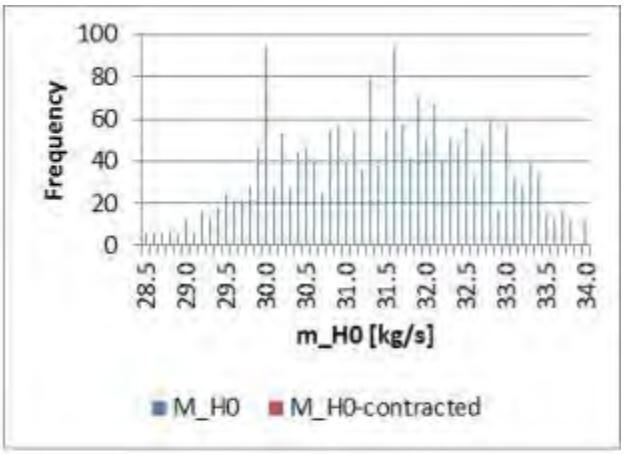

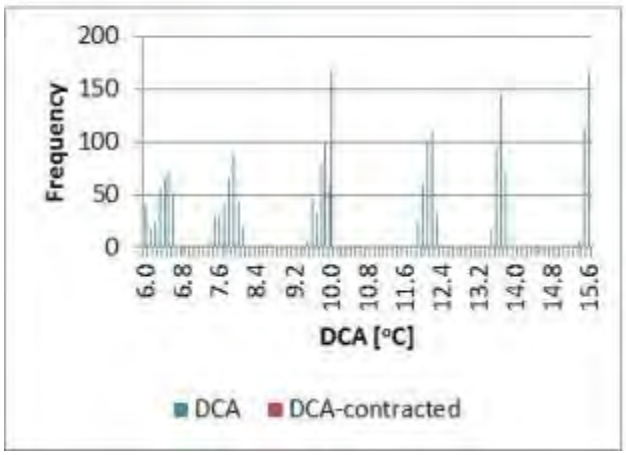

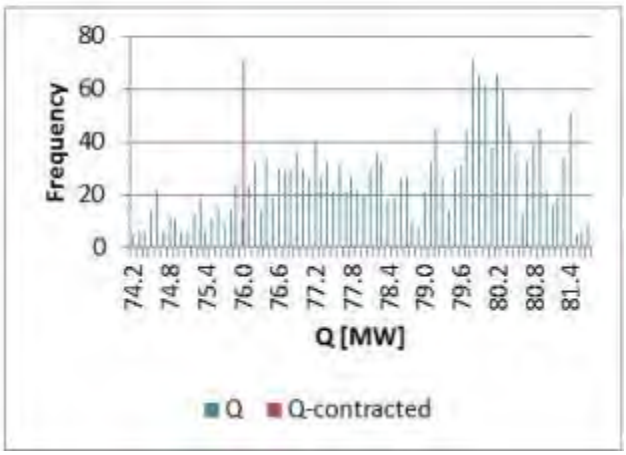

E-22. Tabular and graphical representation of results for the PS08 LP1 FWH

PS08 LP1 FWH								
	Units	**Min**	**Mean**	**Max**	**Claim**[56]	Δ_1	Δ_2	**Range**
TTD	[°C]	0.7	1.3	2.9	**1.4**	-0.1	6%	Yes
DCA	[°C]							
DWA	[°C]	-2.8	-1.2	-0.7	**1**	-2.2	103%	No
$\dot{m}_{H0}$	[kg/s]	5.3	5.9	6.1	**5.5**	7%	51%	Yes
U_{DC}	[W/m^{2}K]							
U_{CONC1}	[W/m^{2}K]	1864.7	2726.3	3329.3				
U_{CONR}	[W/m^{2}K]							
U_{DS}	[W/m^{2}K]							
Q_{TOTAL}	[MW]	11.7	13.1	13.5	**12.5**	5%	32%	Yes
A_{CONDS}	[]	1.0	1.0	1.0				

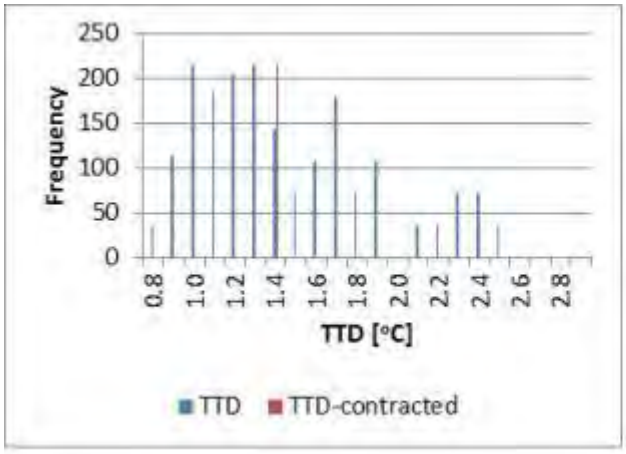

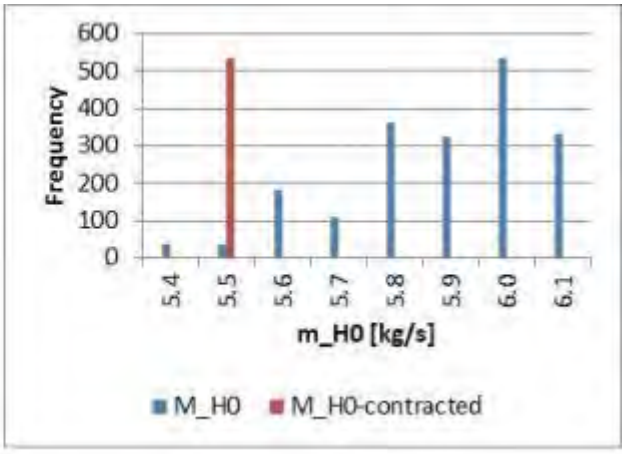

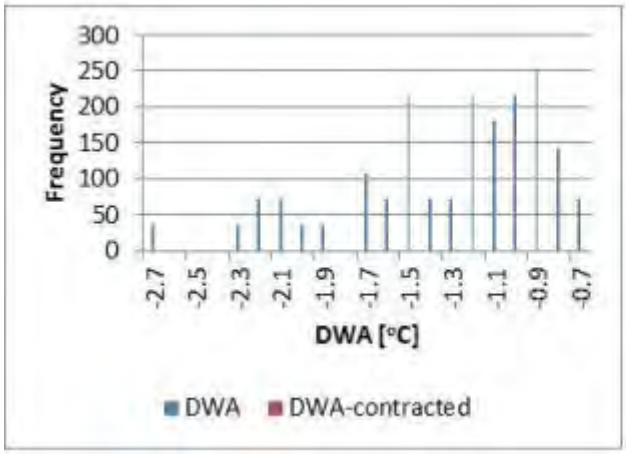

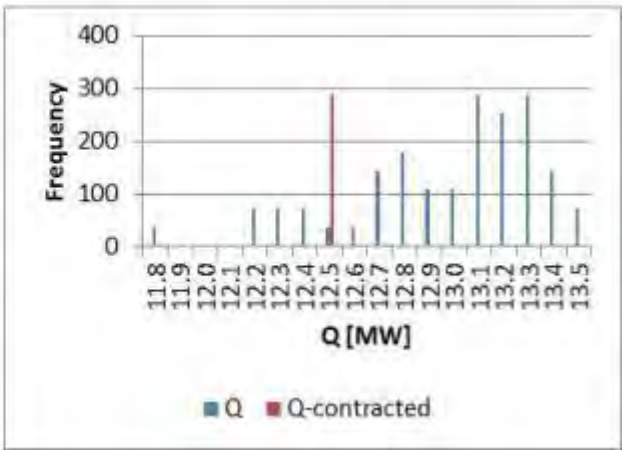

E-23. Tabular and graphical representation of results for the PS08 LP2 FWH

PS08 LP2 FWH								
	Units	**Min**	**Mean**	**Max**	**Claim**[56]	Δ_1	Δ_2	**Range**
TTD	[°C]	0.9	1.7	4.1	**2**	-0.3	10%	Yes
DCA	[°C]							
DWA	[°C]	-3.9	-1.6	-0.8	**1**	-2.6	84%	No
$\dot{m}_{H0}$	[kg/s]	8.0	8.9	9.1	**8.7**	2%	14%	Yes
U_{DC}	[W/m^{2}K]							
U_{CONC1}	[W/m^{2}K]	1941	2861	3514				
U_{CONR}	[W/m^{2}K]							
U_{DS}	[W/m^{2}K]							
Q_{TOTAL}	[MW]	18.0	20.0	20.6	**19.7**	1%	10%	Yes
A_{CONDS}	[]	0.0	5.6	7.5				

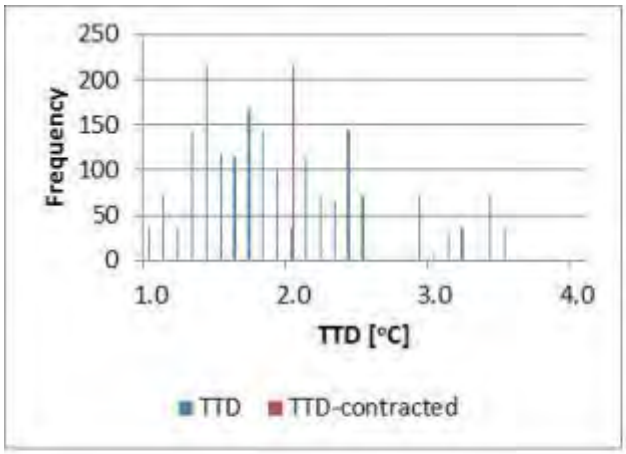

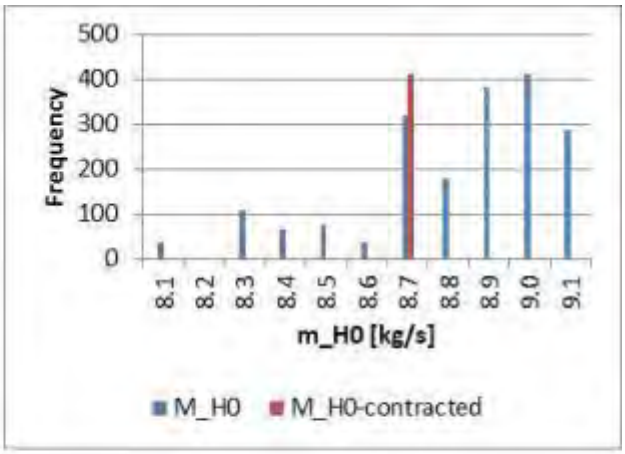

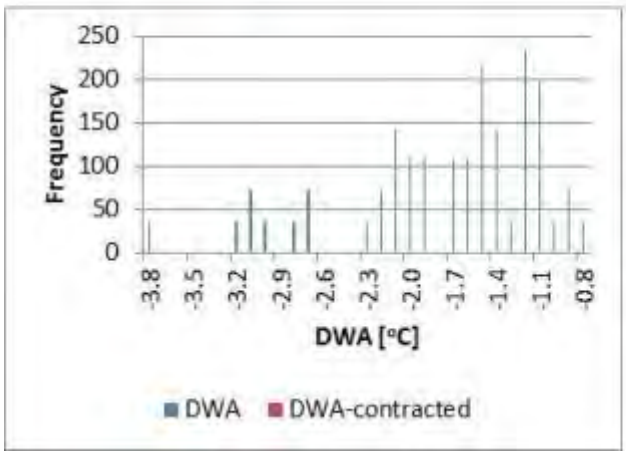

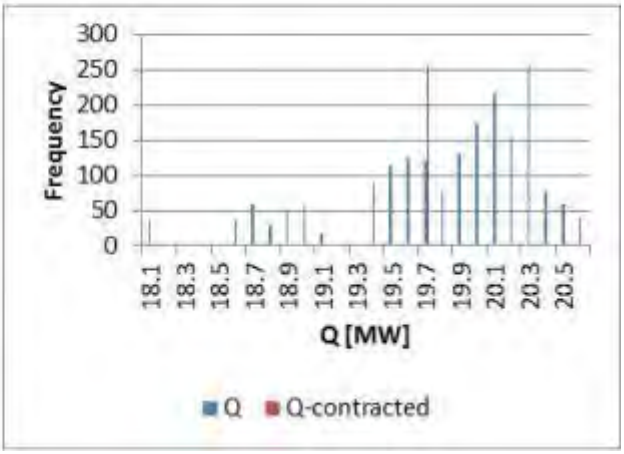

E-24. Tabular and graphical representation of results for the PS08 LP3 FWH

PS08 LP3 FWH								
	Units	**Min**	**Mean**	**Max**	**Claim**[56]	Δ_1	Δ_2	**Range**
TTD	[°C]	1.5	2.3	4.0	**2**	0.3	12%	Yes
DCA	[°C]							
DWA	[°C]	-1.3	-0.2	0.0	**1**	-1.2	88%	No
$\dot{m}_{H0}$	[kg/s]	12.4	13.6	14.2	**13.8**	-1%	10%	Yes
U_{DC}	[W/m^{2}K]							
U_{CONC1}	[W/m^{2}K]							
U_{CONR}	[W/m^{2}K]							
U_{DS}	[W/m^{2}K]							
Q_{TOTAL}	[MW]	28.2	31.0	32.4	**32**	-3%	24%	Yes
A_{CONDS}	[]	225.3	321.0	428.3				

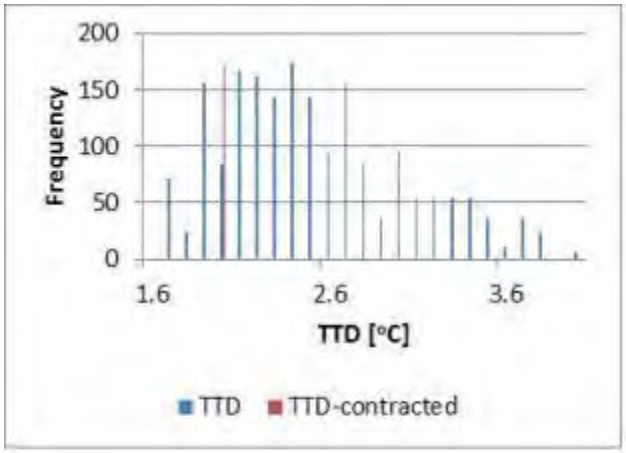

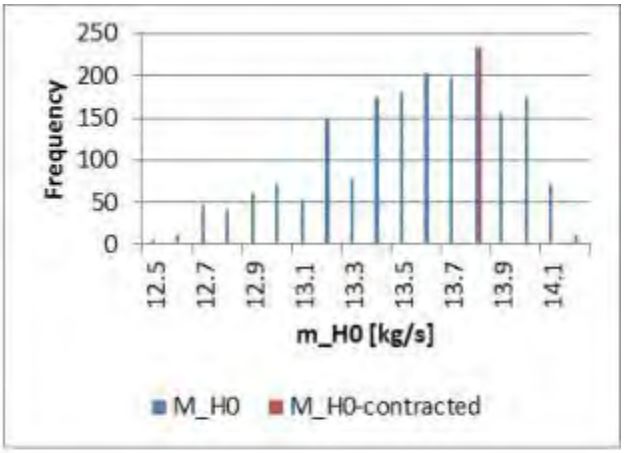

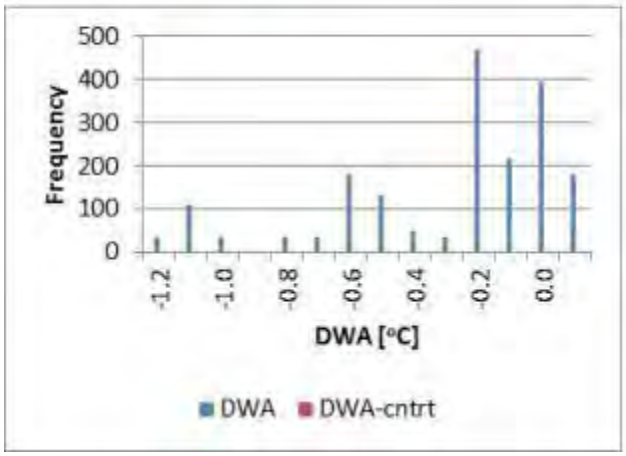

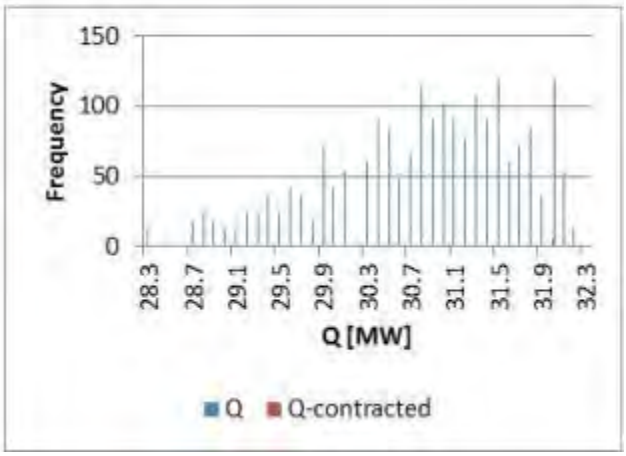

E-25. Tabular and graphical representation of results for the PS08 HP5 FWH

PS08 HP5 FWH								
	Units	**Min**	**Mean**	**Max**	**Claim**[56]	Δ_1	Δ_2	**Range**
TTD	[°C]	-3.7	-0.5	6.5	**0**	-0.5	5%	Yes
DCA	[°C]	3.9	6.7	10.2	**5.6**	0.2	17%	Yes
DWA	[°C]	-7.7	-2.1	-0.1	**1**	-3.1	41%	No
$\dot{m}_{H0}$	[kg/s]	13.4	16.2	17.3	**16.4**	-1%	5%	Yes
U_{DC}	[W/m^{2}K]	2813	3782	4821				
U_{CONC1}	[W/m^{2}K]	2745	4376	5701				
U_{CONR}	[W/m^{2}K]	2688	4305	5622				
U_{DS}	[W/m^{2}K]	423	646	883				
Q_{TOTAL}	[MW]	40.0	47.8	51.2	**47**	2%	7%	Yes
A_{CONDS}	[]	27.1	27.1	27.1				

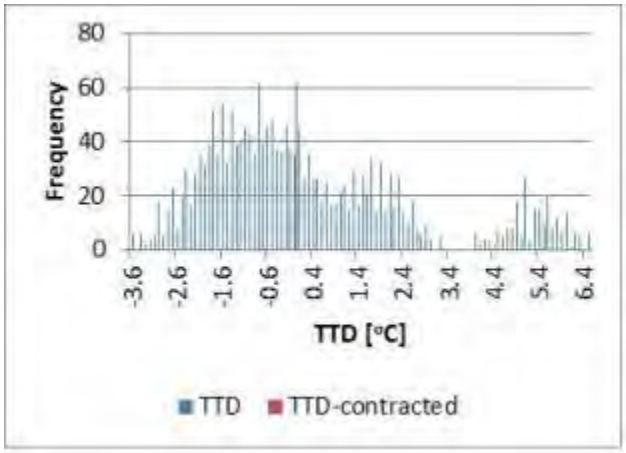

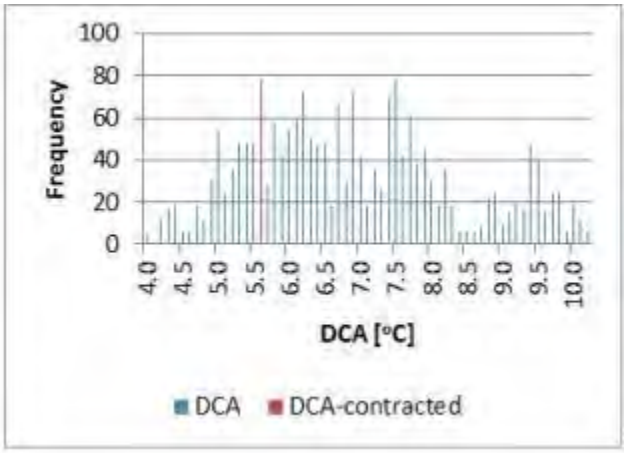

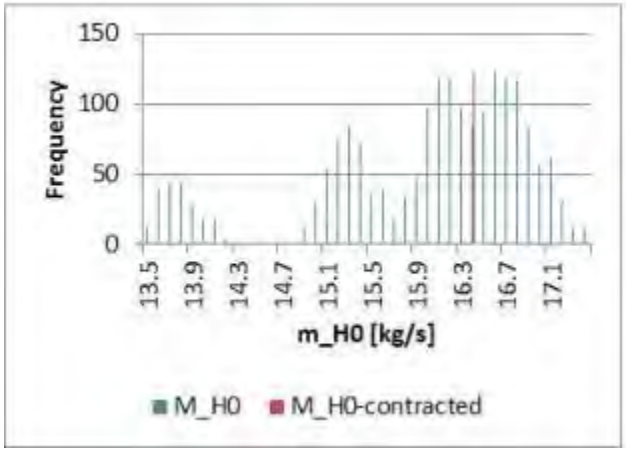

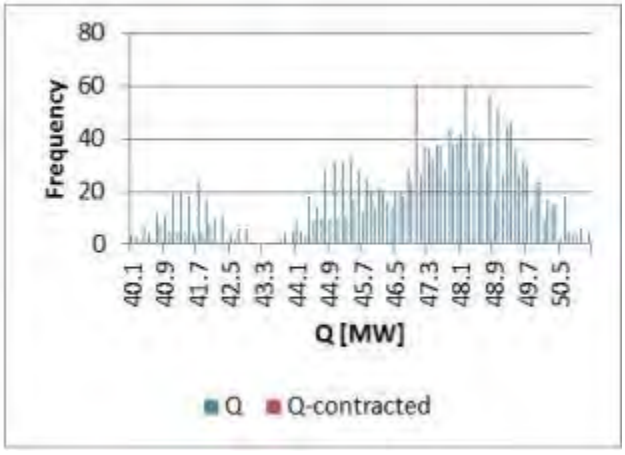

E-26. Tabular and graphical representation of results for the PS08 HP6 FWH

PS08 HP6 FWH								
	Units	**Min**	**Mean**	**Max**	**Claim**[56]	Δ_1	Δ_2	**Range**
TTD	[°C]	-3.4	-0.3	7.9	**0.8**	-1.1	9%	Yes
DCA	[°C]	0.5	1.6	3.3	**5.1**	-0.7	129%	No
DWA	[°C]	-5.6	-0.5	0.9	**1**	-1.5	24%	No
$\dot{m}_{H0}$	[kg/s]	25.6	29.9	31.6	**30.145**	-1%	3%	Yes
U_{DC}	[W/m^{2}K]	2575.9	3387.4	4209.7				No
U_{CONC1}	[W/m^{2}K]	2667.5	4325.3	5751.7				No
U_{CONR}	[W/m^{2}K]	2386.1	3989.5	5351.9				No
U_{DS}	[W/m^{2}K]	669.3	1054.6	1489.8				No
Q_{TOTAL}	[MW]	56.9	66.5	70.2	**66.5**	0%	0%	Yes
A_{CONDS}	[]	45.5	45.5	45.5				

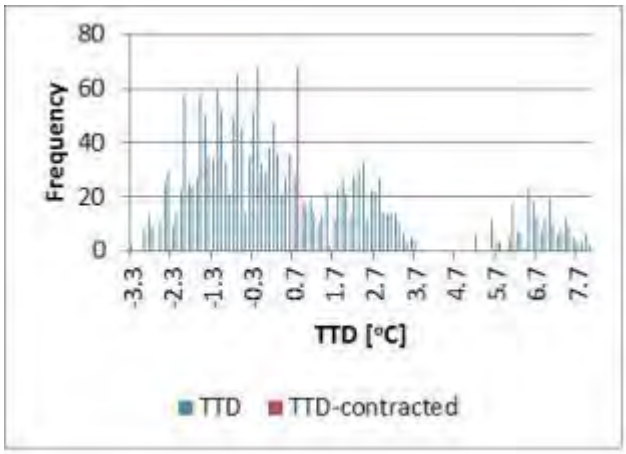

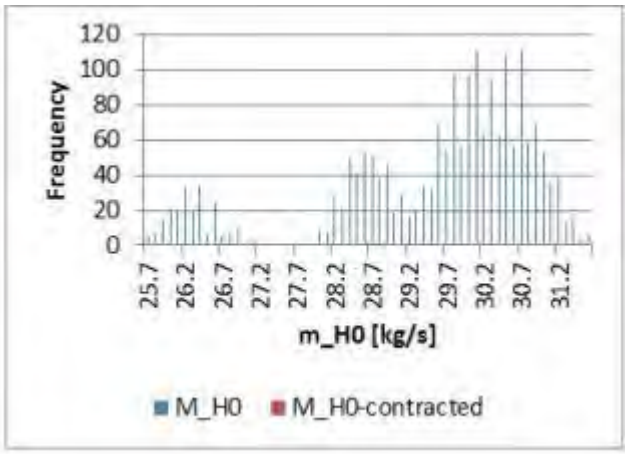

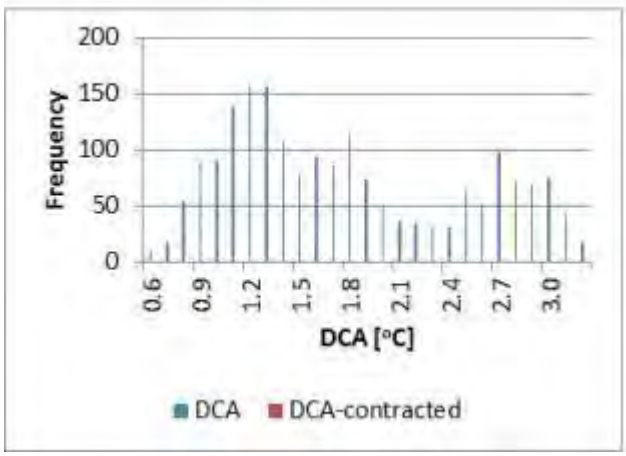

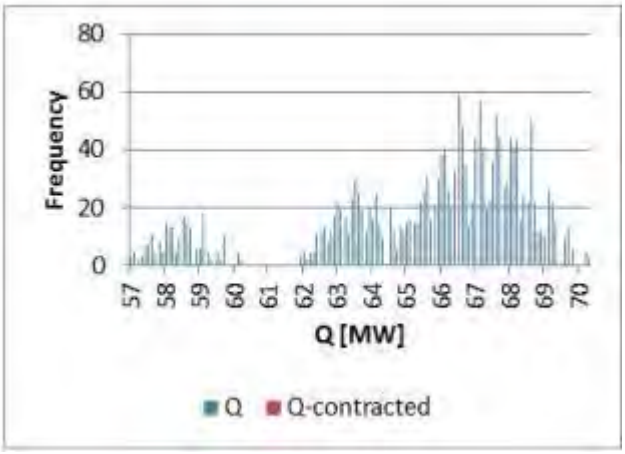

E-27. Tabular and graphical representation of results for the PS16 LP1 FWH

PS16 LP1 FWH								
	Units	**Min**	**Mean**	**Max**	**Claim**[55]	Δ_1	Δ_2	**Range**
TTD	[°C]	1.4	2.4	4.7	**2**	0.4	11%	Yes
DCA	[°C]							
DWA	[°C]	-2.4	-0.5	0.0	**1**	-1.5	61%	No
$\dot{m}_{H0}$	[kg/s]	30.6	32.6	33.4	**32.94**	-1%	14%	Yes
U_{DC}	[W/m^{2}K]							
U_{CONC1}	[W/m^{2}K]	3232.6	4629.8	6101.0	**3477**	33%	40%	Yes
U_{CONR}	[W/m^{2}K]							
U_{DS}	[W/m^{2}K]							
Q_{TOTAL}	[MW]	70.0	74.4	76.3	**75.1**	-1%	11%	Yes
A_{HCONDS}	[m^2]	142.7	256.3	443.3				

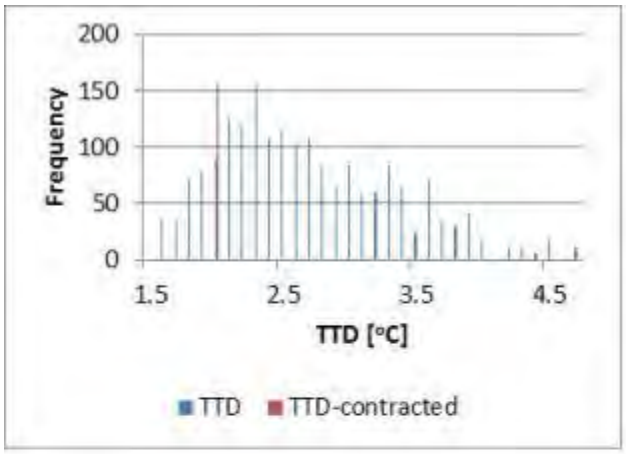

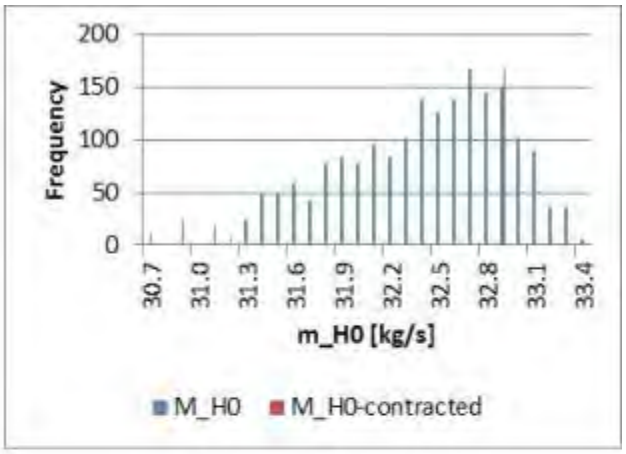

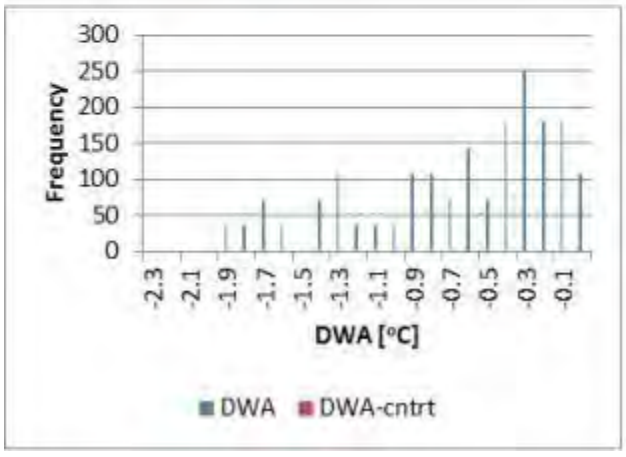

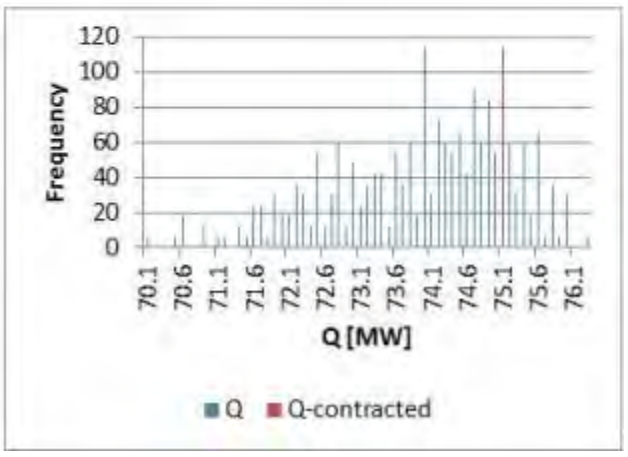

E-28. Tabular and graphical representation of results for the PS16 LP2 FWH

PS16 LP2 FWH								
	Units	**Min**	**Mean**	**Max**	**Claim**[55]	Δ_1	Δ_2	**Range**
TTD	[°C]	1.1	3.7	7.9	**2**	1.7	24%	Yes
DCA	[°C]							
DWA	[°C]	0.7	2.7	3.7	**1**	1.7	56%	Yes
$\dot{m}_{H0}$	[kg/s]	23.4	27.0	29.1	**28.46**	-5%	26%	Yes
U_{DC}	[W/m^{2}K]							
U_{CONC1}	[W/m^{2}K]	3214.0	4674.1	6153.9	**3633**	29%	35%	Yes
U_{CONR}	[W/m^{2}K]							
U_{DS}	[W/m^{2}K]							
Q_{TOTAL}	[MW]	54.8	63.0	67.9	**66.2**	-5%	25%	Yes
A_{HCONDS}	[m^2]	455.4	612.3	728.1				

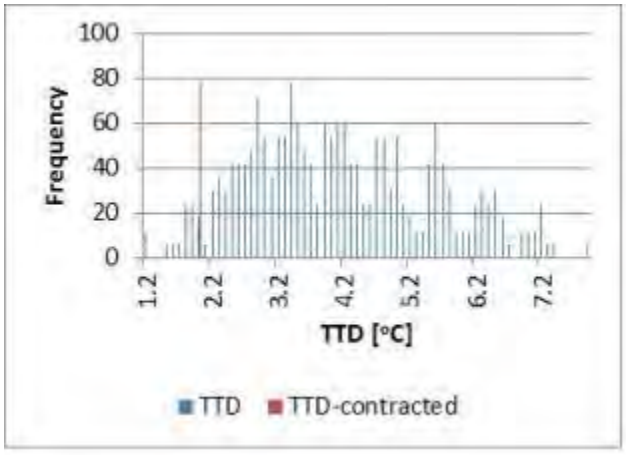

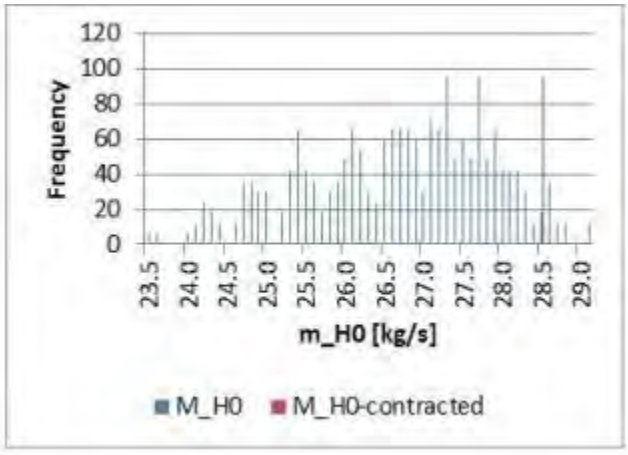

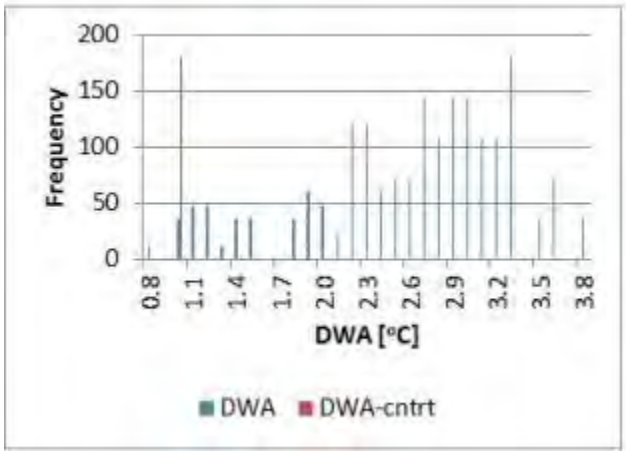

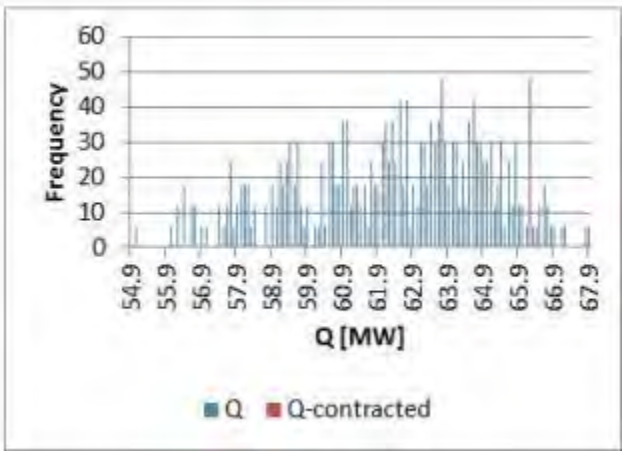

E-29. Tabular and graphical representation of results for the PS16 LP3 FWH

PS16 LP3 FWH								
	Units	**Min**	**Mean**	**Max**	**Claim**[55]	Δ_1	Δ_2	**Range**
TTD	[°C]	-1.2	2.2	8.4	**2**	0.2	2%	Yes
DCA	[°C]	0.0	0.4	1.7	**6**	-5.6	329%	No
DWA	[°C]	-5.1	-0.9	1.4	**1**	-1.9	29%	Yes
$\dot{m}_{H0}$	[kg/s]	19.4	24.8	27.8	**25.3**	-2%	6%	Yes
U_{DC}	[W/m^{2}K]	3198.9	6731.8	12364.7	**1810**	272%	54%	No
U_{CONC1}	[W/m^{2}K]	2980.6	4663.8	6147.7	**3820**	22%	27%	Yes
U_{CONR}	[W/m^{2}K]	3333.2	5176.5	6748.6	**3820**	36%	40%	Yes
U_{DS}	[W/m^{2}K]	252.9	724.3	1392.5	**340**	113%	34%	Yes
Q_{TOTAL}	[MW]	47.8	61.3	68.7	**61.8**	-1%	3%	Yes
A_{HCONDS}	[m^2]	0.0	256.5	448.3				

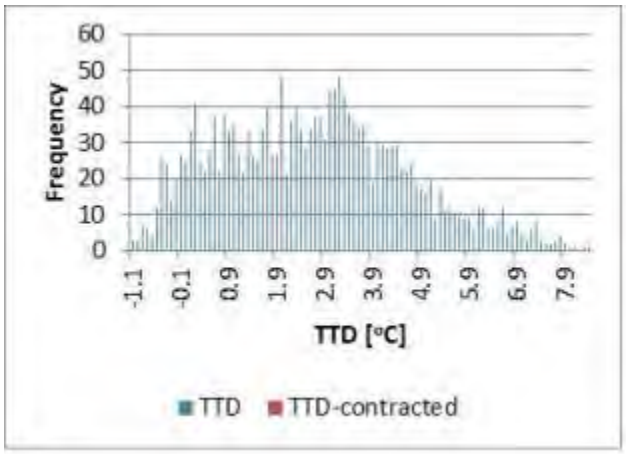

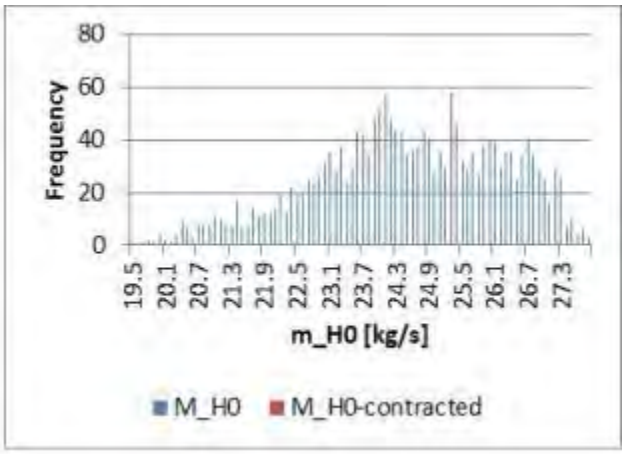

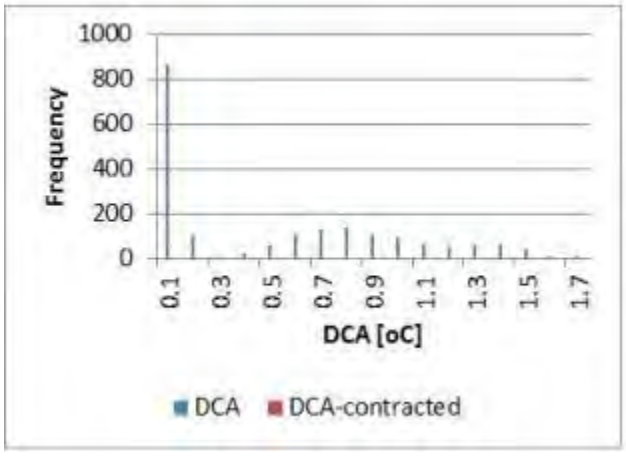

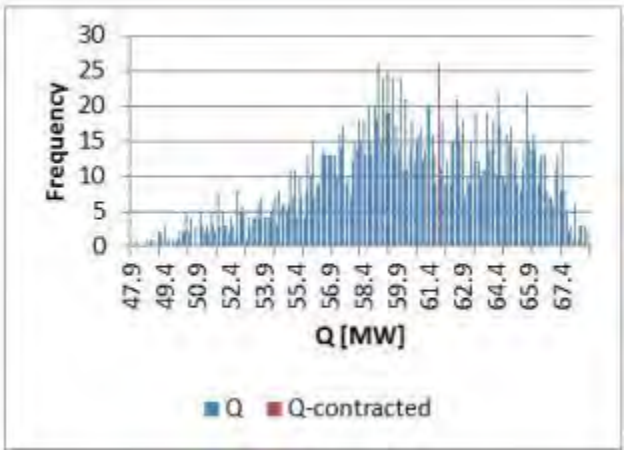

E-30. Tabular and graphical representation of results for the PS16 HP5 FWH

PS16 HP5 FWH								
	Units	**Min**	**Mean**	**Max**	**Claim**[55]	Δ_1	Δ_2	**Range**
TTD	[°C]	-6.0	-2.8	3.9	**-1**	-1.8	18%	Yes
DCA	[°C]	3.7	6.5	10.1	**8**	-1.5	23%	Yes
DWA	[°C]	-4.7	1.3	6.4	**1**	0.3	3%	Yes
$\dot{m}_{H0}$	[kg/s]	16.9	20.4	22.1	**19.325**	6%	21%	Yes
U_{DC}	[W/m^{2}K]	1495.6	2091.8	2732.0	**1876**	12%	17%	Yes
U_{CONC1}	[W/m^{2}K]	2528.0	3906.0	5075.2	**3175**	23%	29%	Yes
U_{CONR}	[W/m^{2}K]	2467.5	3842.9	5013.5	**3175**	21%	26%	Yes
U_{DS}	[W/m^{2}K]	325.6	544.3	802.7	**560**	-3%	3%	Yes
Q_{TOTAL}	[MW]	48.7	58.1	62.6	**54.8**	6%	24%	Yes
A_{HCONDS}	[m^2]	42.2	82.1	82.1				

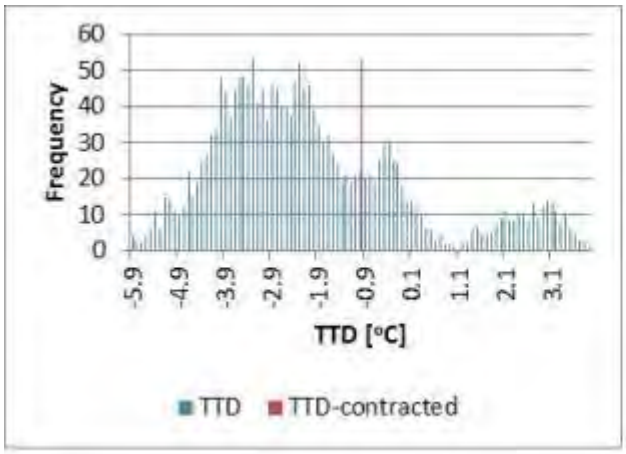

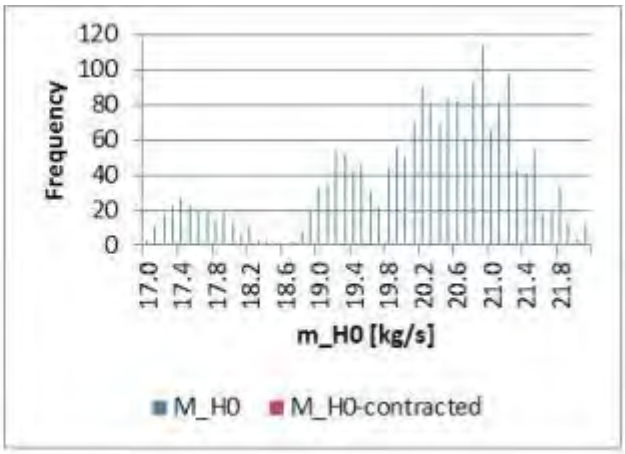

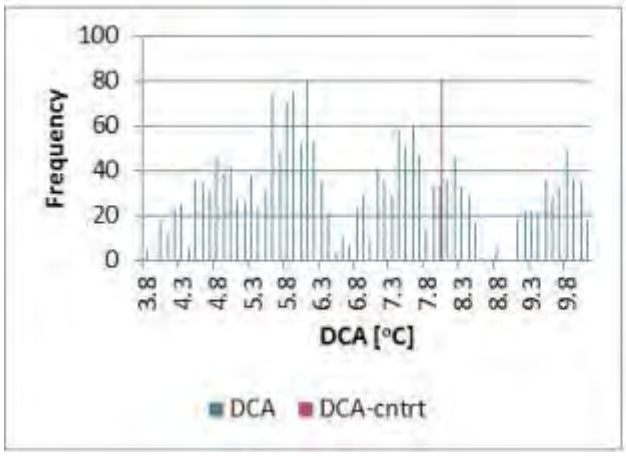

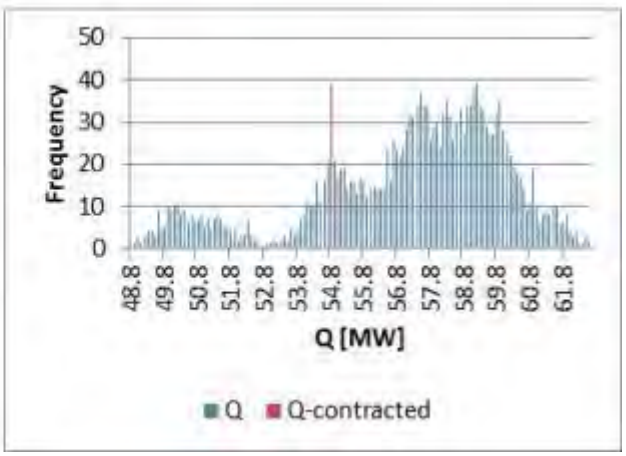

E-31. Tabular and graphical representation of results for the PS16 HP6 FWH

PS16 HP6 FWH								
	Units	**Min**	**Mean**	**Max**	**Claim**[55]	Δ_1	Δ_2	**Range**
TTD	[°C]	-2.3	0.2	5.8	**1**	-0.8	10%	Yes
DCA	[°C]	2.4	5.5	9.3	**8**	-2.5	36%	Yes
DWA	[°C]	-3.3	1.4	4.4	**1**	0.4	5%	Yes
$\dot{m}_{H0}$	[kg/s]	24.3	28.4	30.3	**27**	5%	23%	Yes
U_{DC}	[W/m^{2}K]	1193.6	1785.3	2405.2	**1340**	33%	37%	Yes
U_{CONC1}	[W/m^{2}K]	2173.1	3404.5	4453.1	**2980**	14%	19%	Yes
U_{CONR}	[W/m^{2}K]	2318.1	3556.6	4662.6	**2980**	19%	25%	Yes
U_{DS}	[W/m^{2}K]	396.7	745.2	1189.5	**720**	4%	3%	Yes
Q_{TOTAL}	[MW]	48.6	56.9	60.5	**54.9**	4%	16%	Yes
A_{HCONDS}	[m^2]	69.8	200.8	202.2				

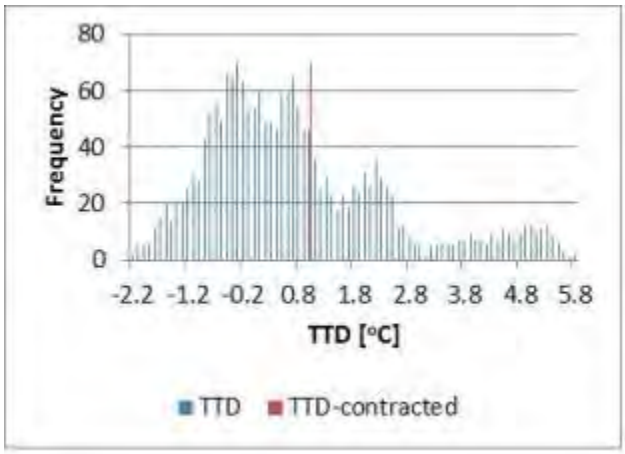

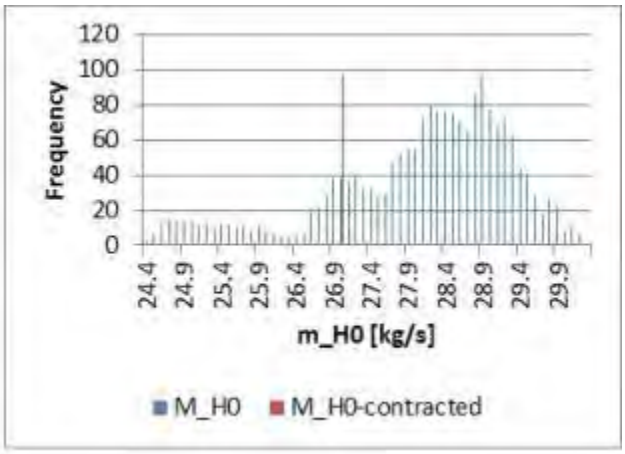

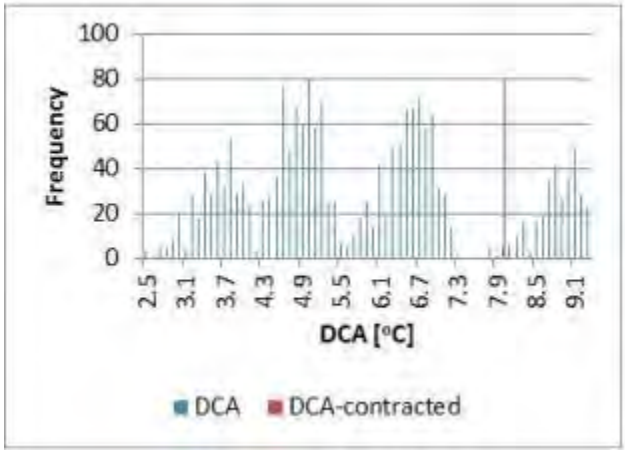

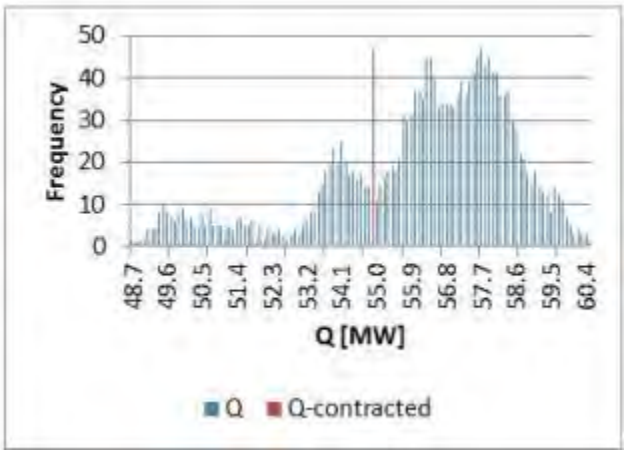

Appendix F. Assessment of Ethics in Research Projects form

EBE Faculty: Assessment of Ethics in Research Projects

Any person planning to undertake research in the Faculty of Engineering and the Built Environment at the University of Cape Town is required to complete this form before collecting or analysing data. When completed it should be submitted to the supervisor (where applicable) and from there to the Head of Department. If any of the questions below have been answered YES, and the applicant is NOT a fourth year student, the Head should forward this form for approval by the Faculty EIR committee: submit to Ms Zulpha Geyer (Zulpha.Geyer@uct.ac.za; Chem Eng Building, Ph 021 650 4791). Students must include a copy of the completed form with the thesis when it is submitted for examination.

Name of Principal Researcher/Student: M.N. ALLIE Department: Mechanical Eng.

If a Student: Degree: MSc Supervisor: Dr Wim Fuls

If a Research Contract indicate source of funding/sponsorship:

Research Project Title: Thermal Modelling of feedwater Heaters

Overview of ethics issues in your research project:

Question 1: Is there a possibility that your research could cause harm to a third party (i.e. a person not involved in your project)?	YES	(NO)
Question 2: Is your research making use of human subjects as sources of data? If your answer is YES, please complete Addendum 2.	YES	(NO)
Question 3: Does your research involve the participation of or provision of services to communities? If your answer is YES, please complete Addendum 3.	YES	(NO)
Question 4: If your research is sponsored, is there any potential for conflicts of interest? If your answer is YES, please complete Addendum 4.	YES	(NO)

If you have answered YES to any of the above questions, please append a copy of your research proposal, as well as any interview schedules or questionnaires (Addendum 1) and please complete further addenda as appropriate.

I hereby undertake to carry out my research in such a way that

- there is no apparent legal objection to the nature or the method of research; and
- the research will not compromise staff or students or the other responsibilities of the University;
- the stated objective will be achieved, and the findings will have a high degree of validity;
- limitations and alternative interpretations will be considered;
- the findings could be subject to peer review and publicly available; and
- I will comply with the conventions of copyright and avoid any practice that would constitute plagiarism.

Signed by:

	Full name and signature	Date
Principal Researcher/Student:	MOHAMMED NAZIER ALLIE	2015-01-29

This application is approved by:

Supervisor (if applicable):	WILHELM FRANZ FULS	2015/2/3
HOD (or delegated nominee): Final authority for all assessments with NO to all questions and for all undergraduate research.	R.D. KNUTSEN	03/02/15
Chair : Faculty EIR Committee For applicants other than undergraduate students who have answered YES to any of the above questions. .		